MASTER

Analysis of an array of cavity-backed stacked path antennas a waveguide simulator approach

Gierstberg, T.A.K.

Award date:
2002

TU/e technische universiteit eindhoven

Faculty of Electrical Engineering
Division Telecommunication Technology and Electromagnetics
Chair of Electromagnetics

Analysis of an Array of Cavity-Backed Stacked Path Antennas: a Waveguide Simulator Approach

by Tom A.K. Gierstberg

EM-10-02

November, 2002

Report of M.Sc. Thesis project performed
at Thales Nederland in collaboration with
the Chair of Electromagnetics of the TU/e

Supervisors:
Prof.dr. A.G. Tijhuis (TU/e)
Ir. M.C. van Beurden (TU/e)
Dr.ir. G.H.C. van Werkhoven (Thales Nederland)

Contents

Chapter 1

Introduction

1.1 General introduction

For the completion of my education at Eindhoven University of Technologie (EUT) I worked on a graduation assignment at Thales Nederland. Thales Nederland is a world-wide particpating and competitive company on the market of building complete radar systems, from antenna to signal processing to visualization and control. Nowadays the main attention is focussed on building large, integrated and multi-functional active antenna arrays, for the purposes of radar and missile guidance. These antenna arrays can be made very large, with respect to the wavelength, which results in a high antenna gain. Also with today's technology it has become possible to steer the main beam almost in any given direction, which makes it possible to scan in azimuth and elevation. It is even possible to set up multiple beams at the same time with the same antenna array.

Antenna arrays, which are capable of performing as mentioned above, are categorized as phased array antennas. These days, phased arrays are being applied more and more often in different fields. For example in mobile communications, in astronomy and in the military. In all applications it is desirable to have low side lobes, such that unwanted signals incident from directions other than the observation direction are suppressed as much as possible. In astronomy it is important to take extra design measures to minimize (thermal) noise. In military applications, phased arrays antennas are used in radar applications. For radar applications, high scan performance and accurate main beam positioning are required.

1.2 Phased array antennas

Phased array antennas are build in all of shapes and sizes. The difference between phased array antennas is mainly formed by the type of elementary radiator out of which the array has been built up. Usually, a phased array antenna consists of several hundreds or thousands of small radiators. Together they form a large aperture with performance levels that easily surpass those of large single aperture antennas, like conventional reflector antennas.

Fast scanning has become possible by the fact that every radiator has its own power supply and phase shifter. However, the drawback is the increasing complexity of the electronics.

The last two decades, a lot of investigation and research is done on microstrip patch arrays, single patches and stacked patches, e.g. [2], [3], [24], [20], [30] [31], mainly because of their excellent performance, low implementation or manufacturing costs and the flexibility in layout during the design proces. In the literature, we find that the bandwidth of arrays consisting of single patches is relatively small: $\pm 10\%$, [20], [30]. This figure can be increased by applying a thicker substrate on which the patches lie [4], [30]. Another solution to increase the bandwidth is to use a second patch stacked above the first, with dielectric layers in between, which results in bandwidth from 20% up to 50 %, [5], [9], [20], [30]. A drawback of the former and also somewhat of the last solution are surface waves in the dielectric substrates. A consequence of this problem is the increase of dielectric losses, deterioration of the radiation efficiency and even worse, introduction of blind spots in the scan range [23] [10]. A possible solution to these unwanted surface waves is to lower the relative permittivity, ε_r, of the substrate. A second possibility is the use of metallized cavities backing the microstrip patches to prevent the surface waves from travelling and thereby preventing their destructive effect [4], [7], [13], [14], [21], [32], [33].

Nowadays during the design and development of phased array antennas more and more attention is focussed on other fields of requirements, for example on: compactness, lightweight, low cost, multi-functional, broadband, etc. Some of these requirements point into the direction of a phased array antenna built from single or stacked patches residing in a cavity.

Large phased arrays are in general modelled by making the assumption that the transverse plane of the antenna face extends towards infinity. Owing to this assumption, one can define a periodicity condition, with which an analysis of a whole array is reduced to a *unit cell*. The *unit cell* is the smallest part of an array from which an array can be build. Note that by assuming and modelling an infinite array, the edge effects which occur in the real finite array are not present. But, before we can examine and analyse these kinds of array phenomena, the whole configuration behind the periodic antenna face has to be analysed. In the case of patches backed by a cavity, and depending on the type of power supply, one can see this configuration as a waveguide structure. A suitable tool for the analysis of waveguide problems is a modal analysis.

1.3 Objective

Besides designing a proper and good functioning antenna with the help of commercial EM-software tools like HFSS, Thales is also interested in gaining insight in what really happens, at a physical level, i.e. currents that are flowing and electromagnetic fields that exist and propagate from the supply-network structure, through the cavity into the outside world, which is called the transmitting case. Once the transmitting case has been characterised the receiving case is also known, owing to reciprocity.

From this we can draw up some rough objectives. First of all, investigation and analysis

of large phased array antennas consisting of stacked patches residing in a cavity. The subjects to which, in general, most of the interest goes out are, scan performance, side lobe levels, bandwidth, low cross-polarization. These are quite a few things to investigate all at once, so we will make a start with the analysis by modelling a waveguide simulator. Our objective thereby will be mainly to find out how the *modes* [1] of the electromagnetic field behave, and to seek for modes, propagating and/or evanescent, with a characteristic behaviour for this specific configuration. Also, will be look at the frequency dependence of separate parts of the antenna and their combinations.

1.4 Method of analysis

For the analysis of this problem we have decided to use integral equations for the magnetic field, solved analytically. Starting form the Marcuvitz-Swinger equation with a properly chosen basis to expand the electromagnetic field in. The choice for integral equations is based on the fact that the problem to be solved is a regular problem for which closed form integrals can be found. Also, it is the most accurate method. The global error which is made, is controllable and can be made as small as possible within certain limits.

What also could have been used is, for example FDTD (Finite Differences Time Domain). Methods based on finite differences are less accurate then integral equations, and for this reason we do not use them.

1.5 Organization report

After the introduction in Chapter 1, we continue with the modelling approach in Chapter 2. It describes how we go from a complex antenna configuration to a configuration divided into subproblems. These subproblems are eventually more simply to solve. Chapter 3 presents a derivation of the Marcuvitz-Swinger equations, suitable for the analysis of waveguide problems. Also, a preview is given of how to arrive at equivalent transmission-line equations by applying a modal representation. In Chapter 4 one can find a description of the waveguide mode functions and we show that they can be used as a suitable basis, for the expansion of the transverse electric and magnetic field constituents. Then in Chapter 5 the equivalent transmission-line equations are deduced together with a source representation. The solution of these transmission-line equations yield the expansion coefficients for the modal field representation. Chapter 6 is completely devoted to the analysis of the iris. First, the so-called modal Green's functions are deduced. Then, the equivalent currents are solved with the method of moments (MoM). Finally, a scattering parameter description is formed, followed by some results. Chapter 7 discusses a patch in a waveguide. The approach is the same as for the iris in Chapter 6. We conclude the analysis in Chapter 8, in which a waveguide simulator is modelled with the components of Chapters 6 and 7. The report ends with some conclusions and recommendations.

[1] later on it will become clear what is understood by "modes"

Chapter 2

Modelling approach

2.1 General

In the preceding chapter we talked about phased array antennas, and with particular interest about phased arrays consisting of patches receding in a cavity. This chapter will be devoted to a more detailed description of such an array geometry and how we intend to form a model which can be analyzed with appropriate tools. In spite of the fact that one of our final objectives is to form a waveguide modulator, which is an approach to model an entire infinite periodic array, we will give a model approach for the entire array, including periodic coupling with free space. In this way the basis for a possible continuation of the analysis is made.

Fig.2.1 shows a cross-section, in the $x - z$-plane, of the phased array of interest. The

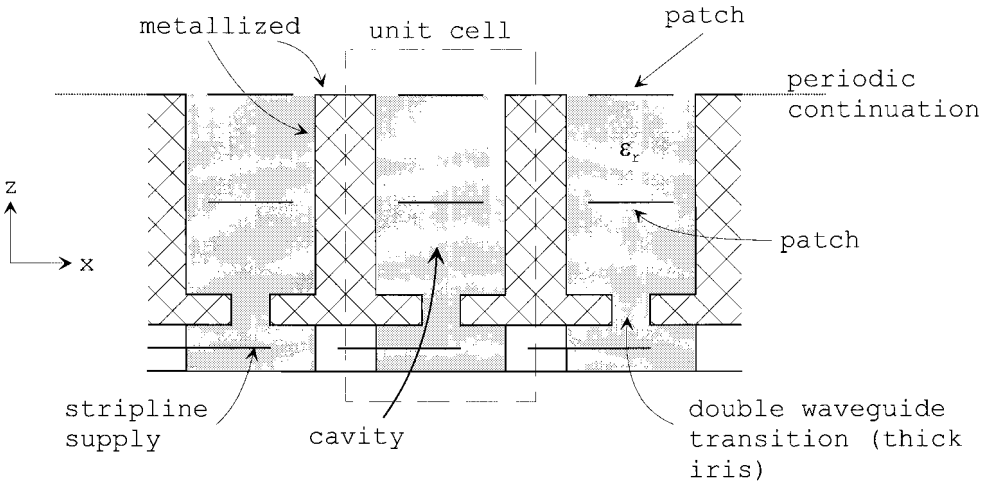

Figure 2.1: *Cross-section of cavity backed stacked patch phased array in $x - z$-plane*

infinite array approach reduces the analysis to a unit cell. Due to this modelling step every elementary radiator, confined in such an unit cell, sees the same environment. Therefore,

it does not matter which unit cell is taken, so, we choose the one in the origin of the coordinate system.

The cavity can be modelled as a piece of waveguide. Further down into the cavity we come to a double waveguide transition, which we will consider as a thick iris. The purpose of the waveguide transition is to couple the cavity to the stripline power-supply. Depending on the geometry of the transition and the position in the transverse plane (x-y-plane), it acts as a filter for the polarization and determines which modes couple and are transmitted. If we pass through the iris we observe the power-supply. The power-supply is a completely closed cavity, except for the iris aperture, in which a stripline ends. The cavity which contains the patches, the iris and the cavity in which the stripline ends are filled with dielectricum with relative permittivity $\varepsilon_r = 3$. In Fig.2.2 the top-view (x-y-plane) of the array is displayed. Observable, is the periodicity. In this case the periodic grid extends

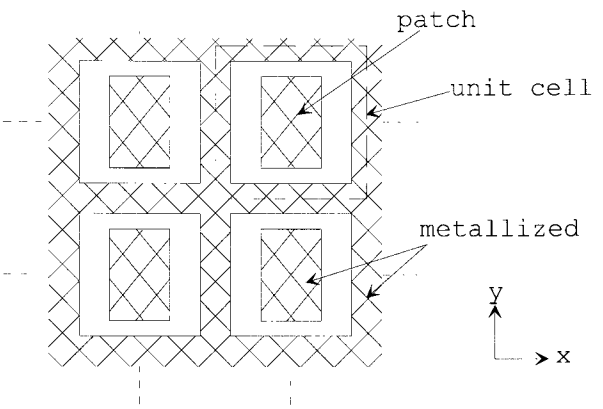

Figure 2.2: *Top view of array in $x-y$-plane*

along the orthogonal x- and y-axis, but it could also be along some triangular grid spacing. The shaded parts are metallized. Furthermore, the cavity, the patches, and the iris all have rectangular shapes.

2.2 Modelling assumptions

For analysis and modelling of a problem it is important to know what assumptions have been made, since these assumptions often give the analysis a certain position in the field of reliability. Also, certain discrepancies compared to practical results can be explained. The first assumption we made is, that all metal is modelled as a Perfect Electric Conductor (PEC).

The patches are made of a very thin layer of coper, printed on a very thin layer of capton, which has a relative permittivity $\varepsilon_r = 3.4$. The thickness of each layer is in the order of a tenth of a millimeter. The capton layers are being neglected for simplicity and because they are very thin and lie transverse to the propagation direction. In practice the

worst that can happen is a small reflection and phase shift. Regarding to the phase shift which the capton can introduce. Each cavity contains layers of capton on which the patchs are printed, so the same phase shift will occur in every cavity along the whole array which makes it no problem. What might form a problem, is if the thickness of the capton layers varies or if the capton is inhomogeneous. This could result in a varying attenuation and phase shift in each cavity. The inhomogeneity and/or anisotropic characteristics of the dielectric filling can also raise problems. Taking into account the fact that a material is inhomogeneous and/or anisotropic would make the analysis much more difficult therefore we assume that all dielectric materials are homogeneous.

Some other imposed assumptions for this system are that it is lineair, time invariant and instantaneously reacting.

In our model we assume that the walls inside the iris are completely metallized and that this metal is a PEC.

2.3 Subdivision of the problem

In some papers, which discus comparable configurations, the hole configuration is usually analysed at once. It is then also a complex approach, in the sense that one can easily make mistakes and get lost in the problem. Therefore, we take a different approach. We divide the problem in parts to simplify the problem. In this way we can tackle the problem step by step and afterwards, the sub-solutions can be used to study the total structure be putting them together.

Looking at Fig.2.1, the configuration can be split into 4 parts viz.,

- Part 1: the iris, Fig.2.3.

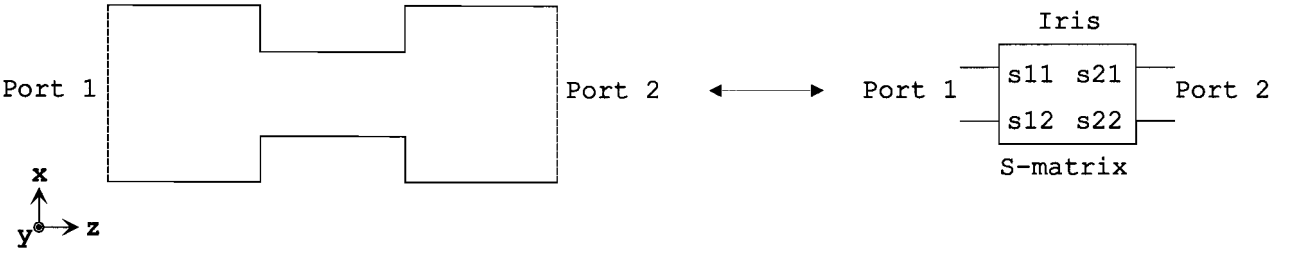

Figure 2.3: *Iris.*

- Part 2: patch in cavity, Fig.2.4.
- Part 3: patch in periodic arrangement, Fig.2.5.
- Part 4: the stripline power-supply, also called the feed. The power-supply is out of the scoop of this analysis.

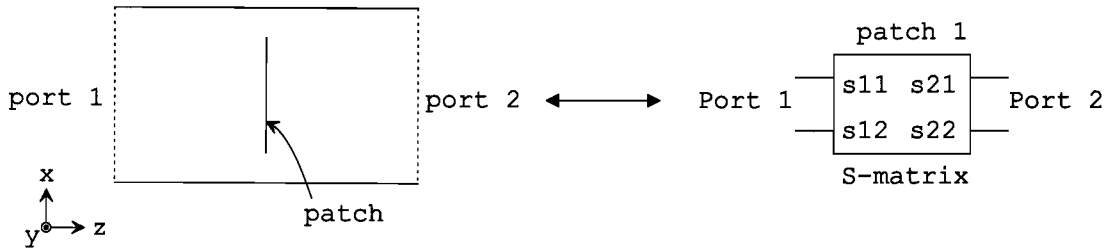

Figure 2.4: *Patch in cavity.*

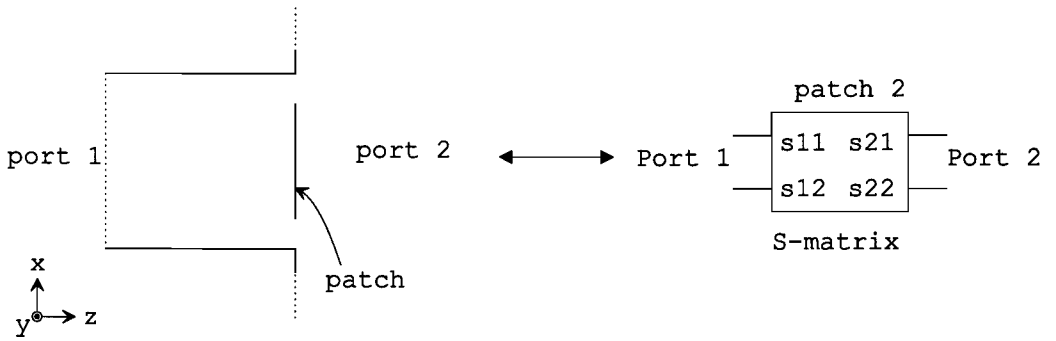

Figure 2.5: *Patch in periodic arrangement.*

The coupling of the different parts afterwards, can be realized by forming scattering parameter descriptions of each part, during the analysis. That's why we illustrated the scattering matrices (S-matrices) in the figures. By coupling the output of one S-matrix to the input of the other, the matrices are combined, to form a compleet system. The results S-matrix description gives us insight into the behaviour of the modes. Before we can work with these S-matrices we have to analyse each part and come to a description that will lend itself to be transformed into scattering parameters.

If it was not yet completely clear, we emphasize it again that we have to deal with waveguide problems. To analyse the electromagnetic fields in waveguides we make use of the Marcuvitz-Swinger equations. The Marcuvitz-Swinger equations describe the transverse electromagnetic fields of an infinitely long of waveguide. A description of the transverse electromagnetic fields is well suited, as it will turn out, for the discontinuities in the transverse plane which are present in our problems. From the Marcuvitz-Swinger equations we can deduce equivalent transmission-line equations which describe the behaviour of each mode in the propagation direction.

To deal with the discontinuities we could use the method of mode matching, which is appropriate in the case of the iris, but not in the case of the patches. Instead, we will apply the methode of moments (MoM). In this way we can use one solution methode for different cases. The method of moments is used to solve integral equations and yields current coefficients of an approximated current distribution. Until now we have not talked

about, or defined any current, but by defining equivalent situations for the cases depicted in Fig.(2.3)-(2.5) we can, with the help of the equivalence theory and uniqueness theorems, introduce equivalent surface current densities. In Fig.(2.6)-(2.8) the equivalent situations are depicted. The equivalent situation is created by closing the apertures with a flat PEC

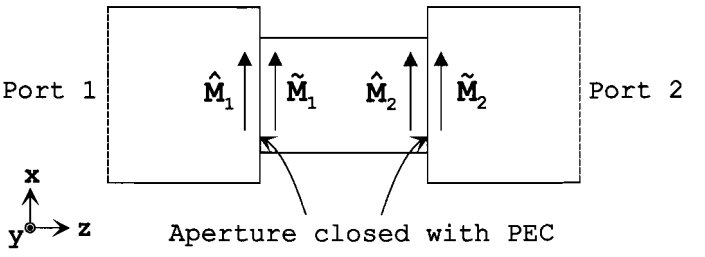

Figure 2.6: *Equivalent configuration of iris.*

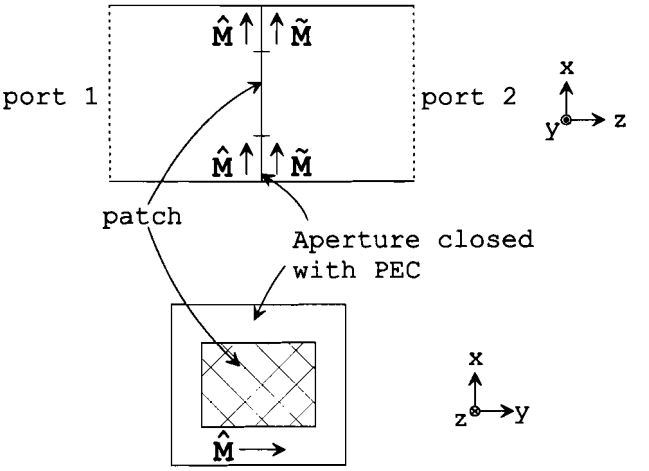

Figure 2.7: *Equivalent configuration of patch in cavity.*

surface and defining at an infinitesimal distance, on both sides of the PEC, magnetic surface current densities. Magnetic surface current densities on the left side of the PEC (i.e. $z = z_a^-$) are defined by $\hat{\mathbf{M}}$ and on the right (i.e. $z = z_a^+$) by $\tilde{\mathbf{M}}$. This was the first step in defining a equivalent situation, the second follows. The situations with the equivalent surface currents, Fig.(2.6)-(2.8), are completely equivalent to the original situations, Fig.(2.3)-(2.5), once Eqs.(2.1) and (2.2) are satisfied.

$$\mathbf{E} \times \mathbf{n}|_{(z_a^-)} = \mathbf{E} \times \mathbf{n}|_{(z_a^+)}, \tag{2.1}$$

$$\mathbf{n} \times \mathbf{H}|_{(z_a^-)} = \mathbf{n} \times \mathbf{H}|_{(z_a^+)}. \tag{2.2}$$

These equations tell us that the tangential fields at the aperture (i.e. $z = z_a$) must be continuous as in the original situation.

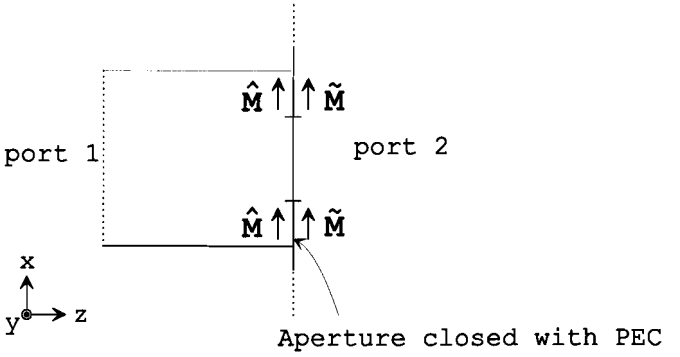

Figure 2.8: *Equivalent configuration of patch in periodic grid.*

The second equation, Eq.(2.2), will be used during the MoM. The first equation, Eq.(2.1), can be satisfied by examining the magnetic surface current densities on the aperture according to the well known relation for the tangential component of the electric field, viz.

$$\mathbf{E} \times \mathbf{n} = \mathbf{M}_s. \tag{2.3}$$

The subscript s is the indication for a surface quantity, which from now on is left out and will be implied until defined otherwise.
For the left side of the aperture, Eq.(2.4) is applicable.

$$\mathbf{E} \times \mathbf{n}|_{(z_a^-)} = -\mathbf{E} \times \mathbf{e}_z|_{(z_a^-)} = \hat{\mathbf{M}}. \tag{2.4}$$

The minus-sign is due to the fact that we defined the normal vector on the aperture in the positive z-direction, thereby becoming equal to the z-directed unit vector and the normal vector needed to determine the tangential electric field on the left of the aperture is directed opposite to the z-directed unit vector.
For the right side of the aperture Eq.(2.5) is applicable.

$$\mathbf{E} \times \mathbf{n}|_{(z_a^+)} = \mathbf{E} \times \mathbf{e}_z|_{(z_a^+)} = \tilde{\mathbf{M}}. \tag{2.5}$$

Then, by combining Eq.(2.4) and (2.5) according Eq.(2.1) we find the relation between the magnetic surface current densities on both sides of the aperture,

$$-\hat{\mathbf{M}} = \tilde{\mathbf{M}}. \tag{2.6}$$

By closing the aperture with PEC's and defining equivalent magnetic surface currents we have created a situation of uniform waveguide sections which are analyzed in an simpler way.

Note: to make significante conclusions or recommendations in relation to the specific configuration in Fig.2.1 it is important to have an accurate and description and model of the stripline power-supply.

Chapter 3

Waveguide problem; General insight applied analysis

In the introduction we discussed the configuration that will be analyzed. We showed how the problem is split up, in order to simplify it, and how that led to four subproblems of which one, the power-supply, is out of the scoop. All cases are waveguide type problems for which the Marcuvitz-Swinger equations are well suited to describe and solve the electromagnetic fields.

This chapter we want to use more as an general introductory to explain and give an idea, a bigger picture, behind the analysis by means of the Marcuvitz-Swinger equations. It gives us an opportunity to derive these equations. An opportunity to show how the transverse field can be expressed in an modal representation. Furthermore, we show how we come to equivalent transmission-line equations, starting from the Marcuvitz-Swinger equations and what the characteristic guided wave solution is for waveguides.

The gained insight will then be further employed and worked out in detail for the particular cases.

3.1 Maxwell's equations

We will start form Maxwell's equations with $e^{j\omega t}$ time dependence:

$$\nabla \times \mathbf{E}(\mathbf{r},\omega) = -j\omega\mathbf{B}(\mathbf{r},\omega) - \mathbf{M}(\mathbf{r},\omega), \tag{3.1}$$

$$\nabla \times \mathbf{H}(\mathbf{r},\omega) = j\omega\mathbf{D}(\mathbf{r},\omega) + \mathbf{J}(\mathbf{r},\omega), \tag{3.2}$$

where,

$\mathbf{E}$ = electric field strength [V/m], $\mathbf{B}$ = magnetic flux density [Vs/m^2],
$\mathbf{H}$ = magnetic field strength [A/m], $\mathbf{J}$ = electric current density [A/m^2],
$\mathbf{D}$ = electric flux density [As/m^2], $\mathbf{M}$ = magnetic current density [V/m^2],

The field quantities are vector fields, indicated bold, and are position ($\mathbf{r}$) and frequency (ω) dependent. The quantities $\mathbf{J}$ and $\mathbf{M}$ represent sources. They are referred to as being exter-

nal, or impressed. Furthermore these sources must obey the laws of charge conservation, defined by the continuity equations,

$$\nabla \cdot \mathbf{M}(\mathbf{r},\omega) = -j\omega\rho_m(\mathbf{r},\omega), \tag{3.3}$$
$$\nabla \cdot \mathbf{J}(\mathbf{r},\omega) = -j\omega\rho_e(\mathbf{r},\omega), \tag{3.4}$$

where,

ρ_e = electric charge density [As/m^3],
ρ_m = magnetic charge density [Vs/m^3].

Taking the divergence of Eq.(3.1) and Eq.(3.2) we arrive at,

$$\nabla \cdot \nabla \times \mathbf{E}(\mathbf{r},\omega) = 0 = -j\omega\nabla \cdot \mathbf{B}(\mathbf{r},\omega) - \nabla \cdot \mathbf{M}(\mathbf{r},\omega), \tag{3.5}$$
$$\nabla \cdot \nabla \times \mathbf{H}(\mathbf{r},\omega) = 0 = \quad j\omega\nabla \cdot \mathbf{D}(\mathbf{r},\omega) + \nabla \cdot \mathbf{J}(\mathbf{r},\omega), \tag{3.6}$$

then by substitution of the charge conservation laws, Eq.(3.3) en Eq.(3.4), we get the dependent equations

$$\nabla \cdot \mathbf{B}(\mathbf{r},\omega) = \rho_m(\mathbf{r},\omega), \tag{3.7}$$
$$\nabla \cdot \mathbf{D}(\mathbf{r},\omega) = \rho_e(\mathbf{r},\omega), \tag{3.8}$$

which are *Gauss' laws* for the electric and magnetic flux densities. Under the assumptions made in Sec.2.2 the following constitutive relations hold

$$\mathbf{B}(\mathbf{r},\omega) = \mu\mathbf{H}(\mathbf{r},\omega), \tag{3.9}$$
$$\mathbf{D}(\mathbf{r},\omega) = \varepsilon\mathbf{E}(\mathbf{r},\omega), \tag{3.10}$$

with

ε = (complex) permittivity [As/Vm],
μ = (complex) permeability [Vs/Am].

Upon substituting Eqs.(3.9)-(3.10) in to Eqs.(3.1)-(3.2) we obtain the final form of Maxwell's equations

$$\nabla \times \mathbf{E}(\mathbf{r},\omega) = -j\omega\mu\mathbf{H}(\mathbf{r},\omega) - \mathbf{M}(\mathbf{r},\omega), \tag{3.11}$$
$$\nabla \times \mathbf{H}(\mathbf{r},\omega) = j\omega\varepsilon\mathbf{E}(\mathbf{r},\omega) + \mathbf{J}(\mathbf{r},\omega), \tag{3.12}$$
$$\nabla \cdot \mathbf{B}(\mathbf{r},\omega) = \rho_m(\mathbf{r},\omega), \tag{3.13}$$
$$\nabla \cdot \mathbf{D}(\mathbf{r},\omega) = \rho_e(\mathbf{r},\omega). \tag{3.14}$$

The position and frequency dependenties will be assumed through out the rest of this report unless indicated otherwise.

3.2 Derivation of Marcuvitz-Swinger equations

For the analysis of the problem, as described in Sec.1, we will use the Marcuvitz-Swinger equations as basis. In this section a derivation of these equations is given. A reason for using these equations is that they give a description of the transverse field quantities which is convenient in our cases, when we arrive at the analysis of the transverse discontinuities. Also the equations can be transformed into equivalent transmission-line equations which can be handled without much difficulty.

For the derivation we will refer to the waveguide depicted in Fig.(3.1). The guide

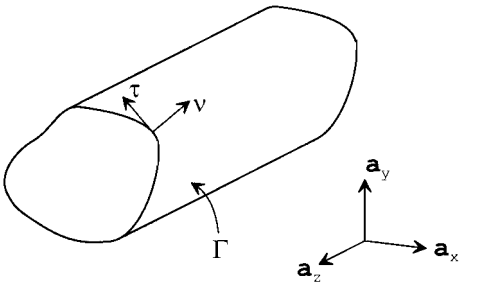

Figure 3.1: *A section of an infinite waveguide with arbitrary cross-section*

extends form $-\infty$ to $+\infty$ along the spatial z-axis and has an arbitrary, but uniform along the z-axis, cross-section. Γ indicates the waveguide wall, $\boldsymbol{\tau}$ is the unity vector tangential to the contour of a cross-section and $\boldsymbol{\nu}$ is the unity vector normal the contour of a cross-section in the plane of that cross-section. Furthermore the assumptions made in Sec.2.2 are applied.

The following can also be obtained form [11],[16]. To derive the Marcuvitz-Swinger from Maxwell's equations we have to eliminate the longitudinal field components from Maxwell's equations, Eq.(3.11)-(3.12). This can be realized by decomposing the vectors and operators into their transverse and longitudinal parts, i.e.

$$\begin{aligned} \mathbf{E} &= \mathbf{E}_t + E_z\mathbf{a}_z, & \mathbf{H} &= \mathbf{H}_t + H_z\mathbf{a}_z, \\ \mathbf{J} &= \mathbf{J}_t + J_z\mathbf{a}_z, & \mathbf{M} &= \mathbf{M}_t + M_z\mathbf{a}_z, \\ \mathbf{r} &= \boldsymbol{\rho} + z\mathbf{a}_z, & \nabla &= \nabla_t + \mathbf{a}_z\frac{\partial}{\partial z}. \end{aligned} \tag{3.15}$$

Next, we apply this decomposition to Maxwell's equations in Eq.(3.11),

$$(\nabla_t + \mathbf{a}_z\frac{\partial}{\partial z}) \times (\mathbf{E}_t + E_z\mathbf{a}_z) = -j\omega\mu(\mathbf{H}_t + H_z\mathbf{a}_z) - (\mathbf{M}_t + M_z\mathbf{a}_z), \tag{3.16}$$

which leads to

$$\nabla_t \times \mathbf{E}_t + \nabla_t \times (E_z\mathbf{a}_z) + \mathbf{a}_z\frac{\partial}{\partial z} \times \mathbf{E}_t + \mathbf{a}_z\frac{\partial}{\partial z} \times (E_z\mathbf{a}_z) + j\omega\mu\mathbf{H}_t + j\omega\mu H_z\mathbf{a}_z = -\mathbf{M}_t - M_z\mathbf{a}_z$$

$$\nabla_t \times \mathbf{E}_t + \nabla_t \times (E_z\mathbf{a}_z) + \mathbf{a}_z \times \frac{\partial\mathbf{E}_t}{\partial z} + \mathbf{a}_z \times \frac{\partial E_z}{\partial z}\mathbf{a}_z + j\omega\mu\mathbf{H}_t + j\omega\mu H_z\mathbf{a}_z = -\mathbf{M}_t - M_z\mathbf{a}_z$$

(3.17)

Equation (3.17) consists of several transverse en longitudinal terms. We will examine term by term and determine of what kind it is. Before we do this we can apply two more simplifications viz.

$$\mathbf{a}_z \times \frac{\partial E_z}{\partial z}\mathbf{a}_z = 0, \tag{3.18}$$

this is trivial, because the cross-product of two vectors lying parallel to each other is zero. The second simplification, involves the term

$$\nabla_t \times (E_z \mathbf{a}_z), \tag{3.19}$$

which can be rewritten with the aid of the following vector identity,

$$\nabla \times (\alpha \mathbf{A}) = \nabla\alpha \times \mathbf{A} + \alpha(\nabla \times \mathbf{A}), \tag{3.20}$$

to

$$\nabla_t \times (E_z \mathbf{a}_z) = \nabla_t E_z \times \mathbf{a}_z + \underbrace{E_z \nabla_t \times \mathbf{a}_z}_{\mathbf{0}}, \tag{3.21}$$

and eventually

$$\nabla_t \times (E_z \mathbf{a}_z) = \nabla_t E_z \times \mathbf{a}_z. \tag{3.22}$$

The fact that the second term on the right-hand side in Eq.(3.21), is equal to zero needs no proof, just write it out. Carry through Eq.(3.18) and Eq.(3.22), Eq.(3.17) can be rewritten according to

$$\nabla_t \times \mathbf{E}_t + \nabla_t E_z \times \mathbf{a}_z + \mathbf{a}_z \times \frac{\partial \mathbf{E}_t}{\partial z} + j\omega\mu\mathbf{H}_t + j\omega\mu H_z \mathbf{a}_z = -\mathbf{M}_t - M_z \mathbf{a}_z. \tag{3.23}$$

Equation (3.23) still contains transverse as well as longitude terms, viz.,

- $\nabla_t \times \mathbf{E}_t$ is a longitudinal term; because it is the cross product of a transverse operator and a transverse vector.
- $\nabla_t E_z \times \mathbf{a}_z$ is a transverse term; because it is the cross product of, the gradient of the z-component of the E-field which gives, a transverse vector and a longitudinal vector.
- $\mathbf{a}_z \times \frac{\partial \mathbf{E}_t}{\partial z}$ is a transverse term; because it is a cross product of a longitudinal vector with a transverse vector.

The remaining terms of Eq.(3.23) do not need further explanation.

At this point we still don't have the kind of equations we can use for the rest of the analysis. Separation of the transverse terms and the longitudinal terms is the following step. First we will split off the transverse terms, as follows

$$\mathbf{a}_z \times (\nabla_t \times \mathbf{E}_t + \nabla_t E_z \times \mathbf{a}_z + \mathbf{a}_z \times \frac{\partial \mathbf{E}_t}{\partial z} + j\omega\mu \mathbf{H}_t + j\omega\mu H_z \mathbf{a}_z) = \mathbf{a}_z \times (-\mathbf{M}_t - M_z \mathbf{a}_z). \quad (3.24)$$

What happend is, we applied the operator $\mathbf{a}_z \times$ to the left of Eq.(3.23). Now, with the aid of the following vector identity,

$$\mathbf{A} \times (\mathbf{B} \times \mathbf{C}) = \mathbf{B}(\mathbf{A} \cdot \mathbf{C}) - \mathbf{C}(\mathbf{A} \cdot \mathbf{B}), \quad (3.25)$$

applied to Eq.(3.24) and some simple mathematical rearrangements we get,

$$-\frac{\partial \mathbf{E}_t}{\partial z} = j\omega\mu \mathbf{H}_t \times \mathbf{a}_z - \nabla_t E_z + \mathbf{M}_t \times \mathbf{a}_z, \quad (3.26)$$

Now that we have an expression for the transverse electric field, by invoking the principle of duality[1] we get an expression for the transverse magnetic field at once viz.,

$$-\frac{\partial \mathbf{H}_t}{\partial z} = j\omega\varepsilon_c \mathbf{a}_z \times \mathbf{E}_t - \nabla_t H_z + \mathbf{a}_z \times \mathbf{J}_t. \quad (3.27)$$

Subsequently we can split off the longitudinal terms by applying the operator, $\vec{a}_z \cdot$, in a same manner as in Eq.(3.24),

$$\mathbf{a}_z \cdot (\nabla_t \times \mathbf{E}_t + \nabla_t E_z \times \mathbf{a}_z + \mathbf{a}_z \times \frac{\partial \mathbf{E}_t}{\partial z} + j\omega\mu \mathbf{H}_t + j\omega\mu H_z \mathbf{a}_z) = \mathbf{a}_z \cdot (-\mathbf{M}_t - M_z \mathbf{a}_z). \quad (3.28)$$

Again, as we did previously by splitting off the transverse part, we apply the vector identity,

$$\mathbf{A} \cdot (\mathbf{B} \times \mathbf{C}) = \mathbf{B} \cdot (\mathbf{C} \times \mathbf{A}) = \mathbf{C} \cdot (\mathbf{A} \times \mathbf{B}), \quad (3.29)$$

and with some mathematical rearrangements we arrive at,

$$j\omega\mu H_z = \nabla_t \cdot (\mathbf{a}_z \times \mathbf{E}_t) - M_z, \quad (3.30)$$

and application of the duality principle yields

$$j\omega\varepsilon_c E_z = \nabla_t \cdot (\mathbf{H}_t \times \mathbf{a}_z) - J_z. \quad (3.31)$$

Summarizing, we have obtained the transverse parts of Eq.(3.11) and Eq.(3.12) written in Eq.(3.32) and Eq.(3.33), respectively

$$-\frac{\partial \mathbf{E}_t}{\partial z} = j\omega\mu \mathbf{H}_t \times \mathbf{a}_z - \nabla_t E_z + \mathbf{M}_t \times \mathbf{a}_z, \quad (3.32)$$

$$-\frac{\partial \mathbf{H}_t}{\partial z} = j\omega\varepsilon_c \mathbf{a}_z \times \mathbf{E}_t - \nabla_t H_z + \mathbf{a}_z \times \mathbf{J}_t. \quad (3.33)$$

[1] $\{\mathbf{E}, \mathbf{H}, \varepsilon, \mu, \mathbf{J}, \mathbf{M}\} \longleftrightarrow \{\mathbf{H}, \mathbf{E}, -\mu, -\varepsilon, -\mathbf{M}, -\mathbf{J}\}$

The longitudinal parts of Eq.(3.11) and Eq.(3.12) written in Eq.(3.34) and Eq.(3.35), respectively

$$j\omega\mu H_z = \nabla_t \cdot (\mathbf{a}_z \times \mathbf{E}_t) - M_z, \tag{3.34}$$

$$j\omega\varepsilon_c E_z = \nabla_t \cdot (\mathbf{H}_t \times \mathbf{a}_z) - J_z. \tag{3.35}$$

Observe that equations (3.32)-(3.35) still contain transverse as well as longitudinal field components. To get equations that only contain transverse field components, we apply the transverse gradient to Eq.(3.34) and Eq.(3.35),

$$\nabla_t H_z = \frac{1}{j\omega\mu}\nabla_t\nabla_t \cdot (\mathbf{a}_z \times \mathbf{E}_t) - \frac{1}{j\omega\mu}\nabla_t M_z, \tag{3.36}$$

$$\nabla_t E_z = \frac{1}{j\omega\varepsilon_c}\nabla_t\nabla_t \cdot (\mathbf{H}_t \times \mathbf{a}_z) - \frac{1}{j\omega\varepsilon_c}\nabla_t J_z, \tag{3.37}$$

and substitute them into Eq.(3.32) and Eq.(3.33) respectively, which results in:

$$-\frac{\partial \mathbf{E}_t}{\partial z} = j\omega\mu\mathbf{H}_t \times \mathbf{a}_z - \frac{1}{j\omega\varepsilon_c}\nabla_t\nabla_t \cdot (\mathbf{H}_t \times \mathbf{a}_z) + \frac{1}{j\omega\varepsilon_c}\nabla_t J_z + \mathbf{M}_t \times \mathbf{a}_z, \tag{3.38}$$

$$-\frac{\partial \mathbf{H}_t}{\partial z} = j\omega\varepsilon_c \mathbf{a}_z \times \mathbf{E}_t - \frac{1}{j\omega\mu}\nabla_t\nabla_t \cdot (\mathbf{a}_z \times \mathbf{E}_t) + \frac{1}{j\omega\mu}\nabla_t M_z + \mathbf{a}_z \times \mathbf{J}_t. \tag{3.39}$$

The identity $\nabla_t\nabla_t\cdot$ is a dyad of the form

$$\nabla_t\nabla_t\cdot = \begin{pmatrix} \partial_x^2 & \partial_x\partial_y \\ \partial_y\partial_x & \partial_y^2 \end{pmatrix}. \tag{3.40}$$

Hence, if we want to further simplify, by taking the terms $\mathbf{H}_t \times \mathbf{a}_z$ and $\mathbf{a}_z \times \mathbf{E}_t$ out of the first and second righthand side terms of Eq.(3.38) and Eq.(3.39), respectively, we have to multiply the first term on the righthand side, in former equations, with the "transverse" identity dyad

$$\underline{\underline{I}}_t = (\mathbf{a}_x\,\mathbf{a}_x + \mathbf{a}_y\,\mathbf{a}_y) = \begin{pmatrix} 1 & 0 \\ 0 & 1 \end{pmatrix}. \tag{3.41}$$

We can now cast the Marcuvitz-Swinger equations in the following form,

$$-\frac{\partial}{\partial z}\begin{pmatrix} \mathbf{E}_t(\boldsymbol{\rho}, z) \\ \mathbf{H}_t(\boldsymbol{\rho}, z) \end{pmatrix} = \begin{pmatrix} j\omega\mu\underline{\underline{\mathcal{L}}} & \mathcal{O} \\ \mathcal{O} & j\omega\varepsilon_c\underline{\underline{\mathcal{L}}} \end{pmatrix}\begin{pmatrix} \mathbf{H}_t(\boldsymbol{\rho}, z) \times \mathbf{a}_z \\ \mathbf{a}_z \times \mathbf{E}_t(\boldsymbol{\rho}, z) \end{pmatrix} + \begin{pmatrix} \mathbf{M}_t^{eq}(\boldsymbol{\rho}, z) \times \mathbf{a}_z \\ \mathbf{a}_z \times \mathbf{J}_t^{eq}(\boldsymbol{\rho}, z) \end{pmatrix}, \tag{3.42}$$

where the operator, $\underline{\underline{\mathcal{L}}}$, is meant symbolically and represents

$$\underline{\underline{\mathcal{L}}} = (\underline{\underline{I}}_t + \frac{1}{k^2}\nabla_t\nabla_t\cdot), \tag{3.43}$$

in which $k = \omega\sqrt{\mu\varepsilon_c}$ is the complex propagation constant. This is due to the fact that the applied dielectric filling of the waveguide is not necessarily lossless and that reveals itself

in the complex epsilon, ε_c. In Eq.(3.42) the equivalent transverse magnetic and electric current distributions are given by

$$\mathbf{M}_t^{eq} = \mathbf{M}_t - \frac{1}{j\omega\varepsilon_c}\nabla_t \times (J_z \mathbf{a}_z) \tag{3.44}$$

$$\mathbf{J}_t^{eq} = \mathbf{J}_t + \frac{1}{j\omega\mu}\nabla_t \times (M_z \mathbf{a}_z) \tag{3.45}$$

which are derived by applying the vector identities in equations (3.20) and (3.25) to the third term in the right-hand side of Eq.(3.38) and Eq.(3.39). We will give a short derivation. Let us start with the third term of Eq.(3.38). If we apply the operator, $\times\mathbf{a}_z$, with it two times and make use of (3.39) we obtain

$$\begin{aligned}(\nabla_t J_z \times \mathbf{a}_z) \times \mathbf{a}_z &= -[\nabla_t J_z(\mathbf{a}_z \cdot \mathbf{a}_z) - \mathbf{a}_z(\mathbf{a}_z \cdot \nabla_t J_z)], \\ &= -\nabla_t J_z.\end{aligned}$$

Apart of a minus sign, it is the same as the third term. Next, apply the other vector identity to the term on the left-hand side between brackets, of the previous equation, transfer the minus-sign of the right-hand side term to the left-hand side term and discard the cross-product with $\mathbf{a}_z$ for a moment. As a result we get,

$$\begin{aligned}-(\nabla_t J_z \times \mathbf{a}_z) &= -\nabla_t \times (J_z \mathbf{a}_z) + J_z(\nabla_t \times \mathbf{a}_z), \\ &= -\nabla_t \times (J_z \mathbf{a}_z).\end{aligned}$$

Once we have obtained this result, Eq.(3.44) can be readily identified. The same successive manipulations can be used to arrive at Eq.(3.45), with one difference viz. we start form $(\mathbf{a}_z \times \nabla_t M_z) \times \mathbf{a}_z$ instead of $(\nabla_t J_z \times \mathbf{a}_z) \times \mathbf{a}_z$.

As we can see in Eq.(3.42), the Macuvitz-Swinger equations only contain the transverse field quantities and still represent Maxwell's equations only rewritten in a somewhat different form. Where Maxwell's equations form a vectorially coupled system of first-order partial differential equations, we now have a vectorially coupled system of second-order partial differential equations, due to the elimination of a field variable viz. the longitudinal one. At first this may not seem an advantage but later on we will see that these can be transformed in equivalent transmission line equations, as mentioned earlier, which are hopefully easier to handle.

3.2.1 Boundary conditions

In general differential equations are not uniquely solvable without knowing something more about the specific problem we are dealing with. Solutions of differential equations leave us always with undetermined constants, or even with higher order terms. Since these constants and/or terms can take on a variety of values, creating infinitely many possible solutions. So, what we have to do is to find out what specific conditions apply to the problem, the so-called boundary conditions. Through the introduction of boundary conditions the

differential equations become completely solvable.
As mentioned before, we assume a waveguide along the z-axis from $-\infty$ t0 $+\infty$. The shape of the cross-section is arbitrary but uniform and the walls are made of a Perfect Electrical Conductor (PEC). With this assumption the following condition holds,

$$\mathbf{n} \times \mathbf{E}(\boldsymbol{\rho}, z)^{tot}|_{\rho=\rho_\Gamma} = \mathbf{0}, \tag{3.46}$$

which implies, that the total tangential component of the electric field evaluated on the waveguide wall ($\boldsymbol{\rho}_\Gamma$) must vanish, with $\mathbf{n}$ the unity vector normal to the waveguide wall, lying in the plane of the cross-section and pointing outward, $\mathbf{E}(\boldsymbol{\rho}, z)^{tot}$ the total electric field on the inside of the waveguide and $\boldsymbol{\rho}_\Gamma$ is a position vector describing the contour of the waveguide wall in the transverse plane. The boundary condition in Eq.(3.46) holds for the Marcuvitz-Swinger equations in Eq.(3.42) but is not directly applicable because the Marcuvitz-Swinger only contain transverse field quantities therefore we are going to rewrite it

$$\mathbf{n} \times (\mathbf{E}_t + E_z \mathbf{a}_z)|_{\rho=\rho_\Gamma} = \mathbf{n} \times \mathbf{E}_t|_{\rho=\rho_\Gamma} + \underbrace{\mathbf{n} \times \mathbf{a}_z}_{-\boldsymbol{\tau}} E_z|_{\rho=\rho_\Gamma} = \mathbf{0}. \tag{3.47}$$

In the third term we see $\mathbf{n} \times \mathbf{a}_z$ which is the unity vector, $-\boldsymbol{\tau}$, tangential to the waveguide wall lying in the plane of the cross-section.
The rewritten boundary condition, as can be seen in Eq.(3.47), now consists of two terms. One term contains the transverse electric field and the other term contains the longitudinal electric field, which doesn't appear in the Marcuvitz-Swinger equations. To have boundary conditions completely restated in transverse field quantities, we have to find another expression for the longitudinal electric field term. Now if we look at Eq.(3.35), for convenience stated below again, we see the solution to the problem.

$$j\omega\varepsilon E_z = \nabla_t \cdot (\mathbf{H}_t \times \mathbf{a}_z) - J_z.$$

Upon assuming that J_z becomes zero in the proces of $\lim_{\rho \uparrow \rho_\Gamma}$, we get

$$E_z|_{\rho=\rho_\Gamma} = \nabla_t \cdot (\mathbf{H}_t \times \mathbf{a}_z)|_{\rho=\rho_\Gamma} = 0. \tag{3.48}$$

Finally the transverse boundary conditions are,

$$\mathbf{n} \times \mathbf{E}_t|_{\rho=\rho_\Gamma} = \mathbf{0}, \tag{3.49}$$

$$\nabla_t \cdot (\mathbf{H}_t \times \mathbf{a}_z)|_{\rho=\rho_\Gamma} = 0. \tag{3.50}$$

For a moment we will go back to the assumption that $J_z = 0$ on the waveguide wall. This restriction, which requires the vanishing of the z component of the applied electric current source on the boundary is consistent with the fact that an applied tangential electric current source on a PEC surface is "short-circuit" and as a consequence cannot radiate any electromagnetic energy. In Appendix A this is explained further.

3.3 Equivalent transmission line equations

It has been mentioned earlier, e.g. Sec. 3.2, that the Marcuvitz-Swinger equations can be cast in equivalent transmission-line equations. In this section we would like to emphasize why and how one can come to equivalent transmission-line equations, without directly solving them. To come to these equations we need an expression for the transverse field components. For this, we will start from [11]. In [11, Sec. 8.1] it is discussed that for a guided wave description of a homogeneous lineair field, thus EM-waves propagating along the spatial z-axis described by Maxwell's equations, the total electromagnetic field can be represented as a superposition of eigenmodes or also called characteristic guided waves of the form $\boldsymbol{\Psi}_\alpha(\boldsymbol{\rho},t)e^{-jk_{z;\alpha}z}$ in which z is the symmetry axis along which guiding takes place, $k_{z;\alpha}$ is the eigenvalue of the α-th mode, $\boldsymbol{\Psi}_\alpha(\boldsymbol{\rho},t)$ is a eigenvector function depending on the transverse position vector $\boldsymbol{\rho}$ and time t. Explicitly, the representation of the total field takes the form,

$$\boldsymbol{\Psi}(\mathbf{r},t) = \sum_\alpha a_\alpha(0)\,\boldsymbol{\Psi}_\alpha(\boldsymbol{\rho},t)\,e^{-jk_{z;\alpha}z} = \sum_\alpha a_\alpha(z)\,\boldsymbol{\Psi}_\alpha(\boldsymbol{\rho},t) \tag{3.51}$$

for source free points. Here, $\boldsymbol{\Psi}(\mathbf{r},t)$ is called a wave function and is an abstract notation for the electromagnetic field quantities,

$$\boldsymbol{\Psi}(\mathbf{r},t) \longrightarrow \left\{ \begin{array}{c} \mathbf{E}(\mathbf{r},t) \\ \mathbf{H}(\mathbf{r},t) \end{array} \right\}$$

The term $a_\alpha(z)$ is defined as the amplitude factor of the α-th mode and takes on the z-dependence. For bounded cross-sections we assume $\boldsymbol{\Psi}_\alpha(\boldsymbol{\rho},t) = \boldsymbol{\Psi}_\alpha(\boldsymbol{\rho})e^{j\omega t}$. The exponential term indicates the time dependence, as stated at the beginning of Sec.3.1 and will be left out. This is described more rigorous in [11, Sec. 1.4]. At the end of this Sec. 1.4 it appears that the field description $\boldsymbol{\Psi}$, is restricted to the transverse field components $\mathbf{E}_t$ and $\mathbf{H}_t$. It turns out, that these are the independent components of the electromagnetic field, in cases of guided waves along the spatial z-axis. It's notation becomes

$$\overline{\boldsymbol{\Psi}}(\mathbf{r}) = \sum_\alpha a_\alpha(z)\,\overline{\boldsymbol{\Psi}}_\alpha(\boldsymbol{\rho}) \qquad\qquad \overline{\boldsymbol{\Psi}}(\mathbf{r}) \longrightarrow \left\{ \begin{array}{c} \mathbf{E}_t(\mathbf{r}) \\ \mathbf{H}_t(\mathbf{r}) \end{array} \right\} \tag{3.52}$$

In [11, Sec. 1.4] eigenvectors are found, and as a result the total wavevector, by making use of Maxwell's equations explicitly. This results in solving a tedious eigenvalue problem. In spite of the fact that this is not the way we are going to follow, it remains true that the electromagnetic field can be represented as a sum of eigenvectors. In Chapter 4 another approach will be discussed.

To be able to resume the derivation of the equivalent transmission line equations we introduce, by analogy of Eq.(3.52), two complete sets of vector functions $\{\mathbf{f}_i^E\}$ and $\{\mathbf{f}_i^H\}$,

which form a basis, by which the transverse electromagnetic field can be expressed as

$$\mathbf{E}_t(\boldsymbol{\rho}, z) = \sum_{i=1}^{\infty} V_i(z)\mathbf{f}_i^E(\boldsymbol{\rho}), \tag{3.53}$$

$$\mathbf{H}_t(\boldsymbol{\rho}, z) = \sum_{i=1}^{\infty} I_i(z)\mathbf{f}_i^H(\boldsymbol{\rho}). \tag{3.54}$$

As we can see, the vector functions represent the transverse dependency and the terms in front, represent the z-dependency and also contain an amplitude coefficient that can become complex. The index i is a multicomponent summation index distinguishing the ith mode or eigenvalue. So what these equations are expressing is that the total transverse field can be thought of as a transversely directed slice for every possible value of z and on such a transversely directed slice the field is exact since it is built up of an infinite sum of eigenvector functions, which form a basis. The solution can be found in the space formed by the eigenvectors.
The expressions in Eq.(3.53) and Eq.(3.54) hold for the problem in our case because the transverse region is bounded. For open guided wave problems the complete spectrum need to be entirely discrete. In open guided wave problems, one or both of the transverse directions is unbounded yielding a continuous spectrum of eigenvalues. In [11, Sec. 3.2], it is shown that only a part of the solutions contain summations supplemented by integrals, meaning that a part of the spectrum has become continuous.

Next, we will insert Eq.(3.53) and Eq.(3.54) into the Marcuvitz-Swinger equations but before that, we make a minor adjustment to Eq.(3.42). On the right-hand site, in the last mentioned equation, we have terms with cross-product of field quantities with z-directed unit vectors. To come to the modified equation, we define two operators $\underline{\underline{\mathcal{D}}}$ and $\underline{\underline{\mathcal{I}}}$ working on vector functions $\mathbf{U}$ and $\mathbf{W}$ who add $\mathbf{U} \times \mathbf{a}_z$ and $\mathbf{a}_z \times \mathbf{W}$ to these vector functions, respectively. Next, we define that $\mathbf{U} = \mathbf{H}_t$ and $\mathbf{W} = \mathbf{E}_t$ giving rise to

$$\underline{\underline{\mathcal{L}}}(\mathbf{H}_t \times \mathbf{a}_z) = \underline{\underline{\mathcal{L}}}\,\underline{\underline{\mathcal{D}}}\,\mathbf{H}_t = \underline{\underline{\mathcal{L}}}^H\,\mathbf{H}_t, \tag{3.55}$$

$$\underline{\underline{\mathcal{L}}}(\mathbf{a}_z \times \mathbf{E}_t) = \underline{\underline{\mathcal{L}}}\,\underline{\underline{\mathcal{I}}}\,\mathbf{E}_t = \underline{\underline{\mathcal{L}}}^E\,\mathbf{E}_t. \tag{3.56}$$

The left-hand sides of Eqs.(3.55) and (3.56) come from Eq.(3.42). The operators $\underline{\underline{\mathcal{L}}}^H$ and $\underline{\underline{\mathcal{L}}}^E$ transform Eq.(3.42) into

$$-\frac{\partial}{\partial_z}\begin{pmatrix}\mathbf{E}_t(\boldsymbol{\rho}, z)\\ \mathbf{H}_t(\boldsymbol{\rho}, z)\end{pmatrix} = \begin{pmatrix}j\omega\mu\underline{\underline{\mathcal{L}}}^H & \mathcal{O}\\ \mathcal{O} & j\omega\epsilon\underline{\underline{\mathcal{L}}}^E\end{pmatrix}\begin{pmatrix}\mathbf{H}_t(\boldsymbol{\rho}, z)\\ \mathbf{E}_t(\boldsymbol{\rho}, z)\end{pmatrix} + \begin{pmatrix}\mathbf{M}_t^{eq}(\boldsymbol{\rho}, z) \times \mathbf{a}_z\\ \mathbf{a}_z \times \mathbf{J}_t^{eq}(\boldsymbol{\rho}, z)\end{pmatrix}. \tag{3.57}$$

With Eq.(3.53) and Eq.(3.54) substituted into Eq.(3.57) we get

$$-\sum_{i=1}^{\infty}\frac{dV_i(z)}{dz}\,\mathbf{f}_i^E(\boldsymbol{\rho}) = j\omega\mu\sum_{i=1}^{\infty} I_i(z)\,\underline{\underline{\mathcal{L}}}^H\,\mathbf{f}_i^H(\boldsymbol{\rho}) + (\mathbf{M}_t^{eq}(\boldsymbol{\rho}, z) \times \mathbf{a}_z), \tag{3.58}$$

$$-\sum_{i=1}^{\infty}\frac{dI_i(z)}{dz}\,\mathbf{f}_i^H(\boldsymbol{\rho}) = j\omega\varepsilon\sum_{i=1}^{\infty} V_i(z)\,\underline{\underline{\mathcal{L}}}^E\,\mathbf{f}_i^E(\boldsymbol{\rho}) + (\mathbf{a}_z \times \mathbf{J}_t^{eq}(\boldsymbol{\rho}, z)). \tag{3.59}$$

Subsequently we take the inner product of Eq.(3.58) with $\mathbf{f}_j^E(\boldsymbol{\rho})$ $(j = 1, 2, ...)$ and the inner product of Eq.(3.59) with $\mathbf{f}_j^H(\boldsymbol{\rho})$ hereby introducing an inner product of two vector function as

$$\langle \mathbf{f}, \mathbf{g} \rangle = \int_S \mathbf{f} \cdot \mathbf{g}^* \, dS \tag{3.60}$$

which leads to

$$-\sum_{i=1}^{\infty} \frac{dV_i(z)}{dz} \langle \mathbf{f}_i^E, \mathbf{f}_j^E \rangle = j\omega\mu \sum_{i=1}^{\infty} I_i(z) \langle \underline{\underline{\mathcal{L}}}^H \mathbf{f}_i^H, \mathbf{f}_j^E \rangle + \langle (\mathbf{M}_t^{eq} \times \mathbf{a}_z), \mathbf{f}_j^E \rangle, \tag{3.61}$$

$$-\sum_{i=1}^{\infty} \frac{dI_i(z)}{dz} \langle \mathbf{f}_i^H, \mathbf{f}_j^H \rangle = j\omega\varepsilon \sum_{i=1}^{\infty} V_i(z) \langle \underline{\underline{\mathcal{L}}}^E \mathbf{f}_i^E, \mathbf{f}_j^H \rangle + \langle (\mathbf{a}_z \times \mathbf{J}_t^{eq}), \mathbf{f}_j^H \rangle. \tag{3.62}$$

where only the significant spatial coordinate variables are shown. These equations can be rewritten more clearly in a matrix-vector notation

$$-\underline{\underline{N}}^E \cdot \frac{d\mathbf{V}}{dz} = j\omega\mu \underline{\underline{L}}^H \cdot \mathbf{I} + \mathbf{v}, \tag{3.63}$$

$$-\underline{\underline{N}}^H \cdot \frac{d\mathbf{I}}{dz} = j\omega\varepsilon \underline{\underline{L}}^E \cdot \mathbf{V} + \mathbf{i}. \tag{3.64}$$

We assume that it is evident that $\mathbf{V}$ and $\mathbf{I}$ are column vectors of dimensions $(n \times 1)$ and $\underline{\underline{N}}^E$, $\underline{\underline{N}}^H$, $\underline{\underline{L}}^E$ and $\underline{\underline{L}}^H$ are matrices of dimensions $(n \times n)$ with $n = \infty$.

These last equations, Eq.(3.63) and Eq.(3.64), tell us that by choosing, or even better, by constructing a suitable vectorial basis we can have influence on the type of matrices we get, determined by the inner products of the vector functions. If we can construct a orthonormal basis which obeys the boundary conditions we will get diagonal matrices implying, a separate system of equivalent transmission-line equations for every mode. From this system of first order coupled differential equations the coefficients V_i and I_i can be solved. Together with the constructed vectorial basis the total transverse fields are formed, Eqs.(3.53)-(3.54). In this way we have an efficient analysis tool to tackle waveguide problems and especially discontinuities in the transverse plane of which we have quite a few.

In theory, the infinite sum in Eqs.(3.53)-(3.54) can be handled and will lead to an exact solution but in practice this sum has to be truncated because of the reason that our computer is finite. A satisfactory answer, good approximation, can still be reached by taking into account sufficient coefficients.

Chapter 4

Waveguide mode functions; Construction of basis

In the preceding chapter we have shown how we end up with an analysis tool for guided waves along a spatial axis, for instance the z-axis, starting from Maxwell's equations. A important point in here is the construction of a suitable vectorial basis in which the solution of the transverse electromagnetic field can be constructed. In this chapter we are going to construct a suitable basis. A brief preview of what is coming ahead. Point of departure are the source free counterparts of the Marcuvitz-Swinger equations from which we find equations for the $\boldsymbol{\rho}$-depended parts of the transverse fields, the mode functions $\mathbf{e}$ and $\mathbf{h}$, expressed as a function of the $\boldsymbol{\rho}$-depended longitudinal field constituents e_z and h_z. Therefore we will make use, among other things, of the characteristic wave solution. This line of approach results in a rather simple problem for the $\boldsymbol{\rho}$-depended longitudinal field constituents, e_z and h_z to solve, viz. scalar Helmholtz equations. As it will turn out, the mentioned field constituents possess orthogonality properties and with the help of scalar functions, normalisation can be achieved, which yields an suitable orthonormal basis.

4.1 Waveguide mode functions

On the basis of what has been written in Sec. 3.3 and on what is physically acceptable, when looking to a waveguide lying along the z-axis, Fig.(3.1), the characteristic guided waves will be sought in the following general form,

$$\boldsymbol{\Psi}(\mathbf{r}) = \boldsymbol{\Psi}(\boldsymbol{\rho})e^{-jk_z z}, \tag{4.1}$$

again assuming $e^{j\omega t}$ for the time dependency.
The variable $\boldsymbol{\Psi}$ refers to the vectorial field quantities $\mathbf{E}(\mathbf{r})$ as well as $\mathbf{H}(\mathbf{r})$

$$\boldsymbol{\Psi}(\mathbf{r}) \longrightarrow \left\{ \begin{array}{c} \mathbf{E}(\mathbf{r}) \\ \mathbf{H}(\mathbf{r}) \end{array} \right\} \tag{4.2}$$

Writing the field quantities explicitly in this general form

$$\mathbf{E}(\mathbf{r}) = \mathbf{E}(\boldsymbol{\rho})e^{-jk_z z}, \tag{4.3}$$

$$\mathbf{H}(\mathbf{r}) = \mathbf{H}(\boldsymbol{\rho})e^{-jk_z z}, \tag{4.4}$$

gives us a basic approach to find a solution for the waveguide mode functions.

Finding the waveguide mode functions comes down to solving an eigenvalue problem, because waveguide mode functions are eigenfunction solutions to source-free differential equations applied with appropriate boundary conditions. If Maxwell's equations are applied to the characteristic solution form of Eqs.(4.3) and (4.4) we end up with a tedious differential eigenvalue problem, see e.g. [11, Sec.1.4 and Sec.8.2]. There is a method to circumvent this, which comes down to expressing the $\boldsymbol{\rho}$-depended transverse field in the $\boldsymbol{\rho}$-depended longitudinal field, as done in e.g. [8], [16], [19]. As a consequence we will end up with a scalar eigenvalue problem.

For this, we start by separating the fields in Eq.(4.3) and Eq.(4.4) in its transverse

$$\mathbf{E}_t(\boldsymbol{\rho}, z) = A^E\, \mathbf{e}(\boldsymbol{\rho})\, e^{-jk_z z}, \tag{4.5}$$

$$\mathbf{H}_t(\boldsymbol{\rho}, z) = A^H\, \mathbf{h}(\boldsymbol{\rho})\, e^{-jk_z z}, \tag{4.6}$$

and longitudinal parts

$$E_z(\boldsymbol{\rho}, z) = A^E\, e_z(\boldsymbol{\rho})\, e^{-jk_z z}, \tag{4.7}$$

$$H_z(\boldsymbol{\rho}, z) = A^H\, h_z(\boldsymbol{\rho})\, e^{-jk_z z}. \tag{4.8}$$

Herein, A^E and A^H represent amplitude coefficients that might become complex, $\mathbf{e}(\boldsymbol{\rho})$ and $\mathbf{h}(\boldsymbol{\rho})$ are the waveguide mode functions or eigenvector functions and k_z is the longitudinal wavenumber. For all clarity we will drop the $\boldsymbol{\rho}$- and z-dependency but they stay valid until noted otherwise.

To find a solution to the above postulated method we make use of the source-free counter parts of Eqs.(3.32)-(3.33), stated below for clarity,

$$-\frac{\partial \mathbf{E}_t}{\partial z} = j\omega\mu \mathbf{H}_t \times \mathbf{a}_z - \nabla_t E_z, \tag{4.9}$$

$$-\frac{\partial \mathbf{H}_t}{\partial z} = j\omega\varepsilon_c \mathbf{a}_z \times \mathbf{E}_t - \nabla_t H_z, \tag{4.10}$$

and substitute Eqs.(4.5)-(4.8), which lead to

$$-A^E\, \mathbf{e}\, \frac{\partial}{\partial z}(e^{-jk_z z}) = j\omega\mu A^H[\mathbf{h} \times \mathbf{a}_z]e^{-jk_z z} - A^E\, \nabla_t e_z\, e^{-jk_z z}, \tag{4.11}$$

$$-A^H\, \mathbf{h}\, \frac{\partial}{\partial z}(e^{-jk_z z}) = j\omega\varepsilon_c A^E[\mathbf{a}_z \times \mathbf{e}]e^{-jk_z z} - A^H\, \nabla_t h_z\, e^{-jk_z z}, \tag{4.12}$$

and eventually

$$\mathbf{e} = \frac{\omega\mu}{k_z}\frac{A^H}{A^E}[\mathbf{h} \times \mathbf{a}_z] - \frac{1}{jk_z}\nabla_t e_z, \tag{4.13}$$

$$\mathbf{h} = \frac{\omega\varepsilon_c}{k_z}\frac{A^E}{A^H}[\mathbf{a}_z \times \mathbf{e}] - \frac{1}{jk_z}\nabla_t h_z. \tag{4.14}$$

We see that the source-free counter parts of the Marcuvitz-Swinger equations are no longer of the partial differential kind but are now transformed to two equations who are lineair depended and if we look closely, we can eliminate the mutual dependency and completely express the mode functions in the $\boldsymbol{\rho}$-depended parts of the longitudinal fields, by taking the cross-product of $\mathbf{a}_z$ with Eq.(4.13), thus $\mathbf{a}_z\times$ on the left side, and taking the cross-product of Eq.(4.14) with $\mathbf{a}_z$, thus $\times\mathbf{a}_z$ on the right side. After this we substitute the modified equations in one another and this gives rise to

$$\mathbf{e}(\boldsymbol{\rho}) = -j\,\frac{\omega\mu}{k_t^2}\frac{A^H}{A^E}\left(\nabla_t h_z(\boldsymbol{\rho})\times\mathbf{a}_z\right) - j\,\frac{k_z}{k_t^2}\,\nabla_t e_z(\boldsymbol{\rho}), \tag{4.15}$$

and in a analogue way we get

$$\mathbf{h}(\boldsymbol{\rho}) = -j\,\frac{\omega\varepsilon_c}{k_t^2}\frac{A^E}{A^H}\left(\mathbf{a}_z\times\nabla_t e_z(\boldsymbol{\rho})\right) - j\,\frac{k_z}{k_t^2}\,\nabla_t h_z(\boldsymbol{\rho}). \tag{4.16}$$

In this derivation we made use of

$$k_t^2 = \omega^2\varepsilon_c\mu - k_z^2 = k^2 - k_z^2, \tag{4.17}$$

which is the transverse wavenumber.

As we can see in Eqs.(4.15)-(4.16) and as was mentioned before, the $\boldsymbol{\rho}$-depended transverse field quantities are completely expressed in, and depended on the longitudinal field quantities.

What we must do now, is constructing an expression for longitudinal field quantities $e_z(\boldsymbol{\rho})$ and $h_z(\boldsymbol{\rho})$.

4.2 Longitudinal field

In this section we will try to find an appropriate expression for the longitudinal field terms $e_z(\boldsymbol{\rho})$ and $h_z(\boldsymbol{\rho})$. In the preceding section we used the source free counterparts of the Marcuvitz-Swinger equations stated, in Eqs.(3.32)-(3.33), to find equations for the waveguide mode functions. We can use the same approach to find a solution to the current problem. Therefore, we use the source free counterparts of Eqs.(3.34)-(3.35), for convenience stated below again,

$$j\omega\varepsilon_c E_z = \nabla_t\cdot(\mathbf{H}_t\times\mathbf{a}_z), \tag{4.18}$$

$$j\omega\mu H_z = \nabla_t\cdot(\mathbf{a}_z\times\mathbf{E}_t). \tag{4.19}$$

Subsequently, we substitute Eqs.(4.5)-(4.8) into Eq.(4.18) and Eq.(4.19) and end up with

$$j\omega\varepsilon_c A^E\, e_z = A^H\,\nabla_t\cdot(\mathbf{h}\times\mathbf{a}_z), \tag{4.20}$$

$$j\omega\mu A^H\, h_z = A^E\,\nabla_t\cdot(\mathbf{a}_z\times\mathbf{e}). \tag{4.21}$$

In the above equations, the transverse field quantities $\mathbf{e}$ and $\mathbf{h}$ can be replaced by the in Eq.(4.15) and (4.16) found expressions, respectively, yielding

$$j\omega\varepsilon_c A^E e_z = -j\frac{\omega\varepsilon_c}{k_t^2}\frac{A^E A^H}{A^H}\nabla_t\cdot((\mathbf{a}_z\times\nabla_t e_z)\times\mathbf{a}_z) - j\frac{k_z}{k_t^2}\nabla_t\cdot(\nabla_t h_z\times\mathbf{a}_z). \tag{4.22}$$

(4.23)

Now, we apply Eq.(3.25) to the first term on the right-hand and the vector identity in Eq.(4.24) to the second term on the right-hand side

$$\nabla\cdot(\mathbf{A}\times\mathbf{B}) = \mathbf{B}\cdot(\nabla\times\mathbf{A}) - \mathbf{A}\cdot(\nabla\times\mathbf{B}), \tag{4.24}$$

yielding

$$(\nabla_t^2 + k_t^2)e_z(\boldsymbol{\rho}) = 0, \tag{4.25}$$

which is a Helmholtz equation. For Eq.(4.21) we get the same equation, of course now for h_z, by a similar derivation.

$$(\nabla_t^2 + k_t^2)h_z(\boldsymbol{\rho}) = 0, \tag{4.26}$$

This scalar eigenvalue problem is easier to handle than the vectorial eigenvalue problem as mentioned briefly in Sec.(3.3).

To make the solution to these differential equations unique, these equations must be accompanied by appropriate boundary conditions. In section 3.2.1 we stated one, viz. $\boldsymbol{\nu}\times\mathbf{E}^{tot}|_{\boldsymbol{\rho}=\boldsymbol{\rho}_\Gamma} = \mathbf{0}$, as a result of the fact that we assumed a waveguide with PEC walls. This condition eventually got into the form of Eq.(3.48) and Eq.(3.49), and with help of Eq.(4.5) and Eq.(4.7) we get

$$\boldsymbol{\nu}\times\mathbf{e}|_{\boldsymbol{\rho}=\boldsymbol{\rho}_\Gamma} = \mathbf{0}, \tag{4.27}$$

$$e_z|_{\boldsymbol{\rho}=\boldsymbol{\rho}_\Gamma} = 0. \tag{4.28}$$

We note that Eq.(4.28) is directly applicable to Eq.(4.25). Because we are looking for boundary conditions, which are valid for longitudinal field quantities, equation Eq.(4.27), containing a transverse field quantity, has to be modified. This, can be resolved by invoking Eq.(4.15),

$$\boldsymbol{\nu}\times\mathbf{e} = -j\frac{\omega\mu}{k_t^2}\frac{A^H}{A^E}\boldsymbol{\nu}\times(\nabla_t h_z\times\mathbf{a}_z) - j\frac{k_z}{k_t^2}\boldsymbol{\nu}\times\nabla_t e_z. \tag{4.29}$$

With the help of Eq.(3.25) and the fact that $\boldsymbol{\nu} = \boldsymbol{\tau}\times\mathbf{a}_z$, the cross-products on the right-hand side are converted into

$$\boldsymbol{\nu}\times(\nabla_t h_z\times\mathbf{a}_z) = \nabla_t h_z\,(\boldsymbol{\nu}\cdot\mathbf{a}_z) - \mathbf{a}_z(\boldsymbol{\nu}\cdot\nabla_t h_z) = -\mathbf{a}_z\frac{\partial h_z}{\partial\nu}, \tag{4.30}$$

$$\boldsymbol{\nu}\times\nabla_t e_z = (\boldsymbol{\tau}\times\mathbf{a}_z)\times\nabla_t e_z = -[\boldsymbol{\tau}(\nabla_t e_z\cdot\mathbf{a}_z) - \mathbf{a}_z(\nabla_t e_z\cdot\boldsymbol{\tau})] = \mathbf{a}_z\frac{\partial e_z}{\partial\tau}, \tag{4.31}$$

which are the directional derivatives to, respectively, the normal and the tangent of the waveguide wall. Next we evaluate Eq.(4.29) with the directional derivatives substituted, on the waveguide wall $\boldsymbol{\rho} = \boldsymbol{\rho}_\Gamma$,

$$\boldsymbol{\nu} \times \mathbf{e}\,|_{\rho=\rho_\Gamma} = \mathbf{0} = -\omega\mu\frac{A^H}{A^E}\frac{\partial h_z}{\partial \nu}\,\mathbf{a}_z|_{\rho=\rho_\Gamma} + k_z\frac{\partial e_z}{\partial \tau}\,\mathbf{a}_z|_{\rho=\rho_\Gamma} = \frac{\partial h_z}{\partial \nu}\,\mathbf{a}_z|_{\rho=\rho_\Gamma}. \tag{4.32}$$

The term with e_z vanishes in view of Eq.(4.28). Furthermore, the above equation tells us that the longitudinal constituent of the magnetic field (tangential magnetic field) on the waveguide wall must be constant and at the same time provides us with a boundary condition for Eq.(4.26).

So, up till now we have found the following expressions for the longitudinal constituents of the electromagnetic field,

$$(\nabla_t^2 + k_t^2)e_z = 0, \qquad e_z|_{\rho=\rho_\Gamma} = 0, \tag{4.33}$$

$$(\nabla_t^2 + k_t^2)h_z = 0, \qquad \frac{\partial h_z}{\partial \nu}|_{\rho=\rho_\Gamma} = 0. \tag{4.34}$$

On the previous page we show the same kind of equation for the longitudinal constituent of the electric as well as for the longitudinal constituent of the magnetic field, but the problem that they eventually describe is completely different, which is brought about by the boundary conditions. Because of the boundary conditions, Eq.(4.33) is also called a scalar Dirichlet boundary-value problem and Eq.(4.34) is also called a scalar Neumann boundary-value problem.

Now that we have derived a description of the $\boldsymbol{\rho}$-depended longitudinal field components e_z and h_z, as well as the $\boldsymbol{\rho}$-depended transverse field components $\mathbf{e}$ and $\mathbf{h}$, for a waveguide depicted in Fig.(3.1) we can distinguish between 2 mode types out of which the electromagnetic field in the waveguide can be build up. They are,

- TE-modes, transverse electric modes. In this case the longitudinal component $e_z(\boldsymbol{\rho})$ vanishes.
- TM-modes, transverse magnetic modes. In this case the longitudinal component $h_z(\boldsymbol{\rho})$ vanishes.

In [11, Sec.8.2.f], it's proven, under the assumptions of a waveguide with PEC walls and of which the cross-section is filled with a homogeneous dielectric, as we assume, that it is possible to separate the field in TE- and TM-modes.

4.3 Orthogonality and normalisation mode functions

With what is treated up to here, we could just calculate the $\boldsymbol{\rho}$-depended longitudinal field constituents e_z, h_z and with these the mode functions $\mathbf{e}$, $\mathbf{h}$. Subsequently, use these mode functions $\mathbf{e}$ and $\mathbf{h}$) as a basis, to construct a space, of which the solution of the

transverse electromagnetic field may perhaps be an element. But, we still don't have an answer to the question whether the vector mode functions form a suitable basis and a complete set to express the transverse field quantities in. By suitable basis we mean an orthonormal one, if possible, so that later on use can be made of orthogonaliy properties. An orthonormal basis is the most compact description of a vector space. Adding an extra basis vector, of which afterwards appears, that can be constructed out of two or more already existing basis vectors and doesn't give any additional information. An answer to the question could be, checking the vectors for mutual independence or maybe applying some kind of orthogonalisation algorithm. The check for mutual independence is redundant (or superfluous) if orthogonality can be proven first or at the same time, because independency is enclosed by orthogonality. As it will turn out orthogonality holds for both (e_z, h_z) and $(\mathbf{e}, \mathbf{h})$.

By using the mentioned distinction between the mode types we shall look further into the mode functions.

4.3.1 TE modes

In the case of TE modes, which have $e_z = 0$, we have the following set of equations to our disposal,

$$(\nabla_t^2 + k_t''^2)\, h_z = 0, \qquad \frac{\partial h_z}{\partial \nu}|_{\boldsymbol{\rho}=\boldsymbol{\rho}_\Gamma} = 0, \tag{4.35}$$

$$\mathbf{h}'' = -j\,\frac{k_z''}{k_t''^2}\nabla_t h_z, \tag{4.36}$$

$$\mathbf{e}'' = -j\,\frac{\omega\mu}{k_t''^2}\frac{A^H}{A^E}\,(\nabla_t h_z \times \mathbf{a}_z). \tag{4.37}$$

To be able to distinguish between TE modes and TM modes we will work with primes. TE modes are indicated by a *double prime.*

If we look to the above set of equations there is still a undetermined quotient of two factors, A^H/A^E, prohibiting the outcome of an unique solution. It is not of particular interest to find a value for each coefficient, but rather to find a value for the quotient. We could have left out the amplitude factors A^H, A^E, or chosen them equal to one, at the beginning, Eq.(4.5)-(4.8). As a consequence the mode functions $(\mathbf{e}'', \mathbf{h}'')$, which we want to use as basis vector functions would have had dimension of voltage and ampere respectively, which is uncommon. One can see this by using Eq.(4.13), with $e_z = 0$ substituted, or by substituting Eq.(4.36) into Eq.(4.37), both result in,

$$\mathbf{e}'' = \frac{\omega\mu}{k_z''}(\mathbf{h}'' \times \mathbf{a}_z). \tag{4.38}$$

Writing down the variables of above equation in their unit yields,

$$[\mathbf{e}''] = \frac{\frac{rad}{s}\frac{Vs}{Am}}{\frac{rad}{m}}\,\frac{A}{m} = \frac{V}{A}\,\frac{A}{m} = \frac{V}{m}, \tag{4.39}$$

from which we indeed obtain, that $\mathbf{e}''$ and $\mathbf{h}''$ contain units of voltage and ampere, respectively, otherwise the relation would not hold. This is all a bit trivial and not the focus of our main attention but its relevancy will show in a moment. Hence, $\omega\mu/k_z''$ has the unit of V/A=Ω which is a impedance [1]. Now, if the quotient of the amplitude factors A^H, A^E is chosen in such away that the factor $\omega\mu/k_z''$ is being compensated, the units of voltage and ampere are shifted to the coefficients V'' and I'', which appear in the modal representation of the electromagnetic fields, Eqs.(3.52)-(3.53) and the 2-norm of the mode functions can be made equal. The 2-norm of a function is the inner-product of this function with itself. We define

$$\frac{A^H}{A^E} = Y_\infty'' = \frac{1}{Z_\infty''} = \frac{k_z''}{\omega\mu}, \tag{4.40}$$

which is called, according to the literature [11, Sec.2.2], [16, Sec.4.4.1], [27, Sec.12.3], the modal characteristic admittance. This leads to the following relation between $\mathbf{e}''$ and $\mathbf{h}''$

$$\mathbf{e}'' = \mathbf{h}'' \times \mathbf{a}_z, \tag{4.41}$$

$\mathbf{e}''$ and $\mathbf{h}''$ still have dimensions of m^{-1}, meaning that h_z also has dimension m^{-1}. In Appendix(B.2) a derivation is given, which proves that the mode functions are orthogonal. For this use is made of the fact that the Neumann boundary-value problem has orthogonal eigenfunctions and that the eigenvalues $k_t''^2$ are real and positive. This is clarified in Appendix(B.1) and (B.4) respectively. Having established the orthogonality and an equal 2-norm between the mode functions we can look at the normalization of the mode functions. Normalisation of the mode functions can be obtained by enforcing the 2-norm to unity, as follows, using Eq.(B.21) as a point of departure,

$$< \mathbf{h}_i'', \mathbf{h}_i'' >=\| \mathbf{h}_i'' \|^2= 1 = \frac{\mid k_{z;i}'' \mid^2}{k_{t;i}''^2} \int_S \mid h_{z;i} \mid^2 \, d\sigma. \tag{4.42}$$

We refer to Eq.(B.17) for the definition of the inner-product. An obvious solution is finding an substitute for the term $h_{z;i}$, we therefore introduce a scalar function and make it proportional to $h_{z;i}$ according

$$h_{z;i} = -j \frac{k_{t;i}''}{k_{z;i}''} \psi_i. \tag{4.43}$$

Substitution of Eq.(4.43) into Eq.(4.42) leads to

$$\| \mathbf{h}_i'' \|^2 = \frac{\mid k_{z;i}'' \mid^2}{k_{t;i}''^2} \int_S \left| \frac{k_{t;i}''}{k_{z;i}''} \psi_i \right|^2 d\sigma = \int_S \mid \psi_i \mid^2 \, d\sigma = < \psi_i, \psi_i >= 1, \tag{4.44}$$

indicating that the scalar function has to be normalized according

$$< \psi_i, \psi_j > = \delta_{ij}, \tag{4.45}$$

[1] not a resistance because k_z is depending on k which again is depended of ε_c which can be complex

where δ_{ij} is the Kronecker delta function defined as

$$\delta_{ij} = \begin{cases} 1 & i = j, \\ 0 & i \neq j. \end{cases} \tag{4.46}$$

We have come to a L^2-norm for $\mathbf{h}_i''$ equal to unity and simultaneously for $\mathbf{e}_i''$, by means of Eq.(4.41). As a consequence of using the scalar function, the longitudinal field constituent $h_{z;i}(\boldsymbol{\rho})$, is no longer normalized.

Eventually we conclude, with field quantities expressed in terms of the scalar function ψ,

$$(\nabla_t^2 + k_t''^2)\,\psi_i = 0, \qquad \frac{\partial \psi_i}{\partial \nu}\Big|_{\boldsymbol{\rho}=\boldsymbol{\rho}_\Gamma} = 0, \tag{4.47}$$

$$h_{z;i} = -j\,\frac{k_t''}{k_z''}\,\psi_i, \tag{4.48}$$

$$\mathbf{h}_i'' = -\frac{1}{k_t''}\nabla_t\,\psi_i, \tag{4.49}$$

$$\mathbf{e}_i'' = -\frac{1}{k_t''}\,(\nabla_t\,\psi_i \times \mathbf{a}_z), \tag{4.50}$$

The solution to the Neumann boundary-value problem for a rectangular waveguide can be found in Appendix(C.1). From this appendix we obtain completeness of the function ψ_i, assuring that $\mathbf{h}''$ and $\mathbf{e}''$ form complete sets, $\{\mathbf{e}''\}$, $\{\mathbf{h}''\}$, together with there orthonormality the mode functions form a suitable basis to construct a solution for the transverse electromagnetic field.

4.3.2 TM modes

In case of TM modes, meaning that $h_z = 0$, we have the following set of equation, at our disposal, derived from Eq.(4.15) and Eq.(4.16),

$$(\nabla_t^2 + k_t'^2)\,e_z = 0, \qquad e_z|_{\boldsymbol{\rho}=\boldsymbol{\rho}_\Gamma} = 0, \tag{4.51}$$

$$\mathbf{e}' = -j\,\frac{k_z'}{k_t'^2}\nabla_t e_z, \tag{4.52}$$

$$\mathbf{h}' = -j\,\frac{\omega\varepsilon_c}{k_t'^2}\frac{A^E}{A^H}\,(\mathbf{a}_z \times \nabla_t e_z). \tag{4.53}$$

TM modes are distinguished by a *single prime*.

There is a lot of analogy between the treatment presented for TE modes and the oncoming treatment for TM modes. So, in view of this, we will be somewhat briefer in our description of the TM modes.

In Eq.(4.53) we also got a quotient of 2 amplitude factors, A^E/A^H, inverse to the one in Eq.(4.37). In the TE case we defined it as an admittance, now it will be defined as a

modal characteristic impedance, as

$$Z'_{\infty} = \frac{k'_z}{\omega \varepsilon_c}. \tag{4.54}$$

By the above definition, the following simple relation is formed between the mode functions

$$\mathbf{h}' = \mathbf{a}_z \times \mathbf{e}'. \tag{4.55}$$

As a result the unity of voltage and ampere, of respectively $\mathbf{e}'$ and $\mathbf{h}'$, are replaced to the coefficients V' and I' of the modal representation and the 2-norm of the mode functions become equal. The mode functions are also orthogonal, just like their counterparts in the TE case.

$$< \mathbf{e}'_i, \mathbf{e}'_j >= 0 \qquad i \neq j, \tag{4.56}$$

$$< \mathbf{h}'_i, \mathbf{h}'_j >= 0 \qquad i \neq j. \tag{4.57}$$

See Appendix(B.2) for a derivation.

Next, we are arrived at the normalisation of the mode functions. This goes by analogy with Eq.(4.42), viz.

$$< \mathbf{e}'_i, \mathbf{e}'_i >=\| \mathbf{e}'_i \|^2= 1 = \frac{\mid k'_{z;i} \mid^2}{k'^2_{t;i}} \int_S \mid e_{z;i} \mid^2 \, d\sigma. \tag{4.58}$$

Again we introduce a scalar function, ϕ_i, proportional to $e_{z;i}$, according to

$$e'_{z;i} = -j \, \frac{k'_{t;i}}{k'_{z;i}} \, \phi_i, \tag{4.59}$$

by which the 2-norm of $\mathbf{e}'_i$ and $\mathbf{h}'_i$ is set to unity, under the condition that the scalar function obeys

$$< \phi_i, \phi_j >= \delta_{ij}. \tag{4.60}$$

This last condition is satisfied during the solution of the Dirichlet boundary-value problem.

Summarizing we've got

$$(\nabla_t^2 + k_t'^2)\phi_i = 0, \qquad \phi|_{\boldsymbol{\rho}=\boldsymbol{\rho}_\Gamma} = 0, \tag{4.61}$$

$$e'_{z;i} = -j \, \frac{k'_t}{k'_z} \, \phi_i, \tag{4.62}$$

$$\mathbf{e}'_i = -\frac{1}{k'_t} \nabla_t \phi_i, \tag{4.63}$$

$$\mathbf{h}'_i = -\frac{1}{k'_t} (\mathbf{a}_z \times \nabla_t \phi_i). \tag{4.64}$$

The solution to the Dirichlet boundary-value problem for a rectangular waveguide is found in Appendix(C.2). The Dirichlet boundary-value problem, also yields completeness of the scalar function ϕ_i, just like its counterpart ψ_i, with which we assume that it assures completeness of the mode functions, $\{\mathbf{e}'\}$, $\{\mathbf{h}'\}$. Thus, the TM mode functions also form a suitable basis.

4.4 Modal field representation

In the preceding section we have seen that the mode functions can be used as a basis for the construction of the transverse electric and magnetic fields. Since we know that the mode functions form complete sets we can expand the electric and magnetic fields in it. In fact they become exact if we take along a infinite number of modes into account.

Continuing in the notation we used for the transverse fields in Sec.3.3 and the knowledge that fields can be build up out of TE and TM modes, we can write the transverse components of the electromagnetic field in a so-called modal representation, as follows

$$\mathbf{E}_t(\boldsymbol{\rho}, z) = \sum_i V_i'(z)\mathbf{e}_i'(\boldsymbol{\rho}) + \sum_i V_i''(z)\mathbf{e}_i''(\boldsymbol{\rho}) = \sum_{i;\alpha} V_i^\alpha(z)\mathbf{e}_i^\alpha(\boldsymbol{\rho}), \tag{4.65}$$

$$\mathbf{H}_t(\boldsymbol{\rho}, z) = \sum_i I_i'(z)\mathbf{h}_i'(\boldsymbol{\rho}) + \sum_i I_i''(z)\mathbf{h}_i''(\boldsymbol{\rho}) = \sum_{i;\alpha} I_i^\alpha(z)\mathbf{h}_i^\alpha(\boldsymbol{\rho}). \tag{4.66}$$

with index i, $i \in [0, \infty)$, indicating the mode number and index α, $\alpha \in \{'', '\}$, indicating the mode type. V_i^α, I_i^α are the modal voltage and current coefficients, respectively, containing an amplitude coefficient and a z-dependency.

Up till now our main attention was focused at gaining a representation or expression for the transverse components of the electromagnetic fields. To get an expression for the total electromagnetic fields we also need an expression for the longitudinal field components, since $\mathbf{E} = \mathbf{E}_t + E_z\mathbf{a}_z$ and $\mathbf{H} = \mathbf{H}_t + H_z\mathbf{a}_z$. From Eq.(4.18) and Eq.(4.19) we know that the longitudinal field components can be derived from the transverse ones, as

$$j\omega\varepsilon_c E_z = \nabla_t \cdot (\mathbf{H}_t \times \mathbf{a}_z), \tag{4.67}$$

$$j\omega\mu H_z = \nabla_t \cdot (\mathbf{a}_z \times \mathbf{E}_t). \tag{4.68}$$

First we concentrate on Eq.(4.67) for the calculation of the longitudinal electric field component. By substitution of Eq.(4.66) and subsequently applying Eq.(4.55) one obtains

$$j\omega\varepsilon_c E_z = \nabla_t \cdot \left[\sum_i I_i'(\mathbf{h}_i' \times \mathbf{a}_z)\right] = \sum_i I_i' \nabla_t \cdot \mathbf{e}_i'. \tag{4.69}$$

Note that since E_z can only exist for mode type TM, the index α of the summation is restricted to TM ($= '$), explicitly written in the above equation and we assume that differentiation and summation can be interchange. Next, we have to take care of the divergence of the TM electric mode function. The in Sec.4.3.2 derived equations can be used, but there is an other lucid manner viz. by means of the divergency of the electric flux density. In the source-free case, the divergence of the electric flux density is zero, implicating that the divergence of the electric field is zero also. Splitting up the nabla operator and the electric field in their transverse and longitudinal components, we get

$$\nabla \cdot \mathbf{E} = \nabla_t \cdot \mathbf{E}_t + \underbrace{\nabla_t \cdot \mathbf{a}_z}_{0} E_z + \underbrace{\frac{\partial \mathbf{E}_t}{\partial z} \cdot \mathbf{a}_z}_{0} + \frac{\partial E_z}{\partial z} = 0 \tag{4.70}$$

In Eqs.(4.5) and (4.7) at the beginning of this section we postulated some characteristic wave solution for the transverse en longitudinal field components which we can apply to Eq.(4.70), resulting in

$$A^E e^{-jk_z z} \nabla_t \cdot \mathbf{e} - jk_z A^E e^{-jk_z z} e_z = 0, \tag{4.71}$$

$$\nabla_t \cdot \mathbf{e} = jk_z e_z. \tag{4.72}$$

Finally, the longitudinal electric field component takes the form

$$E_z = \sum_i I_i' Z_{\infty;i}' e_{z;i}. \tag{4.73}$$

As for the longitudinal magnetic field, we can make a similar derivation to end up with

$$H_z = \sum_i V_i'' Y_{\infty;i}'' h_{z;i}. \tag{4.74}$$

Of course, now the summation is restricted to TE modes, otherwise H_z could not exist.

It is valid to expand the longitudinal fields in their $\boldsymbol{\rho}$-depended longitudinal constituents e_z and h_z because they form a suitable basis.

Chapter 5

Equivalent transmission lines

This chapter will show how equivalent transmission line equations can be deduced from the Marcuvitz-Swinger equations. In Sec.3.3, we already mentioned that the Marcuvitz-Swinger equations that they can be cast in equivalent transmission line equations. For this, we expanded the transverse fields in a infinite sum of vector functions and substituted them into the Marcuvitz-Swinger equations. At that point we did not yet know what kind of function we should use, except that they should form a complete set. In the preceding chapter we derived the mode functions and found that they form a orthonormal basis. This, together with the fact that the mode functions are eigen functions of the system, makes them suitable for the description of waveguide characteristics.

5.1 Transmission line equations

We will start by repeating the Marcuvitz-Swinger equations, Eq.(3.42),

$$-\frac{\partial}{\partial z}\begin{pmatrix}\mathbf{E}_t(\boldsymbol{\rho},z)\\ \mathbf{H}_t(\boldsymbol{\rho},z)\end{pmatrix}=\begin{pmatrix}j\omega\mu\underline{\underline{\mathcal{L}}} & \mathcal{O}\\ \mathcal{O} & j\omega\varepsilon_c\underline{\underline{\mathcal{L}}}\end{pmatrix}\begin{pmatrix}\mathbf{H}_t(\boldsymbol{\rho},z)\times\mathbf{a}_z\\ \mathbf{a}_z\times\mathbf{E}_t(\boldsymbol{\rho},z)\end{pmatrix}+\begin{pmatrix}\mathbf{M}_t^{eq}(\boldsymbol{\rho},z)\times\mathbf{a}_z\\ \mathbf{a}_z\times\mathbf{J}_t^{eq}(\boldsymbol{\rho},z)\end{pmatrix}, \tag{5.1}$$

By invoking the modal representation for the transverse fields we arrive at

$$-\sum_{i;\alpha}\frac{dV_i^\alpha}{dz}\,\mathbf{e}_i^\alpha=j\omega\mu\sum_{i;\alpha}I_i^\alpha\,\underline{\underline{\mathcal{L}}}(\mathbf{h}_i^\alpha\times\mathbf{a}_z)+\mathbf{M}_t^{eq}\times\mathbf{a}_z \tag{5.2}$$

$$-\sum_{i;\alpha}\frac{dI_i^\alpha}{dz}\,\mathbf{h}_i^\alpha=j\omega\varepsilon_c\sum_{i;\alpha}V_i^\alpha\,\underline{\underline{\mathcal{L}}}(\mathbf{a}_z\times\mathbf{e}_i^\alpha)+\mathbf{a}_z\times\mathbf{J}_t^{eq} \tag{5.3}$$

where,

$$\underline{\underline{\mathcal{L}}}=(\underline{\underline{I}}_t+\frac{1}{k^2}\nabla_t\nabla_t\cdot). \tag{5.4}$$

As before, the inner-product of Eq.(5.2) and (5.3) is taken with $\mathbf{e}_j^\beta$ and $\mathbf{h}_j^\beta$, respectively, in which j is a mode number index and β is a mode type index, TM or TE. Then, with the

use of $\mathbf{e} = \mathbf{h} \times \mathbf{a}_z$ and the othogonality property, $< \mathbf{e}_i^\alpha, \mathbf{e}_j^\beta > = < \mathbf{h}_i^\alpha, \mathbf{h}_j^\beta > = \delta_{ij}$, we obtain

$$-\frac{dV_j^\alpha}{dz} = j\omega\mu \sum_{i;\alpha} I_i^\alpha < \underline{\underline{\mathcal{L}}}\mathbf{e}_i^\alpha, \mathbf{e}_j^\beta > + v_j^\beta, \tag{5.5}$$

$$-\frac{dI_j^\alpha}{dz} = j\omega\varepsilon_c \sum_{i;\alpha} V_i^\alpha < \underline{\underline{\mathcal{L}}}\mathbf{h}_i^\alpha, \mathbf{h}_j^\beta > + i_j^\beta. \tag{5.6}$$

with v_j^β, i_j^β being called the modal voltage source and current source, respectively, defined as

$$v_j^\beta = < \mathbf{M}_t^{eq} \times \mathbf{a}_z, \mathbf{e}_j^\beta >, \tag{5.7}$$

$$i_j^\beta = < \mathbf{a}_z \times \mathbf{J}_t^{eq}, \mathbf{h}_j^\beta > . \tag{5.8}$$

The inner-products involving the operator $\underline{\underline{\mathcal{L}}}$ are not trivial.Therefore, in AppendixD a short derivation is given. With these intermediate results, Eqs.(5.5) and (5.6) can be cast directly in their final form, the so-called equivalent transmission line equations

$$-\frac{dV_i^\alpha(z)}{dz} = jk_{z;i}^\alpha I_i^\alpha(z) Z_{\infty;i}^\alpha + v_i^\alpha(z), \tag{5.9}$$

$$-\frac{dI_i^\alpha(z)}{dz} = jk_{z;i}^\alpha V_i^\alpha(z) Y_{\infty;i}^\alpha + i_i^\alpha(z). \tag{5.10}$$

Note that we have written all indices, j and β, into their former notation.

As was already postulated in Sec.3.3 and now more solidly proven, every mode has its own set of ordinary first-order system of differential equations by, which the voltage and current coefficients can be determined. This finds its origin in the fact that the modes are orthogonal. Under the assumption that the dielectric filling stays homogeneous, these specific equivalent transmission-line equations can handel changes in material parameters along the z-axis, by continuity of the voltage and current, which follows from the continuity of the tangential electric and magnetic field over the dielectric junction. The above-mentioned, is only valid in the case of a waveguide with a uniform cross-section, since the mode functions don't change, are orthogonal and are independent of material parameters. In case of discontinuities in the waveguide cross section other, extra steps during the analysis are necessary, to solve the electromagnetic fields since the mode functions change at the discontinuity, which leads to mode coupling.

We can represent the transmission-line equations schematically by rewriting the differential equations as difference equation followed by their physical interpretation as

$$-\frac{V(z+\Delta z) - V(z)}{\Delta z} \doteq jk_z I(z) Z_\infty + v(z), \tag{5.11}$$

$$-\frac{I(z+\Delta z) - I(z)}{\Delta z} \doteq jk_z I(z) Y_\infty + i(z). \tag{5.12}$$

For clarity we have left out the mode-number index i and the mode type index α. Fig.(5.1) and (5.2) represent Eq.(5.11) and (5.12) schematically, respectively.

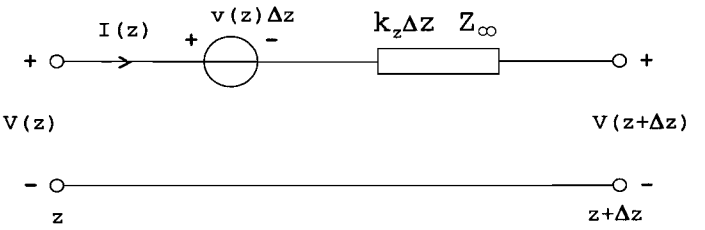

Figure 5.1: *Section equivalent transmission line with modal voltage source*

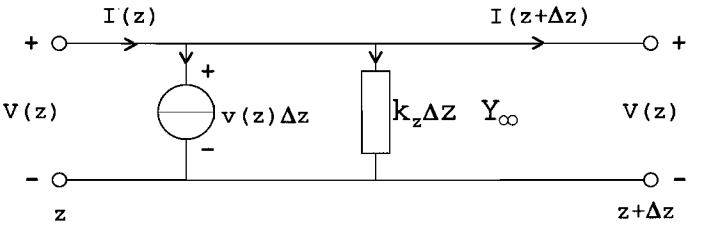

Figure 5.2: *Section equivalent transmission line with modal current source*

5.2 Source representation

There is one last thing about the equivalent transmission-line equations that should be discussed, viz. the modal voltage source and the modal current source in Eqs.(5.7) and (5.8). We will be brief about this. Substituting the equivalent transverse source distributions of Eqs.(3.44) and (3.45) into Eq.(5.7) and Eq.(5.8) respectively, we obtain

$$v_i^\alpha = < \mathbf{M}_t \times \mathbf{a}_z, \mathbf{e}_i^\alpha > - \frac{1}{j\omega\varepsilon_c} < \nabla_t \times (J_z \mathbf{a}_z) \times \mathbf{a}_z, \mathbf{e}_i^\alpha >, \tag{5.13}$$

$$i_i^\alpha = < \mathbf{a}_z \times \mathbf{J}_t, \mathbf{h}_i^\alpha > + \frac{1}{j\omega\mu} < \mathbf{a}_z \times \nabla_t \times (M_z \mathbf{a}_z), \mathbf{h}_i^\alpha > . \tag{5.14}$$

In our problem we don't have to deal with sources distributed along the z-axis so J_z and M_z vanish and thereby the second term on the right-hand side in above equations. Then, by making use of the relation $\mathbf{e}_i^\alpha = \mathbf{h}_i^\alpha \times \mathbf{a}_z$, see Eqs.(4.41) and (4.55), the modal voltage and current source for TM as well as for TE modes are

$$v_i^\alpha = < \mathbf{M}_t, \mathbf{h}_i^\alpha >, \tag{5.15}$$

$$i_i^\alpha = < \mathbf{J}_t, \mathbf{e}_i^\alpha > . \tag{5.16}$$

Suppose $\mathbf{M}_t(\mathbf{r})$ and $\mathbf{J}_t(\mathbf{r})$ would be a transversely directed magnetic and electric dipool, respectively, at source point $\mathbf{r}_0$ represented like

$$\mathbf{M}^d(\mathbf{r}) = \delta(\mathbf{r} - \mathbf{r}_0)\mathbf{M}^0, \qquad \mathbf{J}^d(\mathbf{r}) = \delta(\mathbf{r} - \mathbf{r}_0)\mathbf{J}^0, \tag{5.17}$$

with d indicating a dipool, δ dirac delta-functie and $\mathbf{M}^0$ an arbitrary transversely directed constant unity vector, then we obtain

$$\begin{aligned} v_i^\alpha(z) =< \mathbf{M}^d, \mathbf{h}_i^\alpha > &= \int_S \delta(\mathbf{r}-\mathbf{r}_0)\mathbf{M}^0 \cdot \mathbf{h}_i^{\alpha *}\, dA = \mathbf{M}^0 \cdot \mathbf{h}_i^{\alpha *}\delta(z-z_0) \\ &= v_i^{0;\alpha}\,\delta(z-z_0), \end{aligned} \tag{5.18}$$

$$i_i^\alpha(z) =< \mathbf{J}^d, \mathbf{e}_i^\alpha > = i_i^{0;\alpha}\,\delta(z-z_0), \tag{5.19}$$

for the model voltage and current source respectively.

Next, we will look at a magnetic surface current density. In general there is not just one dipole as excitation. Usually there is some arbitrary volumetric current source distribution as excitation. Such a source distribution can be thought of as being built-up out of an infinite number of dipoles. With the help of the superposition theorem we can formulate this as

$$\mathbf{M}(\mathbf{r}) = \int_{V'} \mathbf{M}(\mathbf{r}')\delta(\mathbf{r}-\mathbf{r}')\, dV', \tag{5.20}$$

in which the source points in the source volume V' are being indicated by $\mathbf{r}'$. Assuming a surface current density transverse to the propagation direction (z) at some arbitrary but fixed point $z = z_0$. We can take Eq.(5.20) as starting point and modify it to obtain an expression for the magnetic surface current density, see Eq.(5.21).

$$\mathbf{M}_t(\mathbf{r}) = \int_{S'} \mathbf{M}_t(\boldsymbol{\rho}', z_0)\delta(\boldsymbol{\rho}-\boldsymbol{\rho}')\, dS'\, \delta(z-z_0) = \mathbf{M}_t(\boldsymbol{\rho}, z_0)\delta(z-z_0). \tag{5.21}$$

The subscript t indicates that it is a transverse current, and the source points on surface S' are indicated by $\boldsymbol{\rho}'$. With this result we obtain the following modal voltage and current source

$$v_i^\alpha(z) =< \mathbf{M}_t(\boldsymbol{\rho}, z_0), \mathbf{h}_i^\alpha > \delta(z-z_0) = v_i^\alpha(z_0)\delta(z-z_0), \tag{5.22}$$

$$i_i^\alpha(z) =< \mathbf{J}_t(\boldsymbol{\rho}, z_0), \mathbf{e}_i^\alpha > \delta(z-z_0) = i_i^\alpha(z_0)\delta(z-z_0). \tag{5.23}$$

Eq.(5.23) is derived by defining an transversely electric surface current density by analogy to Eq.(5.21).

For a further treatment of arbitrary source distributions in guided wave problems see [11], [16].

Chapter 6

Iris; double waveguide junction

6.1 Introduction

The first subproblem we encounter is the iris, as defined in Sec.1. An iris, and particularly in our case a thick iris, can be seen as a double waveguide transition spaced closely after one and other. With the theory derived up till now in Sec.4 and Sec.5, we should be able to model and analyse a thick iris. Having to deal with abrupt discontinuities in the cross-section of waveguides, which we have in the case of an iris, is something that is not yet been reviewed. That particular problem is going to be discussed and solved in this chapter. The most frequently applied methods to solve discontinuities in the cross-section of waveguides are mode matching [12], and the moment method (MoM) [15]. We decided to apply a Galerkin type of MoM.

In the end, it is not our aim to reconstruct the complete electric and magnetic field, but we are more interested in the behaviour of the modes. By this we mean that we want to get some knowledge of the modes that play an important role, modes with a relevant contribution. Are they propagating or evanescent? The reason why we are particularly interested in the modes is because of the fact that the structure is very compact compared to the wave length. Because of this, there is a lot of interaction between the transverse distortions, not only by propagating modes but also by evanescent modes. Thus it is important to produce the proper kind of information, which contains the characteristics of the problem. The modes which the biggest magnitude, transporting the most (complex) power, are the most important. A description in scattering parameters, S-matrix, will be the objective.

6.2 Configuration

For the analysis of the thick iris we use the configuration depicted in Fig.(6.1a). There, we see an arbitrary double waveguide transition consisting of a waveguide, coming from $z = -\infty$, with some specific uniform cross-section. At point $z = z_1$ we encounter an abrupt junction in the cross-section of the waveguide. After this first junction the waveguide

continues with a smaller cross-section until point $z = z_2$ where we have again an abrupt junction which enlarges the waveguide cross-section to continue uniformly in the direction of $z = +\infty$. Electromagnetic fields are incident on the junctions form the left and the right. Fig.(6.1b) represents the equivalent situation. Through the fact that we closed of

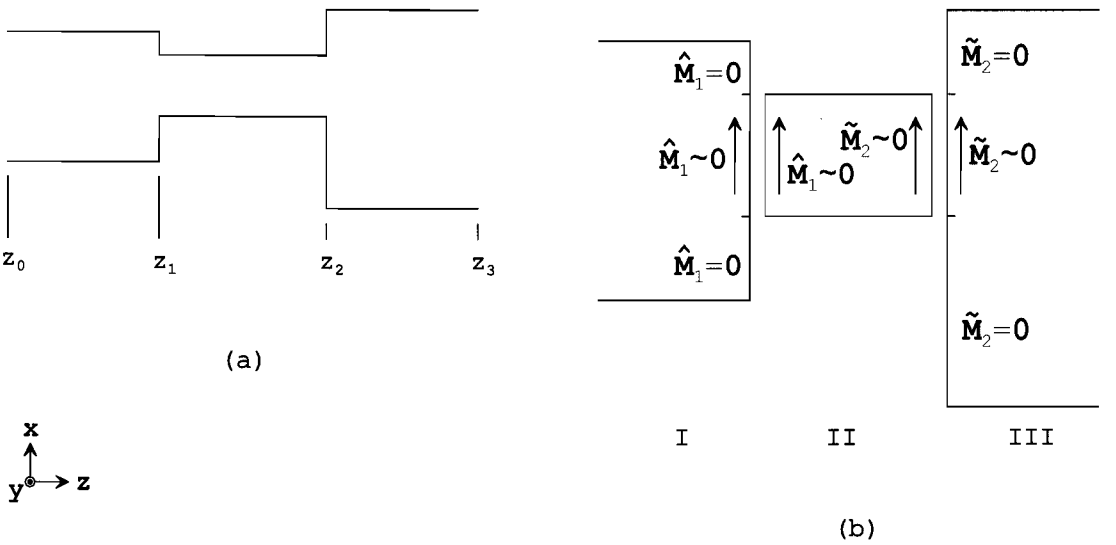

Figure 6.1: *a) A double waveguide junction, forming a thick iris, in an infinitely long waveguide. b) The equivalent representation with equivalent magnetic currents defined on the aperture closed with a PEC.*

the apertures with a infinitely thin PEC, three regions (sections) are created, indicated with I, II, III. Note that we now have uniform waveguide sections, which ideally fit the description in terms of equivalent transmission-lines. Once again the waveguide walls are PECs, the dielectric filling is homogeneous and can have a loss tangent, $\tan\delta$.

6.3 Solving transmission line equations; Modal Green's functions

In this section we are going to find expressions for the modal voltage and current coefficients, V and I, by solving the equivalent transmission line equations for the three defined sections.

First, before we start solving V and I for the different cases, we want to have some clarity about the behaviour of a (equivalent) magnetic dipole located on an infinitesimal small distance from a transversely directed PEC wall, closing of the waveguide cross-section completely, which is equivalent to a shorted transmission line. This is still a bit unclear, because a magnetic dipole on a infinitesimal small distance from a PEC is a limit proces of $\lim l \downarrow 0$, with l a small distance between PEC and dipole. The case of section-I will be used to make a compleet derivation. For the other cases just the derived final outcome will be used.

6.3.1 Section I

CASE: distance l in lim $l \downarrow 0$

Consider Fig.(6.2). The corresponding equivalent transmission line equations are

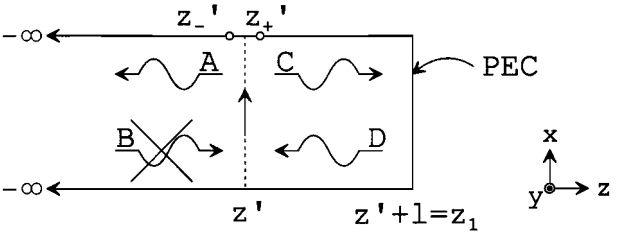

Figure 6.2: *Waveguide section I from Fig.(6.1) with on a distance l from the PEC wall a magnetic dipole. Indicated are the waves generated by the dipole.*

$$-\frac{dV}{dz} = jk_z\, I\, Z_\infty + p\delta(z - z'), \tag{6.1}$$

$$-\frac{dI}{dz} = jk_z\, V\, Y_\infty \tag{6.2}$$

where $p = 1V$. The mode-type and mode-number indices are left out. There is no modal current source because we're dealing with a magnetic dipole. The way to solve these first order coupled differential equations is to first find the homogeneous solution and then use this homogeneous solution to find the particular solution.

For the homogeneous solution, we discard the modal voltage source v and substitute Eqs.(6.1) and (6.2) it to one another to obtain

$$\frac{d^2V}{dz^2} + k_z^2\, V = 0, \tag{6.3}$$

$$\frac{d^2I}{dz^2} + k_z^2\, I = 0. \tag{6.4}$$

Now, if we only consider Eq.(6.4) we have as general solution

$$I(z) = \begin{cases} Ae^{jk_z(z-z')} + Be^{-jk_z(z-z')} & z < z', \\ Ce^{-jk_z(z-z')} + De^{jk_z(z-z')} & z > z'. \end{cases} \tag{6.5}$$

To get a unique solution to Eq.(6.4) we have to obey certain boundary conditions. If we look at Fig.(6.2) and consider $z < z'$ under the assumption that there are no sources for $z < z'$, the waveguide has a uniform cross-section and the fact that the source has to obey the radiation condition at infinity, we conclude that B=0, meaning that all waves are outgoing propagating or evanescent. If we consider $z > z'$ we have a boundary at $z = z' + l$

consisting of a PEC, which causes the out-going wave with amplitude C to reflect and there by creating a reflected wave with amplitude D. This can be transformed into the boundary condition $\mathbf{a}_z \times \mathbf{E}|_{z=z'+l} = \mathbf{E}_t|_{z=z'+l} = 0 \Rightarrow V|_{z=z'+l} = 0$ and from Eq.(6.2) this implies that $\frac{dI}{dz}|_{z=z'+l} = 0$. The result is

$$C = D\, e^{2jk_z l} \tag{6.6}$$

We now turn over the attention to the source jump at $z = z'$. This can be taken into account by demanding continuity of $I(z)$ on z', which comes from $\mathbf{a}_z \times (\mathbf{H}^{z'_-} - \mathbf{H}^{z'_+})|_{z=z'} = \mathbf{0}$, and results in

$$A = C + D. \tag{6.7}$$

Then by integrating over the source with the following inhomogeneous differential equation for $I(z)$, obtained by taking the derivative of Eq.(6.2) and substituting it into Eq.(6.1)

$$\frac{d^2 I}{dz^2} + k_z^2\, I = jk_z Y_\infty\, \delta(z - z'), \tag{6.8}$$

$$\Rightarrow \lim_{\epsilon \downarrow 0} \int_{z'-\epsilon}^{z'+\epsilon} \left(\frac{d^2 I}{dz^2} + k_z^2 I \right) dz = jk_z Y_\infty \lim_{\epsilon \downarrow 0} \int_{z'-\epsilon}^{z'+\epsilon} \delta(z - z')dz,$$

$$\Rightarrow \qquad \left[\partial_z I|_{z=z'_+} - \partial_z I|_{z=z'_-} \right] = jk_z Y_\infty, \tag{6.9}$$

If we work out Eq.(6.9) by taking the derivative of I from Eq.(6.5), substitute the appropriate constraints for z and apply Eqs.(6.6)-(6.7), we end up with the following expressions for the coefficients A,B, C and D

$$A = -Y_\infty \cos(k_z l)\, e^{-jk_z l}, \tag{6.10}$$

$$B = 0, \tag{6.11}$$

$$C = -\frac{1}{2} Y_\infty, \tag{6.12}$$

$$D = -\frac{1}{2} Y_\infty\, e^{-2jk_z l}. \tag{6.13}$$

These coefficients applied to Eq.(6.5) yield the final expression for $I(z)$

$$I_i^{\alpha;\mathrm{I}}(z) = \begin{cases} -Y_{\infty;i}^{\alpha;\mathrm{I}} \cos(k_{z;i}^{\alpha;\mathrm{I}} l)\, e^{jk_{z;i}^{\alpha;\mathrm{I}}(z-z'-l)} & z \le z', \\ -Y_{\infty;i}^{\alpha;\mathrm{I}}\, e^{-jk_{z;i}^{\alpha;\mathrm{I}} l} \cos(k_{z;i}^{\alpha;\mathrm{I}}[z - z' - l]) & z \ge z'. \end{cases} \tag{6.14}$$

The superscript 'I' is of course the indication for section-I. The other indices are known from former considerations. Note the standing wave between the dipole and the PEC wall for $z > z'$. By rewriting Eq.(6.2) as

$$V = -\frac{1}{jk_z} Z_\infty \frac{dI}{dz}, \tag{6.15}$$

and substitution of Eq.(6.14) we directly obtain the model voltage coefficients

$$V_i^{\alpha;\mathrm{I}}(z) = \begin{cases} \cos(k_{z;i}^{\alpha;\mathrm{I}} l)\, e^{jk_{z;i}^{\alpha;\mathrm{I}}(z-z'-l)} & z \leq z', \\ j\, e^{-jk_{z;i}^{\alpha;\mathrm{I}} l}\, \sin(k_{z;i}^{\alpha;\mathrm{I}}[z-z'-l]) & z \geq z'. \end{cases} \tag{6.16}$$

Worthwhile to evaluate is $I(z)$ and $V(z)$ on $z = z'$ to check if they are oke. We find for $I(z)$ that it is continuous, as required, because there is no electric surface current. For $V(z)$ we find that it is discontinuous. The discontinuity has a magnitude of one. The discontinuity is as expected because of $\mathbf{a}_z \times (\mathbf{E}^{z'-} - \mathbf{E}^{z'+})|_{z=z'} = \mathbf{M}_s$ in which the magnetic surface current $\mathbf{M}_s$ in our case is a delta-puls $p\delta(z-z')$ with a magnitude of, indeed, $p = 1$.

Going back to the beginning of Sec.6.3 we can, now the expressions of the modal voltage and current coefficients are known, examine what happens if the dipole moves towards the PEC wall. With distances l going to zero, the condition $z \geq z'$ converts to $z \downarrow z'$. For $I(z)$ we find

$$\lim_{l \downarrow 0} I_i^{\alpha;\mathrm{I}}(z) = \begin{cases} -Y_{\infty;i}^{\alpha;\mathrm{I}}\, e^{jk_{z;i}^{\alpha;\mathrm{I}}(z-z')} & z \leq z', \\ -Y_{\infty;i}^{\alpha;\mathrm{I}} & z \downarrow z'. \end{cases} \tag{6.17}$$

In Eq.(6.17) we see that the lower case is just a special form of the upper case, which makes the lower redundant. For $V(z)$ we find

$$\lim_{l \downarrow 0} V_i^{\alpha;\mathrm{I}}(z) = \begin{cases} e^{jk_{z;i}^{\alpha;\mathrm{I}}(z-z')} & z \leq z', \\ 0 & z \downarrow z'. \end{cases} \tag{6.18}$$

The discrepancy in Eq.(6.18) between the upper and lower case for $z = z'$ is because of the impressed source. And of course, approaching the dipole with a PEC from the right V must become zero because of the fact that the tangential component of the electric field must vanish upon reaching a PEC.

CASE: distance l is zero

In this section we will look for a correct description of a magnetic dipole spaced infinitely close to a PEC wall without having to work out the limit proces each time. We take Fig.(6.3) as reference. We depart from the fact that Eqs.(6.1)-(6.5) still hold. The difference begins after the last equation. For the case, $l \neq 0$ we see that there exists a standing wave between the dipole at z' and the PEC wall at $z' + l$, in Eqs.(6.14)-(6.15) on the second line given by the cosinus and sinus term, respectively. This standing wave is caused by the interference between the incident wave on the PEC wall and the reflected wave form the PEC. Then, with the distance l going towards zero we obtain, in Eqs.(6.17) and (6.18), that the standing wave has disappeared. From this we conclude that a dipole placed on an infinitesimal distance from a PEC only radiates away from the PEC. So, we are left with the homogeneous solution form Eq.(6.5)

$$I(z) = Ae^{jk_z(z-z')} \qquad z < z'. \tag{6.19}$$

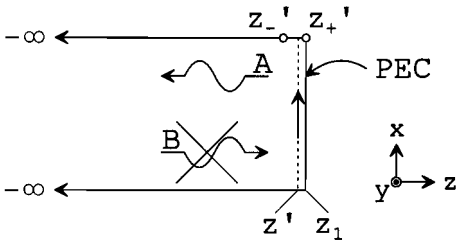

Figure 6.3: *Waveguide section I from Fig.(6.1) with a magnetic dipole on an infinitesimal distance form PEC. Indicated are the waves generated by the dipole.*

The amplitude coefficient B=0 for the same reasons as in the previous case. We have only one unknown that can be solved by taking the source into account, which comes down to integrating over the source with help of the one-dimensional inhomogeneous Helmholtz equation for *I(z)*, as was done in Eq.(6.8) and Eq.(6.9). Eq.(6.9) can be further reduced to

$$-\partial_z I|_{z=z'_-} = jk_z Y_\infty, \tag{6.20}$$

because an expression for *I(z)* with $z > z'$ doesn't exist. Solving Eq.(6.20) readily provides us with the solution for A,

$$A = -Y_\infty. \tag{6.21}$$

The final expressions for *I(z)* and *V(z)* are

$$I_i^{\alpha;\mathrm{I}}(z) = -Y_{\infty;i}^{\alpha;\mathrm{I}}\, e^{jk_{z;i}^{\alpha;\mathrm{I}}(z-z')} \qquad z \le z', \tag{6.22}$$

$$V_i^{\alpha;\mathrm{I}}(z) = e^{jk_{z;i}^{\alpha;\mathrm{I}}(z-z')} \qquad z \le z', \tag{6.23}$$

and are similar to Eq.(6.17) and (6.18). So for the calculation of a dipole, parallel and very close to a PEC we only have to consider the out-going waves and integrate over the source.

Note that what we have been calculating just now, according to the literature [11], are the so called modal Green's functions. So

$$I(z) \longrightarrow G_I(z, z'), \tag{6.24}$$

$$V(z) \longrightarrow G_V(z, z'), \tag{6.25}$$

with I and V as subscript indicating that the Green's function is related to modal current and voltage coefficients. Then, replacing a transverse magnetic dipole by a transverse magnetic surface current distribution, which gives a modal voltage source representation as in Eq.(5.22), the modal voltage and current coefficients as a result of this surface current density are found as

$$I_i^{\alpha;\mathrm{I}}(z) = \lim_{z\to z_1} \int G_{I;i}^{\alpha;\mathrm{I}}(z, z')\, v_i^{\alpha;\mathrm{I}}(z')\, \delta(z - z')dz' = -Y_{\infty;i}^{\alpha;\mathrm{I}}\, v_i^{\alpha;\mathrm{I}}(z_1)\, e^{jk_{z;i}^{\alpha;\mathrm{I}}(z-z_1)}, \tag{6.26}$$

$$V_i^{\alpha;\mathrm{I}}(z) = \lim_{z\to z_1} \int G_{V;i}^{\alpha;\mathrm{I}}(z, z')\, v_i^{\alpha;\mathrm{I}}(z')\, \delta(z - z')dz' = v_i^{\alpha;\mathrm{I}}(z_1)\, e^{jk_{z;i}^{\alpha;\mathrm{I}}(z-z_1)}. \tag{6.27}$$

for $z \leq z_1$, with $v_i^{\alpha;\mathrm{I}}(z_1) =< \hat{\mathbf{M}}_1(\boldsymbol{\rho}, z_1), \mathbf{h}_i^{\alpha;\mathrm{I}} >$ and the magnetic current is a transversly directed surface current.

6.3.2 Section II

Consider Fig.(6.4). For this problem Eqs.(6.1)-(6.4) hold. We now have to deal with

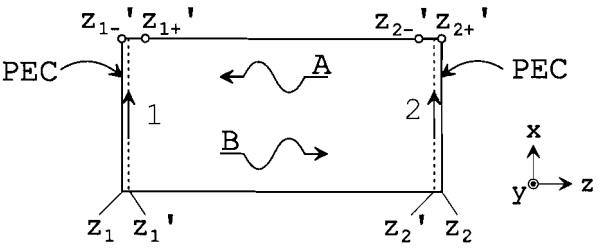

Figure 6.4: *Waveguide section II from Fig.(6.1) with magnetic dipoles on an infinitesimal distance form the PECs. Indicated are the waves generated by the dipole.*

two sources. Because the problem is described by linear equations we can apply the superposition principle to find the total solution for the two sources. This means for the homogeneous solution of $I(z)$

$$I_1(z) = Ae^{jk_z(z-z_1')} + Be^{-jk_z(z-z_1')} \qquad z_1' < z < z_2, \tag{6.28}$$

$$I_2(z) = Ae^{jk_z(z-z_2')} + Be^{-jk_z(z-z_2')} \qquad z_1 < z < z_2', \tag{6.29}$$

where the subscripts 1 and 2 of the modal current coefficient $I(z)$ indicate source 1 and source 2 at z_1' and z_2', respectively. Because the sources are confined to a completely closed cavity, the existence of back and forth travelling waves is evident.

Only source 1

We begin by solving the problem for source 1 (source 2 is absent). To get a unique solution to Eq.(6.28), two unknown amplitude coefficients must be recovered A and B. Therefore we need two boundary conditions. The first is for $z = z_2$, the PEC wall, and the other is taking into account the source at z_1'. According to the former we obtain

$$\mathbf{a}_z \times \mathbf{E}|_{z=z_2} = 0 \longrightarrow V|_{z=z_2} = 0 \longrightarrow \partial_z I_1|_{z=z_2} = 0, \tag{6.30}$$

which gives us

$$B = A\, e^{2jk_z(z_2-z_1')}. \tag{6.31}$$

Further, by integrating over the source in the inhomogeneous Helmholtz equation, we take

into account the source jump

$$\lim_{\epsilon \downarrow 0} \int_{z_1'-\epsilon}^{z_1'+\epsilon} \left(\frac{d^2 I_1}{dz^2} + k_z^2 I_1 \right) dz = jk_z Y_\infty \lim_{\epsilon \downarrow 0} \int_{z_1'-\epsilon}^{z_1'+\epsilon} \delta(z - z')dz, \tag{6.32}$$

$$[\partial_z I_1|_{z=z_{1+}'} - \underbrace{\partial_z I_1|_{z=z_{1-}'}}_{0}] = jk_z Y_\infty. \tag{6.33}$$

Working out the derivative of $I_1(z)$ and filling in the constraint for z results in

$$-B + A = Y_\infty. \tag{6.34}$$

Two unknowns A, B, two equations, Eq.(6.31), (6.34), gives us the solution for the amplitude terms A and B

$$A = \frac{-Y_\infty \, e^{-jk_z(z_2 - z_1')}}{2j \sin[k_z(z_2 - z_1')]}, \tag{6.35}$$

$$B = \frac{-Y_\infty \, e^{jk_z(z_2 - z_1')}}{2j \sin[k_z(z_2 - z_1')]}. \tag{6.36}$$

The above results applied to Eq.(6.28) gives the complete expression for $I_1(z)$

$$I_1(z) = \frac{-Y_\infty \cos[k_z(z - z_2)]}{j \sin[k_z(z_2 - z_1')]} \qquad z_1' \leq z \leq z_2. \tag{6.37}$$

Note the standing wave in the numerator, which is the effect of the back and forth travelling waves between the PEC walls.

Only source 2

The way of solving the problem for only source 2 is analogous to the previous treatment.

$$I_2(z) = \frac{Y_\infty \cos(k_z[z - z_1])}{j \sin(k_z[z_1 - z_2'])} \qquad z_1 \leq z \leq z_2'. \tag{6.38}$$

Total solution

The Eqs.(6.37) and (6.38) are again in fact modal Green's functions. We can find the response to a transverse directed magnetic surface current density in the same way as done in Eq.(6.24) and (6.26). The result is

$$I_{1;p}^{\alpha;\mathrm{II}}(z) = \int G_{I_1;p}^{\alpha;\mathrm{II}}(z, z_1') \, v_p^{\alpha;\mathrm{II}}(z_1') \, \delta(z - z_1') \, dz_1' = \frac{-Y_{\infty;p}^{\alpha;\mathrm{II}} \, v_p^{\alpha;\mathrm{II}}(z_1') \cos(k_{z;p}^{\alpha;\mathrm{II}}[z - z_2])}{j \sin(k_{z;p}^{\alpha;\mathrm{II}}[z_2 - z_1'])}, \tag{6.39}$$

$$I_{2;p}^{\alpha;\mathrm{II}}(z) = \int G_{I_2;p}^{\alpha;\mathrm{II}}(z, z_2') \, v_p^{\alpha;\mathrm{II}}(z_2') \, \delta(z - z_2') \, dz_2' = \frac{Y_{\infty;p}^{\alpha;\mathrm{II}} \, v_p^{\alpha;\mathrm{II}}(z_2') \cos(k_{z;p}^{\alpha;\mathrm{II}}[z - z_1])}{j \sin(k_{z;p}^{\alpha;\mathrm{II}}[z_1 - z_2'])}, \tag{6.40}$$

with $v_p^{\alpha;\mathrm{II}}(z_1') =< \tilde{\mathbf{M}}_1(\boldsymbol{\rho}, z_1'), \mathbf{h}_p^{\alpha;\mathrm{II}} >$ and $v_p^{\alpha;\mathrm{II}}(z_2') =< \hat{\mathbf{M}}_2(\boldsymbol{\rho}, z_2'), \mathbf{h}_p^{\alpha;\mathrm{II}} >$. For section-II we use p as mode number indicator. Adding up the partial solutions, $I_{1;p}^{\alpha;\mathrm{II}}(z)$ and $I_{2;p}^{\alpha;\mathrm{II}}(z)$, yields the total solution

$$\begin{aligned} I_p^{\alpha;\mathrm{II}}(z) &= I_{1;p}^{\alpha;\mathrm{II}}(z) + I_{2;p}^{\alpha;\mathrm{II}}(z) \\ &= \frac{-Y_{\infty;p}^{\alpha;\mathrm{II}}\, v_p^{\alpha;\mathrm{II}}(z_1')\, \cos(k_{z;p}^{\alpha;\mathrm{II}}[z - z_2])}{j \sin(k_{z;p}^{\alpha;\mathrm{I}}[z_2 - z_1'])} + \frac{Y_{\infty;p}^{\alpha;\mathrm{II}}\, v_p^{\alpha;\mathrm{II}}(z_2')\, \cos(k_{z;p}^{\alpha;\mathrm{II}}[z - z_1])}{j \sin(k_{z;p}^{\alpha;\mathrm{II}}[z_1 - z_2'])}, \end{aligned} \tag{6.41}$$

In the numerical consideration we put $z_1' = z_1$ and $z_2' = z_2$, see the limit proces in Sec.6.3.1. This gives rise to

$$I_p^{\alpha;\mathrm{II}}(z) = \frac{Y_{\infty;p}^{\alpha;\mathrm{II}}}{j \sin(k_{z;p}^{\alpha;\mathrm{II}}[z_1 - z_2])} \left(v_p^{\alpha;\mathrm{II}}(z_1) \cos(k_{z;p}^{\alpha;\mathrm{II}}[z - z_2]) + v_p^{\alpha;\mathrm{II}}(z_2) \cos(k_{z;p}^{\alpha;\mathrm{II}}[z - z_1]) \right). \tag{6.42}$$

and for the modal voltage coefficient we get according to Eq.(6.15)

$$V_p^{\alpha;\mathrm{II}}(z) = \frac{1}{\sin(k_{z;p}^{\alpha;\mathrm{II}}[z_1 - z_2])} \left(v_p^{\alpha;\mathrm{II}}(z_1) \sin(k_{z;p}^{\alpha;\mathrm{II}}[z - z_2]) - v_p^{\alpha;\mathrm{II}}(z_2) \sin(k_{z;p}^{\alpha;\mathrm{II}}[z - z_1]) \right). \tag{6.43}$$

valid for $z_1 \leq z \leq z_2$.

6.3.3 Section III

Consider Fig.(6.5). The derivation of the modal current and voltage coefficients for section-

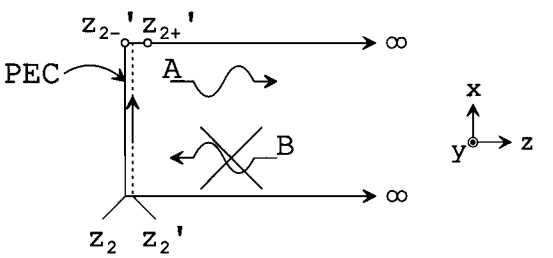

Figure 6.5: *Waveguide section III with magnetic a dipole on an infinitesimal distance form the PEC. Indicated are the waves generated by the dipole.*

III goes in exactly the same as for section-I. The only difference is that the dipole now radiates in the positive z-direction instead of the negative. As a consequence, the homogeneous solution that must be used is

$$I(z) = Ae^{-jk_z(z - z_2')} \qquad z > z_2', \tag{6.44}$$

Next, by using the two boundary conditions, the one at infinity and the one at the source location, the unknown amplitude term A can be recovered and is presented in Eq.(6.21). The solution of this amplitude factor leads us, in fact again to a modal Green's function expression, which then is used to find the modal current and voltage coefficients, as in Eq.(6.26), yielding

$$I_l^{\alpha;\mathrm{III}}(z) = -Y_{\infty;l}^{\alpha;\mathrm{III}}\, v_l^{\alpha;\mathrm{III}}(z_2)\, e^{-jk_{z;l}^{\alpha;\mathrm{III}}(z-z_2)}, \tag{6.45}$$

$$V_l^{\alpha;\mathrm{III}}(z) = v_l^{\alpha;\mathrm{III}}(z_2)\, e^{-jk_{z;l}^{\alpha;\mathrm{III}}(z-z_2)} \tag{6.46}$$

for $z \geq z_2$ and with $v_l^{\alpha;\mathrm{III}}(z_2) =< \tilde{\mathbf{M}}_2(\boldsymbol{\rho}, z_2), \mathbf{h}_l^{\alpha;\mathrm{III}} >$. Note that l is the mode number indicator for section-III.

6.4 Method of Moments formulation

We have arrived at the point from where we can determine the unknown equivalent magnetic surface currents of Fig.(6.1). There is one boundary condition left that has not yet been considered and that still needs to be satisfied. This is the continuity of the total tangential magnetic field over the apertures at $z = z_1$ and $z = z_2$. The conditions are stated below

$$\mathbf{n} \times \mathbf{H}^{\mathrm{I};tot}(\mathbf{r})\Big|_{z=z_1} = \mathbf{n} \times \mathbf{H}^{\mathrm{II};tot}(\mathbf{r})\Big|_{z=z_1} \qquad \mathbf{r} \in S_1^a, \tag{6.47}$$

$$\mathbf{n} \times \mathbf{H}^{\mathrm{II};tot}(\mathbf{r})\Big|_{z=z_2} = \mathbf{n} \times \mathbf{H}^{\mathrm{III};tot}(\mathbf{r})\Big|_{z=z_2} \qquad \mathbf{r} \in S_2^a, \tag{6.48}$$

with S_1^a and S_2^a defined as the surfaces of the apertures closed with thin PEC walls at resp. z_1 and z_2. First, we will work out Eq.(6.47) and by analogy a solution is found for Eq.(6.48).

Junction I → II

Eq.(6.47) is rewritten to

$$\left(\mathbf{H}_t^{\mathrm{I};inc} + \mathbf{H}_t^{\mathrm{I}}(\hat{\mathbf{M}}_1) - \mathbf{H}_t^{\mathrm{II}}(\tilde{\mathbf{M}}_1, \hat{\mathbf{M}}_2)\right)\Big|_{z=z_1} = \mathbf{0}. \tag{6.49}$$

Subscript t stand for *tangential*, which in this case is transverse. The total transverse field in section-I is split up in an incident field denoted by "*inc*" and a field constituent depending on the surface current density $\hat{\mathbf{M}}_1$, see Fig.(6.1). The total transverse magnetic field in section-II at z_1, is reformulated as being dependent of surface current densities $\tilde{\mathbf{M}}_1$ and $\hat{\mathbf{M}}_2$. Eq.(6.49) will be solved numerically by the method of moments. Therefore we introduce a so called *residue* $\mathbf{R}(\mathbf{r})$.

$$\mathbf{R}(\mathbf{r}) = \left(\mathbf{H}_t^{\mathrm{I};inc} + \mathbf{H}_t^{\mathrm{I}}(\hat{\mathbf{M}}_1) - \mathbf{H}_t^{\mathrm{II}}(\tilde{\mathbf{M}}_1, \hat{\mathbf{M}}_2)\right)\Big|_{z=z_1}. \tag{6.50}$$

The residue must be zero on S_1^a. This is somewhat too restrictive so the demand is weakened by weighting the residue to zero with the help of a set of test functions $\mathbf{w}_s(\mathbf{r})$, according

$$\langle \mathbf{R}(\mathbf{r}), \mathbf{w}_s(\mathbf{r}) \rangle = \int_{S^a} \mathbf{R}(\mathbf{r}) \cdot \mathbf{w}_s^*(\mathbf{r}) dA = 0, \tag{6.51}$$

for $s \in \{1, \ldots, N\}$. The test functions are defined unequal to zero on the aperture, $\mathbf{r} \in S_1^a$, and zero elsewhere. Eq.(6.49) therefore becomes

$$\left\langle \mathbf{H}_t^{\mathrm{I};inc}, \mathbf{w}_s \right\rangle + \left\langle \left(\mathbf{H}_t^{\mathrm{I}}(\hat{\mathbf{M}}_1) - \mathbf{H}_t^{\mathrm{II}}(\tilde{\mathbf{M}}_1, \hat{\mathbf{M}}_2) \right), \mathbf{w}_s \right\rangle \Big|_{z=z_1} = \mathbf{0}, \tag{6.52}$$

and because $\mathbf{H}_t^{\mathrm{II}}$ is defined according Eq.(4.66) with $I_i^{\alpha}(z)$ in Eq.(6.42), linearity can be applied, yielding

$$\left\langle \mathbf{H}_t^{\mathrm{I};inc}, \mathbf{w}_s \right\rangle + \left\langle \left(\mathbf{H}_t^{\mathrm{I}}(\hat{\mathbf{M}}_1) - \mathbf{H}_t^{\mathrm{II}}(\tilde{\mathbf{M}}_1) \right), \mathbf{w}_s \right\rangle - \left\langle \mathbf{H}_t^{\mathrm{II}}(\hat{\mathbf{M}}_2), \mathbf{w}_s \right\rangle \Big|_{z=z_1} = \mathbf{0}. \tag{6.53}$$

Subsequently the modal representation of the magnetic field is invoked, Sec.4.4, yielding

$$\left\langle \mathbf{H}_t^{\mathrm{I};inc}, \mathbf{w}_s \right\rangle + \left\langle \left(\sum_i I_i^{\alpha;\mathrm{I}}(\hat{\mathbf{M}}_1)\mathbf{h}_i^{\alpha;\mathrm{I}} - \sum_p I_p^{\alpha;\mathrm{II}}(\tilde{\mathbf{M}}_1)\mathbf{h}_p^{\alpha;\mathrm{II}} \right), \mathbf{w}_s \right\rangle - \left\langle \sum_p I_p^{\alpha;\mathrm{II}}(\hat{\mathbf{M}}_2)\mathbf{h}_p^{\alpha;\mathrm{II}}, \mathbf{w}_s \right\rangle \Big|_{z=z_1} = \mathbf{0}, \tag{6.54}$$

where

$$I_i^{\alpha;\mathrm{I}} = -Y_{\infty;i}^{\alpha;\mathrm{I}} \left\langle \hat{\mathbf{M}}_1, \mathbf{h}_i^{\alpha;\mathrm{I}} \right\rangle e^{jk_{z;i}^{\alpha;\mathrm{I}}(z-z_1)}, \tag{6.55}$$

$$I_p^{\alpha;\mathrm{II}} = \frac{Y_{\infty;p}^{\alpha;\mathrm{II}}}{j \sin(k_{z;p}^{\alpha;\mathrm{II}}[z_1 - z_2])} \Big(\left\langle \tilde{\mathbf{M}}_1, \mathbf{h}_p^{\alpha;\mathrm{II}} \right\rangle \cos(k_{z;p}^{\alpha;\mathrm{II}}[z - z_2]) + \left\langle \hat{\mathbf{M}}_2, \mathbf{h}_p^{\alpha;\mathrm{II}} \right\rangle \cos(k_{z;p}^{\alpha;\mathrm{II}}[z - z_1]) \Big). \tag{6.56}$$

The second step in the MoM is expansion of the unknown magnetic currents. We introduce

$$\hat{\mathbf{M}}_1(\boldsymbol{\rho}) = \sum_r m_r \mathbf{f}_r(\boldsymbol{\rho}) \qquad \boldsymbol{\rho} \in S_1^a, \tag{6.57}$$

$$\hat{\mathbf{M}}_2(\boldsymbol{\rho}) = \sum_q m_q \mathbf{f}_q(\boldsymbol{\rho}) \qquad \boldsymbol{\rho} \in S_2^a, \tag{6.58}$$

in which $\mathbf{f}_r$, $\mathbf{f}_q$ form complete sets of vectorial basis functions and m_r, m_q are the unknown expansion coefficients, which will be solved by the method of moments and $r = q \in \{1, \ldots, N\}$. Then, applying Eqs.(6.55)-(6.58) to Eq.(6.54) and invoking the relation found

in Eq.(2.6) yields

$$-\left\langle \mathbf{H}_t^{\mathrm{I};inc}, \mathbf{w}_s \right\rangle \Big|_{z=z_1} = \Bigg\{ -\sum_r m_r \sum_i Y_{\infty;i}^{\alpha;\mathrm{I}} \left\langle \mathbf{f}_r, \mathbf{h}_i^{\alpha;\mathrm{I}} \right\rangle \left\langle \mathbf{h}_i^{\alpha;\mathrm{I}}, \mathbf{w}_s \right\rangle e^{jk_{z;i}^{\alpha;\mathrm{I}}(z-z_1)} + \sum_r m_r \sum_p \frac{Y_{\infty;p}^{\alpha;\mathrm{II}} \cos(k_{z;p}^{\alpha;\mathrm{II}}[z-z_2])}{j \sin(k_{z;p}^{\alpha;\mathrm{II}}[z_1-z_2])} \left\langle \mathbf{f}_r, \mathbf{h}_p^{\alpha;\mathrm{II}} \right\rangle \left\langle \mathbf{h}_p^{\alpha;\mathrm{II}}, \mathbf{w}_s \right\rangle - \sum_q m_q \sum_p \frac{Y_{\infty;p}^{\alpha;\mathrm{II}} \cos(k_{z;p}^{\alpha;\mathrm{II}}[z-z_1])}{j \sin(k_{z;p}^{\alpha;\mathrm{II}}[z_1-z_2])} \left\langle \mathbf{f}_q, \mathbf{h}_p^{\alpha;\mathrm{II}} \right\rangle \left\langle \mathbf{h}_p^{\alpha;\mathrm{II}}, \mathbf{w}_s \right\rangle \Bigg\} \Bigg|_{z=z_1}. \tag{6.59}$$

In short hand notation, with $z = z_1$ we write

$$I_s^{\mathrm{I};ex} = \sum_r m_r T_{sr}^{\mathrm{I};\mathrm{II}} + \sum_q m_q T_{sq}^{\mathrm{II}}, \tag{6.60}$$

with the following definitions

$$\begin{aligned} T_{sr}^{\mathrm{I};\mathrm{II}} &= T_{sr;i}^{\mathrm{I}} + T_{sr;p}^{\mathrm{II}} \\ &= -\sum_i Y_{\infty;i}^{\alpha;\mathrm{I}} \Pi_{ri}^{\mathrm{I}} \Pi_{is}^{\mathrm{I}} + \sum_p \frac{Y_{\infty;p}^{\alpha;\mathrm{II}} \cos(k_{z;p}^{\alpha;\mathrm{II}}[z_1-z_2])}{j \sin(k_{z;p}^{\alpha;\mathrm{II}}[z_1-z_2])} \Pi_{rp}^{\mathrm{II}} \Pi_{ps}^{\mathrm{II}}, \end{aligned} \tag{6.61}$$

$$T_{sq}^{\mathrm{II}} = -\sum_p \frac{Y_{\infty;p}^{\alpha;\mathrm{II}}}{j \sin(k_{z;p}^{\alpha;\mathrm{II}}[z_1-z_2])} \Pi_{qp}^{\mathrm{II}} \Pi_{ps}^{\mathrm{II}}, \tag{6.62}$$

$$\Pi_{ri}^{\mathrm{I}} = \left\langle \mathbf{f}_r, \mathbf{h}_i^{\alpha;\mathrm{I}} \right\rangle, \tag{6.63}$$

$$\Pi_{is}^{\mathrm{I}} = \left\langle \mathbf{h}_i^{\alpha;\mathrm{I}}, \mathbf{w}_s \right\rangle, \tag{6.64}$$

$$\Pi_{rp}^{\mathrm{II}} = \left\langle \mathbf{f}_r, \mathbf{h}_p^{\alpha;\mathrm{II}} \right\rangle, \tag{6.65}$$

$$\Pi_{ps}^{\mathrm{II}} = \left\langle \mathbf{h}_p^{\alpha;\mathrm{II}}, \mathbf{w}_s \right\rangle, \tag{6.66}$$

$$\Pi_{qp}^{\mathrm{II}} = \left\langle \mathbf{f}_q, \mathbf{h}_p^{\alpha;\mathrm{II}} \right\rangle, \tag{6.67}$$

$$I_s^{\mathrm{I};ex} = -\left\langle \mathbf{H}_t^{\mathrm{I};inc}, \mathbf{w}_s \right\rangle, \tag{6.68}$$

Junction II → III

The following step is satisfying the boundary condition in Eq.(6.48). By analogy with Eq.(6.49) and (6.50) we define a *residue* $\mathbf{R}(\mathbf{r})$, which must be zero on the aperture surface S_2^a, according

$$\mathbf{R}(\mathbf{r}) = \left(\mathbf{H}_t^{\mathrm{II}}(\tilde{\mathbf{M}}_1, \hat{\mathbf{M}}_2) - \mathbf{H}_t^{\mathrm{III}}(\tilde{\mathbf{M}}_2) - \mathbf{H}_t^{\mathrm{III};inc} \right) \Big|_{z=z_2}, \tag{6.69}$$

Then, the demand of the residue is being weakened according Eq.(6.51), the modal representation of the transverse magnetic field is being substituted and we apply the expansion of the magnetic currents yielding

$$
\begin{aligned}
-\left\langle \mathbf{H}_t^{\mathrm{III};inc}, \mathbf{w}_s \right\rangle \Big|_{z=z_2} = \Bigg\{ &+ \sum_r m_r \sum_p \frac{Y_{\infty;p}^{\alpha;\mathrm{II}} \cos(k_{z;p}^{\alpha;\mathrm{II}}[z-z_2])}{j \sin(k_{z;p}^{\alpha;\mathrm{II}}[z_1-z_2])} \left\langle \mathbf{f}_r, \mathbf{h}_p^{\alpha;\mathrm{II}} \right\rangle \left\langle \mathbf{h}_p^{\alpha;\mathrm{II}}, \mathbf{w}_s \right\rangle \\
&- \sum_q m_q \sum_p \frac{Y_{\infty;p}^{\alpha;\mathrm{II}} \cos(k_{z;p}^{\alpha;\mathrm{II}}[z-z_1])}{j \sin(k_{z;p}^{\alpha;\mathrm{II}}[z_1-z_2])} \left\langle \mathbf{f}_q, \mathbf{h}_p^{\alpha;\mathrm{II}} \right\rangle \left\langle \mathbf{h}_p^{\alpha;\mathrm{II}}, \mathbf{w}_s \right\rangle \\
&+ \sum_q m_q \sum_l Y_{\infty;l}^{\alpha;\mathrm{III}} \left\langle \mathbf{f}_q, \mathbf{h}_l^{\alpha;\mathrm{III}} \right\rangle \left\langle \mathbf{h}_l^{\alpha;\mathrm{III}}, \mathbf{w}_s \right\rangle e^{jk_{z;l}^{\alpha;\mathrm{III}}(z-z_2)} \Bigg\} \Big|_{z=z_2}.
\end{aligned}
\tag{6.70}
$$

In short hand notation, with $z = z_2$, one obtain

$$
I_s^{\mathrm{III};ex} = \sum_r m_r T_{sr}^{\mathrm{II}} + \sum_q m_q T_{sq}^{\mathrm{II;III}}, \tag{6.71}
$$

with the definitions

$$
T_{sr}^{\mathrm{II}} = \sum_p \frac{Y_{\infty;p}^{\alpha;\mathrm{II}}}{j \sin(k_{z;p}^{\alpha;\mathrm{II}}[z_1-z_2])} \Pi_{rp}^{\mathrm{II}} \Pi_{ps}^{\mathrm{II}}, \tag{6.72}
$$

$$
\begin{aligned}
T_{sq}^{\mathrm{II;III}} &= T_{sq;p}^{\mathrm{II}} + T_{sq;l}^{\mathrm{III}} \\
&= -\sum_p \frac{Y_{\infty;p}^{\alpha;\mathrm{II}} \cos(k_{z;p}^{\alpha;\mathrm{II}}[z_2-z_1])}{j \sin(k_{z;p}^{\alpha;\mathrm{II}}[z_1-z_2])} \Pi_{qp}^{\mathrm{II}} \Pi_{ps}^{\mathrm{II}} + \sum_l Y_{\infty;l}^{\alpha;\mathrm{III}} \Pi_{ql}^{\mathrm{III}} \Pi_{ls}^{\mathrm{III}},
\end{aligned}
\tag{6.73}
$$

$$
\Pi_{ql}^{\mathrm{III}} = \left\langle \mathbf{f}_q, \mathbf{h}_l^{\alpha;\mathrm{III}} \right\rangle, \tag{6.74}
$$

$$
\Pi_{ls}^{\mathrm{III}} = \left\langle \mathbf{h}_l^{\alpha;\mathrm{III}}, \mathbf{w}_s \right\rangle, \tag{6.75}
$$

$$
I_s^{\mathrm{III};ex} = -\left\langle \mathbf{H}_t^{\mathrm{III};inc}, \mathbf{w}_s \right\rangle. \tag{6.76}
$$

Consequently, we have to solve the following system of equations as a consequence of the method of moments

$$
\begin{aligned}
I_s^{\mathrm{I};ex} &= \sum_r m_r T_{sr}^{\mathrm{I;II}} + \sum_q m_q T_{sq}^{\mathrm{II}}, \\
I_s^{\mathrm{III};ex} &= \sum_r m_r T_{sr}^{\mathrm{II}} + \sum_q m_q T_{sq}^{\mathrm{II;III}},
\end{aligned}
\tag{6.77}
$$

for $s \in \{1, \ldots, (r+q)\}$.

Excitation

The excitation fields, $I_s^{\mathrm{I};ex}$ and $I_s^{\mathrm{III};ex}$ are transverse magnetic fields weighted with a test function. They come from respectively $z = -\infty$ and $z = \infty$, and are incident on the junctions at $z = z_1$ and $z = z_2$, respectively, and then reflected in the direction where they came from, see Fig.(6.6). By applying the modal representation to the incident magnetic

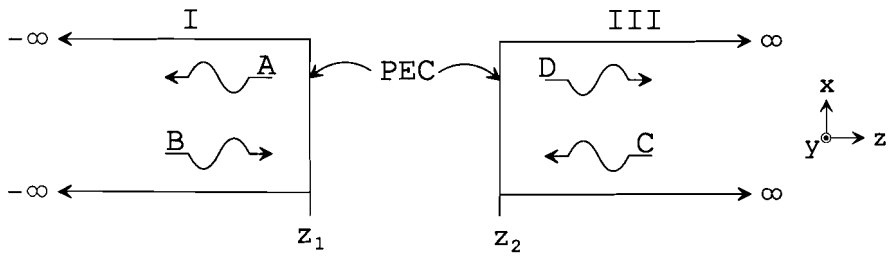

Figure 6.6: *Incident and reflected waves of the magnetic excitation fields in waveguide section-I and -III. Amplitude coefficient A and C represents V^- and B and D represents V^+.*

fields one finds for Eq.(6.68) and (6.76)

$$I_s^{\mathrm{I};ex} = -\sum_i I_i^{\alpha;\mathrm{I}} \left\langle \mathbf{h}_i^{\alpha;\mathrm{I}}, \mathbf{w}_s \right\rangle, \tag{6.78}$$

$$I_s^{\mathrm{III};ex} = -\sum_l I_l^{\alpha;\mathrm{III}} \left\langle \mathbf{h}_l^{\alpha;\mathrm{III}}, \mathbf{w}_s \right\rangle. \tag{6.79}$$

assuming that interchanging the summation and the integration is allowed. The homogeneous modal voltage and current wave equations, Eq.(6.3)-(6.4), yield per mode

$$V^{\mathrm{I}}(z) = V^- e^{jk_z(z-z_1)} + V^+ e^{-jk_z(z-z_1)} \qquad z \le z_1, \tag{6.80}$$

$$\begin{aligned} I^{\mathrm{I}}(z) &= I^- e^{jk_z(z-z_1)} + I^+ e^{-jk_z(z-z_1)} \\ &= Y_\infty^{\mathrm{I}}(-V^- e^{jk_z(z-z_1)} + V^+ e^{-jk_z(z-z_1)}) \\ &= Y_\infty^{\mathrm{I}}(-Ae^{jk_z(z-z_1)} + Be^{-jk_z(z-z_1)}) \quad z \le z_1, \end{aligned} \tag{6.81}$$

$$V^{\mathrm{III}}(z) = V^- e^{jk_z(z-z_2)} + V^+ e^{-jk_z(z-z_2)} \qquad z \ge z_2, \tag{6.82}$$

$$I^{\mathrm{III}}(z) = Y_\infty^{\mathrm{II}}(-Ce^{jk_z(z-z_2)} + De^{-jk_z(z-z_2)}) \quad z \ge z_2, \tag{6.83}$$

By evaluating Eq.(6.80) and (6.82) on resp. z_1 and z_2 we find

$$\left.\begin{array}{ll} V^{\mathrm{I}}(z_1) & = 0 = V^- + V^+, \\ V^{\mathrm{III}}(z_2) & = 0 = V^- + V^+, \end{array}\right\} \longrightarrow \Gamma = \frac{V^-}{V^+} = \frac{A}{B} = \frac{C}{D} - 1, \tag{6.84}$$

Γ is the so-called the reflection coefficient. For I^{I} and I^{III} on resp. z_1 and z_2, this means

$$I^{\mathrm{I}}(z_1) = 2BY_\infty, \tag{6.85}$$

$$I^{\mathrm{III}}(z_2) = -2CY_\infty, \tag{6.86}$$

leading to the final form of the excitation fields

$$I_s^{\mathrm{I};ex} = -\sum_i 2B_i^{\alpha} Y_{\infty;i}^{\alpha;\mathrm{I}} \Pi_{is}^{\mathrm{I}}, \tag{6.87}$$

$$I_s^{\mathrm{III};ex} = -\sum_l -2C_l^{\alpha} Y_{\infty;l}^{\alpha;\mathrm{III}} \Pi_{ls}^{\mathrm{III}}. \tag{6.88}$$

6.4.1 Matrix representation

The system of equations in Eq.(6.77) can be cast into a matrix-vector form $A\mathbf{x} = \mathbf{b}$, from which the unknown vector x, representing the unknown current coefficients, must be solved. Before we can do this we have to look at the definitions we made, Eqs.(6.61)-(6.68) and Eqs.(6.72)-(6.76), to determine what they become in matrix notation, but we begin with some a priori information. By applying the MoM we used $2r$[1] expansion functions and weighted with $2s$ testing functions we know for a fact that matrix A will have dimensions $(2s \times 2r)$, the coefficient vector x, $(2r \times 1)$ and the source vector b, $(2s \times 1)$.

Observing Eqs.(6.61), (6.62), (6.72) and (6.73), we notice that they have the following general structure, $T_{xy} = \sum_j l_j M_{yj} N_{jx}$. It is evident that M_{yj} and N_{jx} correspond to the "Π" constituents. With this knowledge, we're left with l_j. Since T, M and N are all matrices, l_j must also be a matrix otherwise we have contradiction with T being a matrix. Therefore we define

$$[L]_{jj} = l_j \, \delta_{ji}, \qquad i = j, \tag{6.89}$$

indicating that L is a diagonal matrix with dimensions $(j \times j)$. You see that we use the subscript indices as an indication for the dimensions of the matrices. Having deduced all sizes and looking back to the general expression for T we find that $[T]_{xy} \neq [M]_{yj}[L]_{jj}[N]_{jx}$. In order to solve this the transpose, indicated with superscript 'T', has to be taken of the right-hand side

$$[T]_{xy} = \Big([M]_{yj}[L]_{jj}[N]_{jx}\Big)^{\mathrm{T}} = [N]_{jx}^{\mathrm{T}}[L]_{jj}[M]_{yj}^{\mathrm{T}} = [N]_{xj}[L]_{jj}[M]_{jy}. \tag{6.90}$$

Note that the subscript indices change of order after the matrix is transposed. Now we are prepared to represent the problem in matrix form. Eq.(6.77) becomes

$$\begin{bmatrix} [T^{\mathrm{I;II}}]_{sr} & [T^{\mathrm{II}}]_{sq} \\ [T^{\mathrm{II}}]_{sr} & [T^{\mathrm{II;III}}]_{sq} \end{bmatrix} \begin{bmatrix} [m]_r \\ [m]_q \end{bmatrix} = \begin{bmatrix} [I^{\mathrm{I};ex}]_s \\ [I^{\mathrm{III};ex}]_s \end{bmatrix} \tag{6.91}$$

In Appendix G a survey of the intermediate matrices is presented. Appendix E discusses the integrals of Eqs.(6.63)-(6.67) and (6.74)-(6.75) and gives a detailed derivation.

We choose the set of expansion functions equal to the set of test functions. This particular choice is known as Garlerkin's methode [15]. Equal sets of expansion and test functions implies, $r = q = s \in \{1, \ldots, N\}$, as for the mode numbers, used for the field

[1]Note that it should be $r + q$, but earlier on we have defined $r = q$.

expansion, we choose, $i \in \{1,\ldots,M^{\mathrm{I}}\}$, $p \in \{1,\ldots,N\}$ and $l \in \{1,\ldots,M^{\mathrm{III}}\}$. All the indices just mentioned will take on a finite value, are truncated, because the computer is finite and also the memory capacity.

6.4.2 Basis functions

During the formulation of the method of moments in the preceding section we encountered expansion functions, to approximate the unknown magnetic currents, and test functions, which weakened the continuity equation of the magnetic field. We used the same set of functions to cover the both. These, so-called, basis functions should eventually form a complete set in the solution space.

In general, two types of basis functions can be distinguished, entire domain basis functions and subdomain basis functions. The entire domain functions are non-zero over the entire domain, S_1^a, S_2^a, of the unknown function, $\mathbf{M}_1$, $\mathbf{M}_2$. The subdomain functions, on the contrary, differ from zero on only a small subsection of the domain of the unknown function. These subdomain basis functions offer great flexibility when it comes down to the analysis of arbitrary shaped domains, however, often a lot of these subdomain basis functions are needed which could cause excessive computation times and memory problems. In case of entire domain basis functions the number of functions needed is usually much lower.

For the iris problem we have used the mode functions of the magnetic field of section-II as entire domain basis functions. They form good basis functions because we saw that they form a complete set, the functions are zero on the edge, ∂S^a, of the domain of the unknown function so no current can leak from the domain and there are no line charges. Also, the divergence is limited because the domain is finite. Below they are summarised

$$\mathbf{f}_r = \mathbf{w}_s = \mathbf{h}^{\alpha} = \begin{cases} \mathbf{h}'^{\mathrm{II}} = \frac{-2}{k_t'^{\mathrm{II}}\sqrt{AB}} \begin{bmatrix} -k_y^{\mathrm{II}} \sin(k_x^{\mathrm{II}} x)\cos(k_y^{\mathrm{II}} y)\mathbf{a}_x \\ k_x^{\mathrm{II}} \cos(k_x^{\mathrm{II}} x)\sin(k_y^{\mathrm{II}} y)\mathbf{a}_y \end{bmatrix}, \\ \mathbf{h}''^{\mathrm{II}} = \frac{\sqrt{\epsilon_m \epsilon_n}}{k_t''^{\mathrm{II}}\sqrt{AB}} \begin{bmatrix} k_x^{\mathrm{II}} \sin(k_x^{\mathrm{II}} x)\cos(k_y^{\mathrm{II}} y)\mathbf{a}_x \\ k_y^{\mathrm{II}} \cos(k_x^{\mathrm{II}} x)\sin(k_y^{\mathrm{II}} y)\mathbf{a}_y \end{bmatrix}. \end{cases} \tag{6.92}$$

Now that the choice of basis-functions is known, we can say something more about the integrals in Eqs.(6.63)-(Eq.5.4.21) and (6.74)-(6.75). They have a more or less matching character. Waveguide modes of two different sections are being weighted, which yields a scalar coefficient, indicating the contribution of mode i in section-I to mode j in section-II. Moreover, when there is no change in cross-section between the two sections there is no mode coupling between the modes of section-I and -II, what results in diagonal matrices. This seems all a bit trivial, because no distortion means no disruption of the waves, of course. Should there be a disturbance in the cross-section, completely filled matrices will be the result. The same applies for the junction between section-II and -III.

6.5 S-matrix notation

In order to couple the separate modules together, a scattering parameter formulation of each part has to be found. This can be realised by constructing S-matrices. By connecting the ports of the S-matrices in the proper manner, we can evaluated the behavior of the modes on the, new formed, port surfaces of the total coupled system.

In general, the S-matrix formulation is written as

$$[I^{out}] = [S][I^{in}], \tag{6.93}$$

indicating that the outgoing waves represented by I^{out} are due to the incoming waves represented by I^{in}. For the iris, we can write

$$\begin{bmatrix} I^{\mathrm{I};out} \\ I^{\mathrm{III};out} \end{bmatrix} = \begin{bmatrix} s_{11} & s_{12} \\ s_{21} & s_{22} \end{bmatrix} \begin{bmatrix} I^{\mathrm{I};in} \\ I^{\mathrm{III};in} \end{bmatrix}. \tag{6.94}$$

The vector on the left-hand side contains the amplitudes of the outgoing waves on the surface of port 1, in waveguide section-I (upper) and on the surface of port 2, in waveguide section-III (lower), s_{**} are the different scattering parameters, and the vector on the right-hand side contains the amplitudes of the incident waves on the surface of port 1 in section-I (upper) and on the surface of port 2 in section-III (lower). Usually S-matrices are given for the electric field (V), but because we have made an analysis based on the magnetic field (I) we will derive a scattering description based on magnetic field waves.

6.5.1 Incoming and outgoing waves port 1

With the derivation coming up port 1 of the S-matrix lies in section-I directly against the junction between I and II. Port 2 lies in section-III also directly against the junction from III to II. We will start with the description of the incoming and outgoing waves on the surface of port 1, i.e. an amplitude description of the waves on the port surfaces. Fig.6.7 is put in to clarify. With the incident waves we mean the total of waves travelling in the

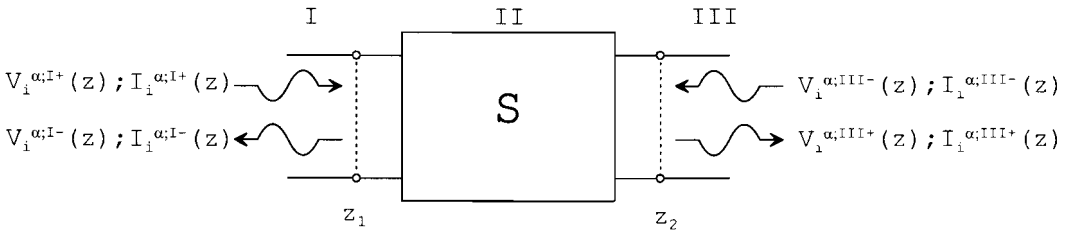

Figure 6.7: *Incident and reflected waves of the magnetic excitation fields in waveguide section I and II. Amplitude coefficient A represents V^- and B represents V^+.*

positive z-direction, indicated with the superscript '+'. The scattered waves correspond

to the total of waves travelling in the negative z-direction, indicated with the superscript '-'. First, a derivation per mode will be given, followed by a matrix notation.

The incoming waves are just the incident waves, but the outgoing waves, because of our modelling technique, consist of the incident waves who are reflected against the PEC wall and waves generated by the equivalent magnetic surface current $\hat{\mathbf{M}}_1$. A description for the incoming and the reflection of the incoming waves can be found with the help of the homogeneous Helmholtz equation. A description of the waves generated by the magnetic current can be found with the inhomogeneous Helmholtz equation, as we have already done in Sec.6.3.1. Eqs.(6.3) and (6.4) yield the homogeneous solutions, per mode, indicated with index 'h'

$$V_i^{\alpha;\mathrm{I};h}(z) = V_i^{\alpha;\mathrm{I}-} e^{jk_{z;i}^{\alpha;\mathrm{I}}(z-z_1)} + V_i^{\alpha;\mathrm{I}+} e^{-jk_{z;i}^{\alpha;\mathrm{I}}(z-z_1)} \qquad z \leq z_1, \tag{6.95}$$

$$I_i^{\alpha;\mathrm{I};h}(z) = Y_{\infty;i}^{\alpha;\mathrm{I}} \left[-V_i^{\alpha;\mathrm{I}-} e^{jk_{z;i}^{\alpha;\mathrm{I}}(z-z_1)} + V_i^{\alpha;\mathrm{I}+} e^{-jk_{z;i}^{\alpha;\mathrm{I}}(z-z_1)} \right] \; z \leq z_1, \tag{6.96}$$

with $V_i^{\alpha;\mathrm{I}-} = A$ and $V_i^{\alpha;\mathrm{I}+} = B$ derived on p.58. From this, we known that the reflection coefficient is $\Gamma = -1$, leading us to

$$I_i^{\alpha;\mathrm{I};h}(z) = B_i^{\alpha} Y_{\infty;i}^{\alpha;\mathrm{I}} \left[e^{jk_{z;i}^{\alpha;\mathrm{I}}(z-z_1)} + e^{-jk_{z;i}^{\alpha;\mathrm{I}}(z-z_1)} \right], \qquad z \leq z_1, \tag{6.97}$$

$$= I_i^{\alpha;\mathrm{I};h-}(z) + I_i^{\alpha;\mathrm{I};h+}(z). \tag{6.98}$$

The particular solution, derived form Eq.(6.26), is

$$I_i^{\alpha;\mathrm{I};p}(z) = -Y_{\infty;i}^{\alpha;\mathrm{I}} \left\langle \hat{\mathbf{M}}_1, \mathbf{h}_i^{\alpha;\mathrm{I}} \right\rangle e^{jk_{z;i}^{\alpha;\mathrm{I}}(z-z_1)}, \tag{6.99}$$

$$= -Y_{\infty;i}^{\alpha;\mathrm{I}} \sum_r m_r \left\langle \mathbf{f}_r, \mathbf{h}_i^{\alpha;\mathrm{I}} \right\rangle e^{jk_{z;i}^{\alpha;\mathrm{I}}(z-z_1)} = I_i^{\alpha;\mathrm{I};p-}(z) \quad \text{for} \quad z \leq z_1. \tag{6.100}$$

The total description of all the waves going through the waveguide cross-section in section-I at some arbitrary point $z \leq z_1$, is

$$\begin{aligned} I_i^{\alpha;\mathrm{I}}(z) = I_i^{\alpha;\mathrm{I};h}(z) + I_i^{\alpha;\mathrm{I};p}(z) &= I_i^{\alpha;\mathrm{I};h-}(z) + I_i^{\alpha;\mathrm{I};h+}(z) + I_i^{\alpha;\mathrm{I};p-}(z) \\ &= I_i^{\alpha;\mathrm{I};h+}(z) + \{I_i^{\alpha;\mathrm{I};h-}(z) + I_i^{\alpha;\mathrm{I};p-}(z)\} \\ &= I_i^{\alpha;\mathrm{I};+}(z) + I_i^{\alpha;\mathrm{I};-}(z). \end{aligned} \tag{6.101}$$

with

$$I_i^{\alpha;\mathrm{I};+}(z) = B_i^{\alpha} Y_{\infty;i}^{\alpha;\mathrm{I}} e^{-jk_{z;i}^{\alpha;\mathrm{I}}(z-z_1)} \qquad z \leq z_1, \tag{6.102}$$

$$I_i^{\alpha;\mathrm{I};-}(z) = B_i^{\alpha} Y_{\infty;i}^{\alpha;\mathrm{I}} e^{jk_{z;i}^{\alpha;\mathrm{I}}(z-z_1)} - Y_{\infty;i}^{\alpha;\mathrm{I}} \sum_r m_r \Pi_{ri}^{\mathrm{I}} e^{jk_{z;i}^{\alpha;\mathrm{I}}(z-z_1)} \quad z \leq z_1. \tag{6.103}$$

Eqs.(6.102) and (6.103) evaluated at $z = z_1$ yields

$$I_i^{\alpha;\mathrm{I};+}(z_1) = B_i^{\alpha} Y_{\infty;i}^{\alpha;\mathrm{I}} = I_i^{\mathrm{I};in}, \tag{6.104}$$

$$I_i^{\alpha;\mathrm{I};-}(z_1) = B_i^{\alpha} Y_{\infty;i}^{\alpha;\mathrm{I}} - Y_{\infty;i}^{\alpha;\mathrm{I}} \sum_r m_r \Pi_{ri}^{\mathrm{I}} = I_i^{\mathrm{I};out}. \tag{6.105}$$

6.5.2 Incoming and outgoing waves port 2

At port2, the incoming waves are the total of waves travelling in the negative z-direction, superscript indication is '-'. The outgoing waves are the total of waves travelling in the positive z-direction. The incoming and outgoing waves and the way they are built up is similar to the description of the preceding section, except now the outgoing waves are partially caused by equivalent magnetic current $\tilde{\mathbf{M}}_2$. For the homogenous part we have

$$\begin{aligned} I_l^{\alpha;\mathrm{III};\mathrm{h}}(z) &= Y_{\infty;l}^{\alpha;\mathrm{III}} \left[-V_l^{\alpha;\mathrm{III}-} e^{jk_{z;l}^{\alpha;\mathrm{III}}(z-z_2)} + V_l^{\alpha;\mathrm{III}+} e^{-jk_{z;l}^{\alpha;\mathrm{III}}(z-z_2)} \right] \\ &= -C_l^{\alpha} Y_{\infty;l}^{\alpha;\mathrm{III}} \left[e^{jk_{z;l}^{\alpha;\mathrm{III}}(z-z_2)} + e^{-jk_{z;l}^{\alpha;\mathrm{III}}(z-z_2)} \right], \\ &= I_l^{\alpha;\mathrm{III};h-}(z) + I_l^{\alpha;\mathrm{III};h+}(z), \qquad z \geq z_2, \end{aligned} \tag{6.106}$$

For the particular solution, with $\hat{\mathbf{M}}_2 = -\tilde{\mathbf{M}}_2$ substituted into Eq.(6.45), we find

$$I_l^{\alpha;\mathrm{III};p}(z) = Y_{\infty;l}^{\alpha;\mathrm{III}} \left\langle \tilde{\mathbf{M}}_2, \mathbf{h}_l^{\alpha;\mathrm{III}} \right\rangle e^{jk_{z;l}^{\alpha;\mathrm{III}}(z-z_2)}, \tag{6.107}$$

$$= Y_{\infty;l}^{\alpha;\mathrm{III}} \sum_q m_q \left\langle \mathbf{f}_q, \mathbf{h}_l^{\alpha;\mathrm{III}} \right\rangle e^{jk_{z;l}^{\alpha;\mathrm{III}}(z-z_2)} = I_l^{\alpha;\mathrm{III};p-}(z) \qquad z \geq z_2. \tag{6.108}$$

In a similar way, we can find a description for the waves going through the cross-section of waveguide section-III at some arbitrary point $z \geq z_2$. We obtain

$$I_l^{\alpha;\mathrm{III}}(z) = I_l^{\alpha;\mathrm{III};+}(z) + I_l^{\alpha;\mathrm{III};-}(z), \tag{6.109}$$

$$I_l^{\alpha;\mathrm{III};-}(z) = -C_l^{\alpha}\, Y_{\infty;l}^{\alpha;\mathrm{III}} e^{jk_{z;l}^{\alpha;\mathrm{III}}(z-z_2)}, \tag{6.110}$$

$$I_l^{\alpha;\mathrm{III};+}(z) = -C_l^{\alpha}\, Y_{\infty;l}^{\alpha;\mathrm{III}} e^{-jk_{z;l}^{\alpha;\mathrm{III}}(z-z_2)} + Y_{\infty;l}^{\alpha;\mathrm{III}} \sum_q m_q \Pi_{ql}^{\mathrm{III}}\, e^{-jk_{z;l}^{\alpha;\mathrm{III}}(z-z_2)}. \tag{6.111}$$

For $z = z_2$, Eqs.(6.110) and (6.111) yield

$$I_l^{\alpha;\mathrm{III};-}(z_2) = -C_l^{\alpha}\, Y_{\infty;l}^{\alpha;\mathrm{III}} = I_l^{\mathrm{III};in}, \tag{6.112}$$

$$I_l^{\alpha;\mathrm{III};+}(z_2) = -C_l^{\alpha}\, Y_{\infty;l}^{\alpha;\mathrm{III}} + Y_{\infty;l}^{\alpha;\mathrm{III}} \sum_q m_q \Pi_{ql}^{\mathrm{III}} = I_l^{\mathrm{III};out}. \tag{6.113}$$

From a structural point of view, the iris is a two port, on one end we've got waveguide section-I and on the other end of the double junction we've got waveguide section-III. However on an electromagnetic level it is a N-port, and 'N' is determined by the number of modes, i=p=l, we take into account in our model to describe the electromagnetic fields. The result of an electromagnetic field encountering, for instance, a waveguide junction along it's propagation path is interaction between the different modes of the two sections. Thereby, creating as a matter of fact a N-port. For a continuous homogeneous cross-section we have a 2-port for every mode.

6.5.3 S-parameters

In matrix-vector-notation the outgoing waves are represented as

$$[I^{\mathrm{I};out}]_i = [Y^{\mathrm{I}}]_{ii}[B^{\alpha}]_i - [Y^{\mathrm{I}}]_{ii}[\Pi^{\mathrm{I}}]^{\mathrm{T}}_{ri}[m]_r = [I^{\mathrm{I};in}]_i - [Y^{\mathrm{I}}]_{ii}[\Pi^{\mathrm{I}}]^{\mathrm{T}}_{ri}[m]_r, \tag{6.114}$$

$$[I^{\mathrm{III};out}]_l = [Y^{\mathrm{III}}]_{ll}[-C^{\alpha}]_l + [Y^{\mathrm{III}}]_{ll}[\Pi^{\mathrm{III}}]^{\mathrm{T}}_{ql}[m]_q = [I^{\mathrm{III};in}]_l + [Y^{\mathrm{III}}]_{ll}[\Pi^{\mathrm{III}}]^{\mathrm{T}}_{ql}[m]_q. \tag{6.115}$$

Then, from Eq.(6.91), expressions for the unknown current vectors can be obtained by writing out the equation as

$$[m]_r = -[T^{\mathrm{I;II}}]^{-1}_{rs}[I^{\mathrm{I};ex}]_s - [T^{\mathrm{I;II}}]^{-1}_{rs}[T^{\mathrm{II}}]_{sq}[m]_q, \tag{6.116}$$

$$[m]_q = -[T^{\mathrm{II;III}}]^{-1}_{qs}[I^{\mathrm{III};ex}]_s - [T^{\mathrm{II;III}}]^{-1}_{qs}[T^{\mathrm{II}}]_{sr}[m]_r. \tag{6.117}$$

Substituting Eqs.(6.116) and (6.117) into one another yields

$$[m]_r = [M]^{-1}_{rr}[T^{\mathrm{I;II}}]^{-1}_{rs}[I^{\mathrm{I};ex}]_s - [M]^{-1}_{rr}[T^{\mathrm{I;II}}]^{-1}_{rs}[T^{\mathrm{II}}]_{sq}[T^{\mathrm{II;III}}]^{-1}_{qs}[I^{\mathrm{III};ex}]_s, \tag{6.118}$$

$$[m]_q = [M]^{-1}_{qq}[T^{\mathrm{II;III}}]^{-1}_{qs}[I^{\mathrm{III};ex}]_s - [M]^{-1}_{qq}[T^{\mathrm{II;III}}]^{-1}_{qs}[T^{\mathrm{II}}]_{sr}[T^{\mathrm{I;II}}]^{-1}_{rs}[I^{\mathrm{I};ex}]_s. \tag{6.119}$$

with

$$[M]^{-1}_{rr} = \left[[\underline{I}]_{rr} - [T^{\mathrm{I;II}}]^{-1}_{rs}[T^{\mathrm{II}}]_{sq}[T^{\mathrm{II;III}}]^{-1}_{qs}[T^{\mathrm{II}}]_{sr}\right]^{-1}, \tag{6.120}$$

$$[M]^{-1}_{qq} = \left[[\underline{I}]_{qq} - [T^{\mathrm{II;III}}]^{-1}_{qs}[T^{\mathrm{II}}]_{sr}[T^{\mathrm{I;II}}]^{-1}_{rs}[T^{\mathrm{II}}]_{sq}\right]^{-1}. \tag{6.121}$$

$[\underline{I}]$ is the identity matrix and matrices $[I^{\mathrm{I};ex}]_s$, $[I^{\mathrm{III};ex}]_s$ can be found in Eqs.(G.21) and (G.22), respectively. Subsequently, applying Eqs.(6.118) and (6.119) to Eqs.(6.114) and (6.115), respectively, we obtain the S-parameters

$$[s_{11}]_{ii} = [\underline{I}]_{ii} + 2[Y^{\mathrm{I}}]_{ii}[\Pi^{\mathrm{I}}]^{\mathrm{T}}_{ri}[M]^{-1}_{rr}[T^{\mathrm{I;II}}]^{-1}_{rs}[\Pi^{\mathrm{I}}]^{\mathrm{T}}_{is}, \tag{6.122}$$

$$[s_{12}]_{il} = -2[Y^{\mathrm{I}}]_{ii}[\Pi^{\mathrm{I}}]^{\mathrm{T}}_{ri}[M]^{-1}_{rr}[T^{\mathrm{I;II}}]^{-1}_{rs}[T^{\mathrm{II}}]_{sq}[T^{\mathrm{II;III}}]^{-1}_{qs}[\Pi^{\mathrm{III}}]^{\mathrm{T}}_{ls}, \tag{6.123}$$

$$[s_{12}]_{li} = 2[Y^{\mathrm{III}}]_{ll}[\Pi^{\mathrm{III}}]^{\mathrm{T}}_{ql}[M]^{-1}_{qq}[T^{\mathrm{II;III}}]^{-1}_{qs}[T^{\mathrm{II}}]_{sr}[T^{\mathrm{II;III}}]^{-1}_{rs}[\Pi^{\mathrm{I}}]^{\mathrm{T}}_{is}, \tag{6.124}$$

$$[s_{22}]_{ll} = [\underline{I}]_{ll} - 2[Y^{\mathrm{III}}]_{ll}[\Pi^{\mathrm{III}}]^{T}_{ql}[M]^{-1}_{qq}[T^{\mathrm{II;III}}]^{-1}_{qs}[\Pi^{\mathrm{III}}]^{T}_{sl}. \tag{6.125}$$

6.5.4 Displacement of S-matrix ports

To gain some knowledge about the magnitude of the modes on a arbitrary point z, for $z \leq z_1$ and $z \geq z_2$, the ports of the S-matrix, which up till now were laid on the junctions z_1 and z_2, must be shifted to a desired place, for instance $z = z_0$ and $z = z_3$ with $z_0 \leq z_1$ and $z_3 \geq z_2$. This shifting of the ports will have an effect on the S-matrix. The distance over which the ports are displaced must be taken in to account by the S-matrix. As a result of the displacement of the ports, the waves encounter a phase shift. In Fig.(6.8) we can see that the present situation is

$$[I^{out}] = [S][I^{in}], \qquad [I^{out}] = \begin{bmatrix} [I^{\mathrm{I};out}]_n \\ [I^{\mathrm{III};out}]_n \end{bmatrix}, \qquad [I^{in}] = \begin{bmatrix} [I^{\mathrm{I};in}]_n \\ [I^{\mathrm{III};in}]_n \end{bmatrix}. \tag{6.126}$$

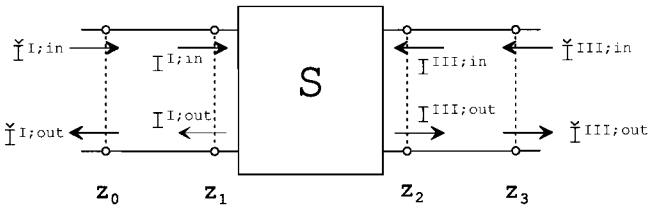

Figure 6.8: *Present ports at z_1, z_2 and new ports, shifted to locations z_0, z_3.*

where n just a general mode number indicator. The new situation will be

$$[\check{I}^{out}] = [\check{S}][\check{I}^{in}], \qquad [\check{I}^{out}] = \begin{bmatrix} [\check{I}^{\mathrm{I};out}]_n \\ [\check{I}^{\mathrm{III};out}]_n \end{bmatrix}, \qquad [\check{I}^{in}] = \begin{bmatrix} [\check{I}^{\mathrm{I};in}]_n \\ [\check{I}^{\mathrm{III};in}]_n \end{bmatrix}. \tag{6.127}$$

Per mode we can determine the phase shift. First we examine the incident waves.

$$I_n^{\alpha;\mathrm{I};in} = e^{-j\theta_n^{\alpha;\mathrm{I}}} \check{I}_n^{\alpha;\mathrm{I};in} \qquad \theta_n^{\alpha;\mathrm{I}} = k_{z;n}^{\alpha;\mathrm{I}}(z_1 - z_0), \tag{6.128}$$

$$I_n^{\alpha;\mathrm{III};in} = e^{-j\theta_n^{\alpha;\mathrm{III}}} \check{I}_n^{\alpha;\mathrm{III};in} \qquad \theta_n^{\alpha;\mathrm{III}} = k_{z;n}^{\alpha;\mathrm{III}}(z_3 - z_2), \tag{6.129}$$

where θ represents the electrical length of the outward shift of the ports. In Eqs.(6.128) and (6.129) we see a negative phase, together with the assumed time convention $e^{j\omega t}$ we have a positive electrical length. This corresponds to what we see in Fig.(6.8). For the new defined waves $\check{I}^{\mathrm{I};in}$, $\check{I}^{\mathrm{III};in}$, at the new position, to get at the position of the present defined waves $I^{\mathrm{I};in}$, $I^{\mathrm{III};in}$, they have to travel an extra distance. In matrix notation

$$\begin{bmatrix} [I^{\mathrm{I};in}]_n \\ [I^{\mathrm{III};in}]_n \end{bmatrix} = \begin{bmatrix} \left[e^{-j\theta^{\mathrm{I}}}\right]_{nn} & \emptyset \\ \emptyset & \left[e^{-j\theta^{\mathrm{III}}}\right]_{nn} \end{bmatrix} \begin{bmatrix} [\check{I}^{\mathrm{I};in}]_n \\ [\check{I}^{\mathrm{III};in}]_n \end{bmatrix}, \tag{6.130}$$

with

$$\left[e^{-j\theta^{\mathrm{I}}}\right]_{nn} = \left[e^{-j\theta_n^{\alpha;\mathrm{I}}}\,\delta_{nj}\right], \tag{6.131}$$

$$\left[e^{-j\theta^{\mathrm{III}}}\right]_{nn} = \left[e^{-j\theta_n^{\alpha;\mathrm{III}}}\,\delta_{nj}\right],. \tag{6.132}$$

For the outgoing waves we find

$$I_n^{\alpha;\mathrm{I};out} = e^{j\theta_n^{\alpha;\mathrm{I}}} \check{I}_n^{\alpha;\mathrm{I};out}, \tag{6.133}$$

$$I_n^{\alpha;\mathrm{III};out} = e^{j\theta_n^{\alpha;\mathrm{III}}} \check{I}_n^{\alpha;\mathrm{III};out}. \tag{6.134}$$

Now there is a positive phase. For the new defined waves, $\check{I}_n^{\alpha;\mathrm{I};out}$ and $\check{I}_n^{\alpha;\mathrm{III};out}$, to get to the position of the present defined waves, $I_n^{\alpha;\mathrm{I};out}$ and $I_n^{\alpha;\mathrm{III};out}$, means that they have travelled to what can be translated to a positive phase. In matrix notation we get

$$\begin{bmatrix} [I^{\mathrm{I};out}]_n \\ [I^{\mathrm{III};out}]_n \end{bmatrix} = \begin{bmatrix} \left[e^{j\theta^{\mathrm{I}}}\right]_{nn} & \emptyset \\ \emptyset & \left[e^{j\theta^{\mathrm{III}}}\right]_{nn} \end{bmatrix} \begin{bmatrix} [\check{I}^{\mathrm{I};out}]_n \\ [\check{I}^{\mathrm{III};out}]_n \end{bmatrix}, \tag{6.135}$$

Substitution of Eqs.(6.130) and (6.135) in Eq.(6.126) yields

$$\begin{bmatrix} \left[e^{j\theta^{\mathrm{I}}}\right]_{nn} & \emptyset \\ \emptyset & \left[e^{j\theta^{\mathrm{III}}}\right]_{nn} \end{bmatrix} \begin{bmatrix} \left[\check{I}^{\mathrm{I};out}\right]_n \\ \left[\check{I}^{\mathrm{III};out}\right]_n \end{bmatrix} = \begin{bmatrix} s_{11} & s_{12} \\ s_{21} & s_{22} \end{bmatrix} \begin{bmatrix} \left[e^{-j\theta^{\mathrm{I}}}\right]_{nn} & \emptyset \\ \emptyset & \left[e^{-j\theta^{\mathrm{III}}}\right]_{nn} \end{bmatrix} \begin{bmatrix} \left[\check{I}^{\mathrm{I};in}\right]_n \\ \left[\check{I}^{\mathrm{III};in}\right]_n \end{bmatrix}, \tag{6.136}$$

which can be rewritten as

$$\begin{bmatrix} \left[\check{I}^{\mathrm{I};out}\right]_n \\ \left[\check{I}^{\mathrm{III};out}\right]_n \end{bmatrix} = \begin{bmatrix} \check{s}_{11} & \check{s}_{12} \\ \check{s}_{21} & \check{s}_{22} \end{bmatrix} \begin{bmatrix} \left[\check{I}^{\mathrm{I};in}\right]_n \\ \left[\check{I}^{\mathrm{III};in}\right]_n \end{bmatrix}, \tag{6.137}$$

with

$$\begin{bmatrix} \check{s}_{11} & \check{s}_{12} \\ \check{s}_{21} & \check{s}_{22} \end{bmatrix} = \begin{bmatrix} \left[e^{-j\theta^{\mathrm{I}}}\right]_{nn} & \emptyset \\ \emptyset & \left[e^{-j\theta^{\mathrm{III}}}\right]_{nn} \end{bmatrix} \begin{bmatrix} s_{11} & s_{12} \\ s_{21} & s_{22} \end{bmatrix} \begin{bmatrix} \left[e^{-j\theta^{\mathrm{I}}}\right]_{nn} & \emptyset \\ \emptyset & \left[e^{-j\theta^{\mathrm{III}}}\right]_{nn} \end{bmatrix}. \tag{6.138}$$

6.6 Power

A formalism that can be used to check if the simulated results are correct is the powerbalance. Calculation of the complex power always begins with the complex Poynting vector integrated over a closed surface

$$P = \oint_S (\mathbf{E} \times \mathbf{H}^*) \cdot \mathbf{n}\, dA, \tag{6.139}$$

in which the normal vector $\mathbf{n}$ is pointing outwards. In case of a waveguide, the waveguide wall can be used as a part of the total closed surface and by defining two separate surfaces S_{z_a} and S_{z_b}, equal to the cross-section, at z_a and z_b, respectively, a total closed surface can formed. In this way the integral of Eq.(6.139) can be split up into three parts

$$P = \int_{S_{z_a}} (\mathbf{E} \times \mathbf{H}^*) \cdot (-\mathbf{a}_z)\, dA + \int_{S_{wall}} (\mathbf{E} \times \mathbf{H}^*) \cdot \mathbf{n}\, dA + \int_{S_{z_b}} (\mathbf{E} \times \mathbf{H}^*) \cdot \mathbf{a}_z\, dA. \tag{6.140}$$

Since the surface of the waveguide wall, indicated with S_{wall} is a PEC, the seconde integral on the right-hand side in Eq.(6.140) doesn't contribute to the power, since

$$(\mathbf{E} \times \mathbf{H}^*) \cdot \mathbf{n} = (\mathbf{n} \times \mathbf{E}) \cdot \mathbf{H}^* = \mathbf{0} \cdot \mathbf{H}^* = 0. \tag{6.141}$$

The argument of the two other integrals can be reduced to

$$(\mathbf{E} \times \mathbf{H}^*) \cdot \mathbf{a}_z = (\mathbf{E}_t \times \mathbf{H}_t^*) \cdot \mathbf{a}_z + \underbrace{(\mathbf{E} \times H_z^* \mathbf{a}_z) \cdot \mathbf{a}_z}_{0} + \underbrace{(E_z \mathbf{a}_z \times \mathbf{H}^*) \cdot \mathbf{a}_z}_{0} + E_z H_z^* \underbrace{(\mathbf{a}_z \times \mathbf{a}_z)}_{0}. \tag{6.142}$$

This is convenient, since we have expressions for the transverse electromagnetic fields, viz. the modal field representation in Eqs.(4.65) and (4.66). If the positions of the surfaces

S_{z_a} and S_{z_b} correspond to the position of the S-matrix ports, we have a description of the nett power flow. By substituting the modal fields into Eq.(6.140) we find the power flow through a port, as follows

$$\begin{aligned} P &= \int_{S_{port1}} (\mathbf{E}_t \times \mathbf{H}_t^*) \cdot \mathbf{a}_z \, dA = \int_{S_{port1}} \left[\sum_i V_i^\alpha \mathbf{e}_i^\alpha \times \sum_j I_j^{\beta *} \mathbf{h}_j^\beta \right] \cdot \mathbf{a}_z \, dA \\ &= \sum_i \sum_j V_i^\alpha I_j^{\beta *} \int_{S_{port1}} [\mathbf{e}_i^\alpha \times \mathbf{h}_j^\beta] \cdot \mathbf{a}_z \, dA = \sum_i \sum_j V_i^\alpha I_j^{\beta *} < \mathbf{e}_i^\alpha, \mathbf{h}_j^\beta \times \mathbf{a}_z > . \end{aligned} \tag{6.143}$$

By invoking the result, $\mathbf{e}_i^\beta = \mathbf{h}_j^\beta \times \mathbf{a}_z$ which can be found in Sec.4.41, the orthogonality condition and the fact that the mode functions are normalised, the innerproduct yields

$$\begin{aligned} &< \mathbf{e}_i^\alpha, \mathbf{e}_j^\beta, > = \delta_{ij} \qquad && \alpha = \beta, \\ &< \mathbf{e}_i^\alpha, \mathbf{e}_j^\beta, > = 0 && \alpha \neq \beta, \end{aligned} \tag{6.144}$$

leading to

$$P = \sum_i V_i^\alpha I_i^{\alpha *} = \sum_i (V_i^{\alpha;+} + V_i^{\alpha;-})(I_i^{\alpha;+} + I_i^{\alpha;-})^* = \sum_i Z_{\infty;i}^\alpha (I_i^{\alpha;+} - I_i^{\alpha;-})(I_i^{\alpha;+} + I_i^{\alpha;-})^*, \tag{6.145}$$

"+" and "-" are referring to the global orientation. In matrix notation, for port 1 in waveguide section-I and port 2 in waveguide section-III, respectively, this becomes

$$P_1^{\mathrm{I}} = [(I^{\mathrm{I};in} - I^{\mathrm{I};out})]_i^{\mathrm{T}} [Y^{\mathrm{I}}]_{ii}^{-1} [(I^{\mathrm{I};in} + I^{\mathrm{I};out})^*]_i, \tag{6.146}$$

$$P_2^{\mathrm{III}} = [(I^{\mathrm{III};out} - I^{\mathrm{III};in})]_i^{\mathrm{T}} [Y^{\mathrm{III}}]_{ii}^{-1} [(I^{\mathrm{III};out} + I^{\mathrm{III};in})^*]_i, \tag{6.147}$$

in which we employed the same wave magnitude notation as for the S-matrix. But, in order to check the powerbalance we need to know what goes in and what goes out. This can be derived form Eqs.(6.146) and (6.147) as follows

$$P_{in1}^{\mathrm{I}} = [I^{\mathrm{I};in}]_i^{\mathrm{T}} [Y^{\mathrm{I}}]_{ii}^{-1} [I^{\mathrm{I};in*}]_i, \tag{6.148}$$

$$P_{in2}^{\mathrm{III}} = [I^{\mathrm{III};in}]_i^{\mathrm{T}} [Y^{\mathrm{III}}]_{ii}^{-1} [I^{\mathrm{III};in*}]_i, \tag{6.149}$$

$$P_{out1}^{\mathrm{I}} = [I^{\mathrm{I};out}]_i^{\mathrm{T}} [Y^{\mathrm{I}}]_{ii}^{-1} [I^{\mathrm{I};out*}]_i, \tag{6.150}$$

$$P_{out2}^{\mathrm{III}} = [I^{\mathrm{III};out}]_i^{\mathrm{T}} [Y^{\mathrm{III}}]_{ii}^{-1} [I^{\mathrm{III};out*}]_i. \tag{6.151}$$

The powerbalance now becomes

$$(P_{in1}^{\mathrm{I}} + P_{in2}^{\mathrm{III}}) - (P_{out1}^{\mathrm{I}} + P_{out2}^{\mathrm{III}}) = 0. \tag{6.152}$$

For shorthand notation we abbreviate the left-hand term in above equation to

$$P_{io} = (P_{in1}^{\mathrm{I}} + P_{in2}^{\mathrm{III}}) - (P_{out1}^{\mathrm{I}} + P_{out2}^{\mathrm{III}}). \tag{6.153}$$

6.7 Normalization

To be able to compare results per mode, in terms of wave amplitudes, we have to normalize the S-matrix and the power calculations. Each mode has a different waveguide admittance for which we have to compensate, by taking this specific admittance per mode into account. Therefore we define per mode

$$\breve{I}_n^{\alpha;a;b} = \frac{I_n^{\alpha;a;b}}{\sqrt{Y_{\infty;n}^{\alpha;b}}} \qquad a = \{\mathrm{I}, \mathrm{III}\} \qquad b = \{in, out\}. \tag{6.154}$$

where n is a general mode number indication. By analogy with Eq.(6.126) we have

$$[I^{out}] = [S][I^{in}], \qquad [I^{out}] = \begin{bmatrix} [I^{\mathrm{I};out}]_n \\ [I^{\mathrm{III};out}]_n \end{bmatrix}, \qquad [I^{in}] = \begin{bmatrix} [I^{\mathrm{I};in}]_n \\ [I^{\mathrm{III};in}]_n \end{bmatrix}, \tag{6.155}$$

Next, we cast Eq.(6.154) into the following matrix form

$$\left[I^{a;b}\right]_n = \left[\sqrt{Y^b}\right]_{nn} \left[\breve{I}^{a;b}\right]_n \qquad a = \{\mathrm{I}, \mathrm{III}\} \qquad b = \{in, out\} \tag{6.156}$$

where

$$\left[\sqrt{Y^b}\right]_{nn} = \left[\sqrt{Y_{\infty;n}^{\alpha;b}}\,\delta_{nj}\right] \qquad a = \{\mathrm{I}, \mathrm{III}\} \qquad b = \{in, out\}. \tag{6.157}$$

Applying Eq.(6.156) to Eq.(6.155) yields

$$\begin{bmatrix} \left[\sqrt{Y^{\mathrm{I}}}\right]_{nn} & \emptyset \\ \emptyset & \left[\sqrt{Y^{\mathrm{III}}}\right]_{nn} \end{bmatrix} \begin{bmatrix} [\breve{I}^{\mathrm{I};out}]_n \\ [\breve{I}^{\mathrm{III};out}]_n \end{bmatrix} = \begin{bmatrix} s_{11} & s_{12} \\ s_{21} & s_{22} \end{bmatrix} \begin{bmatrix} \left[\sqrt{Y^{\mathrm{I}}}\right]_{nn} & \emptyset \\ \emptyset & \left[\sqrt{Y^{\mathrm{III}}}\right]_{nn} \end{bmatrix} \begin{bmatrix} [\breve{I}^{\mathrm{I};in}]_n \\ [\breve{I}^{\mathrm{III};in}]_n \end{bmatrix}, \tag{6.158}$$

from which we can deduce the generalized scattering matrix

$$\begin{bmatrix} \breve{s}_{11} & \breve{s}_{12} \\ \breve{s}_{21} & \breve{s}_{22} \end{bmatrix} = \begin{bmatrix} \left[\sqrt{Z^{\mathrm{I}}}\right]_{nn} & \emptyset \\ \emptyset & \left[\sqrt{Z^{\mathrm{III}}}\right]_{nn} \end{bmatrix} \begin{bmatrix} s_{11} & s_{12} \\ s_{21} & s_{22} \end{bmatrix} \begin{bmatrix} \left[\sqrt{Y^{\mathrm{I}}}\right]_{nn} & \emptyset \\ \emptyset & \left[\sqrt{Y^{\mathrm{III}}}\right]_{nn} \end{bmatrix}. \tag{6.159}$$

Subsequently the power can be normalized. This is done by substitution of Eq.(6.154) or (6.156) into Eqs.(6.145)-(6.151), which yields

$$P_1^{\mathrm{I}} = [(\breve{I}^{\mathrm{I};in} - \breve{I}^{\mathrm{I};out})]_n^{\mathrm{T}} [Y^{\mathrm{I}}]_{nn}^{-1} [\,|Y^{\mathrm{I}}|\,]_{nn} [(\breve{I}^{\mathrm{I};in} + \breve{I}^{\mathrm{I};out})^*]_n, \tag{6.160}$$

$$P_2^{\mathrm{III}} = [(\breve{I}^{\mathrm{III};out} - \breve{I}^{\mathrm{III};in})]_n^{\mathrm{T}} [Y^{\mathrm{III}}]_{nn}^{-1} [\,|Y^{\mathrm{III}}|\,]_{nn} [(\breve{I}^{\mathrm{III};out} + \breve{I}^{\mathrm{III};in})^*]_n. \tag{6.161}$$

and of course

$$P^{\mathrm{I}}_{in1} = [\check{I}^{\mathrm{I};in}]^{\mathrm{T}}_{n}[Y^{\mathrm{I}}]^{-1}_{nn}[\,|Y^{\mathrm{I}}|\,]_{nn}[\check{I}^{\mathrm{I};in^*}]_{n}, \tag{6.162}$$

$$P^{\mathrm{III}}_{in2} = [\check{I}^{\mathrm{III};in}]^{\mathrm{T}}_{n}[Y^{\mathrm{III}}]^{-1}_{nn}[\,|Y^{\mathrm{III}}|\,]_{nn}[\check{I}^{\mathrm{III};in^*}]_{n}, \tag{6.163}$$

$$P^{\mathrm{I}}_{out1} = [\check{I}^{\mathrm{I};out}]^{\mathrm{T}}_{n}[Y^{\mathrm{I}}]^{-1}_{nn}[\,|Y^{\mathrm{I}}|\,]_{nn}[\check{I}^{\mathrm{I};out^*}]_{n}, \tag{6.164}$$

$$P^{\mathrm{III}}_{out2} = [\check{I}^{\mathrm{III};out}]^{\mathrm{T}}_{n}[Y^{\mathrm{III}}]^{-1}_{nn}[\,|Y^{\mathrm{III}}|\,]_{nn}[\check{I}^{\mathrm{III};out^*}]_{n}. \tag{6.165}$$

Note that $|Y| = \sqrt{YY^*}$.

6.8 Results

Now that the analysis of the iris has finished, the model is implemented into the computer. We choose to use the mathematical software programme MATLAB as simulation tool. The choice for MATLAB is rather simple, it is user friendly and surely in the field of electromagnetics a lot of people know how to use it. A drawback is the high internal memory requirement and long computation times. This is the consequence of the fact that it is a high level programming language.

There are a number of things we would like to show and discuss, starting with the verification of the model. After this we will look into the question of convergence and finally we'll show results of the iris.

6.8.1 Verification

In the preceding sections we have discussed and shown a possible way of analysing an iris. Of course there are other approaches for analysing an iris, but they all have to yield the same outcome eventually, or yet better said, show at least resemblance in the trend. So, a good way to check the verification of our model and analysis is to find literature and results which handle junctions between rectangular waveguides but with a different approach.

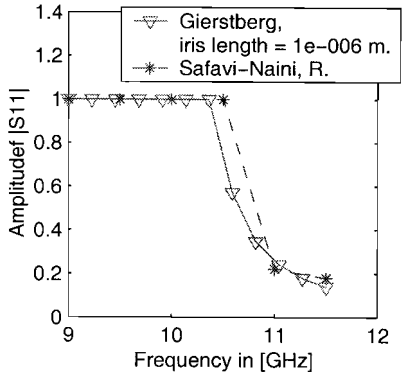

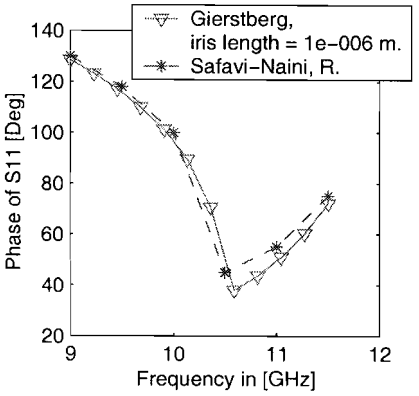

Figure 6.9: *Characteristics of a single junction. Upper: reflection coefficient, of incident mode* TE_{10} *from larger waveguide. Lower: phase of reflection coefficient. Dimensions of waveguides in millimeters are* $A = 22.85$, $B = 10.05$, $C = E = 14.28$, $D = F = 6.5$, $a_2 = 4.285$ *and* $b_2 = 1.775$. *See Fig.E.1 for explanation of variables.*

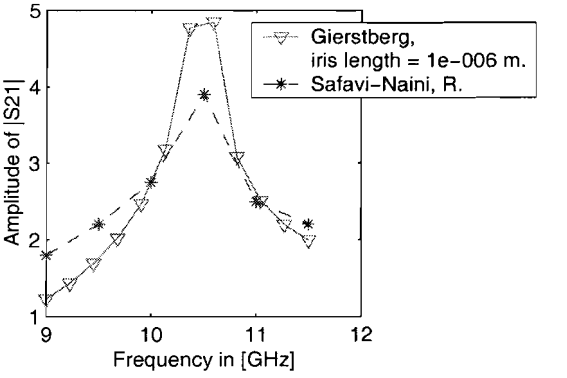

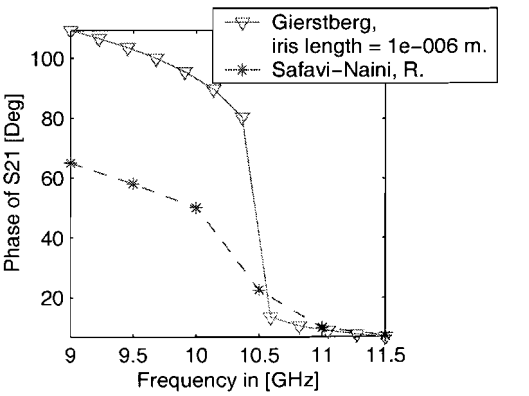

Figure 6.10: *Upper: transmission coefficient, of incident mode* TE_{10}. *Lower: phase of transmission coefficient. Dimensions are stated in Fig.6.9.*

We will use the results from Safavi-Naini and Macphie [28] as a reference. They make use of a mode expansion and the principle of conservation of complex power. The numerical results presented in this paper will be used for the verification of our model and analysis, and at the same time used to look into the behaviour of an iris by varying parameters.

We start with the results of Fig.6.9. What we see here is the reflection coefficient and phase of the electric field. The corresponding configuration consists of a abrupt single junction between two centered rectangular waveguides with different cross-sections. Port 1 of the S-matrix lies in the large waveguide directly against the aperture, port 2 lies directly against the other side of the aperture in the smaller waveguide. We simulated this situation by giving section-III the same cross-section as section-II (the iris), together forming the waveguide with the smaller cross-section and by placing the surface on which we determine the equivalent magnetic current $\mathbf{M}_2$ as close as possible to the aperture formed by section-I and section-II, on which equivalent current $\mathbf{M}_1$ is determined. In this way we try to place

the S-matrix ports as close together as possible, to reduce any phase shift in the iris. The length and other dimensions are indicated in the figure. For the incident field we used the TE_{10} mode, coming from the waveguide with the large cross-section. Furthermore, in [28] the waveguide is filled with air, $\varepsilon_r = 1$, and has no losses, $\tan\delta = 0$. However for us to obtain corresponding results we had to introduce a very small loss tangent of $\tan\delta = 10^{-10}$, giving the propagation constants k_z of all the evanescent modes a very small real part. Only in this way, a stable answer was achieved in all verification cases. The number of modes used in the expansion of the magnetic field, the expansion of the equivalent magnetic currents and the testing of the tangential fields on the aperture surfaces is $i = p = l = s = r = q = 312$. The first three integers are mode number indicators, introduced in Secs.6.3.1, 6.3.2 and 6.3.3, respectively, the last three integers can be found in Eqs.6.51, 6.57 and 6.58 respectively. These 312 modes consist of TM as well as TE modes, more specific 144 TM and 168 TE. There is good correspondence of the TE_{10} reflection coefficient and its phase, certainly the tendency is in agreement. Below the 10.49 GHz the reflection is equals one because the smaller waveguide operates in cutoff. Mapping the amplitude and phase figures in the Smith chart, we start out, for low frequencies, with a high impedance which has a inductive behaviour. For increasing frequency, until the cutoff frequency is reached, the impedance's amplitude stays unchanged but its inductive behaviour varies a little according the decrease of the phase. Then, the reflection descends rapidly, the impedance and the inductive behaviour become small and real power starts to flow into the smaller waveguide.

In Fig.6.10 the transmission coefficient and its phase are depicted. The trend of the curves correspond reasonably, only in the amplitude graph there is some discrepancy. The peak in the amplitude of the transmission coefficient comes form a nonsymmetric S-matrix, for which we have not yet found an explanation. Apparently, strange things happen at the frequency that the smaller guide is beyond cutoff. The peak in the transmission corresponds with the decrease of the reflection. Below cutoff, the phase of s_{21}, also shows some deviation. If section-II is made longer, phase deviations appear above cutoff, too. This can be imputed to the increasing distance between the S-matrix ports, which introduces an extra phase shift.

The next case we examine is a thick iris. The configuration is as follows. Section-I and III are the waveguides with equal cross-sections and are connected with each other by means of section-II (forming the iris) which has a smaller cross-section. The various dimensions are mentioned in the comment under Fig.6.11. The parameters of the dielectric filling are again $\varepsilon_r = 1$ and $\tan\delta = 10^{-10}$, in order to get a stable answer. Fig.6.11 displays the reflection coefficient and phase of the TE_{10} incident wave from section-I. The S-matrix ports are placed directly on the junctions. There is a good correspondence between the data of the paper and our results. At 10.05 GHz the reflection is nearly disappeared and the phase makes a dump of about 180° indicating that the iris is at resonance, The resistance of the iris impedance is close to one and the reactance is zero. The number of modes taken along to produce these results is 312 for each waveguide section.

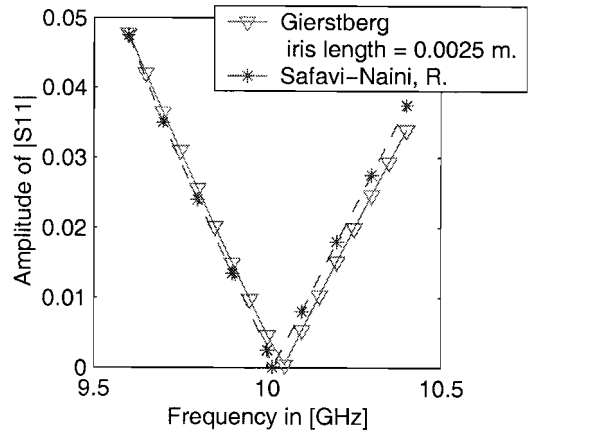

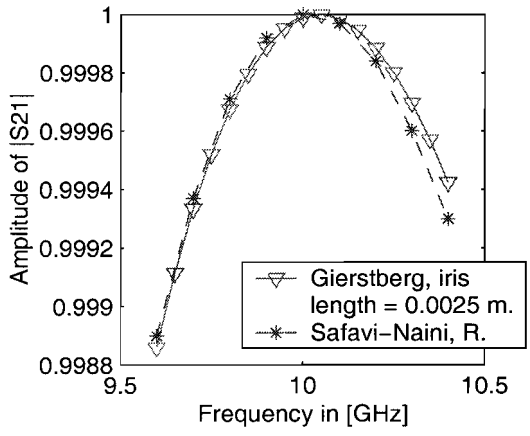

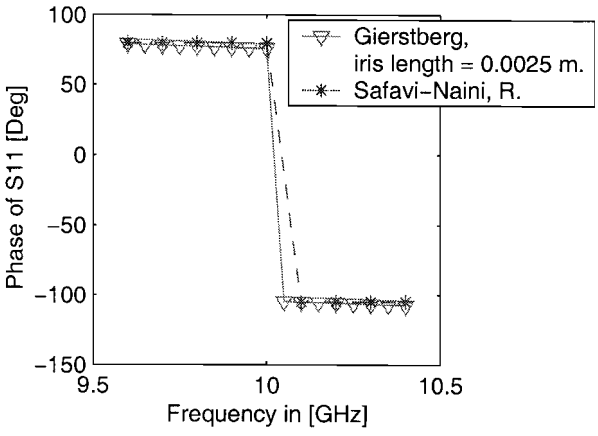

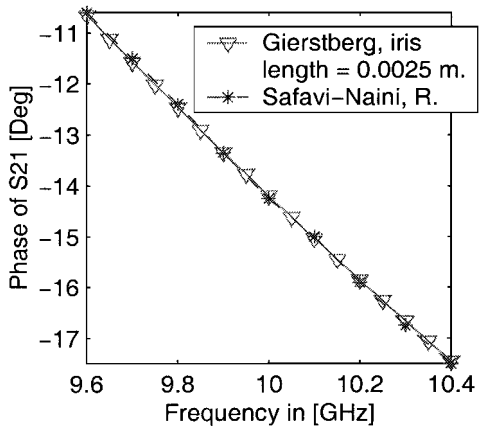

Figure 6.11: *Characteristics of a thick symmetric iris. Upper: reflection coefficient, of incident mode TE_{10}. Lower: phase of reflection coefficient. Dimensions of waveguides in millimeters are A=E=22.85, B=F=10.05, C=18 D=6.6, a_2=4.2 and b_2=1.7.*

Figure 6.12: *Characteristics of a thick symmetric iris. Upper: transmission coefficient, of incident mode TE_{10}. Lower: phase of transmission coefficient.*

Fig.6.12 shows the frequency dependence of the TE_{10} transmission coefficient for the thick iris. The frequency on which the transmission reaches its maximum equals the frequency where reflection is at its lowest. In the phase graphs of the reflection and the transmission, we notice that as the frequency rises the iris goes from inductive to a capacitive behaviour, since the phase goes from positive to negative. Again we see corresponding results. Note that our results for an iris (a double waveguide junction) are better than our results for a single junction, since we have a model for a double junction.

We will continue with some more comparisons but we will focus on the consequences of varying dimensional parameters of the iris. We will investigate a varying iris width along the x-direction for two different lengths of the iris, while the height of the iris in y-direction is kept constant. The configuration is as discussed in the previous case section-I and -III

are the larger waveguides, section-II is the smaller. By equally changing the jump in cross-section, also called step, at both sides of the iris aperture, the three sections remain centered during the width variation of the iris. The number of modes we used is 312, of which 144 TM and 168 TE, in each section. For a TE_{10} incident mode field, the steps along x and y

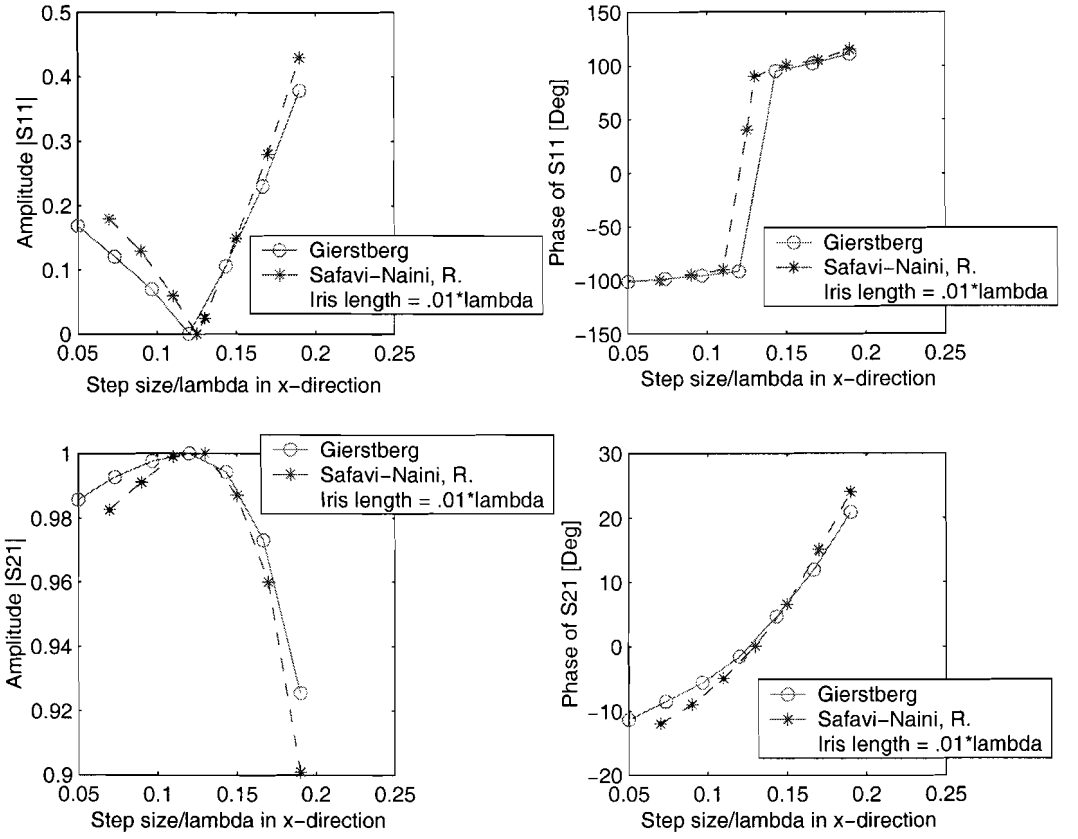

Figure 6.13: *Thin symmetric iris. Upper: reflection coefficient and phase, of incident mode TE_{10}, as function of step size a_2 in wavelengths. Lower: transmission coefficient and phase. Dimensions in wavelengths are $A=E=0.85\lambda$, $B=F=0.4\lambda$, $D=0.225\lambda$ and iris length$=0.01\lambda$.*

exhibit inductive and capacitive effects, respectively. We can see this in the phase graph of Fig.6.13. It start with a negative phase which means a negative reactance, implying a capacitance and end up with a positive phase which means a positive reactance, implying a inductance. This can also be seen from Fig.6.14, which depicts the components of the TE_{10} mode field. Squeezing the waveguide along the y-direction influences the electric field and the capacitance. On the contrary, squeezing the waveguide along the x-direction influences the magnetic field and the inductance.

In Fig.6.13 and Fig.6.15 the reflection and transmission coefficients and there phase curves are depicted for a thin and a thick iris, respectively, as function of step size per wavelength. This step size, as recently said, is the jump in cross-section which the waveguide makes at the junction. The mentioned wavelength is of a wave, at 10 GHz, travelling through a

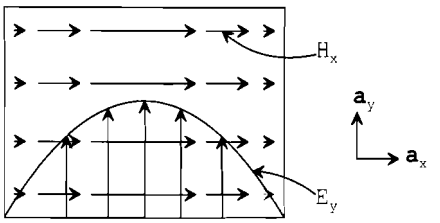

Figure 6.14: *The electric- and magnetic-field components of TE_{10} mode.*

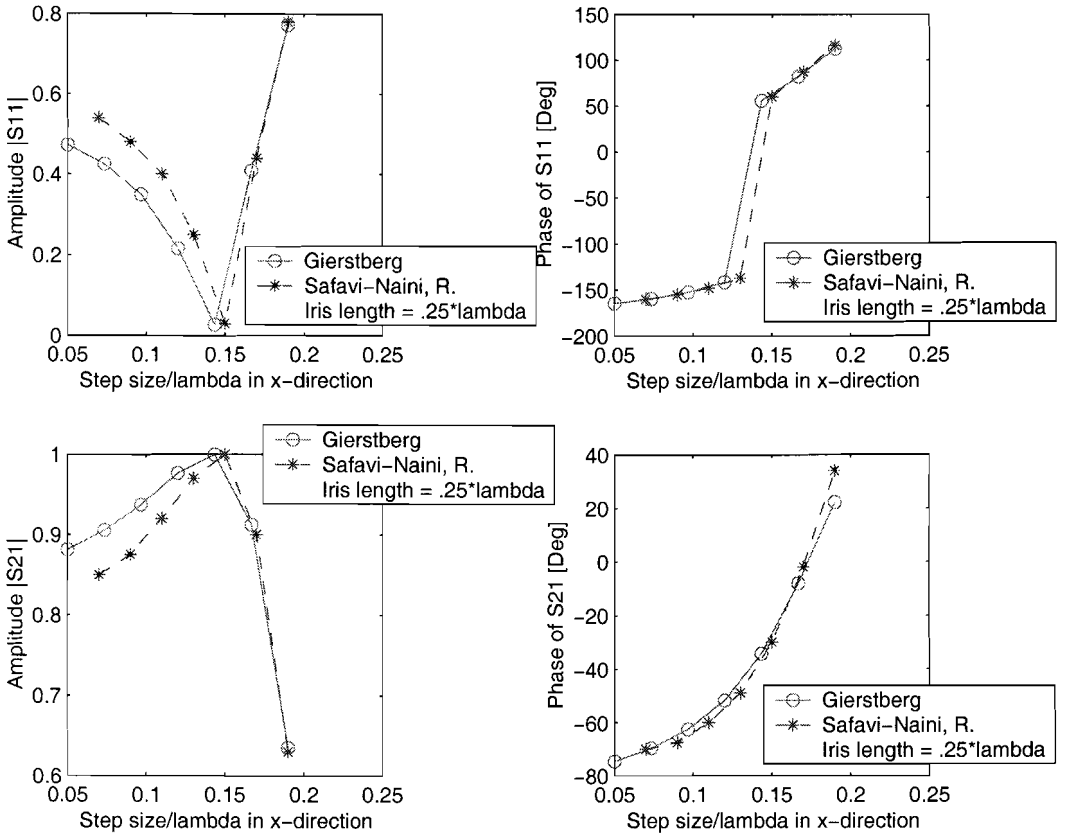

Figure 6.15: *Thick symmetric iris. Upper: reflection coefficient and phase as function of step size a_2 in wavelengths. Lower: transmission coefficient and phase. Iris length=0.25λ, see Fig.6.13 for remaining dimensions.*

space filled with the same dielectric material as the interior of the waveguide, $\varepsilon_r = 1$ and $\tan\delta = 0$ representing free space thus, which yields a wavelength of $\lambda \simeq 3$ cm.

Furthermore, in case of the thin iris we see at step-size/$\lambda = 0.12$ that the reflection vanishes, as a result of the fact that the inductive behaviour and the capacitive behaviour, caused by the steps in the x- and y-direction, cancel one another. At that point it is also visible that the phase graph goes from a negative phase to a positive phase, indicating

a small reactive part. For the thick iris, the characteristics have become narrower and resonance occurs at about step-size/$\lambda = 0.15$. So, we can say that a thicker iris introduces a higher selectivity and the cross-sectional dimensions must be changed to maintain in resonance. The selectivity increase is probable the cause of the decrease in coupling between the two sides. The length of the iris has its influence on the impedance.

Also an interesting quantity to visualise and to gain information from to check if the analysis and calculations went correct, are the equivalent magnetic currents in the aperture of the iris. Eventually, we applied the method of moments during the analysis to derive the currents. For the case of a thick iris case, which is discussed in Figs.6.11 and 6.11, we have plotted the equivalent magnetic current $\mathbf{M}_1$. The x- and y-directed current components of $\mathbf{M}_1$, on the aperture between sections-I and II at $z = z1$ are given in Figs.6.16 and 6.17, respectively.

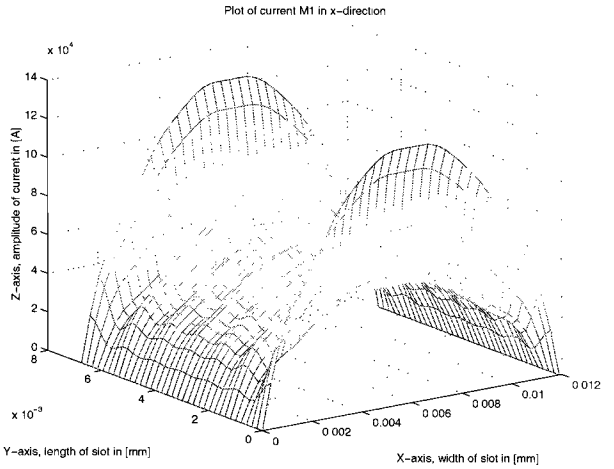

Figure 6.16: *x-directed equivalent magnetic current. Incident field mode is* TE_{10}.

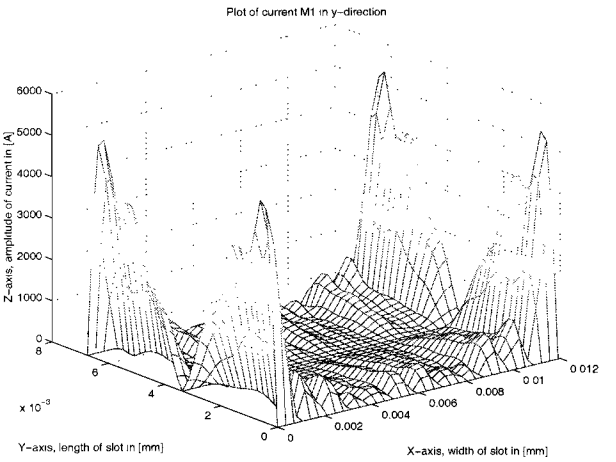

Figure 6.17: *y-directed equivalent magnetic current. Incident field mode is* TE_{10}.

Notice the singular behaviour of the current at the edges of the aperture. This is a correct behaviour caused by the sharp edges of the waveguide wall. The irregularities in the singularities of the x-component are not completely according expectations. Further on in this report the current shape will be more thoroughly discussed and explain, in the discussion of convergence.

To come to certain results we had to take along, as mentioned, 312 waveguide mode. Up till now it is not yet explained how we came to this number. It has to do with the convergence of the problems. The convergence is determined by means of the s_{11} scattering parameter as a function of the number of waveguide modes. Fig.6.18 shows the results of convergence, for the case of the thick iris. Visible is the absolute value of the s_{11} parameter its phase and the condition number of the MoM matrix. As indicated in the figure, 312 modes is at the point where the s_{11} curve has just past a small jump and again seems to have found a stable course. Together with the fact that the condition number of the MoM

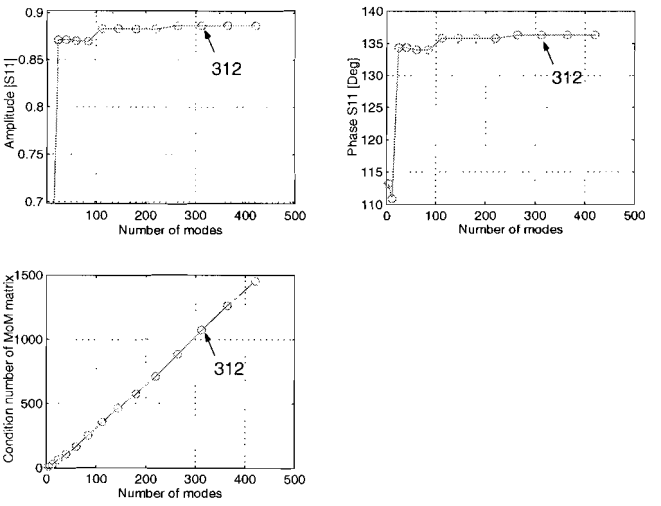

Figure 6.18: *Convergence graphs, determined by means of scattering parameters.*

matrix stays confined is indication enough for us to assume that the amount of applied modes correct.

After the "Results", Sec.6.8, we discuss a method to determine the convergence of problems, of which we though, at first, was a good, correct and reliable idea annex concept. Unfortunately, it does not work because of to weak constraints.

6.8.2 Iris, dubbel waveguide junction

The verification of the results has shown that our analysis and modelling is correct. Based on this, we will show and discus different results of an iris (slot) what qua geometry and size correspond with the reality. We begin by mentioning that we have sorted the modes by their propagation constants in the z-direction (k_z) as follows, from fast to slow propagating modes, meaning from large to small real values and from slow to fast evanescent modes, that is from small to large imaginary values. We start with a canonical case. Section-I, -II and -III all have the same cross-section, the dimensions are $A = C = E = 13.4$ mm and $B = D = F = 13.5$ mm in x and y direction, respectively. The length of the sections is 15 mm, 25 mm and 15 mm, respectively. See Fig.E.1 and Fig.6.1 for explanation. The dielectric filling has parameters $\varepsilon_r = 3$ and $\tan\delta = 0$. The incident field is mode TE_{01} from waveguide section-I, with a frequency of 10 GHz. For the computations we used 4 waveguide modes. In Fig.6.19, amplitude and phase of modes, of above described situation are depicted. In the upper graph, one can see the amplitude of the modes, according to $20\log_{10}[\cdot]$. At 0 dB, the incident wave in section-I is visible, propagating (increasing z) towards the transition between section-I and -II. According to our model approach, the incident field should continue propagating in section-II without any disturbance in amplitude. In our model we separated section-I from -II by closing of the cross-section

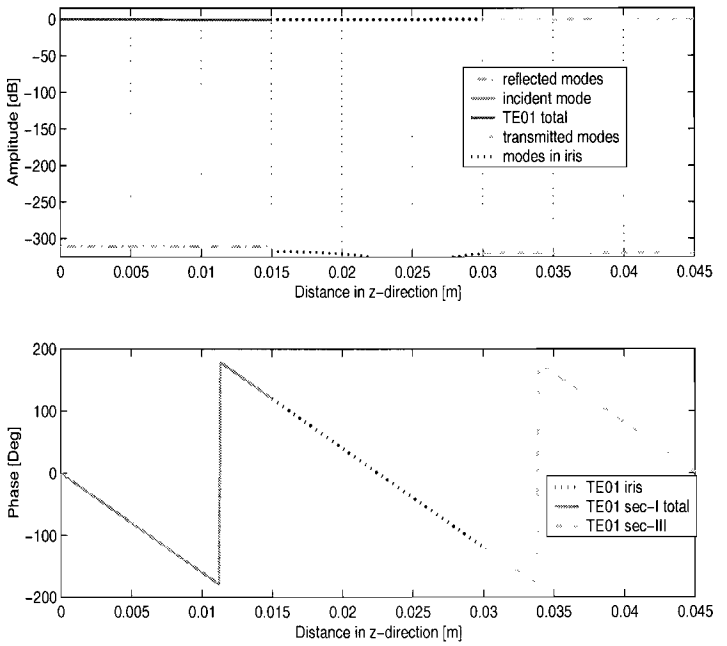

Figure 6.19: *Amplitude and phase of mode TE_{01} propagating in $+z$ direction. Parameters are: $A = C = E = 13.4$ mm, $B = D = F = 13.5$ mm, $\varepsilon_r = 3$, $\tan\delta = 0$, number of modes taken along in computations is 312.*

with a thin PEC and demanding continuity of the electric and magnetic field. Upon crossing the transition between section-II and -III, we expect the same behavior of the TE_{01} mode. This behaviour is observed in the top graph of Fig.6.19. The straight green line at -312 dB along the first 15 mm is the TE_{01} reflected incident field which tell us that we reached machine precision. In the lower graph, the phase of the incident field is plotted, propagating through the three sections. Just like the amplitude, the fase is continuous across the transitions between the sections, as expected.

In Fig.6.20, the reflected and transmitted modes on the transition between section-I and -II and between section-II and -III, respectively are given. We see five modes, three reflected and two transmitted, lying around -312 dB, and one well below -600 dB. Usually, displaying quantities at these levels is nonsense. However, we don't have a good explanation why the modes concentrate around two levels. Probably the contribution of weighting (inner-product) one mode with another is less than the contribution of weighting another pair. In Table 6.1, the modes that are concentrated around the -312 dB are given by number and type.

In Fig.6.21 the x-directed equivalent magnetic current is shown and in Fig.6.22 the y-directed current, note the scale of the vertical axis in both figures. The y-directed current has the precise form of the TE_{01} mode, which clarifies why the incident mode propagates through the three sections without being obstructed by the closed cross-sections.

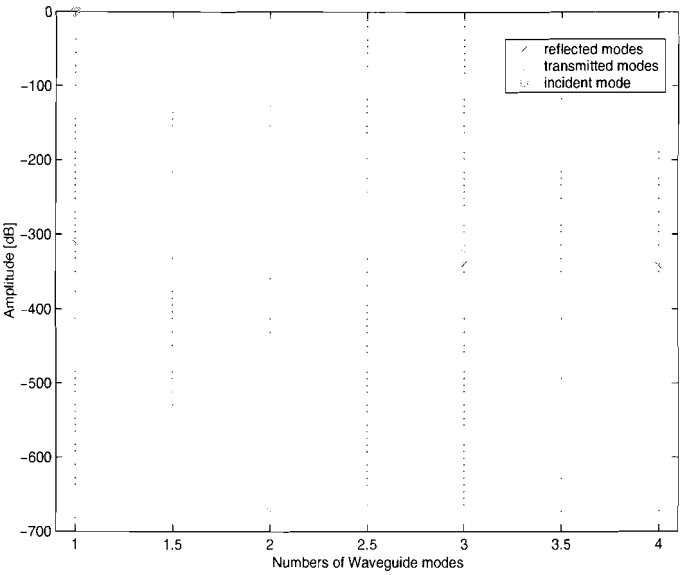

Figure 6.20: *Amplitude of reflected and transmitted modes on the surface of junction I-II and II-III at $z = z_1$ and $z = z_2$, respectively.*

i	1	3	4
(n,m)	(0,1)	(1,1)	(1,1)
type	TE	TM	TE

Table 6.1: *Mode number i, mode indicators (n, m) and the mode type of the modes lying around -312 dB in Fig.(6.20).*

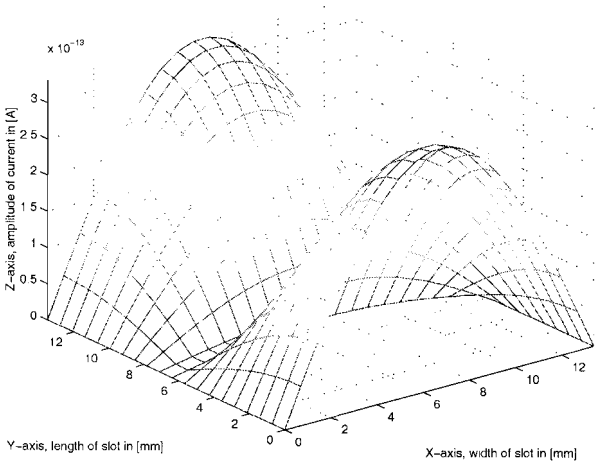

Figure 6.21: *x-directed equivalent magnetic surface current M1 at z_1, for canonical case.*

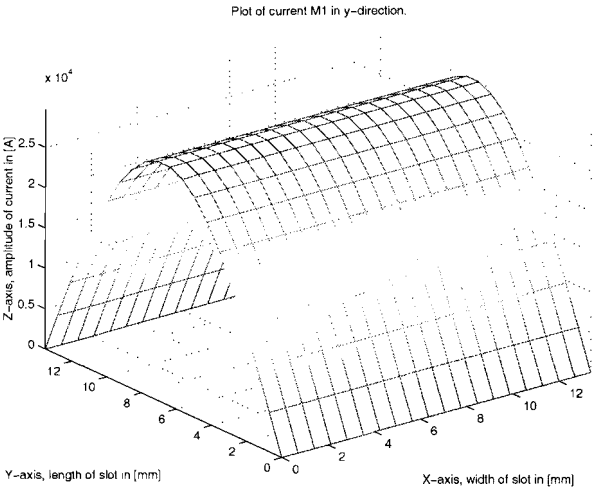

Figure 6.22: *y-directed equivalent magnetic surface current M1 at z_1, for canonical case.*

Looking at Tabel.6.1 and at the x-directed current, we notice that the shape of the current corresponds exactly to the two modes with mode indices (1,1). So, the two modes around the -312 dB are caused by the fact, that the x-directed current is not exactly zero, which in turn can be relate partially to the matching of the modes. The x- and y-directed equivalent magnetic current at z_2 have exactly the same form. Table 6.2 shows some power figures, on the position at the S-matrix ports. We continue our discussion by considering the same

	Real(·)	Imag(·)
$\mathbf{P}^{\mathbf{I}}_{\mathbf{in1}} =$	1	0
$\mathbf{P}^{\mathbf{I}}_{\mathbf{out1}} =$	$7.7184.10^{-32}$	$3.6617.10^{-49}$
$\mathbf{P}^{\mathbf{III}}_{\mathbf{out2}} =$	1	$2.7472.10^{-33}$
$\mathbf{P}_{\mathbf{io}} =$	0	$-2.7472.10^{-33}$

Table 6.2: *Power figures for canonical case, at port 1 and 2 of the S-matrix, that is at* $z_0 = 0$ *mm and* $z_3 = 55$ *mm, respectively.*

configuration as above, except that waveguide section-II is squeezed in de x-direction, such that $C = 2.1$ mm. In this way, we have formed an iris, which is centered with respect to the cross-sections of section-I and -III. For an incident TE_{01} mode, this means that we squeeze in the E-plane, (see Fig.6.14), thereby influencing the capacitance. In Fig.6.23, the magnitude and phase progress in the z-direction are plotted. The amplitude graph shows significant changes, because of the change in cross-section. This causes mode coupling, as we have seen in the discussion of the integrals in Appendix E. As a consequence, equivalent magnetic currents, of considerable magnitude show up on the apertures, at $z_1 = 15$ mm and $z_2 = 40$ mm, generating a number of modes well above the -312 dB. These modes are then radiated in the three different sections. Horizontal lines are propagating modes (k_z=real), the skew lines are evanescent modes (k_z=imaginary) which drop fast over 15 mm. In the amplitude graph, one can find a symmetry axis at $z = 27.5$ mm, for the evanescent modes. This is according expectations, since we have a symmetric iris, over all three spatial axes. In section-I, at 0 dB we have the TE_{01} incident field and right under it we have, at -0.38 dB, the reflected incident field. The horizontal line in section-III at -10.74 dB is the transmitted mode TE_{01}.

We have some figures to confirm the correctness. Table 6.3 contains some power figures and shows the scattering parameters of the incident field mode. The real power is completely carried by the only propagating mode, TE_{01}, and the evanescent modes are responsible for the imaginary part of the complex power. Because of the evanescent modes, the imaginary power decreases over increasing distance. P^{I}_{out1} and P^{III}_{out1} are round off figures. The powerbalance, P_{io}, is calculated with the fully accurate figures.

In section-II we see a standing wave, formed by the interference of the only back and forth travelling wave viz., mode TE_{01}. It has a SWR of $s = \frac{I_{max}}{I_{min}} = 6.9908$. In 6.28 one can see how I is defined, as the linear combination of the back and forth travelling wave. At the minima, of the standing wave pattern the impedance is at its minimum, this can

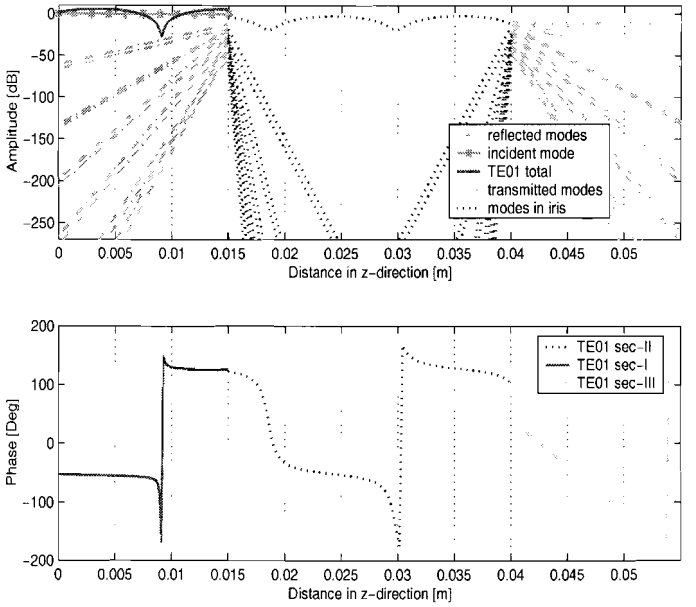

Figure 6.23: *Upper: amplitude of several modes, lower: phase of TE_{01} mode propagating in $+z$ direction. Parameters are: $A = E = 13.4$ mm, $B = D = F = 13.5$ mm, $C = 2.1$ mm, $a_2 = 5.65$ mm, $\varepsilon_r = 3$, $tan\delta = 0$, number of modes taken along in computations is 312.*

Power		
	Real(·)	Imag(·)
$\mathbf{P}^{\mathbf{I}}_{\mathbf{in1}} =$	1	0
$\mathbf{P}^{\mathbf{I}}_{\mathbf{out1}} =$	$9.1564.10^{-1}$	$-5.7943.10^{-7}$
$\mathbf{P}^{\mathbf{III}}_{\mathbf{out2}} =$	$8.4362.10^{-2}$	$-1.6594.10^{-6}$
$\mathbf{P}_{\mathbf{io}} =$	$-2.2264.10^{-16}$	$2.2389.10^{-6}$
Scattering parameters		
$\mathbf{s}_{\mathbf{11}} =$	$-3.1378.10^{-1}$	$-9.0398.10^{-1}$
$\mathbf{s}_{\mathbf{21}} =$	$-2.7439.10^{-1}$	$9.5243.10^{-2}$
$\mid \mathbf{s}_{\mathbf{11}} \mid^2 + \mid \mathbf{s}_{\mathbf{21}} \mid^2 =$	1	

Table 6.3: *Power values and scattering parameters on port 1 and 2 of the S-matrix, at $z_0 = 0$ mm and $z_3 = 55$ mm, respectively.*

be seen in the phase plot of Fig.6.23. At this point the phase makes a jump. In the Smith chart the curve would cross the real axis. Also derived from the standing wave is the so-called "waveguide wavelength" which is twice the distance between two successive minima. Observed out of the plot we get $\lambda_{waveguide} = 2.2553$ cm and calculated it is $\lambda_{waveguide} = 2.2552$ cm. In the phase plot of Fig.6.23, we see mode TE_{01} propagating in section-III. In section-I a deviating phase curve is observed, caused by the interference between the incident mode and its reflection. At $z = 15$ mm, that is the junction between section-I and section-II, the phases not completely connect. This also happens at $z = 40$ mm, that

is the junction between section-II and section-III. We will go into some more detail with respect to these phase jumps. Therefore we have preformed 4 tests, with respect to the iris width and length, divided into two cases.

Case 1: The iris is centered and has a width of $C = 9.2$ mm and a length varies from $(z_2 - z_1) = \frac{\lambda}{2}$ to $(z_2 - z_1) = \frac{\lambda}{4}$. All other parameters remain the same. Note, Figs.6.24 and 6.25 are magnified details from one phase graph, just as Figs.6.26 and 6.27.

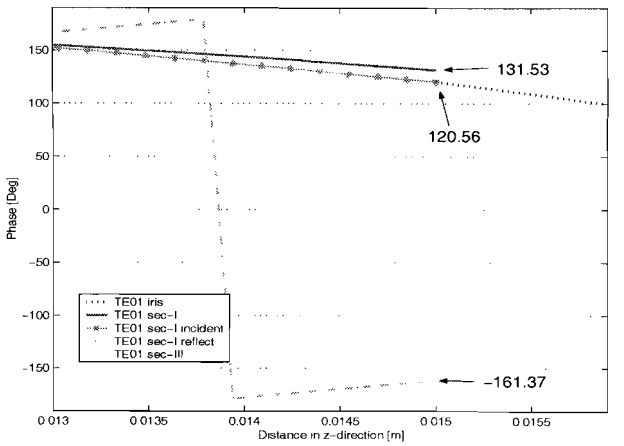

Figure 6.24: *Different TE_{01} phase components at junction I-II. Iris width is* 9.2 *mm and length is* $\frac{\lambda}{2}$.

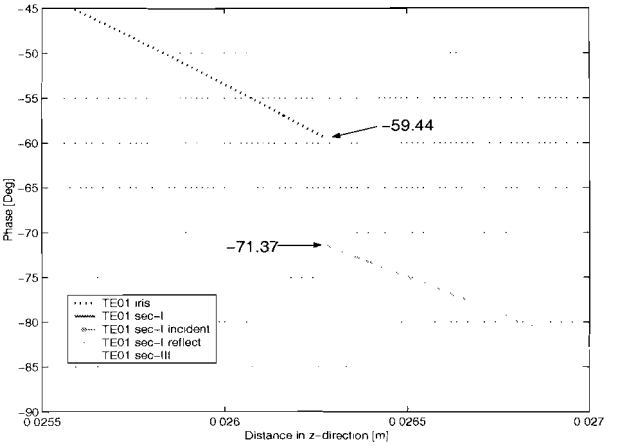

Figure 6.25: *Different TE_{01} phase components at junction II-III. Iris width is* 9.2 *mm and length is* $\frac{\lambda}{2}$.

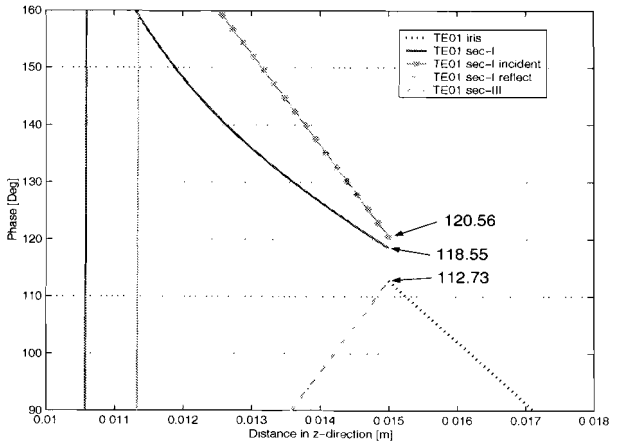

Figure 6.26: *Different TE_{01} phase components at junction I-II. Iris width is* 9.2 *mm and length is* $\frac{\lambda}{4}$.

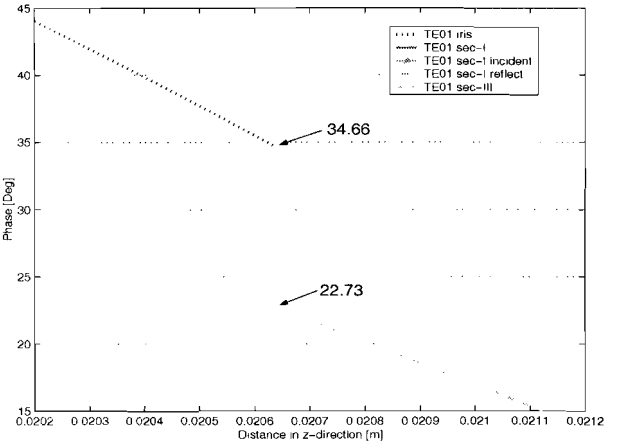

Figure 6.27: *Different TE_{01} phase components at junction II-III. Iris width is* 9.2 *mm and length is* $\frac{\lambda}{4}$.

From Figs.6.25 and 6.27, we observe that the iris produces a phase jump of 11.93° at the junction between section-II and section-III, independent of the length of the iris. In

contrast, (see Figs.6.24 and 6.26), depending on the length of the iris, the phase of incident mode TE_{01} in section-I has a good match with the phase of mode TE_{01} in section-II, or, the reflected mode TE_{01} in section-I has a good match with the mode TE_{01} in section-II.

For the iris length, we have deliberately chosen a good matching case, $\frac{\lambda}{2}$, and a bad matching case, $\frac{\lambda}{4}$, and Table 6.4, a bit later on, gives some comparison between the amplitude values for the TE_{01} mode.

Case 2: The width is reduced to $C = 2.1$ mm and still centered, and the length varies again from $(z_2 - z_1) = \frac{\lambda}{2}$ to $(z_2 - z_1) = \frac{\lambda}{4}$. Other parameter remain the same.

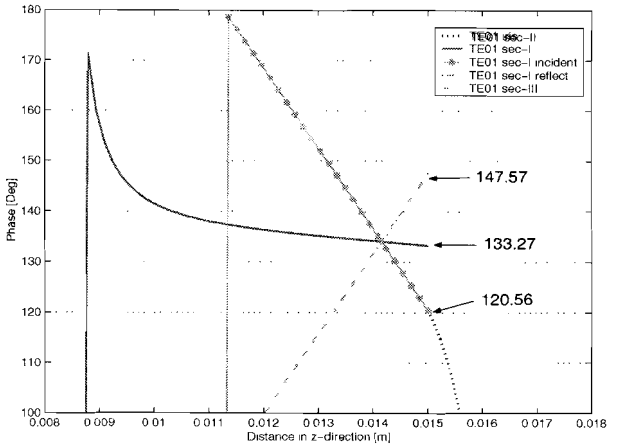

Figure 6.28: *Different TE_{01} phase components at junction I-II. Iris width is* 2.1 *mm and length is* $\frac{\lambda}{2}$.

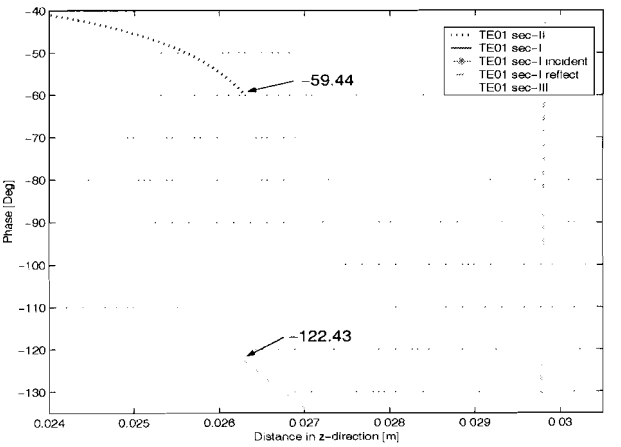

Figure 6.29: *Different TE_{01} phase components at junction II-III. Iris width is* 2.1 *mm and length is* $\frac{\lambda}{2}$.

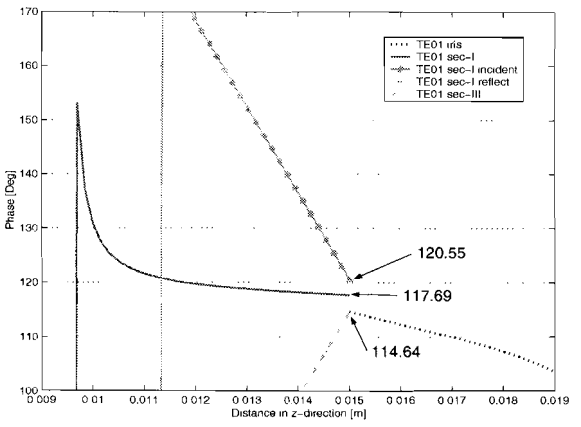

Figure 6.30: *Different TE_{01} phase components at junction I-II. Iris width is* 2.1 *mm and length is* $\frac{\lambda}{4}$.

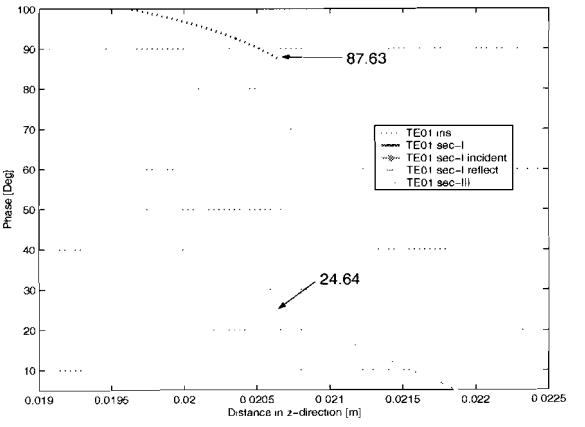

Figure 6.31: *Different TE_{01} phase components at junction II-III. Iris width is* 2.1 *mm and length is* $\frac{\lambda}{4}$.

Due to the decrease in width of the iris we notice an increase in the phase jump at the

junction between section-II and section-III, for both the lengths of the iris. It has become 62.99°, see Figs.6.29 and 6.31. In Figs.6.28 and 6.30 we see that, depending on the length of the iris, the phase of incident mode TE_{01} in section-I, has a good match with the phase of mode TE_{01} in section-II, or, the reflected mode TE_{01} in section-I has a good match with the mode TE_{01} in section-II.

A comparison between amplitude values for this case is shown in Table 6.4. From these

Iris width	$0.4079\lambda = 9.2mm$		$0.0931\lambda = 2.1mm$	
Iris length	$\frac{\lambda}{2}$	$\frac{\lambda}{4}$	$\frac{\lambda}{2}$	$\frac{\lambda}{4}$
$\mathbf{TE_{01}}$**reflect**	$-13.69dB$	$-9.22dB$	$-1.003dB$	$-0.518dB$
$\mathbf{TE_{01}}$**transmit**	$-0.189dB$	$-0.555dB$	$-6.856dB$	$-9.49dB$

Table 6.4: *Reflection and transmission amplitude values of TE_{01} mode, in section-I and -III, respectively, with varying iris dimensions*

two cases we can draw the following conclusions. By decreasing the iris-width, we notice an increase in the phase jump at $z = z_2$, that is the junctions between section-II and section-III. One and other can be explained by the change in impedances, what is caused by the discontinuity in cross-section. In [22, p.404-406] we obtained a first order summary of a thick iris, in which is explained that the change in width is represented by a capacitance, as already mentioned by us, and the length of the iris can be represented by an induction, equivalent with extra distance. The influence of iris-length on the impedance is small but, the ratio of the iris-width with the adjacent larger waveguide, on the other hand, has a large influence on the impedance. The decreasing iris-width also leads to an increase of the standing wave in the iris. For an iris-width of 9.2 mm, we observed a SWR of 1.5124 and for an iris-width of 2.1 mm we observed a SWR of 6.99, form which we can conclude that the mismatch enlarges. Also we noticed that, the higher the SWR becomes, the sharper the shape of the standing wave becomes at its minima (derivative is no longer continuous), and the ripple on the phase of mode TE_{01} in the iris becomes higher (see fig.6.23). The length of the iris determines how well the incident field matches on the iris and apparently has no influence on the phase jump that exists at z_2, the junction between section-II and section-III.

We also noticed, by a decreasing iris width, an increase in amplitude, 10 to 20 dB, of the evanescent modes, reflected and transmitted form the iris (solid and dashed skew lines in sections-I and -III in Fig.6.23). This indicates that the field disturbances become worse as the iris is getting smaller.

In Sec.(6.7) we discussed the normalization of the power and the scattering parameters, to form a generalized scattering matrix. To get normalized scattering parameters, we had to multiply the S-matrix at the front by a diagonal matrix containing the square roots of the mode impedances and at the rear with a diagonal matrix containing the square roots of the mode admittances (see Eq.(6.159)). In case sections-I and -III have the same cross-section and dielectric filling, the impedances per mode, in I and III, are the same.

So, in fact every mode is multiplied by the square root of its impedance and subsequently multiplied with the square root of its admittance, which cancel each other. Therefore the normalisation can be left out.

The next step is sizing down the length of the iris and putting the ports of the S-matrix close to the junctions. The length of the iris is reduced to $\frac{1}{2}$ mm and the S-matrix ports are positioned at a distance of 1 mm from the waveguide junctions, thereby making the effective lengths of sections-I and -III also 1 mm. In Fig.6.32, the magnitude of several modes and the phase of mode TE_{01} are displayed.

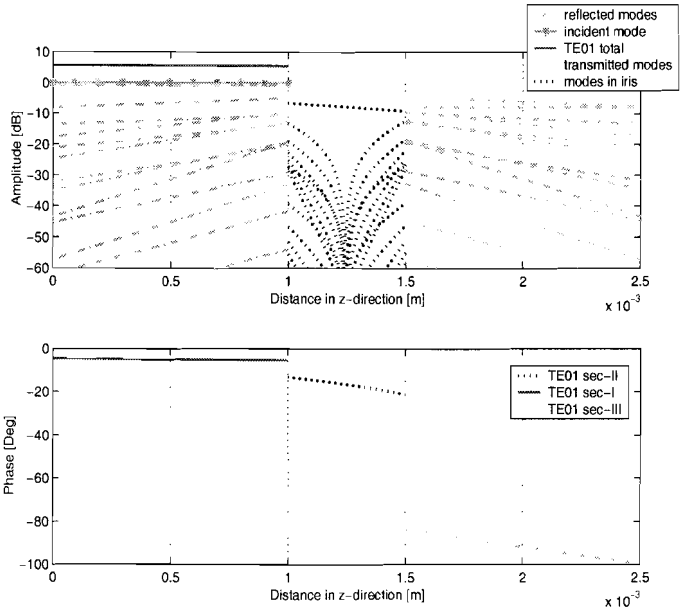

Figure 6.32: *Upper: amplitude of several modes, lower: phase of TE_{01} mode propagating in +z direction. Parameters are: $A = E = 13.4$ mm, $B = D = F = 13.5$ mm, $C = 2.1$ mm, $a_2 = 5.65$ mm, $\varepsilon_r = 3$, $tan\delta = 0$, number of modes taken along in computations is 312.*

Mode TE_{01} is reflected at a level of -0.7511 dB and transmitted at -7.991 dB. Compared to the long iris, (Fig.6.23), less signal is being reflected and more transmitted. The evanescent modes in the iris now really play a role in the coupling between the two junctions. Still, a phase jump of 62.99° is observed, at the junction of section-II with section-III, exactly according statements concluded previously. On the junction of section-I with section-II we now have a mismatch of 7.92°. The powerbalance, indicates a nett real power of $-8.8818.10^{-16}$ W and a nett imaginary power of $1.9967.10^{-1}$ W. Also the scattering parameters of the TE_{01} mode in Table 6.5 show convince results.

In Fig.6.33, the amplitude of the incident mode, the reflected modes in section-I and the transmitted modes in section-III on the S-matrix ports 1 and 2, respectively, are displayed. The S-matrix ports lie at $z_0 = 0$ mm and $z_3 = 2.5$ mm. Compared to the preceding cases, the canonical and the long iris, there are quite a few modes with a considerable contribution at the position of the S-matrix ports. Table 6.6 contains detailed information

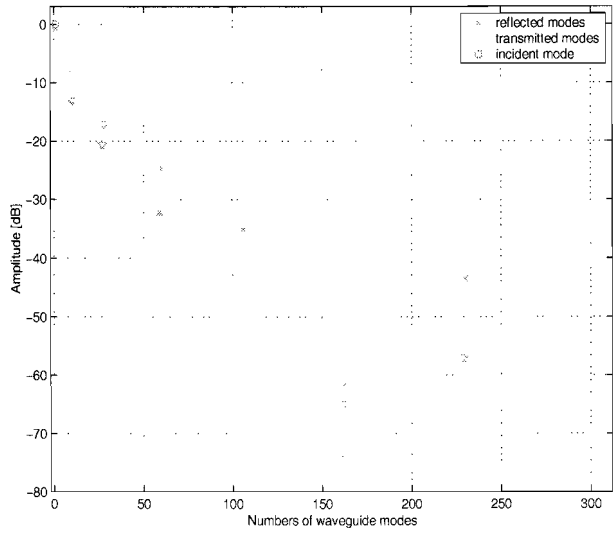

Figure 6.33: *Amplitude of reflected and transmitted modes at the position of S-matrix port 1 and 2, both at 1 mm distance removed form the waveguide junctions.*

of these modes. From Fig.6.33 and Table 6.6 one can notice a regularity in the mode indices

mode	TE_{01}
$\mathbf{s_{11}} =$	$9.0399.10^{-1} - j1.5486.10^{-1}$
$\mathbf{s_{21}} =$	$-6.7288.10^{-2} - j3.928.10^{-1}$
$\mid \mathbf{s_{11}} \mid^2 + \mid \mathbf{s_{21}} \mid^2 =$	1

Table 6.5: *Scattering parameters of mode TE_{01} on the port surfaces of the S-matrix, at $z_0 = 0$ mm and $z_3 = 2.5$ mm.*

mode number	1	9	10	27	28	59	60	105	106	161	162	229	230
(n, m)	(0,1)	(2,1)	(2,1)	(4,1)	(4,1)	(6,1)	(6,1)	(8,1)	(8,1)	(10,4)	(10,1)	(12,1)	(12,1)
mode type	TE	TM	TE	TM	TE	TM	TE	TM	TE	TM	TE	TM	TE
Reflect modes [dB]	-0.751	-8.217	-13.64	-21.18	-17.6	-32.19	-24.64	-45.25	-35.04	-74.1	-61.88	-57.27	-43.43
Transmit modes [dB]	-7.99	-7.755	-13.18	-20.7	-17.12	-31.69	-24.13	-44.63	-34.42	-77.22	-65	-57.08	-43.24

Table 6.6: *Modes depicted in Fig.6.33.*

(n, m) of the higher order modes. More specific, the reflection and transmission coefficients of the modes with n even and m equal to one, corresponding to x and y,respectively, are

larger qua magnitude. This can be explained as follows. The explanation for $m = 1$ is obvious, the y-dimension of the waveguide is uniform over the three sections, so there is no cause for generating higher order modes. To explain that n even, we will take a look at the TE and TM mode functions of the magnetic field Eq.(6.166), and realize that the cross-sections of all three sections are *centered*, thus forming a *symmetric* iris.

$$\mathbf{h}^{\alpha} = \begin{cases} \mathbf{h}' = \frac{-2}{k_t' \sqrt{AB}} \begin{bmatrix} -(\frac{m\pi}{D}) \sin(\frac{n\pi}{C}x) \cos(\frac{m\pi}{D}y)\mathbf{a}_x \\ (\frac{n\pi}{C}) \cos(\frac{n\pi}{C}x) \sin(\frac{m\pi}{D}y)\mathbf{a}_y \end{bmatrix}, \\ \mathbf{h}'' = \frac{\sqrt{\epsilon_m \epsilon_n}}{k_t'' \sqrt{AB}} \begin{bmatrix} (\frac{n\pi}{C}) \sin(\frac{n\pi}{C}x) \cos(\frac{m\pi}{D}y)\mathbf{a}_x \\ (\frac{m\pi}{D}) \cos(\frac{n\pi}{C}x) \sin(\frac{m\pi}{D}y)\mathbf{a}_y \end{bmatrix}, \end{cases} \tag{6.166}$$

If we apply n *even* and m equal to one to h_y^{α}, we find half a sine for the y-dependence, and p times a whole cosine for the x-dependence, with $p \in \{1, 2, 3, ...\}$, over the aperture of the iris. As a consequence, we have a completely positive function over the iris aperture in the y-direction, and in the x-direction a completely positive or negative function, depending of p, over the iris aperture, which will give rise to a contribution during integration over the aperture. This explains why n should be *even*. On the other hand, if we have a sine for the x-dependence in the magnetic field mode functions (see h_x^{α}) we can also create, with n *odd*, completely positive or negative function values over the aperture of the iris, leading to contributions during integration. However, because the y-dependence of h_x^{α} is a cosine, which is an *odd* function on the aperture domain, the total contribution of h_x^{α} vanishes. This explains the modes in Table 6.6, and at the same time it explains which component of the magnetic field produces a contribution.

Not visible in Fig.6.33 that there is again a cluster of modes around -325 dB and around -625 dB. There is not a real pattern in it, the only thing is that they come in pairs of mode types, logically, h_x' and h_x'', and, h_y' and h_y'', are equal except for a constant amplitude factor.

In Fig.6.34 and Fig.6.35, the x- and y-directed currents are plotted. As a consequence of the step in the cross-section in the x-dimension and closing of the aperture with a thin PEC, there exists a y-directed current with a singular behaviour towards the edges. The x-directed component, as in the canonical case, is very small because there is no change in the y-dimension of the waveguide cross-section. All these results are derived by taking along $N = 12$ and $M = 12$ resulting in 312 modes of which 144 TM and 168 TE modes. This was determined by looking at the convergence of the s_{11} parameter of mode TE_{01}, visible in Fig.6.36.

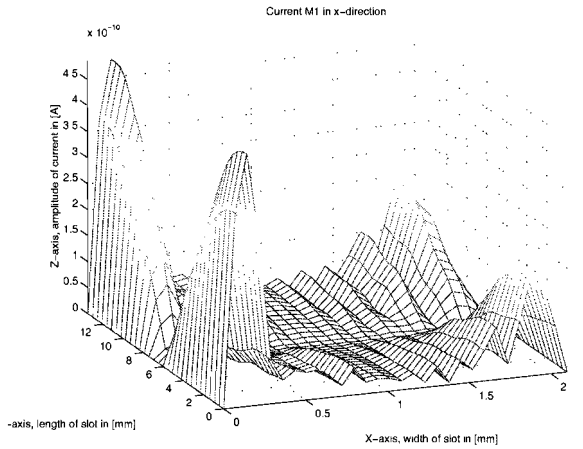

Figure 6.34: *x-directed equivalent magnetic surface current M1 at z_1. Dimensions of iris in x- and y-direction are $C = 2.1$ mm and $D = 13.5$ mm, respectively.*

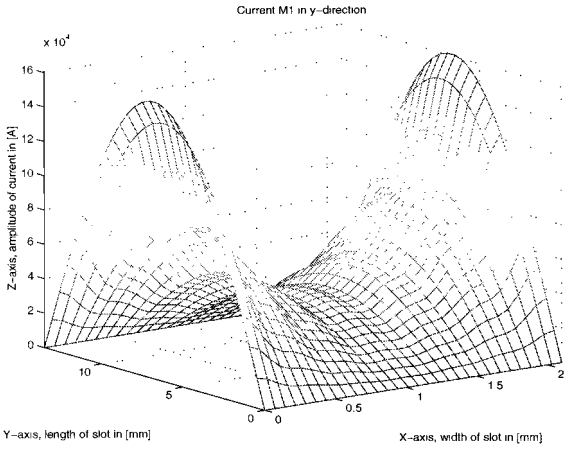

Figure 6.35: *y-directed equivalent magnetic surface current M1 at z_1. Dimensions of iris in x- and y-direction are $C = 2.1$ mm and $D = 13.5$ mm, respectively.*

At a number of 312 modes the s_{11} is well stabilized. Although the graph is still increasing

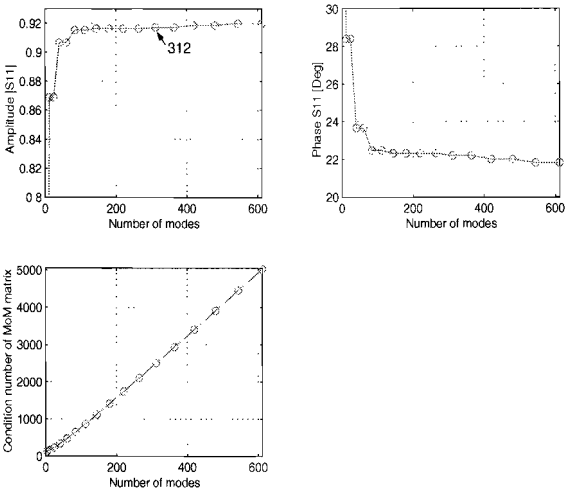

Figure 6.36: *Upper left: convergence of s_{11} of mode TE_{01}, upper right: convergence of corresponding phase, lower left: L^2-norm condition number of MoM matrix.*

very slowly no more modes are taken along. If one looks at het condition number of the MoM matrix, it is klimming linearly with the number of modes.

We would like to discus two last results. We start with frequency dependence of the s_{11} parameter for different lengths of the iris. In Fig.6.37, amplitudes and phases are displayed. Notice the varying distance between the minima of the s_{11} graphs, for the various iris lengths. This is due to the reflected field at the first waveguide junction and

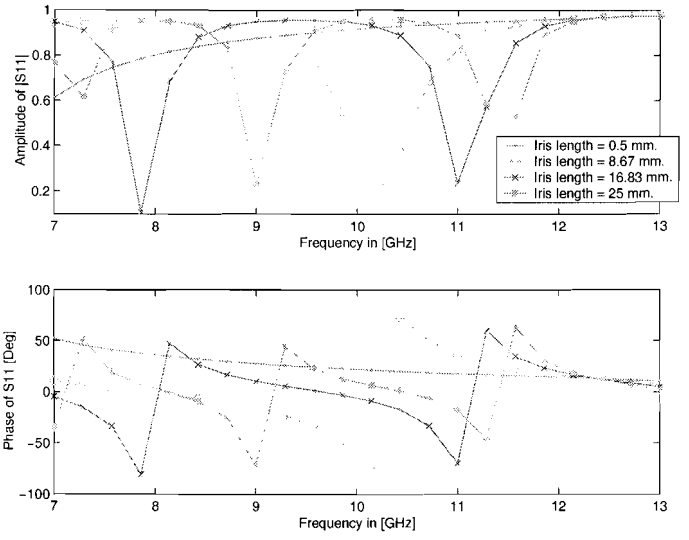

Figure 6.37: *Upper: amplitude of s_{11}, lower: corresponding phase progress. Incident mode is TE_{01}.*

the reflected field at the second junction, which both interfere with the incident field. The distance between the minima is getting shorter as the length of the iris increases.

The longer the iris gets, the longer the transmitted incident wave has to propagate through the iris before it is reflected at the second junction and reaches the first junction again, to be reflected again, and, transmitted into section-I to start interfering with the incident wave and its first reflection. This propagation, back and forth, through the iris causes a certain phase shift with the reflected incident wave at the first junction. Interpreting the frequency range of above graph in waveguide wavelengths, the range then starts with large wavelengths and ends with small wavelengths. Depending on the wavelength and the length of the iris, the interference of the reflected wave at the first junction and the reflected wave at the second junction with the incident wave matches (are constructief resulting in a low s_{11}) or doesn't matches (are destructive resulting in a high s_{11}).

The last results are related to the current graphs obtain from the thick iris case during the verification. As one can see, the current shapes are not convincing, since they are very rough, and especially the singular part of the x-component, in Fig.6.16. But, we would like to say and make clear that these currents are certainly in order. For the resulting current shape a lot depends on the dimensions of the aperture.

So, to make our point we have simulated an iris with of arbitrary size. The dimensional parameters are, $A = E = 13.4$ mm, $B = F = 13.5$ mm, $C = 2.1$ mm, $D = 9.5$ mm, $a_2 = 5.65$ mm, $b_2 = 2$ mm, $\varepsilon_r = 3$, $\tan\delta = 0$ and the number of modes taken along is 312. The incident field is the TE_{01} mode, which causes the currents presented in Figs.6.38 and 6.39. The polarization is in the y-direction, so the magnitude of the y-component of the current is the largest. The x-component has become much smoother and more convincing than before.

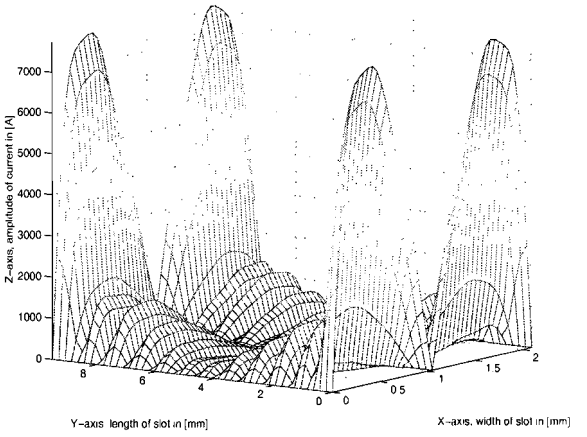

Figure 6.38: *x-directed equivalent magnetic surface current M1 at z_1. Dimensions of iris in x- and y-direction are $C = 2.1$ mm and $D = 9.5$ mm, respectively. Grid size is 45 by 45.*

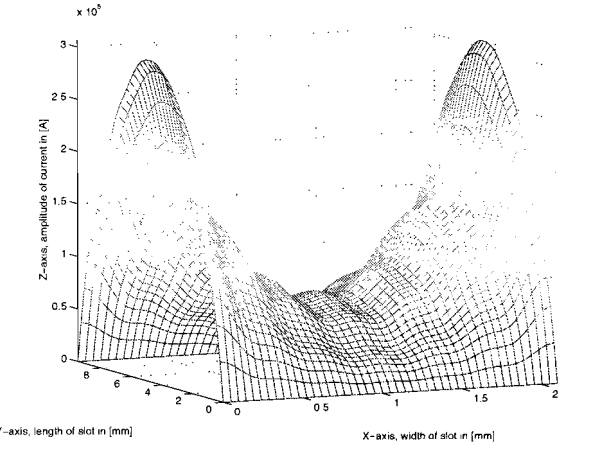

Figure 6.39: *y-directed equivalent magnetic surface current M1 at z_1. Dimensions of iris in x- and y-direction are $C = 2.1$ mm and $D = 9.5$ mm, respectively. Grid size is 45 by 45.*

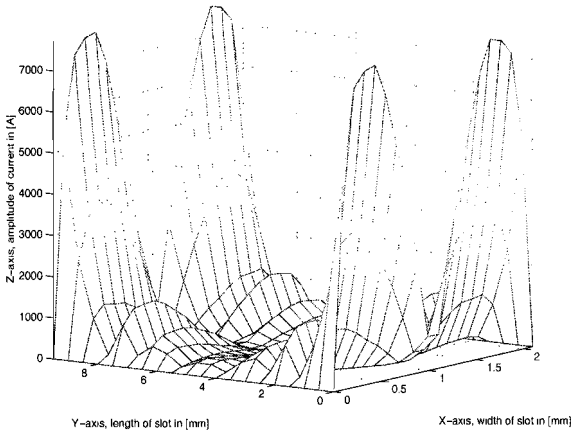

Figure 6.40: *x-directed equivalent magnetic surface current M1 at z_1. Dimensions of iris in x- and y-direction are $C = 2.1$ mm and $D = 9.5$ mm, respectively. Grid size is 20 by 20.*

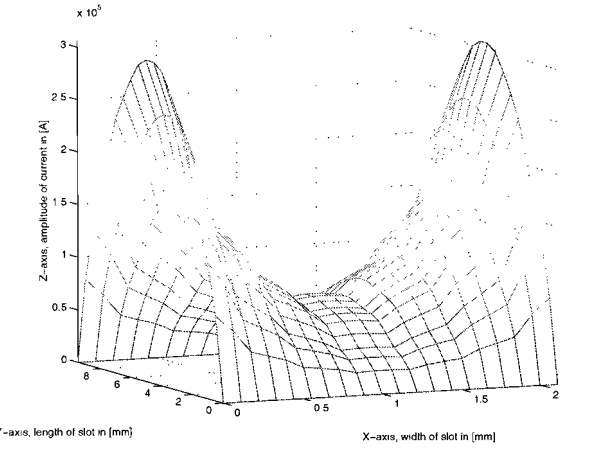

Figure 6.41: *y-directed equivalent magnetic surface current M1 at z_1. Dimensions of iris in x- and y-direction are $C = 2.1$ mm and $D = 9.5$ mm, respectively. Grid size is 20 by 20.*

In Figs.6.40 and 6.41 the same currents are plotted as in Figs.6.38 and 6.39, only in the first two mentioned figures, the x- and y-axis are divided in 20 equidistant points and in the last two mentioned figures the x- and y-axis are divided in 45 equidistant points. As one can see, in spit of the fact that entire domain basis functions are applied, the choice of mesh size to determine the point on which the current is plotted has its influence on the current shapes to a certain extent.

6.9 Convergence

In the preceding sections of this chapter, an analysis was made of the iris, with which the modes can be investigated on for instance, the propagation of modes, the power each mode transports, the magnitude of the modes on the cross-section at a particular point along the waveguide, etc. During Sec.6.8 these quantities have been reviewed, but the one thing that is still not clarified, is the number of modes that we took along during the computations. So now, we would like to focus on the convergence of our numerical method. What means that we will take a look at the minimum number of modes we need to take into account during the simulations to get a stable and reliable answer. By extending the approximations (the truncated summations), by taking the limit to infinity, i.e. $\lim N \rightarrow \infty$, $\lim M \rightarrow \infty$, the computations should converge to an exact solution, but because of the finiteness of the computer this will never be reached. It is not necessary to take along that many modes, to still get a reliable and accurate solution.

Normally, convergence can best be proven on the basis of first hand information and not through some derived parameter. So, what we are going to do is, trying to show convergence by imposing a L^2-norm on the difference of two successive current image (representations). If we are correct, the more modes we take along the more accurate the current mapping becomes. Hence, the difference between the currents goes to towards zero and also the L^2-norm. Later on more about that!

The currents are represented as

$$\mathbf{M}_a = \sum_{i=1}^{O} m'_{i;a}\mathbf{h}'_i + \sum_{i=1}^{P} m''_{i;a}\mathbf{h}''_i, \tag{6.167}$$

$$\mathbf{M}_b = \sum_{i=1}^{Q} m'_{i;b}\mathbf{h}'_i + \sum_{i=1}^{R} m''_{i;b}\mathbf{h}''_i, \tag{6.168}$$

with $Q > O$ and $R > P$. Next, taking the difference of the currents yields

$$\boldsymbol{\Delta}_{\mathbf{M}(i)} = \mathbf{M}_a - \mathbf{M}_b = \sum_{i=1}^{O} \Delta'_{m_i}\mathbf{h}'_i - \sum_{i=O+1}^{Q} m'_{i;b}\mathbf{h}'_i + \sum_{i=1}^{P} \Delta''_{m_i}\mathbf{h}''_i - \sum_{i=P+1}^{R} m''_{i;b}\mathbf{h}''_i, \tag{6.169}$$

where

$$\Delta'_{m_i} = m'_{i;a} - m'_{i;b}, \tag{6.170}$$

$$\Delta''_{m_i} = m''_{i;a} - m''_{i;b}. \tag{6.171}$$

Note that i consists of mode number indicators (n, m) and that $m'_{i;a} - m'_{i;b} = m'_{(n,m);a} - m'_{(n,m);b}$, indeed depends on the combination of (n, m) and not on the absolute value of i. So, the second and fourth term on the right-hand side in Eq.(6.169) consist of modes (n, m) that are not covered by the modes of current $\mathbf{M}_1$. Next, we introduce an L^2 inner

product and the induced norm as

$$\langle \mathbf{\Delta}_{\mathbf{M}(i)}, \mathbf{\Delta}_{\mathbf{M}(j)} \rangle = \int_{S^a} \mathbf{\Delta}_{\mathbf{M}(i)} \cdot (\mathbf{\Delta}_{\mathbf{M}(j)})^* \, d\sigma, \tag{6.172}$$

$$\| \mathbf{\Delta}_{\mathbf{M}(i)} \| = \sqrt{\langle \mathbf{\Delta}_{\mathbf{M}(i)}, \mathbf{\Delta}_{\mathbf{M}(i)} \rangle}, \tag{6.173}$$

respectively, where S^a is the aperture on which the current is defined. By substitution of Eq.(6.169) in Eq.(6.172) we get

$$\begin{aligned} \langle \mathbf{\Delta}_{\mathbf{M}(i)}, \mathbf{\Delta}_{\mathbf{M}(j)} \rangle = & \sum_{i=1}^{O} \sum_{j=1}^{O} \Delta'_{m_i} (\Delta'_{m_j})^* \int_{S^a} \mathbf{h}'_i \cdot \mathbf{h}'_j \, d\sigma + \sum_{i=O+1}^{Q} \sum_{j=O+1}^{Q} m'_{i;b} (m'_{j;b})^* \int_{S^a} \mathbf{h}'_i \cdot \mathbf{h}'_j \, d\sigma \\ & + \sum_{i=1}^{P} \sum_{j=1}^{P} \Delta''_{m_i} (\Delta''_{m_j})^* \int_{S^a} \mathbf{h}''_i \cdot \mathbf{h}''_j \, d\sigma + \sum_{i=P+1}^{R} \sum_{j=P+1}^{R} m''_{i;b} (m''_{j;b})^* \int_{S^a} \mathbf{h}''_i \cdot \mathbf{h}''_j \, d\sigma. \end{aligned} \tag{6.174}$$

Applying the orthogonality condition to Eq.(6.174), yields

$$\langle \mathbf{\Delta}_{\mathbf{M}(i)}, \mathbf{\Delta}_{\mathbf{M}(i)} \rangle = \sum_{i=1}^{O} \| \Delta'_{m_i} \|^2 + \sum_{i=O+1}^{Q} \| m'_{i;b} \|^2 + \sum_{i=1}^{P} \| \Delta''_{m_i} \|^2 + \sum_{i=P+1}^{R} \| m''_{i;b} \|^2 = \| \mathbf{\Delta}_{\mathbf{M}(i)} \|^2 \tag{6.175}$$

Excluded from Eq.(6.174) are the cross terms, because they don't contribute. This has two reasons. Firstly, there are constituents that contain the following the term $< \mathbf{h}'_i, \mathbf{h}''_j >$ which is zero for all i, j. Secondly, some constituents have summations corresponding to $\sum_{i=1}^{O} \sum_{j=O+1}^{Q}$ which as a result yield $< \mathbf{h}'_i, \mathbf{h}'_j >= 0$.

Eq.(6.175) depicts exactly what we explained previously. When the current mapping doesn't change anymore the first and third term on the right hand-side, containing differences of current coefficients, vanish. We will call the first and third term the *difference parts* from now on. Taking along more modes, when appears that the current image doesn't change anymore, has no effect on the outcome because their contribution will be zero, so, the second and fourth term on the right hand-side vanish also. The second and fourth term we will call *rest parts*. To get a better view on the convergence proces we will normalise Eq.(6.175) by dividing it by the squared norm of $\mathbf{M}_b$ which is stated in the expression below

$$\langle \mathbf{M}_b, \mathbf{M}_b \rangle = \sum_{i=1}^{Q} \| m'_{i;b} \|^2 + \sum_{i=1}^{R} \| m''_{i;b} \|^2 = \| \mathbf{M}_b \|^2 . \tag{6.176}$$

The case, for which we will investigate the convergence on basis of the current is as follows. We consider a thick iris with the following dimensions (in millimeter) $A = E = 22.85$, $B = F = 10.05$, $C = 11.9$, $D = 6.75$, $a_2 = 5.475$, $b_2 = 1.65$ and iris length

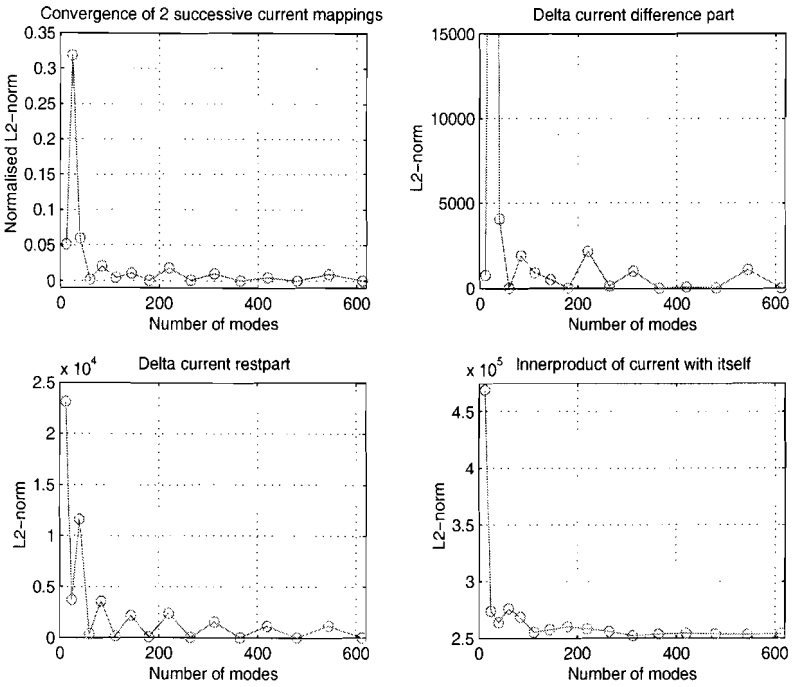

Figure 6.42: *Convergence of the equivalent magnetic current as a function of the number of modes, in the case of a thick iris.*

$(z_2 - z_1)$=3.9. We have an incident TE_{10} mode field and the frequency is 10 GHz. In Fig.6.42 the L^2-norm applied to the difference of two current mappings, determined by successive numbers of modes, is depicted together with some intermediate results. From the figure it is not completely clear if the idea or method by which we wanted to show convergence is working successfully. The normalised L^2-norm (upper left) starts wiggling around the 0.005 already after taking along 60 modes (fourth circle in graph). In the upper right is displayed the L^2-norm of what we call the *difference part* of the current. This corresponds to the first and the third term on the right-hand side of Eq.(6.175), these contain differences between current coefficients of modes with corresponding mode indicators, $(n, m) = i$. Each circle in the graph is a summation of differences between current coefficients. Notice that this curve wiggles around 900 and does not really converge in contrast to what we hoped. In the lower left corner of Fig.6.42, we see the L^2-norm of the what we call *rest part*. It corresponding to the second and fourth term on the right-hand side of Eq.(6.175), which contain current coefficients of modes who are present in current $\mathbf{M}_b$ and not in current $\mathbf{M}_a$. As one sees, the oscillations seem to decay but whether we can speak of a converging behaviour? We remark here that the points which seem to be zero, are not zero. This is because of the scale, they are in the order of 10 to 150. In the lower right graph of Fig.6.42 shows the squared norm of the current $\mathbf{M}_b$, used for the normalization.

The question now is, does it of doesn't it converge, or are the finally obtain results not

clear enough to say useful things about the convergence? To answer this question, we have plotted the absolute value of the current coefficients of the four terms on the right-hand side of Eq.6.175, *difference* and *rest parts* for TM as well as for TE modes. This is presented in Fig.6.43 for currents determined with 264 modes (squares) and 312 modes (circles). In

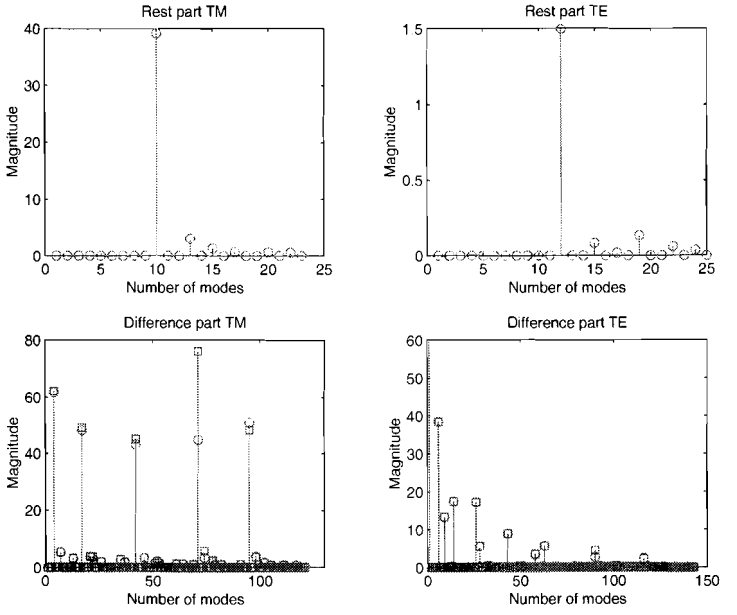

Figure 6.43: *Magnitude of current coefficients of rest part and difference part as function of number of modes, for the current determined with 264 modes (squares) and 312 modes. The amplitude of the first mode in the lower right graph is 484.*

the upper graphs the *rest parts* for TM (left) and TE (right) are displayed. In both graphs there is a large peak which represents a relevant contribution in both cases of mode (1,12). In the lower graphs, the *difference parts* for TM (left) and TE (right) are given. The mode indices (n, m) of the modes that contribute the most (large peaks) when we take along 264 modes, compared to when we take along 312 modes, do not change. Only the magnitude of a few of them changes, with one exceptional case. This is in fact not only true for the modes with the largest contribution, but also for the modes with smaller contributions, the effect is just better visible for the larger peaks. In the lower right graph of Fig.6.43, only a part of the first mode can be seen, because its amplitude is so high, (484). The first mode is namely the incident mode field TE (1,0).

The mode numbers (n, m) of the first five TM modes and the first five TE modes with the largest contribution, of the lower two graphs in Fig.6.43, are stated in Table 6.7

In Fig.6.44 we have depicted the same quantities as in Fig.6.43 only now, we took into account 544 modes (squares) and 612 modes (circles), in order to see what happens if we make a jump in the number of modes we use in the MoM. As one can see in the upper left graph, the magnitude of the modes in the TM *rest part* has strongly decreased, compared to the preceding results. Concerning the TE *rest part* a whole other mode with

	Mode indices				
TM difference part	(1,2)	(1,4)	(1,6)	(1,8)	(1,10)
TE difference part	(1,0)	(3,0)	(1,2)	(5,0)	(7,0)

Table 6.7: *Mode indices (n, m) of first five largest current coefficients of TM and TE difference part.*

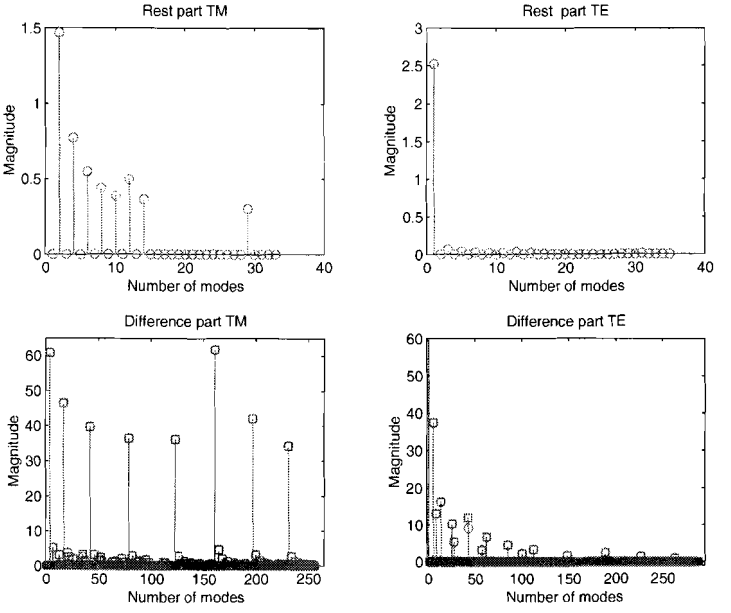

Figure 6.44: *Magnitude of current coefficients of rest part and difference part as function of number of modes, for current determined with 544 modes (squares) and 612 modes (circles). The amplitude of the first mode in the lower right graph is 484.*

a somewhat larger magnitude has come up. This overal decreasing behaviour in the graphs of the current *rest parts* corresponds to the curve in the lower left graph of Fig.6.42.

In the lower left graph of Fig.6.44, we see three more modes with a relevant contribution and the differences in magnitude have become smaller compared to the lower left graph in Fig.6.43. Also, the magnitude of the first five relevant contributing TM modes has changed somewhat. In the lower right graph there are not much differences. In Table 6.8 we have given the mode indices of the modes with largest magnitude, from left to right for al the four graphs.

In general, we can conclude from Figs.(6.43) and (6.44) that, the effect of taking along more and more modes, is the appearance of more current coefficients with a considerable contribution. The mode indices (n, m) of these contributing coefficients, referring to the TM and TE current *difference parts*, appear to stay unchanged when the number of modes which are taken into account are increased. The differences in magnitudes, on the other hand, seem to get smaller.

Then, if we go back to the x- and y-directed equivalent magnetic currents in Figs.6.16

	Mode indices							
TM rest	(17,2)	(17,4)	(17,6)	(17,8)	(17,10)	(17,12)	(17,14)	(17,16)
TE rest	(71,0)							
TM difference	(1,2)	(1,4)	(1,6)	(1,8)	(1,10)	(1,12)	(1,14)	(1,16)
TE difference	(1,0)	(3,0)	(1,2)	(5,0)	(7,0)	(1,4)	(9,0)	

Table 6.8: *Mode indices* (n, m) *of the largest current coefficients of all four graphs of Fig.6.44.*

and 6.17, we remember the singular behaviour of the current components along the edges. Back then, we already mentioned that this was caused by the sharp edges in the waveguide. In theory the current would become infinitely large at the edge. With the MoM we try to approximate this singular current by expanding it in a sum of weighting coefficients and basis functions, and as one has been able to read, we applied the waveguide modes (sinus and cosinus functions) as basis functions. The steep flanks of these singularities can be made exact (in analogy with the Fourier series) if an infinite number of waveguide modes are taken along. Sinusoidal functions behave very regularly and have continuous derivatives. So, to approximate singularities, a lot of such functions are needed. We have been able to see this in the figures where the magnitude of current coefficients are plotted. Comparing the graphs where we took 312 modes into account, (Fig.6.43), and 612 modes, (Fig.6.44), one can observe this effect of approximating a singular function with regular functions viz. in the last figure there are more largely contributing current coefficients, represented by the large peaks.

After having seen the preceding results, one could ask himself one other thing viz., is it possible to use an L^2-norm in this case? We have reason enough it should, based on the following. The corners that the waveguide makes at the edges of the aperture, the aperture on which the equivalent magnetic current are going to be determined, have an angle of 90°. According to [17, p.569] this introduces singularities, which we saw in Figs.6.16 and 6.17, of order $\frac{1}{\sqrt[3]{x}}$. This kind of functional behaviour can be captured with an L^2-norm, which answers that question.

Returning to the question of, does the convergence work yes or no?, we say eventually no, and we can also explain where the problem is at. We overlooked something during the discussion of our idea to demonstrate convergence. There was written that if, the differences between the current coefficients would go to zero, the L^2-norm would also go to zero. Unfortunately, the L^2-norm contains summations of differences which not necessarily have to converge if the difference-terms go to zero. The fact that the differences between the coefficients go the zero is at the most a necessary condition.

Therefore, we decided to check for convergence by means of an alternative parameter viz. the scattering parameter. It was probably also been possible to use a different norm e.g. the L^1-norm.

Chapter 7

Patch in waveguide

7.1 Introduction

An analysis of a patch in a waveguide is a second problem which we would like to discuss. The theory for handling waveguide problems, which we discussed in Chapters 3-5 and applied to the iris problem, is also applicable to the patch problem. Basically the patch can have an arbitrary flat shape. In our problem, the patch has a rectangular shape, made of an infinitely thin PEC and is placed perpendicular to the propagation direction, thereby forming a disturbance in the longitudinal direction. The method of moments, as before, is a suitable tool to deal with this problem. The foundation we developed for the iris can also be applied here.

Agian it's our objective to analyse the behavior of the modes by means of an S-matrix. Fig.7.1(a) depicts the situation. We start from an infinitely long waveguide along the

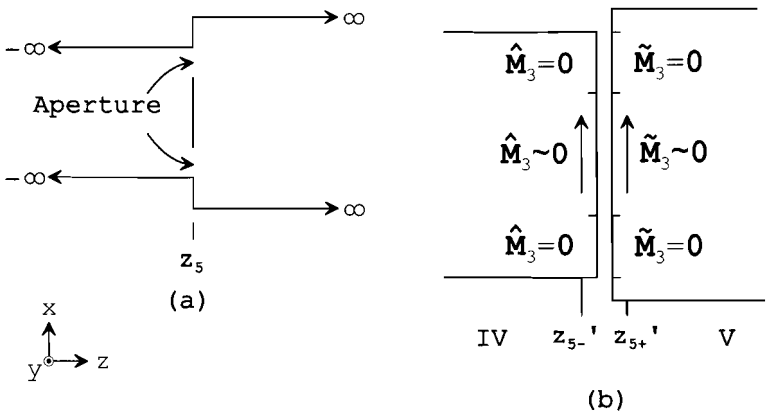

Figure 7.1: *(a) A microstrip patch, made of a thin PEC in an infinitely long waveguide. (b) The equivalent system with equivalent magnetic currents defined on the aperture closed with a PEC.*

spatial z-axis. At $z = z_5$ there is a patch in the waveguide, with dimensions $l_x = K$ and $l_y = L$. As indicated in Fig.7.1(a) there is accounted for an abrupt transition in the

waveguide cross-section at the position of the patch. In Fig.7.1(b) the equivalent situation is given. The aperture, i.e. the area between the patch and the waveguide wall is closed by a thin PEC, thereby creating two regions named section-IV and section-V. Section-IV has cross-sectional x- and y-dimensions G and H, respectively and section-V has cross-sectional x- and y-dimensions Q and R.

7.2 Solving transmission line equations; Modal Green's functions

The analysis starts with finding the solution to the equivalent transmission line equations for section-IV and -V. There is a lot of analogy with the iris case. The method we used for section-I and -III in Sec.6.3.1 and Sec.6.3.3 can be directly applied to section-IV and -V.

For section-IV we find

$$I_i^{\alpha;\mathrm{IV}}(z) = \int G_{I;i}^{\alpha;\mathrm{IV}}(z, z'_{5-})\, v_i^{\alpha;\mathrm{IV}}(z'_{5-})\, \delta(z - z'_{5-}) dz'_{5-} = -Y_{\infty;i}^{\alpha;\mathrm{IV}}\, v_i^{\alpha;\mathrm{IV}}(z_5)\, e^{jk_{z;i}^{\alpha;\mathrm{IV}}(z-z_5)}, \quad (7.1)$$

for $z \leq z_5$ and with $v_i^{\alpha;\mathrm{IV}}(z_5) =< \hat{\mathbf{M}}_3(\boldsymbol{\rho}, z_5), \mathbf{h}_i^{\alpha;\mathrm{IV}} >$.

For section-V we find

$$I_p^{\alpha;\mathrm{V}}(z) = \int G_{I;p}^{\alpha;\mathrm{V}}(z, z'_{5+})\, v_p^{\alpha;\mathrm{V}}(z'_{5+})\, \delta(z - z'_{5+}) dz'_{5+} = -Y_{\infty;p}^{\alpha;\mathrm{V}}\, v_p^{\alpha;\mathrm{V}}(z_5)\, e^{-jk_{z;p}^{\alpha;\mathrm{V}}(z-z_5)}, \quad (7.2)$$

for $z \geq z_5$ and with $v_p^{\alpha;\mathrm{V}}(z_5) =< \tilde{\mathbf{M}}_3(\boldsymbol{\rho}, z_5), \mathbf{h}_p^{\alpha;\mathrm{V}} >$. On numerical basis we substituted $z'_{5-} = z_5$ in the right-hand side of Eq.(7.1), and $z'_{5+} = z_5$ in the right-hand side of Eq.(7.2)

7.3 Method of moments formulation

The next step in the analysis of the patch is to set up the method of moments formulation. This formulation is based on the boundary conditions at the aperture which demand continuity of the tangential electric and magnetic field over the aperture. In Chapter 2 we showed that the continuity of the tangential electric field has been used to define equivalent magnetic surface currents and, as in the case of the iris, the continuity of the tangential magnetic field remains to be enforced. For this we can write

$$\mathbf{n} \times \mathbf{H}^{\mathrm{IV};tot}(\mathbf{r})\Big|_{z=z_5} = \mathbf{n} \times \mathbf{H}^{\mathrm{V};tot}(\mathbf{r})\Big|_{z=z_5} \qquad \mathbf{r} \in S_5^a, \quad (7.3)$$

where S_5^a is the aperture surface, confined between the patch and the waveguide wall at $z = z_5$, and $\mathbf{n}$ is the aperture surface normal vector. Eq.(7.3) can be written as

$$\left(\mathbf{H}_t^{\mathrm{IV};inc} + \mathbf{H}_t^{\mathrm{IV}}(\hat{\mathbf{M}}_3) - \mathbf{H}_t^{\mathrm{V}}(\tilde{\mathbf{M}}_3) - \mathbf{H}_t^{\mathrm{V};inc}\right)\Big|_{z=z_5} = \mathbf{0}, \quad (7.4)$$

where t is an indication for *tangential* components, which correspond to the transverse fields. The total transverse magnetic fields in sections-IV and -V can be split up in an incident field denoted by "inc" and a field depending on the equivalent magnetic current $\mathbf{M}_3$. We intent to solve the unknown current numerical, with the help of this equation. As in the case of the iris we therefore define a so-called *residue*, $\mathbf{R}(\mathbf{r})$, according

$$\mathbf{R}(\mathbf{r}) = \left(\mathbf{H}_t^{\mathrm{IV};tot} - \mathbf{H}_t^{\mathrm{V};tot}\right)\Big|_{z=z_5}, \tag{7.5}$$

This residue must be zero on $S_{z_5}^a$. Because, this is somewhat too restrictive, we weaken the demand by testing the residue to zero with help of a set of testing functions $\mathbf{w}_s(\mathbf{r})$, according to the definition in Eq.(6.51). The test functions are defined as, unequal on the aperture surface $\mathbf{r} \in S_{z_5}^a$, and zero elsewhere. The subscript of the test functions indicates an ordering of the test functions, $s \in \{1, \ldots, N\}$. Eq.(7.4) becomes

$$\left\langle \left(\mathbf{H}_t^{\mathrm{IV};inc} - \mathbf{H}_t^{\mathrm{V};inc}\right), \mathbf{w}_s \right\rangle + \left\langle \left(\mathbf{H}_t^{\mathrm{IV}}(\hat{\mathbf{M}}_3) - \mathbf{H}_t^{\mathrm{V}}(\tilde{\mathbf{M}}_3)\right), \mathbf{w}_s \right\rangle \Big|_{z=z_5} = \mathbf{0}, \tag{7.6}$$

The magnetic fields depending on the magnetic surface current $\mathbf{M}_3$ are written in their modal field representation as follows

$$\left\langle \left(\mathbf{H}_t^{\mathrm{IV};inc} - \mathbf{H}_t^{\mathrm{V};inc}\right), \mathbf{w}_s \right\rangle + \left\langle \left(\sum_i I_i^{\alpha;\mathrm{IV}}(\hat{\mathbf{M}}_3)\mathbf{h}_i^{\alpha;\mathrm{IV}} - \sum_p I_p^{\alpha;\mathrm{V}}(\tilde{\mathbf{M}}_3)\mathbf{h}_p^{\alpha;\mathrm{V}} \right), \mathbf{w}_s \right\rangle \Big|_{z=z_5} = \mathbf{0}, \tag{7.7}$$

with

$$I_i^{\alpha;\mathrm{IV}}(z) = -Y_{\infty;i}^{\alpha;\mathrm{IV}} \left\langle \hat{\mathbf{M}}_3, \mathbf{h}_i^{\alpha;\mathrm{IV}} \right\rangle e^{jk_{z;i}^{\alpha;\mathrm{IV}}(z-z_5)}, \tag{7.8}$$

$$I_p^{\alpha;\mathrm{V}}(z) = -Y_{\infty;p}^{\alpha;\mathrm{V}} \left\langle \tilde{\mathbf{M}}_3, \mathbf{h}_p^{\alpha;\mathrm{V}} \right\rangle e^{-jk_{z;p}^{\alpha;\mathrm{V}}(z-z_5)}. \tag{7.9}$$

The next step is the expansion of the unknown current $\mathbf{M}_3$ in a complete set of vectorial basis functions, $\mathbf{f}_r$, and their corresponding unknown expansion coefficients m_r, where $r \in \{1, \ldots, N\}$:

$$\hat{\mathbf{M}}_3(\boldsymbol{\rho}) = \sum_r m_r \mathbf{f}_r(\boldsymbol{\rho}) \qquad \boldsymbol{\rho} \in S_5^a. \tag{7.10}$$

Substituting Eqs.(7.8)-(7.10) into Eq.(7.7) and using the relation $\tilde{\mathbf{M}}_3 = -\hat{\mathbf{M}}_3$, defined in Eq.2.6, yields

$$\left\langle \left(\mathbf{H}_t^{\mathrm{IV};inc} - \mathbf{H}_t^{\mathrm{V};inc}\right), \mathbf{w}_s \right\rangle \Big|_{z=z_5} = \left\{ \sum_r m_r \sum_i Y_{\infty;i}^{\alpha;\mathrm{IV}} \left\langle \mathbf{f}_r, \mathbf{h}_i^{\alpha;\mathrm{IV}} \right\rangle \left\langle \mathbf{h}_i^{\alpha;\mathrm{IV}}, \mathbf{w}_s \right\rangle e^{jk_{z;i}^{\alpha;\mathrm{IV}}(z-z_5)} \right.$$
$$\left. + \sum_r m_r \sum_p Y_{\infty;p}^{\alpha;\mathrm{V}} \left\langle \mathbf{f}_r, \mathbf{h}_p^{\alpha;\mathrm{V}} \right\rangle \left\langle \mathbf{h}_p^{\alpha;\mathrm{V}}, \mathbf{w}_s \right\rangle e^{-jk_{z;p}^{\alpha;\mathrm{V}}(z-z_5)} \right\} \Big|_{z=z_5}.$$

(7.11)

In shot hand notation it becomes

$$I_s^{ex} = \sum_r m_r T_{sr}^{\mathrm{IV;V}}, \tag{7.12}$$

where

$$T_{sr}^{\mathrm{IV;V}} = \sum_i Y_{\infty;i}^{\alpha;\mathrm{IV}} \Pi_{ri}^{\mathrm{IV}} \Pi_{is}^{\mathrm{IV}} + \sum_p Y_{\infty;p}^{\alpha;\mathrm{V}} \Pi_{rp}^{\mathrm{V}} \Pi_{ps}^{\mathrm{V}}, \tag{7.13}$$

$$\Pi_{ri}^{\mathrm{IV}} = \left\langle \mathbf{f}_r, \mathbf{h}_i^{\alpha;\mathrm{IV}} \right\rangle, \tag{7.14}$$

$$\Pi_{is}^{\mathrm{IV}} = \left\langle \mathbf{h}_i^{\alpha;\mathrm{IV}}, \mathbf{w}_s \right\rangle, \tag{7.15}$$

$$\Pi_{rp}^{\mathrm{V}} = \left\langle \mathbf{f}_r, \mathbf{h}_p^{\alpha;\mathrm{V}} \right\rangle, \tag{7.16}$$

$$\Pi_{ps}^{\mathrm{V}} = \left\langle \mathbf{h}_p^{\alpha;\mathrm{V}}, \mathbf{w}_s \right\rangle, \tag{7.17}$$

$$I_s^{ex} = \left\langle \left(\mathbf{H}_t^{\mathrm{IV};inc} - \mathbf{H}_t^{\mathrm{V};inc} \right), \mathbf{w}_s \right\rangle. \tag{7.18}$$

Excitation

The excitation vector, I_s^{ex}, can be given a more specific form by writing the incident transverse magnetic fields in their modal field expression. From Eq.(7.18) we get

$$I_s^{\mathrm{IV};ex} = \left\langle \mathbf{H}_t^{\mathrm{IV};inc}, \mathbf{w}_s \right\rangle = \sum_i I_i^{\alpha;\mathrm{IV}} \left\langle \mathbf{h}_i^{\alpha;\mathrm{IV}}, \mathbf{w}_s \right\rangle, \tag{7.19}$$

$$I_s^{\mathrm{V};ex} = -\left\langle \mathbf{H}_t^{\mathrm{V};inc}, \mathbf{w}_s \right\rangle = -\sum_p I_p^{\alpha;\mathrm{V}} \left\langle \mathbf{h}_p^{\alpha;\mathrm{V}}, \mathbf{w}_s \right\rangle. \tag{7.20}$$

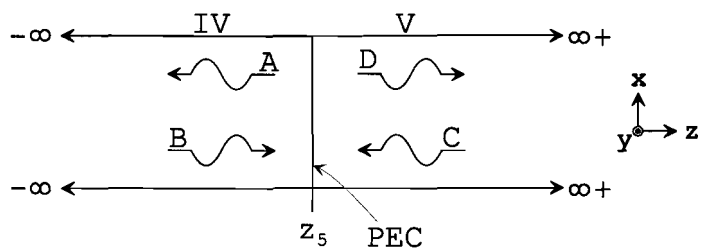

Figure 7.2: *Incident and reflected waves of the excitation field in section-IV and -V.*

Then, by means of Fig.(7.2) we find

$$I^{\mathrm{IV}}(z_5) = 2BY_\infty^{\mathrm{IV}}, \tag{7.21}$$

$$I^{\mathrm{V}}(z_5) = -2CY_\infty^{\mathrm{V}}. \tag{7.22}$$

and subsequently

$$I_s^{\mathrm{IV};ex} = \sum_i 2B_i^{\alpha} Y_{\infty;i}^{\alpha;\mathrm{IV}} \Pi_{is}^{\mathrm{IV}}, \tag{7.23}$$

$$I_s^{\mathrm{V};ex} = -\sum_p -2C_p^{\alpha} Y_{\infty;p}^{\alpha;\mathrm{V}} \Pi_{ps}^{\mathrm{V}}. \tag{7.24}$$

Appendix G gives a survey of the MoM formulation in matrix notation. In Appendix F the integrals of Eqs.(7.14)-(7.17) are worked out.

7.3.1 Basis functions & Test functions

In contrast to the iris case, the aperture is disturbed by a patch. Therefore, we need other basis functions. Since the patch can have an arbitrary shape, which requires a higher degree of flexibility of the basis functions. Subdomain basis functions fulfil this need. Therefore we have chosen the RWG basis function named after its inventors **R**ao, **W**ilton and **G**lisson, [25]. Since we apply Garlerkin's methode during the method of moments, the basis en test functions will be the same in type and number. The RWG basis function is defined as

$$\mathbf{f}_r = \mathbf{w}_s = \mathbf{g}_n(\mathbf{r}) = \begin{cases} \frac{l_n}{2A_n^+}\boldsymbol{\rho}_n^+, & \boldsymbol{\rho}_n^+ = \mathbf{r} - \mathbf{r}_R, \quad \mathbf{r} \text{ in } T_n^+ \\ \frac{l_n}{2A_n^-}\boldsymbol{\rho}_n^-, & \boldsymbol{\rho}_n^+ = \mathbf{r}_U - \mathbf{r}, \quad \mathbf{r} \text{ in } T_n^-, \\ \mathbf{0} \quad \text{otherwise} \end{cases} \tag{7.25}$$

where $\mathbf{r}_R$ and $\mathbf{r}_U$ can be found in Fig.7.3. The RWG function is a proper basis function. We will quickly mention some important properties. For a detailed discussion we refer to [25].
The most important properties of the RWG-function are:

- The basis function has no component normal to the outer boundary of its support formed by the triangle pair T_n^- and T_n^+ (this excludes the common edge). Therefore, no charge can flow of the triangle pair and there is no line charge.

- In contrast to the boundary formed by the outer contour of the triangle pair, there exists a component of the current normal to the common edge that is constant and continuous across this common edge.

- The factors $\frac{l_n}{2A_n^+}$ and $\frac{l_n}{2A_n^-}$ set the current density component normal to the common edge to unity. From which we can conclude that the triangle pair is line charge free. The boundary condition derived from the conservation of charge can be used to check this.

- The divergence of $\mathbf{g}_n$ which is proportional the charge density on the triangle pair remains finite. The mentioned quantities are surface quantities owing to the type of

problem.

$$\nabla_s \cdot \mathbf{g}_n = \begin{cases} \frac{l_n}{2A_n^+} \nabla_s \cdot \mathbf{r} = \frac{l_n}{A_n^+}, \\ \frac{l_n}{2A_n^-} \nabla_s \cdot (-\mathbf{r}) = \frac{-l_n}{A_n^-}, \\ \mathbf{0} \qquad \text{otherwise.} \end{cases} \tag{7.26}$$

with $\mathbf{r} = x\mathbf{a}_x + y\mathbf{a}_y$

In Fig.7.3, a RWG basis function is depicted. Visible are two triangles T_n^+ and T_n^-, joined together via one of there sides, forming the common edge. On every two adjacent triangles, a RWG basis function can be defined. R is the free vertex of T_n^+ with position vector $\mathbf{r}_R$ and U is the free vertex of T_n^- with position vector $\mathbf{r}_U$. The vector $\mathbf{r}$ is a position vector of an arbitrary point.

In general, every triangle will have three neighbours, depending on the shape of the specific domain. Assuming every triangle has three neighbours, three basis functions $\mathbf{g}_n = \frac{l_n}{2A_n}\boldsymbol{\rho}_n$, with $n \in \{1, 2, 3\}$, per triangle can be defined. By combining them, according $l_2\boldsymbol{\rho}_1 - l_1\boldsymbol{\rho}_2$ and $l_3\boldsymbol{\rho}_1 - l_1\boldsymbol{\rho}_3$ a constant vector of arbitrary length and direction can be constructed, in this way any linear varying vector field on the triangles can be created. With

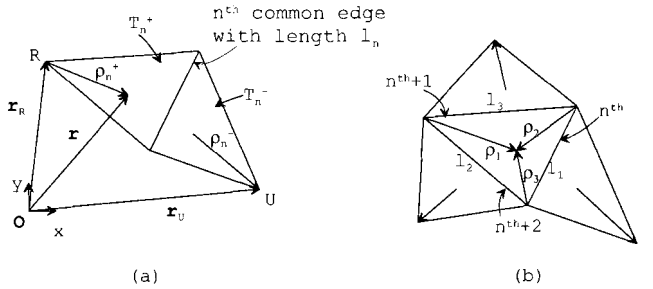

Figure 7.3: *(a) A RWG basis function, defined on two adjacent triangles, T_n^+ with area A_n^+ and T_n^- with area A_n^-. (b) Triangle T_n^+ and its adjacent triangles forming three basis functions.*

7.4 S-matrix notation

From the MoM, it is possible to construct an S-matrix for the patch. There is a lot of resemblance with the iris case. The S-matrix notation is defined as

$$\begin{bmatrix} I^{\mathrm{IV};out} \\ I^{\mathrm{V};out} \end{bmatrix} = \begin{bmatrix} s_{11} & s_{12} \\ s_{21} & s_{22} \end{bmatrix} \begin{bmatrix} I^{\mathrm{IV};in} \\ I^{\mathrm{V};in} \end{bmatrix}. \tag{7.27}$$

Port 1 lies in waveguide section-IV at $z = z_5$. Port 2 is placed in section-V at $z = z_5$.

Incoming and outgoing waves port 1

By analogy with Sec.6.5.1, we find the following expressions for the incoming and outgoing waves, per mode, at port 1 at $z = z_5$

$$I_i^{\alpha;\mathrm{IV};+}(z_5) = B_i^{\alpha} Y_{\infty;i}^{\alpha;\mathrm{IV}} = I_i^{\mathrm{IV};in}, \tag{7.28}$$

$$I_i^{\alpha;\mathrm{IV};-}(z_5) = B_i^{\alpha} Y_{\infty;i}^{\alpha;\mathrm{IV}} - Y_{\infty;i}^{\alpha;\mathrm{IV}} \sum_r m_r \Pi_{ri}^{\mathrm{IV}} = I_i^{\mathrm{I};out}, \tag{7.29}$$

where the outgoing waves are partially caused by $\hat{\mathbf{M}}_3$.

Incoming and outgoing waves port 2

Concerning the incoming and outgoing waves at port 2, together with the results of Sec.6.5.2, we find the following expressions at $z = z_5$, per mode,

$$I_p^{\alpha;\mathrm{V};-}(z_5) = -C_p^{\alpha}\, Y_{\infty;p}^{\alpha;\mathrm{V}} = I_p^{\mathrm{V};in}, \tag{7.30}$$

$$I_p^{\alpha;\mathrm{V};+}(z_5) = -C_p^{\alpha}\, Y_{\infty;p}^{\alpha;\mathrm{V}} + Y_{\infty;p}^{\alpha;\mathrm{V}} \sum_r m_r \Pi_{rp}^{\mathrm{V}} = I_p^{\mathrm{V};out}. \tag{7.31}$$

where we have used the fact that $\hat{\mathbf{M}}_3 = -\tilde{\mathbf{M}}_3$, because the outgoing waves in section-V are partially caused by $\tilde{\mathbf{M}}_3$.

7.4.1 S-parameters

To find the S-parameters, we will use the matrix-vector-notation. The outgoing waves in section-IV and section-V are given by

$$[I^{\mathrm{IV};out}]_i = [Y^{\mathrm{IV}}]_{ii}[B^{\alpha}]_i - [Y^{\mathrm{IV}}]_{ii}[\Pi^{\mathrm{IV}}]_{ri}^{\mathrm{T}}[m]_r = [I^{\mathrm{IV};in}]_i - [Y^{\mathrm{IV}}]_{ii}[\Pi^{\mathrm{IV}}]_{ri}^{\mathrm{T}}[m]_r, \tag{7.32}$$

$$[I^{\mathrm{V};out}]_p = [Y^{\mathrm{V}}]_{pp}[-C^{\alpha}]_p + [Y^{\mathrm{V}}]_{pp}[\Pi^{\mathrm{V}}]_{rp}^{\mathrm{T}}[m]_r = [I^{\mathrm{V};in}]_p + [Y^{\mathrm{V}}]_{pp}[\Pi^{\mathrm{V}}]_{rp}^{\mathrm{T}}[m]_r. \tag{7.33}$$

Eq.(7.12) written in matrix-vector-notation yields

$$[I^{ex}]_s = [T^{\mathrm{IV};\mathrm{V}}]_{sr}[m]_r, \tag{7.34}$$

from which an expression for the unknown magnetic current coefficients can be derived, as

$$[m]_r = [T^{\mathrm{IV};\mathrm{V}}]_{rs}^{-1}[I^{ex}]_s = 2[T^{\mathrm{IV};\mathrm{V}}]_{rs}^{-1}[\Pi^{\mathrm{IV}}]_{is}^{\mathrm{T}}[I^{\mathrm{IV};in}]_i - 2[T^{\mathrm{IV};\mathrm{V}}]_{rs}^{-1}[\Pi^{\mathrm{V}}]_{ps}^{\mathrm{T}}[I^{\mathrm{V};in}]_p. \tag{7.35}$$

Substitution of Eq.(7.35) in Eq.(7.32) and (7.33) yields the S-parameters

$$[s_{11}]_{ii} = [\underline{I}]_{ii} - 2[Y^{\mathrm{IV}}]_{ii}[\Pi^{\mathrm{IV}}]_{ri}^{\mathrm{T}}[T^{\mathrm{IV};\mathrm{V}}]_{rs}^{-1}[\Pi^{\mathrm{IV}}]_{is}^{\mathrm{T}}, \tag{7.36}$$

$$[s_{12}]_{ip} = 2[Y^{\mathrm{IV}}]_{ii}[\Pi^{\mathrm{IV}}]_{ri}^{T}[T^{\mathrm{IV};\mathrm{V}}]_{rs}^{-1}[\Pi^{\mathrm{V}}]_{ps}^{\mathrm{T}}, \tag{7.37}$$

$$[s_{12}]_{pi} = 2[Y^{\mathrm{V}}]_{pp}[\Pi^{\mathrm{V}}]_{rp}^{\mathrm{T}}[T^{\mathrm{IV};\mathrm{V}}]_{rs}^{-1}[\Pi^{\mathrm{IV}}]_{is}^{\mathrm{T}}, \tag{7.38}$$

$$[s_{22}]_{pp} = [\underline{I}]_{pp} - 2[Y^{\mathrm{V}}]_{pp}[\Pi^{\mathrm{V}}]_{rp}^{\mathrm{T}}[T^{\mathrm{IV};\mathrm{V}}]_{rs}^{-1}[\Pi^{\mathrm{V}}]_{ps}^{\mathrm{T}}. \tag{7.39}$$

7.4.2 Displacement of S-matrix ports

About the displacement of the S-matrix ports of the patch we will be brief. The idea behind it is already explained in Sec.6.5.4, so we will give the final equations. If port 1 and 2 are shifted to $z = z_4$ and $z = z_6$, respectively, with $z_4 \leq z_5$ and $z_6 \geq z_5$, we obtain

$$\begin{bmatrix} \left[\check{I}^{\mathrm{IV};out}\right]_n \\ \left[\check{I}^{\mathrm{V};out}\right]_n \end{bmatrix} = \begin{bmatrix} \check{s}_{11} & \check{s}_{12} \\ \check{s}_{21} & \check{s}_{22} \end{bmatrix} \begin{bmatrix} \left[\check{I}^{\mathrm{IV};in}\right]_n \\ \left[\check{I}^{\mathrm{V};in}\right]_n \end{bmatrix}, \tag{7.40}$$

where

$$\begin{bmatrix} \check{s}_{11} & \check{s}_{12} \\ \check{s}_{21} & \check{s}_{22} \end{bmatrix} = \begin{bmatrix} \left[e^{-j\theta^{\mathrm{IV}}}\right]_{nn} & \emptyset \\ \emptyset & \left[e^{-j\theta^{\mathrm{V}}}\right]_{nn} \end{bmatrix} \begin{bmatrix} s_{11} & s_{12} \\ s_{21} & s_{22} \end{bmatrix} \begin{bmatrix} \left[e^{-j\theta^{\mathrm{IV}}}\right]_{nn} & \emptyset \\ \emptyset & \left[e^{-j\theta^{\mathrm{V}}}\right]_{nn} \end{bmatrix}. \tag{7.41}$$

and

$$\theta_n^{\alpha;\mathrm{IV}} = k_{z;n}^{\alpha;\mathrm{IV}}(z_5 - z_4), \tag{7.42}$$

$$\theta_n^{\alpha;\mathrm{V}} = k_{z;n}^{\alpha;\mathrm{V}}(z_6 - z_5). \tag{7.43}$$

7.5 Power

To determine the power that flows through the ports of the patch S-matrix we use

$$P_1^{\mathrm{IV}} = [(\check{I}^{\mathrm{IV};in} - \check{I}^{\mathrm{IV};out})]_n^{\mathrm{T}}[Y^{\mathrm{IV}}]_{nn}^{-1}[\,|Y^{\mathrm{IV}}|\,]_{nn}[(\check{I}^{\mathrm{IV};in} + \check{I}^{IV;out})^*]_n, \tag{7.44}$$

$$P_2^{\mathrm{V}} = [(\check{I}^{\mathrm{V};out} - \check{I}^{\mathrm{V};in})]_n^{\mathrm{T}}[Y^{\mathrm{V}}]_{nn}^{-1}[\,|Y^{\mathrm{V}}|\,]_{nn}[(\check{I}^{\mathrm{V};out} + \check{I}^{\mathrm{V};in})^*]_n, \tag{7.45}$$

in analogy with Sec.6.6. As one can see, we directly incorporated the normalization according to Eq.(6.154). To check the nett power flow through the ports a powerbalance can be set up, according to

$$(P_{in1}^{\mathrm{IV}} + P_{in2}^{\mathrm{V}}) - (P_{out1}^{\mathrm{IV}} + P_{out2}^{\mathrm{V}}) = 0. \tag{7.46}$$

where

$$P_{in1}^{\mathrm{IV}} = [\check{I}^{\mathrm{IV};in}]_n^{\mathrm{T}}[Y^{\mathrm{IV}}]_{nn}^{-1}[\,|Y^{\mathrm{IV}}|\,]_{nn}[\check{I}^{\mathrm{IV};in^*}]_n, \tag{7.47}$$

$$P_{in2}^{\mathrm{V}} = [\check{I}^{\mathrm{V};in}]_n^{\mathrm{T}}[Y^{\mathrm{V}}]_{nn}^{-1}[\,|Y^{\mathrm{V}}|\,]_{nn}[\check{I}^{\mathrm{V};in^*}]_n, \tag{7.48}$$

$$P_{out1}^{\mathrm{IV}} = [\check{I}^{\mathrm{IV};out}]_n^{\mathrm{T}}[Y^{\mathrm{IV}}]_{nn}^{-1}[\,|Y^{\mathrm{IV}}|\,]_{nn}[\check{I}^{\mathrm{IV};out^*}]_n, \tag{7.49}$$

$$P_{out2}^{\mathrm{V}} = [\check{I}^{\mathrm{V};out}]_n^{\mathrm{T}}[Y^{\mathrm{V}}]_{nn}^{-1}[\,|Y^{\mathrm{V}}|\,]_{nn}[\check{I}^{\mathrm{V};out^*}]_n. \tag{7.50}$$

The left-hand side of Eq.(7.46) is shorten to

$$P_{io} = (P_{in1}^{\mathrm{IV}} + P_{in2}^{\mathrm{V}}) - (P_{out1}^{\mathrm{IV}} + P_{out2}^{\mathrm{V}}). \tag{7.51}$$

7.6 Results

We will start the verification of the software and the analysis we preformed previously. For the verification we make use of results coming from, the same paper as used for the iris, i.e. [28], and we will make use a canonical case. The canonical case also makes it possible to draw comparisons between the two canonical cases, that of the iris and the patch. These "comparisons" are in view of the difference in applied basis-functions. If all is correct, both canonical cases must produce corresponding results, to some extent.

Furthermore, results of a patch in a waveguide will be presented, in the form of currents, amplitude and phase progress of modes, scattering-parameters and some power figures. Also the frequency dependency of the s_{11} in a range around 10 GHz is shown.

Of course, some results concerning the convergence of problems will be discussed as well. And finally, we will see what happens if the mesh changed.

7.6.1 Verification

We consider an abrupt single waveguide transition between two rectangular centered waveguides, with different cross-sectional dimensions, as in Fig.7.4. The waveguide with the larger cross-section, referred to as section-IV, has the dimensions $G = 22.85$ mm and $H = 10.05$ mm, in x- and y-direction, respectively. The smaller waveguide, referred to as section-V, has dimensions $Q = 14.28$ mm and $R = 6.5$ mm, in x- and y-direction, respectively. The dielectric parameters are: $\tan\delta = 0$ and $\varepsilon_r = 1$. From the larger waveguide the

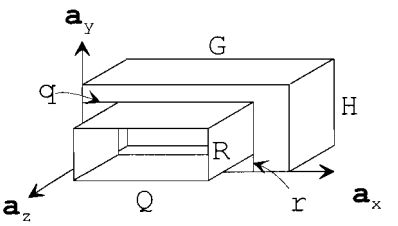

Figure 7.4: *Single waveguide transition. Dimensions of waveguides are* $G = 22.85$ *mm,* $H = 10.05$ *mm,* $Q = 14.28$ *mm,* $R = 6.5$ *mm,* $q = 4.285$ *mm and* $r = 1.775$ *mm.*

mode TE_{10} is incident on the junction at $z_5 = 1$ mm, over a frequency range of 9 GHz up to 11.5 GHz.

Figs.7.5 and 7.6 show the reflection and transmission coefficient with corresponding phase progress of mode TE_{01}, respectively. These figures also contain the results obtained from [28], in which the same case is simulated. The upper graph of Fig.7.5 depicts the magnitude of the reflection coefficient. Below a frequency of 10.49 GHz the smaller waveguide in in cutoff and the incident mode is completely reflected, $|s_{11}| = 1$. A small increase of the frequency causes real power to start flowing into the smaller guide and the s_{11} drops rapidly. The magnitude of the transmission coefficient s_{21} and its corresponding phase, in Fig.7.6, are not exactly matching as the amplitude and phase of the s_{11}, but the trend

is visible. During the verification tests of the iris we witnessed a similar deviation in the results, see Fig.6.10. This is the result of an asymmetric S-matrix. Note that the quantities in above figures are generalized scattering parameters of the E-field, on the junction between the two waveguides.

In Table 7.1, power figures and the powerbalance are given, obtained at a distance of 1 mm on both sides of the junction.

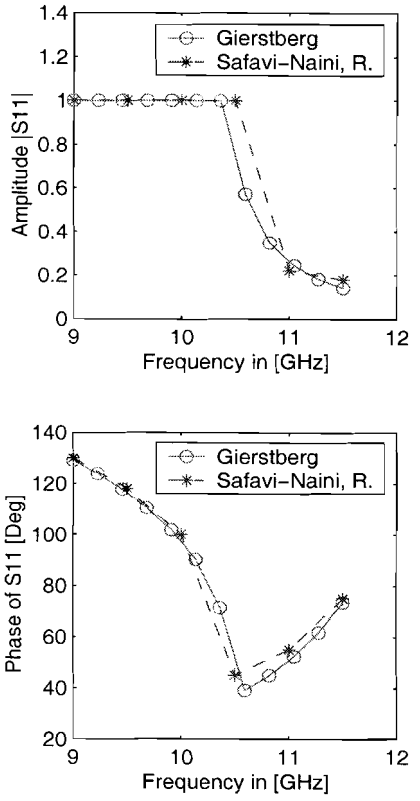

Figure 7.5: *Characteristics of a single junction. Upper: reflection coefficient, of incident mode* TE_{10}. *Lower: phase of reflection coefficient. Dimensions of waveguides in millimeters are* $G = 22.85$, $G = 10.05$, $Q = 14.28$ $R = F = 6.5$, $q = 4.285$ *and* $r = 1.775$.

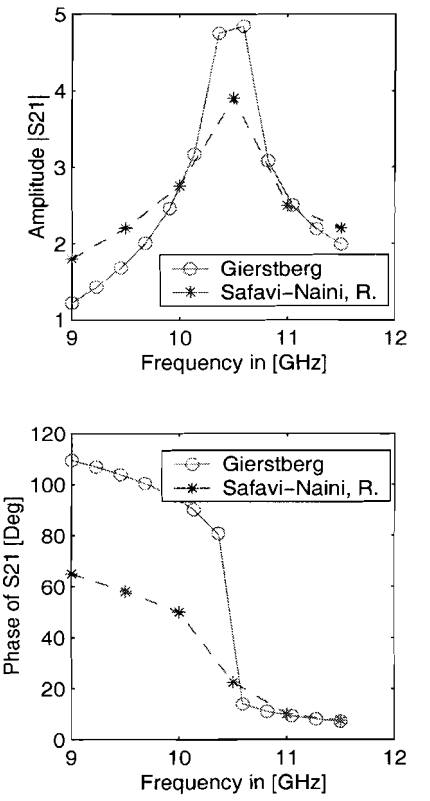

Figure 7.6: *Characteristics of a single junction. Upper: transmission coefficient, of incident mode* TE_{10}. *Lower: phase of transmission coefficient. Dimensions are stated in Fig.6.9.*

The values are obtained at a frequency of 10.7 GHz, which means that the smaller waveguide operates no longer in cutoff. The quantities P_1^{IV} and P_2^{V} is the power that flows through the waveguide cross-sections at $z_4 = 0$ mm and $z_6 = 2$ mm, respectively. These values and those of P_{out1}^{IV} and P_{out2}^{V} are round off figures. The powerbalance, P_{io}, is calculated with the fully accurate figures. For these results we used 277 RWG's and took along 1300 modes ($N = 25, M = 25$) of which 675 TE and 625 TM. The mesh we applied in the aperture between the waveguides is plotted in Fig.7.7. The preceding results considered,

	Real(·)	Imag(·)
$\mathbf{P}^{IV}_{in1} =$	1	0
$\mathbf{P}^{IV}_{out1} =$	$1.9081.10^{-1}$	$2.583.10^{-1}$
$\mathbf{P}^{V}_{out2} =$	$8.0919.10^{-1}$	$5.6946.10^{-3}$
$\mathbf{P}_{io} =$	$-2.2204.10^{-15}$	$-2.64.10^{-1}$
$\mathbf{P}^{IV}_{1} =$	$8.0919.10^{-1}$	$6.0167.10^{-2}$
$\mathbf{P}^{V}_{2} =$	$8.0919.10^{-1}$	$5.6946.10^{-3}$

Table 7.1: *Power values at port 1 and 2 of the S-matrix, that is at* $z_4 = 0$ *mm and* $z_6 = 2$ *mm, respectively.*

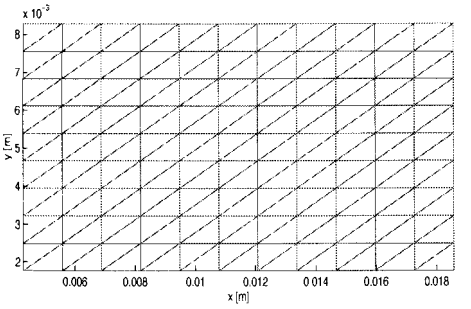

Figure 7.7: *The mesh in the aperture of the waveguide junction consisting of 277 RWG's. The dimensions of the aperture are* $x = 14.28$ *mm,* $y = 6.5$ *mm. The lower left corner is shifted over* $\mathbf{x} = (q, r) = (1.775, 4.285)$ *mm.*

we can say that we have obtained reasonable results.

The second test to verify of our model is a canonical case. We take a waveguide with a uniform cross-section. The waveguide is split up into two sections at the point $z = z_5$, forming a section-IV, which starts at $z = z_4$ and ends at $z = z_5$, and a section-V, which starts at $z = z_5$ and ends at $z = z_6$. They have the dimensions, $G = Q = 13.4$ mm and $H = R = 13.5$ mm, in x- and y-direction, respectively. The length of section-IV is $(z_5 - z_4) = 15$ mm and the length of section-V is $(z_6 - z_5) = 15$ mm. The parameters of the dielectric filling are $\tan\delta = 0$, $\varepsilon_r = 3$. The field incident from section-IV is a TE_{01} mode, with a frequency of 10 GHz. In our model, we have closed of the entire cross-section, at $z = z_5$, with a thin PEC. The intention of this example is more or less twofold. At first, one can see how well the RWG's preform and secondly, compare the application of RWG's with waveguide modes for the MoM.

Again, the modes are sorted according to their propagation constant k_z, as mentioned in Sec.6.8.2. In Fig.7.8, the amplitude in dB, according $20 \cdot \log_{10}[.]$, and the phase, in degrees, of the TE_{01} mode are given. According to our expectations, the incident field propagates across the closed cross-section at $z_5 = 15$ mm without any discontinuity. The phase is a continuous descending line across z_5. For this result we used $r = s = 280$ RWG basis-functions and $i = p = 840$ waveguide modes, before the s_{11} was down to approximately

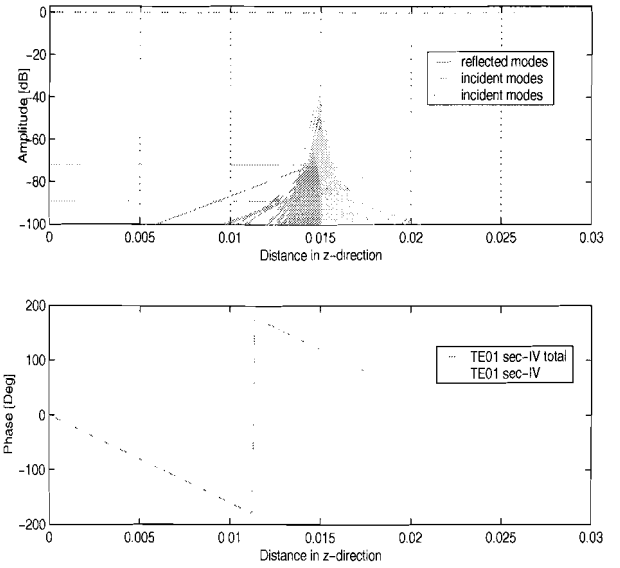

Figure 7.8: *Amplitude and phase plot of incident mode TE_{01} as function of propagation direction z, for canonical case. Dimensions of waveguides are $G = Q = 13.4$ mm, $H = R = 13.5$ mm. Dielectric parameter are $tan\delta = 0$, $\varepsilon_r = 3$. Number of waveguide modes taken along is 840.*

zero. We would like to point out to the just mentioned number of basis-functions and used waveguide modes At this point the condition number of the MoM-matrix had a value of 51. The number of waveguide modes used to expand the magnetic field in is in this case much higher than in the case of the iris, there we used only 4 waveguide modes as basis-function. The number of subdomain basis-functions (280 RWG's) is also much larger than the number of entire domain basis-functions (4 waveguide modes). This confirms some of the advantages that are mentioned in Sec.6.4.2 about entire domain basis-functions. Taking the spectral domain in mind, one can interpret the RWG basis-functions weighted with waveguide modes as the spectral representation of a RWG. Seen from this perspective, the fact that we need more and more waveguide modes to get the problem converged, as the number of RWG's increases means that, or beter said is caused the fact that their spectral representation is slowly descending and thereby very wide, demanding a lot of modes, if one wants a good approximation.

Looking at the amplitude graph in Fig.7.8, the reflection of the incident wave in section-IV is at a level of -72.17 dB, and in case where we used waveguide modes this is at -312 dB. The evanescent modes begin at a level of -30 dB, against -300 dB in the canonical case of the iris. But, as one can see they drop 40 dB over 1 mm, and at 15 mm distance they have completely vanished and only three negligible propagating modes are left. Already we can conclude that waveguide modes used as basis-functions preform better than RWG basis-functions. This was to be expected, since waveguide modes are eigenfunctions of the system and have an orthogonality property what manifests itself during the weighting of the waveguide modes. The RWG's don't have these advantages, what results in the fact

more waveguide modes are needed before the problem converges.

Similar as of the iris, there is again a clustering of modes around -90 dB and -340 dB. We have examined the modes in the clusters on type and mode indices (n, m), but there is no pattern. Both clusters contain TE as well as TM modes, with even and odd mode indices. In Fig.7.9, the reflected and transmitted modes on the junction between section-

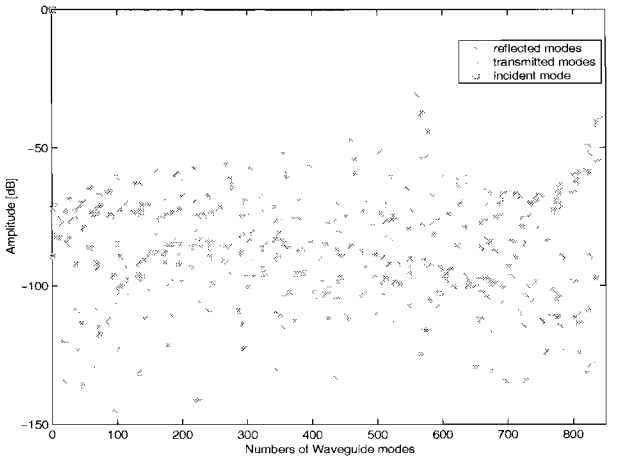

Figure 7.9: *Amplitude of reflected and transmitted mode on the junction of section-IV to -V, at* $z_5 =$ 15 *mm.*

IV and -V, clustered around the -90 dB, are plotted. Almost all the modes lie below the -50 dB, except for a few evanescent modes with a large imaginary propagation constant k_z, which vanish quickly.

In Figs.7.10 and 7.11, the x-component and the y-component of the equivalent magnetic current are displayed. The x-component shows a unexpected behaviour at the edges. Compared to the y-component, the x-directed component can be neglected, but compared to the x-directed component in Fig.6.21 it is large. Having seen the x-directed current, a few modes lying around the -90 dB can perhaps be explained, as in the canonical case of the iris. Perhaps it is the way we meshed the RWG's, or is it a numerical problem!? We then could think about a poor conditioned system, or the order in which the RWG's appear in the the linear system.

If the y-component is compared to the in Fig.6.22 displayed y-component, we see a close resemblance. The mesh we applied is given in Fig.7.14.

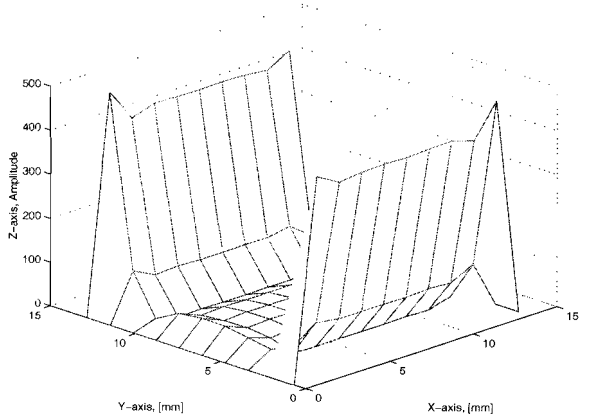

Figure 7.10: *x-directed equivalent magnetic surface current M3 at z_5. Canonical case.*

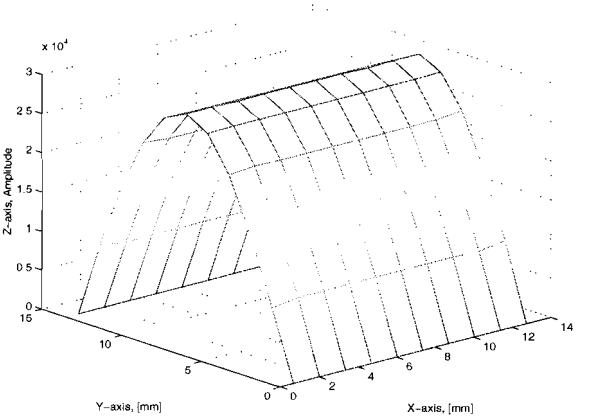

Figure 7.11: *y-directed equivalent magnetic surface current M3 at z_5. Canonical case.*

In view of x-directed component in Fig.7.10 we let another mode field be incident on the patch viz., TM_{11}, to see if everything goes correct for a different incident field and to see how the current behaves. In Figs.7.12 and 7.13 we observe the H-field of mode TM_{11} in the shape of the current, which is as expected. This gives us some more confidence in the correctness of the modelling and analysis.

Table 7.2 contains power and scattering parameter values. The power is the contribution of all modes, the scattering parameters involve only mode TE_{01}. All entries in Table 7.2 are round off figures, but P_{io} and $|s_{11} + s_{21}|$ are calculated with full accuracy. The real power is almost completely determined by mode TE_{01}. If we look at Fig.7.8, we see in section-IV and -V three horizontal lines, indicating propagating modes, which means that they transport real power. Since their values lie below -70 dB, their contribution wil be very small.

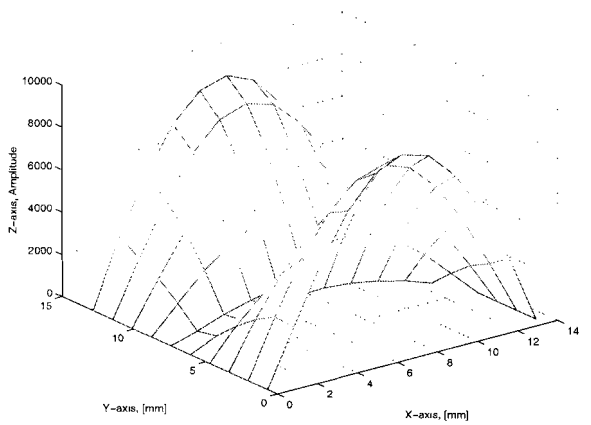

Figure 7.12: *x-directed equivalent magnetic surface current M3 at z_5, for the canonical case.*

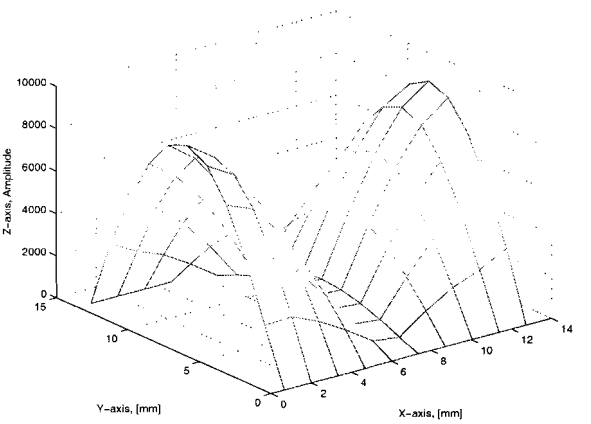

Figure 7.13: *y-directed equivalent magnetic surface current M3 at z_5, for the canonical case.*

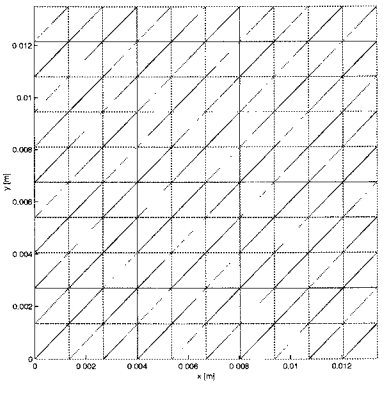

Figure 7.14: *Mesh for canonical case, yielding 280 RWG's. Dimensions:* $x = 13.4$ *mm and* $y = 13.5$ *mm.*

Power		
	Real(·)	Imag(·)
$\mathbf{P}_{\mathbf{in1}}^{\mathbf{IV}} =$	1	0
$\mathbf{P}_{\mathbf{out1}}^{\mathbf{IV}} =$	$6.1953.10^{-8}$	$-1.167.10^{-12}$
$\mathbf{P}_{\mathbf{out2}}^{\mathbf{V}} =$	1	$-1.167.10^{-12}$
$\mathbf{P}_{\mathbf{io}} =$	$1.2773.10^{-11}$	$2.3339.10^{-12}$
Scattering parameters		
$\mathbf{s}_{\mathbf{11}} =$	$2.1577.10^{-4}$	$-1.191.10^{-4}$
$\mathbf{s}_{\mathbf{21}} =$	$-4.8326.10^{-1}$	$-8.7548.10^{-1}$
$\lvert\mathbf{s}_{\mathbf{11}}\rvert^2 + \lvert\mathbf{s}_{\mathbf{21}}\rvert^2 =$	1	

Table 7.2: *Power and scattering values on port 1 and 2 of the S-matrix, at* $z_4 = 0$ *mm and* $z_6 = 30$ *mm, respectively, for canonical case.*

7.6.2 Patch in waveguide

In this section, we will discuss some result for a rectangular patch, formed of a thin PEC, placed in the transverse plane, and centered in a uniform waveguide. The dimensions of sections-IV and -V, and the parameter of the dielectric filling, are the same as in the canonical case, except for the length of the sections. The lengths are both 1 mm. Because both the waveguide sections have equal cross-sections and dielectric parameters, a generalization of the scattering matrix is not necessary. The dimensions of the patch are $x = 6.6$ mm and $y = 11$ mm. From section-IV, a mode TE_{01} is incident on the patch at $z_5 = 1$ mm. Fig.7.15 gives an impression of the amplitude and the phase progress of the modes, resulting from the incident wave on the patch. In the upper graph, at 0 dB in section-IV is the incident mode. At -2.541 dB we see the reflection and together with the incident mode they form a standing wave visible above the 0 dB. At -3.537 dB, in section-V, we find the transmitted part of mode TE_{01}. Furthermore, we see in both sections a lot of slowly decreasing (evanescent) modes with a large magnitude, even at a distance of 1 mm from the patch. These modes have to be taken along as incident fields for an object placed at

that distance. The consequence would be a highly coupled system. Again, as was the case

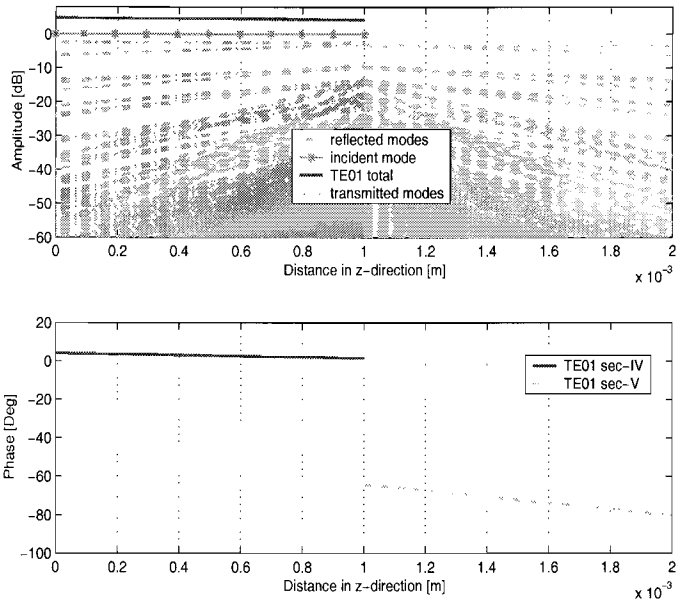

Figure 7.15: *Upper: amplitude progress of several modes, lower: phase progress of mode* TE_{01}*, in section-IV and -V. Waveguide dimensions* $G = Q = 13.4$ *mm,* $H = R = 13.5$ *mm, patch dimensions* $x = 6.6$ *mm,* $y = 11$ *mm.*

during the results of the iris, we notice a discontinuity in the phase of mode TE_{01}, this time it is approximately 66°. The incident field is being scattered partially and partially forced through the aperture around the patch, thereby encountering sudden changes, viz. the modes that can exist in the aperture have different wavenumbers, propagation constants and experience other impedances which cause the phase jump. For the iris, we saw that, a larger discontinuity in the cross-sections corresponds to a larger phase discontinuity. By analogy, we expect that a smaller aperture corresponds to a larger phase jump. The phase curve of mode TE_{01} in section-IV is a horizontal line, logically, because it corresponds to the standing wave in the graph above it.

For clarity, we have plotted the reflected and transmitted modes on port 1 and 2 in Fig.7.16 The modes with a amplitude above the -40 dB are gathered in Table 7.3, to get a better impression which modes play a role. Looking at the entries of Table 7.3 they are no longer that evident and simply to reason. This is mainly caused by the type of problem, a less simple aperture shape and the type of applied basis-functions. The dominant characteristics are resident in, the inner-products of waveguide modes and RWG basis-functions and the MoM matrix. Drawing conclusions from this isn't that quite obvious and as simple as was the case when we had inner-products of waveguide modes with each other. All modes accept the dominant one are unwanted, so 9,10,13,19 etc., because they give rise to cross-polarization

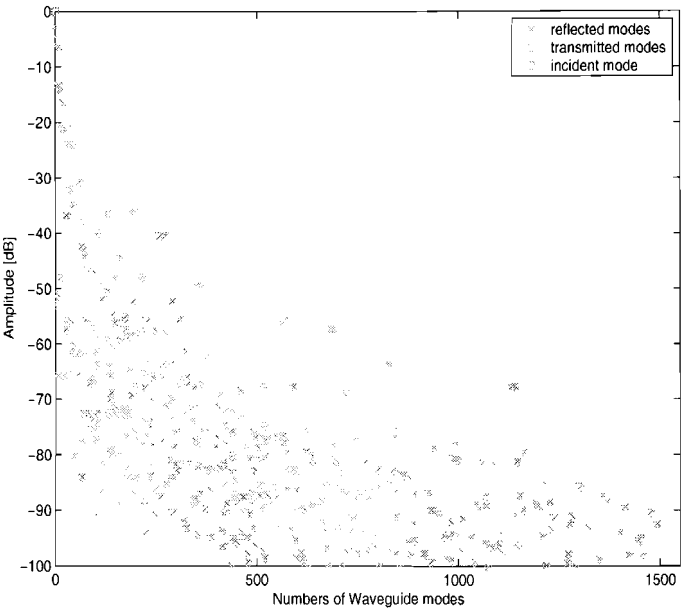

Figure 7.16: *Reflected and transmitted modes on the surface of port 1 and 2 of the S-matrix, both at 1 mm distance of patch.*

i	1	9	10	13	19	20	27	28	35	38	39	45
(n,m)	(0,1)	(2,1)	(2,1)	(0,3)	(2,3)	(2,3)	(4,1)	(4,1)	(0,5)	(4,3)	(4,3)	(2,5)
Type	TE	TM	TE	TE	TM	TE	TM	TE	TE	TM	TE	TM
Amp.[dB]	-2.54	-6.26	-13.37	-14.33	-21.18	-16.57	-21.2	-36.92	-23.65	-31.14	-31.94	-34.94
i	46	59	66	105	125	132	187	194				
(n,m)	(2,5)	(6,1)	(4,5)	(8,1)	(0,9)	(2,9)	(0,11)	(2,11)				
Type	TE	TM	TE	TM	TE	TE	TE	TE				
Amp.[dB]	-24.38	-30.84	-37.95	-39.91	-36.1	-36.22	-35.98	-35.93				

Table 7.3: *Mode number i, mode indicators (n,m) and the mode type of the modes lying above -40 dB in Fig.(7.16) are presented.*

In Table 7.4 we have written down some power figures and the scattering parameters of mode TE_{01} to support the found results.

Figs.7.17 and 7.18 show the x- and y-component of the equivalent surface current density $\mathbf{M}_3$.

Power		
	Real(·)	Imag(·)
$\mathbf{P}_{\mathbf{in1}}^{\mathbf{IV}} =$	1	0
$\mathbf{P}_{\mathbf{out1}}^{\mathbf{IV}} =$	$5.5709.10^{-1}$	$-1.3862.10^{-1}$
$\mathbf{P}_{\mathbf{out2}}^{\mathbf{V}} =$	$4.4291.10^{-1}$	$-1.3862.10^{-1}$
$\mathbf{P}_{\mathbf{io}} =$	$5.3807.10^{-8}$	$2.7724.10^{-1}$
Scattering parameters $\mathbf{TE}_{01}$		
$\mathbf{s}_{11} =$	$7.355.10^{-1}$	$1.2699.10^{-1}$
$\mathbf{s}_{21} =$	$1.1324.10^{-1}$	$-6.5581.10^{-1}$
$\lvert\mathbf{s}_{11}\rvert^2 + \lvert\mathbf{s}_{21}\rvert^2 =$	1	

Table 7.4: *Power and scattering values on port 1 and 2 of the S-matrix, at $z_4 = 0$ mm and $z_6 = 2$ mm, respectively. Patch is position at $z_5 = 1$ mm.*

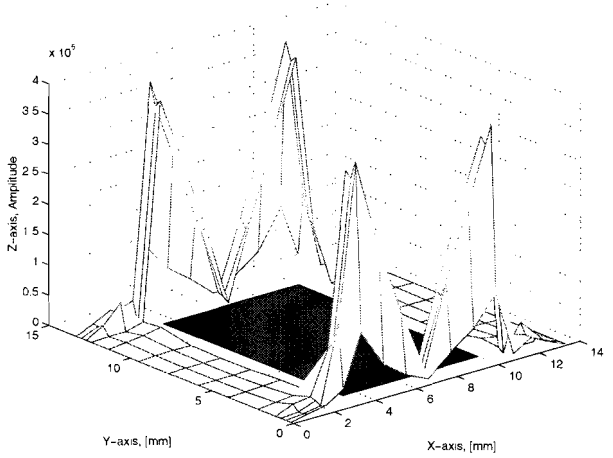

Figure 7.17: *x-component of equivalent magnetic current M3, in case of a patch of sizes $x = 6.6$ mm and $y = 11$ mm, with 1512 modes taken along during the computations.*

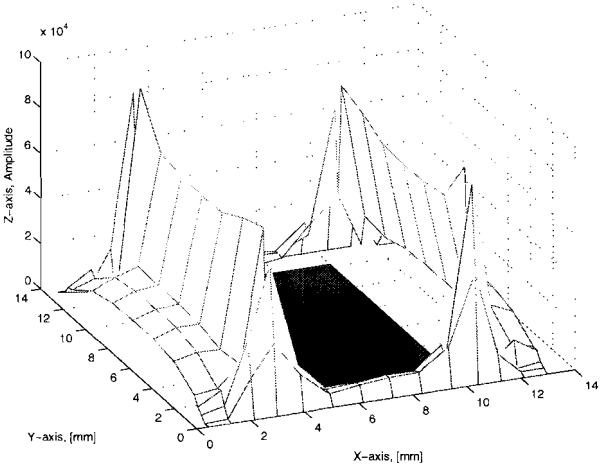

Figure 7.18: *y-component of equivalent magnetic current M3.*

In both figurers, at a level of $0dB$, there are even coloured rectangular surfaces visible representing the transversely placed patch. We notice that the current exhibits a singular behaviour along the edges of the patch. The singular behaviour is the result of the fact that the edge of the patch forms a corner 180°. The exact order of the singularities, at the corners and the edges of the patch, can be determined by solving the homogeneous Helmholtz equation for spherical coordinates, for that we refer to [17, Chap.9]. The fact that the current forms ridges along the y-directed edges of the patch, and the forming of pointed singularities at the corners of the patch, visible in the x-directed current plot, has also something to do with the polarization of the incident field. This is mode TE_{01}, consisting out of component H_y, making the current in the y-direction the dominant main polarized current component. The x-directed current is the cross polarized component.

The pikes at the corners are probably cause by the fact that the current is forced around the corners, creating a increase of the surface current density.

The mesh we used for the discretisation of the aperture is shown in Fig.7.19. It consists of 440 RWG basis-functions.

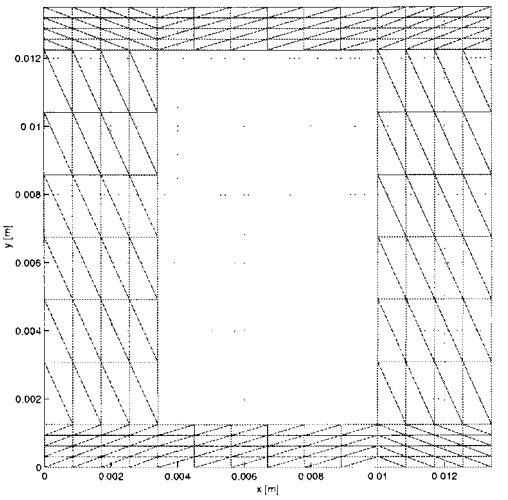

Figure 7.19: *Aperture around patch meshed with 440 RWG's. Patch size is:* $x = 6.6$ *mm,* $y = 11$ *mm*

Also, we looked at the frequency dependence of the patch. It is eventually of interest, since often a wide working range is desired, to know how the patch behaves over a certain frequency range. In a range of 20 % frequency bandwidth, the reflection coefficient varies from 0.68 to 0.83. At about 12.81 GHz the reflection coefficient s_{11} is near 1. Ergo, all power is reflected and only evanescent modes exist at the other side of the patch.

7.6.3 Convergence

During the verification of the results obtained with of our model, with those from [28] we mentioned that we took along 1300 modes. This was based on the convergence graphs in Fig.7.21. There, we see the scattering parameter s_{11} of the incident mode TE_{10} as a function of the number of modes taken into account, its phase and the condition number of the MoM-matrix. Based on these three quantities, the number of modes used during the calculations was chosen. Although the the amplitude graph of s_{11} is stil increasing slowly, the magnitude of the last few points, from 684 till 1860 modes, all lie close together, indicating that the solution is stabilizing and slowly converging to a final solution. In the graph below, the condition number of the MoM-matrix is given. We observe that it reaches its minimum, of about 420, between 1300 and 1404 modes, and starts klimming again afterwards. This indicates that the answers for a higher number of modes will become less accurate. Therefore, the combination of the mentioned graphs and the fact that we have a memory resource problem, has led to the fact that we have chosen to take along

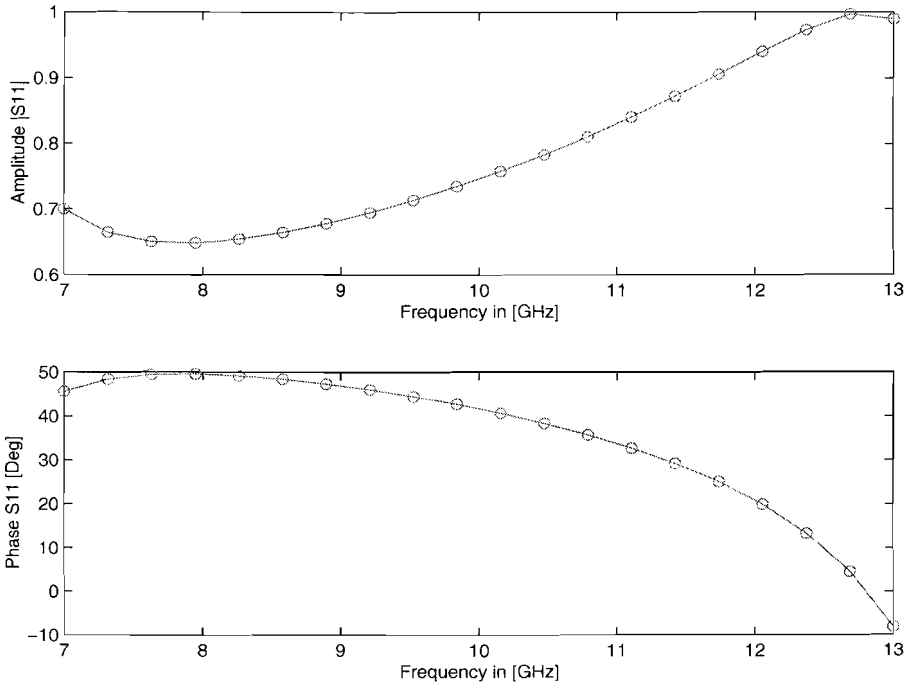

Figure 7.20: *Upper: Frequency dependency of patch with dimensions $x = 6.6$ mm and $y = 11$ mm for incident field mode TE_{01}. Lower: Corresponding phase progress.*

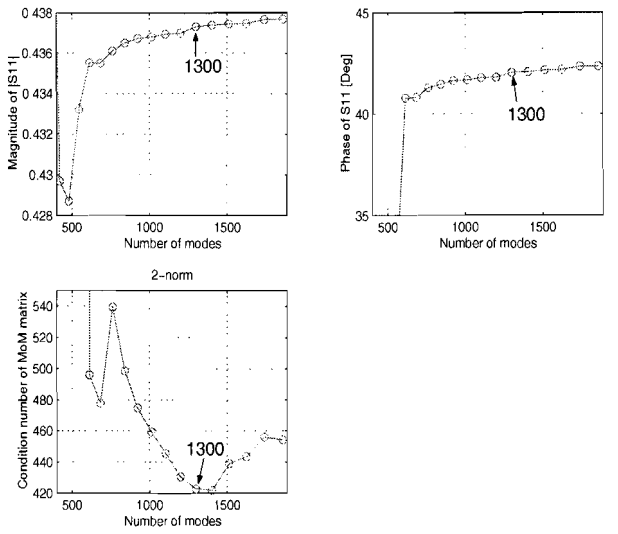

Figure 7.21: *Upper: convergence graphs of s_{11} and corresponding phase, lower: convergence of MoM-matrix's 2-norm. Belonging to first validity case, the single waveguide junction form [28].*

1300 modes. During the other verification case, the canonical case, 840 modes were used

yielding a s_{11} of $2.46 \cdot 10^{-4}$ and a condition number of 51.

In the case of the patch, with the dimensions $x = 6.6$ mm and $y = 11$ mm, the aperture around the patch was meshed with 440 RWG's and, as mentioned, we have taken long 1512 waveguide modes during the computation. This is derived from the information visible in Fig.7.22. In the upper left graph, we see that, from a number of 1512 modes, the s_{11} stabilizes. The phase also stabilizes, at a value of around 42°. The condition number of the MoM-matrix, note the log-scale, is still quite large in the order of magnitude of 10^5, coming from $10^7 - 10^8$, and slowly drops as the number of modes exceeds the value of 1512. Which indicates, that if one adds more modes, no real changes in the increase of accuracy can be expected, and we have checked this based on the current. However, going from 1300 modes to 1512, the condition number drops from $2.7 \cdot 10^8$ to $1.5 \cdot 10^5$, yielding large changes, especially in the current shapes. The x- and y-component of the current derived with the

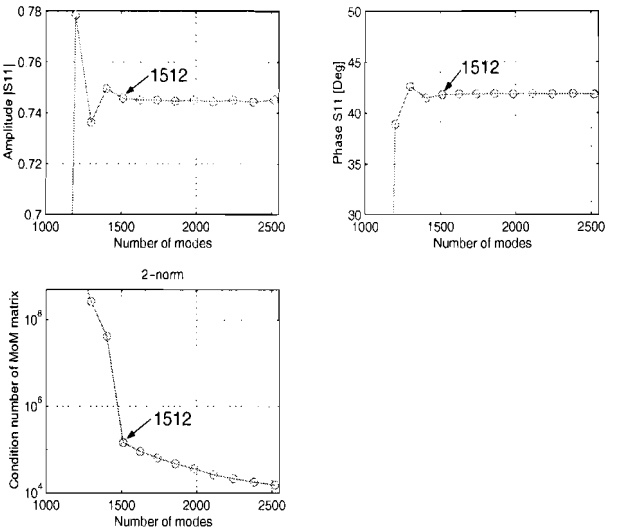

Figure 7.22: *Upper: convergence graphs of* s_{11} *and corresponding phase, lower: convergence of the MoM-matrix's condition number. Convergence belonging to case with patch, having dimensions* $x = 6.6mm$ *and* $y = 11mm$.

help of 1300 modes are depicted in Figs.7.23 and 7.24. The currents obtained with 1512 modes were already given by Figs.7.17 and 7.18. Notice the differences! while compering Figs.7.18 and 7.24. The four singularities, in Fig.7.18, at the corners are disappeared but, the current along the edge of the patch is still there. In Fig.7.24 it is not clearly visible because there is a ratio of about 130, between the singularities and the current along the edge of the patch. We indicated the current along the edge with red arrows. The x-directed current component, in Fig.7.17, is also drastically changed compared to Fig.7.23. In Fig.7.23 we see, what it looks like, the forming of singular behaviour of the current in the four corners, up against the waveguide wall. This seems a bit strange, because the walls of a uniform section of waveguide are no reason to cause singularities. Then, in Fig.7.17 one

notices that the singularities arise along the x-directed edge, mostly towards the corners, of the patch. This is more along the line of expectation.

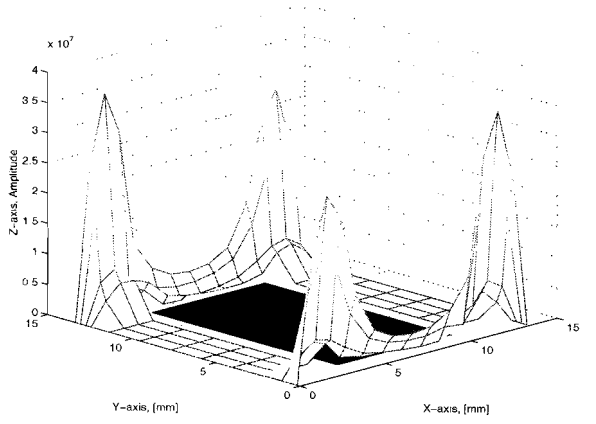

Figure 7.23: *x-component of equivalent magnetic current M3, in case of a patch of sizes* $x = 6.6$ *mm and* $y = 11$ *mm, with 1300 modes taken along during the computations.*

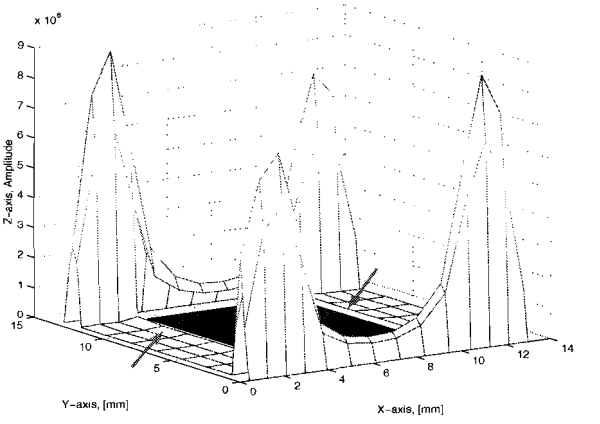

Figure 7.24: *y-component of equivalent magnetic current M3.*

So, as one can see. Just by taking along ± 200 more modes the problem is well converged, the system is must better conditioned, and just because of the better conditioned system the obtained currents are correct.

Also, a sign of a problem that is not yet converged, is the asymmetrical behaviour in the current figure.

7.6.4 Influence of the mesh

In Sec.7.6.1, we observed a image of the x-directed current component that was not in the line of our expectation, see Fig.7.12. There seems to be forming an odd ridge along the waveguide walls in the x-direction. Comparing it's amplitude to y-component of the current its rather small, still, at first its not what we expected after having seen the x-directed current in the canonical case of the iris. This has a few reasons, according to us. First of all. RWG's applied as basis-functions don't exhibit orthogonality properties as waveguide modes do. Secondly, the currents we plotted are not exactly x- and y-directed components. The RWG basis-functions are namely vector functions, defined on a surface e.g. the x-y-plane and not strictly restricted to the orthogonal directions x and y. Therefore, a RWG with a common edge parallel to the y-axis has a flux density across the common edge with a constant and continues x-component and also a insurmountable y-component which is responsible for a larger x-directed current in the figure. By analogy, the same applies for a common edge parallel to the x-axis. Bear in mind the fact that this also occurs during the plotting of the patch current components. As third, how well do the RWG's preform, in approximating an arbitrary directed vector field along an edge of the domain on which

the vector field is defined? In [25] it is being discussed that, and we also mentioned it in Sec.7.3.1, by forming lineair combinations of the three basis-functions on each triangle it is possible to form a linear vector field with arbitrary direction and magnitude. During the description in [25], they assume that every triangle of a flyer has three adjoining triangles, the result being that on each triangle three basis-functions can be defined. In case of a domain in the form of a non-closed surface, the triangles at the edges and especially those in corners, if present, have only one or two adjacent triangles, lacking one or two basis-functions, see Fig.7.25. To what extent is the approximate current still correct and accurate?

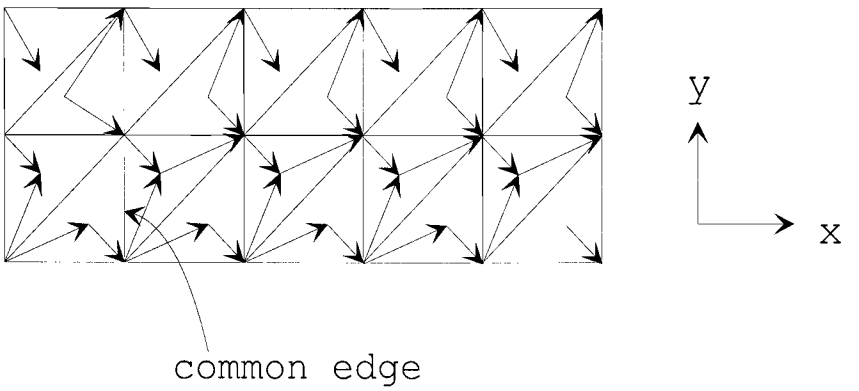

Figure 7.25: *An piece of mesh functioning as example to indicate that triangles adjacent to an edge or corner only contain two of even one basis function. Midpoint of indicated common edge is used as reference point to plot the x-directed component of the current.*

As forth and last. We observed that a part of the problem is situated in the discretisation of the domain on which the current will be determined. The smaller the mesh size the smaller the ridges along the x-direction, in this particular case. We demonstrate this by means of meshing the same surface three different times. The overal structure is kept the same, but mesh size is changed. Figs.7.26(a), 7.14 and 7.26(b) display the applied mesh. The partitioning along the x- and y-direction varies from 5, 10 to 15, respectively. Figs.7.27(a), 7.10 and 7.27(b) show the corresponding x-directed components of the current. The amplitudes of the ridges are 850, 440 and 300 respectively. Furthermore, concerning the main polarization (y) components of the current, no changes are observed due to the varying mesh. One particular thing that is observed in the y-component of the current is, along both y-directed edges, see Fig.7.11, the horizontal lines, perpendicular to the y-axis and parallel to the x-axis, are deviating and only at the ends. This can be explained maybe, by what is indicated with Fig.7.25. Also a fact that can play a role is the order in which the RWG functions appear in the MoM matrix.

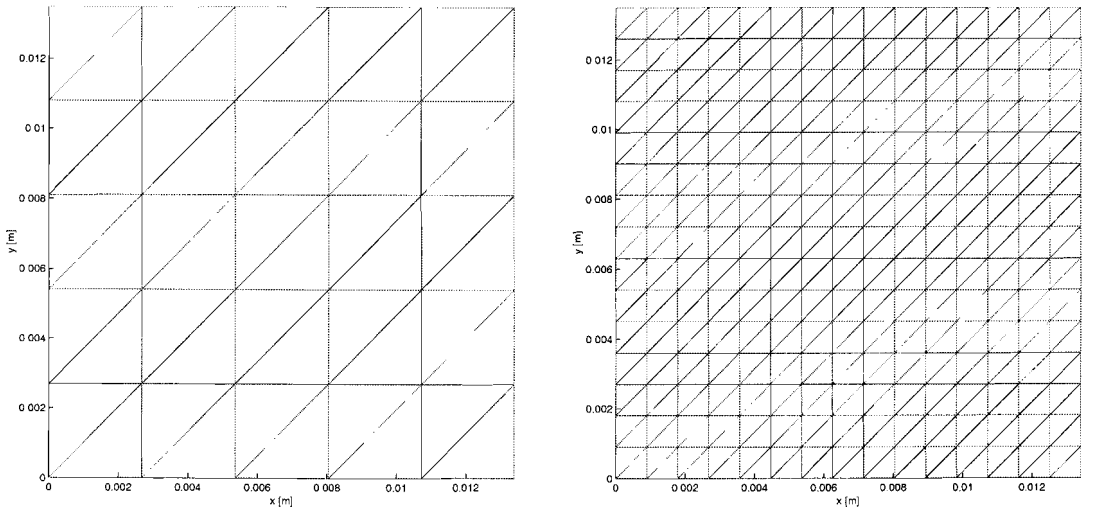

(a) (b)

Figure 7.26: *Meshed cross-section for canonical case. (a)* 5×5 *steps along* x *and* y*, yielding 65 RWG's. (b)* 15×15 *steps along* x *and* y*, yielding 645 RWG's.*

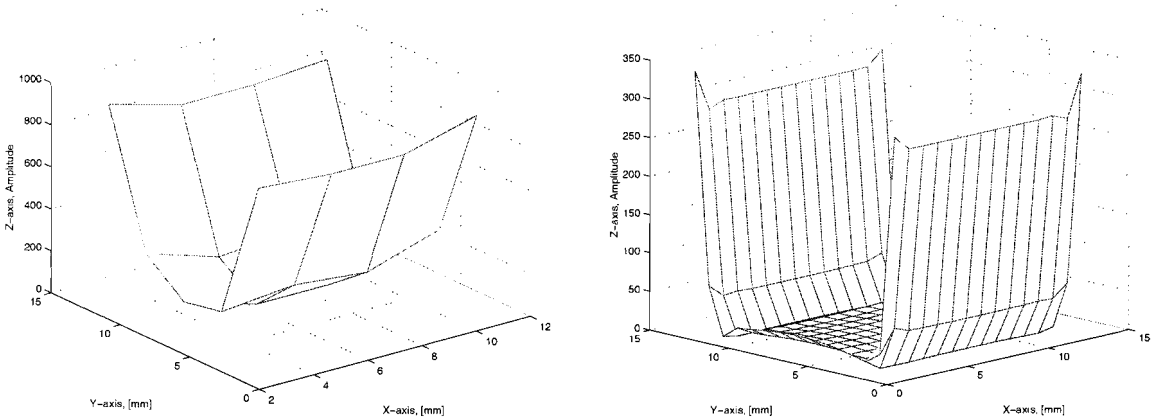

(a) 12 (b)

Figure 7.27: *x-component of equivalent magnetic current* $\mathbf{M}_3$*. (a) Belonging to Fig.7.26(a). (b) Belonging to Fig.7.26(b).*

Chapter 8

Waveguide simulator

In Chapters 6 and 7 we discussed and analysed and iris and a patch in a waveguide. The numerical results we obtained with our software was verified against results found in the literature and by studying their canonical cases. The verification yielded, according expectations, corresponding and correct results. Based on this knowledge we can conclude that our software and analysis is correct so that we can continue with the following step. The coupling of the iris and the patch.

During the introduction, Chapter 1, we explained that our aim was to make a start with the analysis of the array by a waveguide simulator approach. The idea on which this is based can be explained with help of Fig.8.1. In Fig.8.1(a) is depicted a cross-section, in the x-z-plane, of an infinite array of cavity-backed patch antennas in a rectangular periodic grid, as in Fig.2.2. We note , that the infinite array approach is a necessary modelling step if

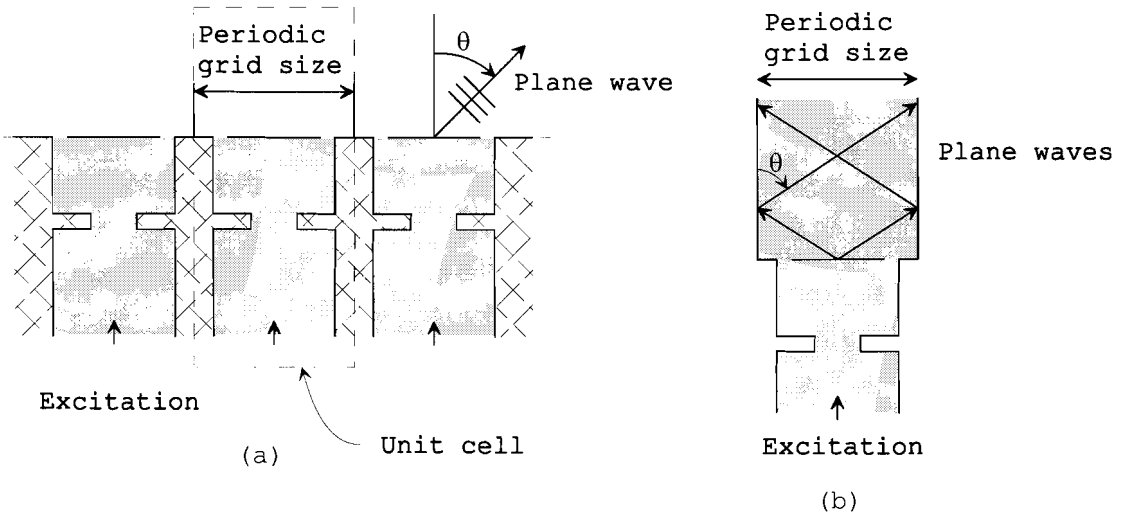

Figure 8.1: *(a) Infinite array of cavity-backed patch antennas in a rectangular periodic grid.(b) Waveguide simulator model.*

one wants to usefully apply a waveguide simulator. Concerning the periodic arrangement of

the array, in general not every arrangement can be handled by a waveguide simulator, there are some restrictions to. A rectangular periodic grid and one type of triangular periodic grid can be approached by a waveguide simulator. We will stick to rectangular periodical grids. Based on these two remarks we can continue the explanation, by again considering Fig.8.1(a). In it is indicated the periodic grid size (cell) which agrees with the unit cell. By placing a rectangular waveguide, made of a PEC and dimensions corresponding to the grid size, on top of the array unit cell with its propagation direction perpendicular to the antenna face, we can neglect all of the rest of the array. We thereby make use of the fact that the walls are PEC's and the symmetry property that the rectangular waveguide posses. With help of image theory the infinite array can be reconstructed. The waveguide walls function as a kind of mirror.

What we have created in this way is a waveguide simulator, as shown in Fig.8.1(b). With the components treated in Chapter 6 and 7 we are able to construct such a waveguide simulator.

With a phased array it is possible to steer the main beam into almost any given directions of the half free space. In general, the radiation properties of the array are a function of the angles θ and ϕ. In Fig.8.1(a) angle θ is indicated, with $\phi = 0°$, for a departing plane wave front, normally called a Floquet mode. With a waveguide simulator it is also possible to study the θ dependency for plane waves, within certain limits. The TE_{01} mode, which we use as excitation can be written as a superposition of two plane waves, as

$$\mathbf{H}''_{01}(\mathbf{r}) = H_y(\mathbf{r})\mathbf{a}_y, \tag{8.1}$$

with

$$H_y(\mathbf{r}) = \Upsilon \sin\left(\frac{\pi}{R}\right) e^{jk_z z} = \Upsilon \left(e^{-jk_z\left(z-\frac{\pi y}{k_z R}\right)} - e^{-jk_z\left(z+\frac{\pi y}{k_z R}\right)}\right), \tag{8.2}$$

where Υ is a constant and R is the dimension of the waveguide in the y-direction. The last term in Eq.(8.2) are two plane waves propagating in the positive z-direction along zigzag paths between the waveguide walls, see Fig.8.1(b). The angle they make with the waveguide wall is

$$\theta = \tan^{-1}\left(\frac{\pi}{k_z R}\right). \tag{8.3}$$

Since θ is depended of k_z and k_z again of the frequency f, according

$$k_z = \sqrt{(2\pi f)^2 \varepsilon\mu - k_t^2}, \tag{8.4}$$

we can by varying the frequency of mode TE_{01} influence the angle θ which the plane waves make with the waveguide wall. We want to note that the illustration made in Fig.8.1(b) corresponds to a TE_{10} mode. This is done to get a clearer picture, but does not change anything about the principle.

To construct a waveguide simulator eventually, we have to couple the iris to the patch.

8.1 Iris coupled to patch

In Chapter 2, modelling approach, we explained the idea, to subdivided the total problem in parts and to form a scattering parameter description of each subproblem. A total model description can then be formed by subsequently cascading the separate S-matrices. At first, the cascading of the S-matrices looks trivial, as long as the matrices have the same size. The output of the one, is the input of the other. But, since the number of waveguide modes, taken along during the computations of the iris and the patch, differ, the sizes of the S-matrices in the two cases also differ from each other resulting in the fact that the S-matrices can no longer be cascade without taken some precautionary measure.

First we will show how to cascade two S-matrices, and after that we'll discuss what to do if the matrices have different sizes. In Fig.8.2 we see two S-matrices that need to be coupled, to form a new system. So, we're looking for a new lineair coupled system of equations describing the relations between the newly inputs a and e, and outputs b and f. From Fig.8.2 we can deduce the following two systems for matrix α and β respectively

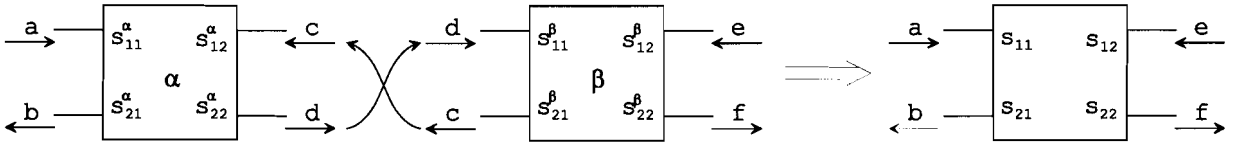

Figure 8.2: *Cascading two S-matrices.*

$$[b] = [s_{11}^{\alpha}][a] + [s_{12}^{\alpha}][c], \tag{8.5}$$
$$[d] = [s_{21}^{\alpha}][a] + [s_{22}^{\alpha}][c]. \tag{8.6}$$

$$[c] = [s_{11}^{\beta}][d] + [s_{12}^{\beta}][e], \tag{8.7}$$
$$[f] = [s_{21}^{\beta}][d] + [s_{22}^{\beta}][e]. \tag{8.8}$$

As suggested previously, we now must find expression for outputs b and f as a function of inputs a and e. Therefore, we substitute Eq.(8.7) into Eq.(8.6), what corresponds to coupling output c of S-matrix β to input c of S-matrix α, yielding

$$[d] = [R_1]^{-1}[s_{21}^{\alpha}][a] + [R_1]^{-1}[s_{22}^{\alpha}][s_{12}^{\beta}][e], \tag{8.9}$$

where

$$[R_1] = [\underline{I}] - [s_{22}^{\alpha}][s_{11}^{\beta}]. \tag{8.10}$$

Likewise we substitute Eq.(8.6) into Eq.(8.7), what corresponds to coupling output d of S-matrix α to input d of S-matrix β, which yields

$$[c] = [R_2]^{-1}[s_{11}^{\beta}][s_{21}^{\alpha}][a] + [R_2]^{-1}[s_{12}^{\beta}][e], \tag{8.11}$$

where

$$[R_2] = [\underline{\underline{I}}] - [s_{11}^{\beta}][s_{22}^{\alpha}]. \tag{8.12}$$

Still unused, are Eq.(8.5) and (8.8). But, this is changed by substituting Eq.(8.12) and (8.10), respectively, resulting in what we had aimed for, outputs b and f as a function of inputs a and e

$$[b] = \left[[s_{11}^{\alpha}] + [s_{12}^{\alpha}][R_2^{-1}][s_{11}^{\beta}][s_{21}^{\alpha}]\right][a] + [s_{12}^{\alpha}][R_2^{-1}][s_{12}^{\beta}][e], \tag{8.13}$$

and

$$[f] = [s_{21}^{\beta}][R_1^{-1}][s_{21}^{\alpha}][a] + \left[[s_{22}^{\beta}] + [s_{21}^{\beta}][R_1^{-1}][s_{22}^{\alpha}][s_{12}^{\beta}]\right][e]. \tag{8.14}$$

From Eqs.(8.13) and (8.14) we can deduce the S-parameter expressions for the new system,

$$[s_{11}] = [s_{11}^{\alpha}] + [s_{12}^{\alpha}][R_2^{-1}][s_{11}^{\beta}][s_{21}^{\alpha}], \tag{8.15}$$

$$[s_{12}] = [s_{12}^{\alpha}][R_2^{-1}][s_{12}^{\beta}], \tag{8.16}$$

$$[s_{21}] = [s_{21}^{\beta}][R_1^{-1}][s_{21}^{\alpha}], \tag{8.17}$$

$$[s_{22}] = [s_{22}^{\beta}] + [s_{21}^{\beta}][R_1^{-1}][s_{22}^{\alpha}][s_{12}^{\beta}]. \tag{8.18}$$

For so far the coupling of S-matrices, of equal sizes. When this is not the case, one must take care that they become equally sized.

The coupling of the iris and the patch brings about this problem. During the computations of the iris, 312 waveguide modes were taken into account, against 1512 waveguide modes for the patch, yielding S-matrices with sizes twice as large as the number of waveguide modes, i.e. 624×624 and 3024×3024, respectively. One can solve the size problem in three ways. First possibility. Enlarge the number of waveguide modes used for the calculations of the iris, to the same number of modes used for the patch. As a consequence, the condition number of the MoM-matrix rises rapidly, see the convergence graphs in the results of the iris Fig.6.36. This implies that we probably are creating dependency in the linear system, therefore the answer, obtained from the the linear system, will no longer be reliable. Subsequently combining two S-matrices would also produce inaccurate results. With other words, no suitable solution.

Second possibility is, size up the S-matrix of the iris to the dimensions of the patch-S-matrix, by adding zeros to the four block matrices $\{s_{11}, s_{12}, s_{21}, s_{22}\}$, in the right way. As a consequence of sizing up the smaller matrix by adding zeros, large matrix multiplications are necessary, which for the most part consist of multiplications by zero, resulting in excessive calculation times and, loss of in information stored in the the higher order modes of the patch. By higher order modes we mean, modes with a large imaginary value for the propagation constant k_z.

The loss of information, stored in the higher order modes of the patch, is actually not so disastrous. These modes are fast evanescent, and only play a role of importance in

the nearest vicinity of the patch. In spite of the fact that we almost enter this region, one has been able to see during the results of the patch, that the contribution of these highly evanescent modes is well below the $-50dB$ and thereby neglected, in general. This brings us to a third possibility. That is, just calculate the subproblems, by taking along enough modes until good convergence is reached. Then, resize the S-matrix of the patch, by leaving out the proper higher order modes of each block matrix, until it has the same dimensions as the S-matrix of the iris. In this way the computation times for coupling the S-matrices stays within acceptable boundaries and enough accuracy is guaranteed. This can be substantiated by the fact that the calculated s-parameters are solutions of converged problems, thereby correct and accurate, and the amount of modes that are left over in the resized patch-S-matrix are responsible for the largest part of the complex power.

8.2 Results

First we will investigate a canonical case, as a first check to see how accurate the coupling between the S-matrices is. This canonical case consists of the coupling of the iris canonical case and the patch canonical case, illustrated in Fig.8.3. All five sections are equal in length, i.e. 15 mm, and equal in cross-section with dimensions $A = C = E = G = Q = 13.4$ mm and $B = D = F = H = R = 13.5$ mm in x and y respectively. The dielectric filling parameters are
$varepsilon_r = 3$ and $\tan\delta = 0$. As incident field we take mode TE_{01}. In Fig.8.4 the results

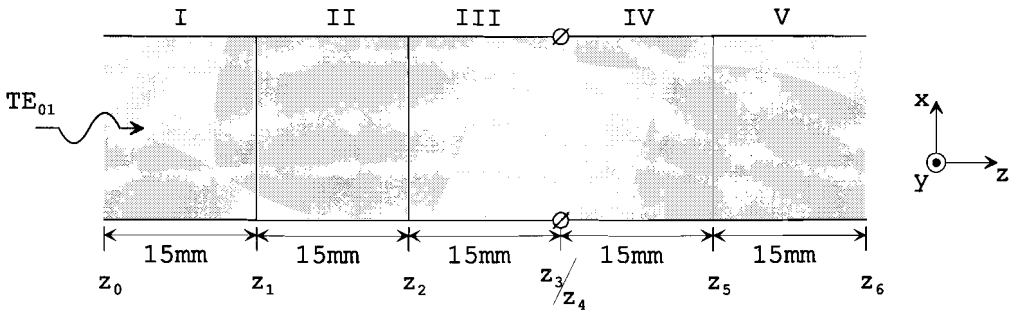

Figure 8.3: *Configuration of an iris coupled to a patch, canonical case. Length of each section is 15 mm and cross-sectional dimensions are 13.4 mm and 13.5 mm in x- and y-direction, respectively.*

are presented and according to our expectations. In the upper graph, the magnitude of the modes is given. At 0 dB in section-I one finds mode TE_{01} and it continues at a level of 0 dB in section-IV. What an indication is of the fact that the mode is propagating through the structure without being disturbed. In the lower graph the phase of mode TE_{01} is shown. The phase shift between the points where the curve ends in section-I and continues in section-V, corresponds exactly to the distance over which mode TE_{01} has travelled. To obtain these results 4 modes were used for the calculations of the iris and 840 modes for the patch. The S-matrix size of the new composite system is 8×8. The two modes at

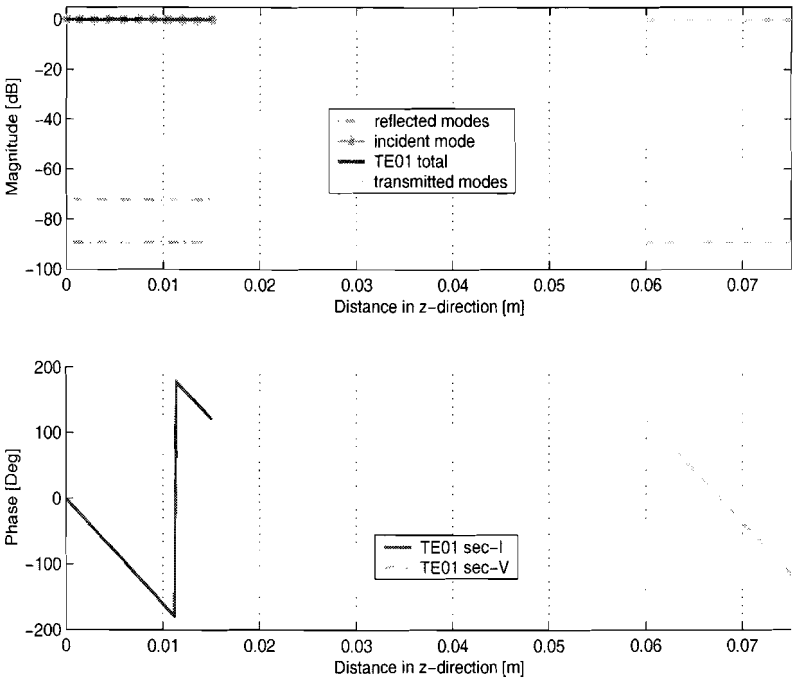

Figure 8.4: *Canonical case of an iris coupled to a patch.*

-72 and -89 dB, in section-I, are TE_{01} and TE_{10}, respectively. The mode at -89 dB, in section-V, is TE_{10}. Not visible are two more modes around -300 dB, viz. TM_{11} and TE_{11} in section-I as well as in section-V.

Table 8.1 contains some power figures and the scattering parameters of mode TE_{01}. The coupling of the iris and the patch seems to go well, what can be concluded from the

Power		
	Real(·)	Imag(·)
$\mathbf{P^{I}_{in1}} =$	1	0
$\mathbf{P^{I}_{out1}} =$	$6.1953.10^{-8}$	$5.1699.10^{-26}$
$\mathbf{P^{V}_{out2}} =$	1	$1.3709.10^{-18}$
$\mathbf{P_{io}} =$	$1.2773.10^{-11}$	$-1.3709.10^{-18}$
Scattering parameters TE_{01}		
$\mathbf{s_{11}} =$	$2.2235.10^{-4}$	$-1.063.10^{-4}$
$\mathbf{s_{21}} =$	$-4.5749.10^{-1}$	$-8.8922.10^{-1}$
$\mathbf{\lvert s_{11}\rvert^2 + \lvert s_{21}\rvert^2} =$	1	

Table 8.1: *Power and scattering values on port 1 and 2 of the S-matrix, at $z_1 = 0$ mm and $z_6 = 75$ mm, respectively.*

canonical results. The next step that we can make with the waveguide simulator is try to construct a configuration which corresponds with a given array. Fig.8.5 displays the

structure which we're going to simulate. The parameter Q and R are the dimensions of

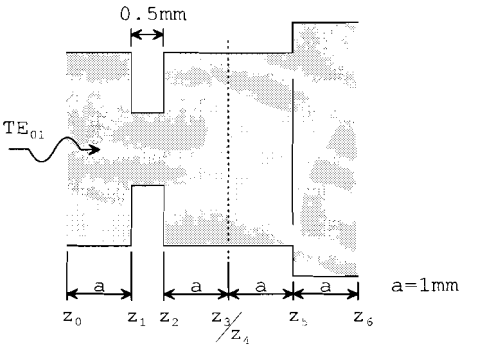

Figure 8.5: *Configuration of an iris coupled to a patch. The lengths of the sections is indicated.The cross-sectional dimensions are* $A = E = G = 13.4$ *mm,* $B = D = F = H = 13.5$ *mm,* $C = 2.1$ *mm,* $Q = 16.4$ *mm and* $R = 16.5$ *mm. Dielectric parameters are* $\varepsilon_r = 3$ *and* $\tan\delta = 0$.

the rectangular periodic gird.

The parameter of interest for the results is the s_{11} as a function of the frequency. Therefore we have made a frequency sweep for the TE_{01} mode, which is incident from section-I. We have also monitored the s_{11} as a function of the angle θ, which we obtained via the relations in Eqs.(8.3) and (??), since θ is dependent of the frequency. Fig.8.6, shows s_{11} as function of the frequency. In Fig.8.7 is displayed the s_{11} as function of the

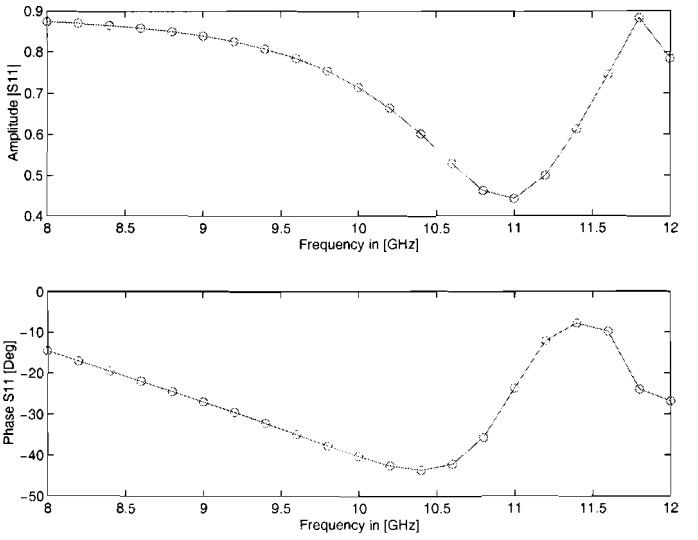

Figure 8.6: *Upper: magnitude of* s_{11} *of incident mode* TE_{01} *as function of frequency. Lower: Corresponding angle.*

angle theta. Note that this is the same plot as in Fig.8.6 only backwards, because of the

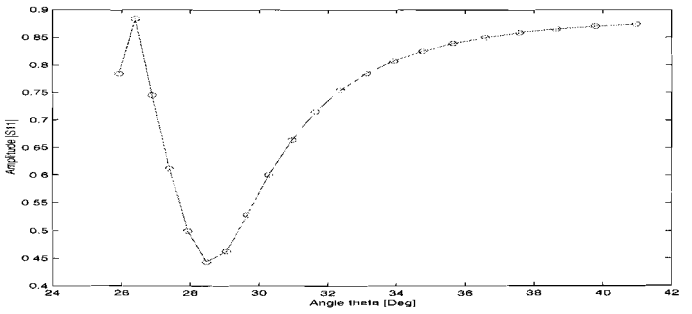

Figure 8.7: *Magnitude of* s_{11} *of incident mode* TE_{01} *as function angle theta.*

fact that, angle θ is reverse proportional to the frequency f, see Eq.(8.3). Furthermore, we notice that the reflection around the center frequency is relatively high.

Chapter 9

Conclusions and Recommendations

9.1 Conclusions

For a phased array consisting of cavity-backed patch antennas, a simple and rigorous method of solution to the problem has been shown. By separating the waveguide structure into several parts a high level of flexibility has been created.

Two sub-problems have been discussed: the iris and a patch in a waveguide. The approach used to model these two problems was to close the apertures with perfect electric conductors (PEC's) and subsequently define equivalent magnetic surface current densities. For this we have made use of the equivalence theory and uniqueness theorems. The equivalent magnetic currents are needed to guarantee continuity of the electric and magnetic fields.

Because of the waveguide-type problems we have deployed the Marcuvitz-Swinger equations and represented the electromagnetic fields in a modal basis. This led to equivalent transmission-line equations, from which we have obtained so-called modal Green's functions. With these Green's functions we formed integral equations which we then solved by applying a Garlerkin method of moments (MoM).

With the obtained results from the MoM, we formed a scattering parameter description of each sub-problem, which has made it possible to connect the two parts. Because we assumed an infinite array in our model, it has become possible to use the coupling of the iris with the patch as a waveguide simulator for the phased array.

9.2 Recommendations

First of all, as long as there are no patches to be analysed with exotic shapes, one could use rooftop basis-functions instead of RWG basis-functions. Because of there orthogonality a good separation in x- and y-direction will be possible.

Secondly, one could uncouple the summations of the Green's function (modal field expansions) and the basis-functions for the equivalent magnetic currents.

Thirdly, one could extend this analysis for a true infinite phased array. This is only a relatively small step. We have to find the Green's function of the periodic arrangement in free space. The Green's function for the waveguide is already known. We can then form an integral equation, and solve this with the MoM.

Further, a modal approach could be employed to create a model for the stripline power-supply.

Finally, one could use the complete software to design a real-life application.

Appendix A

Electric dipole tangential to PEC surface

In this appendix we will show that a current source tangential to a PEC does not radiate any electromagnetic energy.
For this we start from the assumption of a region of space, V, bounded by a large sphere of radius R, with its center at the origin of the coordinate system and its surface is denoted by S_R. In this region there are two bodies, with volumes V^a, V^b with corresponding surfaces S^a and S^b respectively. The subscripts "a" and "b" correspond to two possible time-harmonic electromagnetic "states" in this structure. The first is produced by the given sources $\mathbf{J}^a$, $\mathbf{M}^a$ distributed in some fashion throughout volume V^a, resulting in the fields $\mathbf{E}^a$, $\mathbf{H}^a$. To be clear, in state "a" volume V^b contains no sources so no fields are cause by it. We now look at state "b", which consists of some impressed sources $\mathbf{J}^b$, $\mathbf{M}^b$ distributed in some fashion throughout volume V^b producing the fields $\mathbf{E}^b$, $\mathbf{H}^b$. The sources of state "b" are unrelated to $\mathbf{J}^a$, $\mathbf{M}^a$. In state "b" only volume V^b contains sources and volume V^a contains no sources so no fields result from it. In Fig(A.1), the above described situation is being depicted. Both time-harmonic electromagnetic states obey Maxwell's equations, stated as

$$\begin{aligned} \nabla \times \mathbf{E}^{a,b} &= -j\omega\mu\mathbf{H}^{a,b} - \mathbf{M}^{a,b} \\ \nabla \times \mathbf{H}^{a,b} &= j\omega\varepsilon\mathbf{E}^{a,b} + \mathbf{J}^{a,b} \end{aligned} \tag{A.1}$$

To be complete, $\mathbf{E}^{a,b}$ and $\mathbf{H}^{a,b}$ must satisfy the radiation condition and appropriate boundary conditions.

Even though $\mathbf{E}^a$, $\mathbf{H}^a$ and $\mathbf{E}^b$, $\mathbf{H}^b$ do not exist simultaneously in the space being considered, let us take the quantity

$$\begin{aligned} \nabla \cdot (\mathbf{E}^a \times \mathbf{H}^b - \mathbf{E}^b \times \mathbf{H}^a) &= \mathbf{H}^b \cdot \nabla \times \mathbf{E}^a - \mathbf{E}^a \cdot \nabla \times \mathbf{H}^b \\ &\quad - \mathbf{H}^a \cdot \nabla \times \mathbf{E}^b + \mathbf{E}^b \cdot \nabla \times \mathbf{H}^a \\ &= [\mathbf{E}^b \cdot \mathbf{J}^a - \mathbf{H}^b \cdot \mathbf{M}^a] \\ &\quad - [\mathbf{E}^a \cdot \mathbf{J}^b - \mathbf{H}^a \cdot \mathbf{M}^b], \end{aligned} \tag{A.2}$$

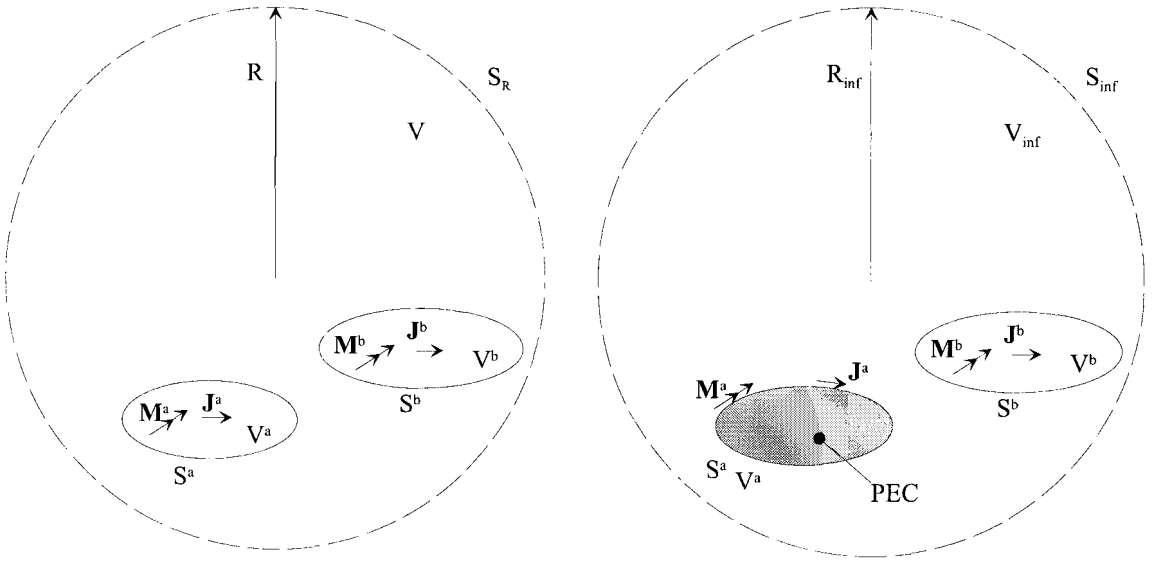

Figure A.1: *(Left) region of Bounded space, volumes "a" and "b" with electric en magnetic source currents, (right) unbounded space, volume "a" filled with PEC and on S^a equivalent surface currents, volume "b" unchanged.*

where there is been made use of the vector identity $\nabla \cdot (\mathbf{A} \times \mathbf{B}) = \mathbf{B} \cdot \nabla \times \mathbf{A} - \mathbf{A} \cdot \nabla \times \mathbf{B}$ and Eq.(A.1). Integrating over the volume V bounded by the surface S_R with unit normal vector $\mathbf{a}_n$ pointing outward from V and applying Gauss' theorem gives the integral form of the Lorentz reciprocity theorem:

$$\begin{aligned} \oint_{S_R} (\mathbf{E}^a \times \mathbf{H}^b - \mathbf{E}^b \times \mathbf{H}^a) \cdot \mathbf{a}_n dS &= \int_V (\mathbf{E}^b \cdot \mathbf{J}^a - \mathbf{H}^b \cdot \mathbf{M}^a)\, dV \\ &\quad - \int_V (\mathbf{E}^a \cdot \mathbf{J}^b - \mathbf{H}^a \cdot \mathbf{M}^b)\, dV \end{aligned} \tag{A.3}$$

Now if we let the radius of the sphere expand to infinity, the former described bounded region becomes all of space which has an infinite volume V_∞ and a surface S_∞. If the sources are still spatially finite, we know that the field far away from the sources obey the Sommerfeld radiation conditions

$$\begin{aligned} &\lim_{r\to\infty} r[Z_0 \mathbf{a}_r \times \mathbf{H}(\mathbf{r}) + \mathbf{E}(\mathbf{r})] = \mathbf{0}, \\ \Leftrightarrow &\lim_{r\to\infty} r[\mathbf{a}_r \times \mathbf{E}(\mathbf{r}) - Z_0 \mathbf{H}(\mathbf{r})] = \mathbf{0}. \end{aligned} \tag{A.4}$$

What they mean is that the fields far from a localized source behave like TEM waves in the r-direction [1] viz. $\mathbf{H}(\theta, \phi) = Y_0 \mathbf{a}_r \times \mathbf{E}(\theta, \phi)$.

[1] In [29] you can read how a localized sources radiate waves and behave as local TEM waves in the far field.

If we apply this condition and use the fact that $\mathbf{a}_r = \mathbf{a}_n$ on the surface S_∞, to the left-hand side of Eq.(A.3) we have

$$\lim_{R\to\infty} \oint_{S_R} (\mathbf{E}^a \times \mathbf{H}^b - \mathbf{E}^b \times \mathbf{H}^a) \cdot \mathbf{a}_n dS = \lim_{R\to\infty} \oint_{S_R} \left[(\mathbf{a}_n \times \mathbf{E}^a) \cdot \mathbf{H}^b - (\mathbf{a}_n \times \mathbf{E}^b) \cdot \mathbf{H}^a \right] dS = 0, \tag{A.5}$$

we see that the contribution of the surface integral becomes zero and Eq.(A.3) reduces to

$$\int_{V_\infty} (\mathbf{E}^b \cdot \mathbf{J}^a - \mathbf{H}^b \cdot \mathbf{M}^a)\, dV = \int_{V_\infty} (\mathbf{E}^a \cdot \mathbf{J}^b - \mathbf{H}^a \cdot \mathbf{M}^b)\, dV. \tag{A.6}$$

It is not necessary to define the boundary fields on S_R, which provide the internal region with information about the sources that exist outside of S_R. After all, it is sensible to assume that as $R \to \infty$ there will be no sources external to S_R and thus no need for the boundary fields and still it is possible to get a unique solution by merely specifying the sources within S_R, [26, Sec.4.10].

Next, we discard the magnetic sources and apply *Love's Equivalence Principle* [6] to the source in volume V^a. This comes down to removing the original source $\mathbf{J}^a$ and defining a equivalent electric surface current density $\mathbf{J}_S^a$ on the surface of V^a, according

$$\mathbf{J}_S^a = \mathbf{a}_n \times \mathbf{H}^a \tag{A.7}$$

This equivalent source produces the same fields outside V^a as the original source, $\mathbf{J}^a$. This equivalent surface current can de treated as if it was an impressed one.

According to Love's principle the field $\{\mathbf{E}, \mathbf{H}\}$ inside V^a become zero. Hence, the material parameters inside V^a can be changed without disturbing those fields. So as a substitute we put in a PEC by which $\mathbf{J}_S^a$ becomes a surface current source tangential and infinitesimally close to the surface of the PEC. Together with the boundary condition $\mathbf{a}_n \times \mathbf{E}|_{S^a} = \mathbf{0}$, the left-hand side of Eq.(A.6) becomes,

$$\int_{V_\infty} \mathbf{E}^b \cdot \mathbf{J}^a\, dV \longrightarrow \int_{S^a} \mathbf{E}_{tan}^b \cdot \mathbf{J}_S^a\, dS = 0. \tag{A.8}$$

It may be obvious that the volume integral over V_∞ reduces to an integral over surface S^a since the source find itself on S^a.
By reciprocity, Eq.(A.6), we have that

$$\int_{V_\infty} \mathbf{E}^a \cdot \mathbf{J}^b\, dV = 0. \tag{A.9}$$

no matter how the source $\mathbf{J}^b$ is chosen. This can only be true if and only if $\mathbf{E}^a = \mathbf{0}$ everywhere. In other words we can conclude that an electric surface current tangential to the surface of a PEC does not produce any electric field (and for that matter no magnetic field either) exterior to that surface.

Appendix B

Orthogonality

In this section it is shown that the $\boldsymbol{\rho}$-depended longitudinal constituent of the electromagnetic field and the mode functions are orthogonal.

B.1 Orthogonality e_z, h_z

The derivation for the longitudinal constituent e_z is the same as for h_z, in this way we can define a scalair substituent like,

$$\xi(\boldsymbol{\rho}) \in \{e_z(\boldsymbol{\rho}), h_z(\boldsymbol{\rho})\}, \tag{B.1}$$

meaning ξ can be e_z as well as h_z. We start with

$$(\nabla_t^2 + k_t^2)\,\xi_i = 0, \tag{B.2}$$
$$(\nabla_t^2 + k_t^2)\,\xi_j^* = 0. \tag{B.3}$$

The superscript $*$ indicates a complex conjugate, the subscripts i and j indicate two different modes i.e. eigensolutions. It is self-evident when $\xi = e_z$, values of k_t^2 are related to TM modes and when $\xi = h_z$, values of k_t^2 are related to TE modes. Next, take the inner-product of Eq.(B.2) and Eq.(B.3) with respectively ξ_j and ξ_i^*, according to

$$< a, b > = \int_S a\, b^* d\sigma, \tag{B.4}$$

and subsequently subtract former equations from each other. This results in

$$\int_S \xi_j^*\, \nabla_t^2\, \xi_i - \xi_i\, \nabla_t^2 \xi_j^*\, d\sigma + (k_{t;i}^2 - k_{t;j}^2) \int_S \xi_i\, \xi_j^*\, d\sigma = 0. \tag{B.5}$$

With the vector identity

$$\nabla_t \cdot (v\mathbf{A}) = \nabla_t \cdot (v \nabla_t \phi) = v \nabla_t^2 \phi + \nabla_t v \cdot \nabla_t \phi, \tag{B.6}$$

we can write the two terms under the first integral as

$$\xi_j^* \nabla_t^2 \xi_i = \nabla_t \cdot (\xi_j^* \nabla_t \xi_i) - \nabla \xi_i \cdot \nabla \xi_j^*, \tag{B.7}$$

$$\xi_i \nabla_t^2 \xi_j^* = \nabla_t \cdot (\xi_i \nabla_t \xi_j^*) - \nabla \xi_j^* \cdot \nabla \xi_i. \tag{B.8}$$

In Eq.(B.7) and Eq.(B.8) we can see that the last two terms on the right-hand side are equal and therefore cancel, thereby restating Eq.(B.5) as

$$\int_S \nabla_t \cdot (\xi_j^* \nabla_t \xi_i - \xi_i \nabla_t \xi_j^*)\, d\sigma = -(k_{t;i}^2 - k_{t;j}^2) \int_S \xi_i\, \xi_j^*\, d\sigma. \tag{B.9}$$

Applying *Gauss'* divergence theorem for $\mathbb{R}^2$ or *Green's* theorem for $\mathbb{R}^2$, we obtain

$$\oint_C (\xi_j^* \nabla_t \xi_i - \xi_i \nabla_t \xi_j^*) \cdot \boldsymbol{\nu}\, dl = -(k_{t;i}^2 - k_{t;j}^2) \int_S \xi_i\, \xi_j^*\, d\sigma. \tag{B.10}$$

where $\boldsymbol{\nu}$ is the outward pointing unity vector normal to the contour. Eq.(B.10) can be reduced further by invoking the directional derivatives as

$$\oint_C \left(\xi_j^* \frac{\partial \xi_i}{\partial \nu} - \xi_i \frac{\partial \xi_j^*}{\partial \nu} \right) dl = -(k_{t;i}^2 - k_{t;j}^2) \int_S \xi_i\, \xi_j^*\, d\sigma. \tag{B.11}$$

In both cases, for $\xi = e_z$ or $\xi = h_z$, the left-hand integral is zero by inspecting the boundary conditions $e_z|_{\boldsymbol{\rho}=\boldsymbol{\rho}_\Gamma} = 0$ and $\partial h_z/\partial \nu|_{\boldsymbol{\rho}=\boldsymbol{\rho}_\Gamma} = 0$, respectively.

This means that

$$\int_S \xi_i\, \xi_j^*\, d\sigma = 0 \qquad \text{for} \qquad k_{t;i}^2 \neq k_{t;j}^2 \quad ; \quad i \neq j \quad ; \quad \xi \in (e_z, h_z), \tag{B.12}$$

in other words, the electric and magnetic longitudinal field constituents are orthogonal.

B.2 Orthogonality e′, e″, h′, h″

Focusing on the equations of the TE and TM mode functions, we see that the expression for $\mathbf{e}'$ and $\mathbf{h}''$ and the expression for $\mathbf{h}'$ and $\mathbf{e}''$ show a lot of similarity.

$$\mathbf{e}' = -j \frac{k_z'}{k_t'^2} \nabla_t e_z, \qquad \mathbf{h}'' = -j \frac{k_z''}{k_t''^2} \nabla_t h_z, \tag{B.13}$$

$$\mathbf{h}' = -j \frac{k_z'}{k_t'^2} (\mathbf{a}_z \times \nabla_t e_z), \qquad \mathbf{e}'' = -j \frac{k_z''}{k_t''^2} (\nabla_t h_z \times \mathbf{a}_z). \tag{B.14}$$

This gives rise to the introduction of vectorial substitutes

$$\boldsymbol{\eta}_i(\boldsymbol{\rho}) = \mathbf{e}'(\boldsymbol{\rho}) \quad \text{or} \quad \boldsymbol{\eta}_i(\boldsymbol{\rho}) = \mathbf{h}''(\boldsymbol{\rho}) \tag{B.15}$$

$$\boldsymbol{\zeta}_i(\boldsymbol{\rho}) = \mathbf{h}'(\boldsymbol{\rho}) \quad \text{or} \quad \boldsymbol{\zeta}_i(\boldsymbol{\rho}) = \mathbf{e}''(\boldsymbol{\rho}). \tag{B.16}$$

By defining an inner-product, according to

$$< \mathbf{a}, \mathbf{b} > = \int_S \mathbf{a} \cdot \mathbf{b}^* d\sigma, \tag{B.17}$$

we can start with the inner-product of the i-th and j-th mode of Eq.(B.13).

B.2.1 Inner-product $\boldsymbol{\eta}$

As a consequence of the introduction of the variable $\boldsymbol{\eta}$, e_z as well as h_z can appear in the inner-product $< \boldsymbol{\eta}_i, \boldsymbol{\eta}_j >$, this is why we will adopt the notation of the preceding section for e_z and h_z, viz. ξ.

$$< \boldsymbol{\eta}_i, \boldsymbol{\eta}_j >= \frac{k_{z;i} k^*_{z;j}}{k^2_{t;i} k^2_{t;j}} \int_S \nabla_t \xi_i \cdot \nabla_t \xi^*_j \, d\sigma. \tag{B.18}$$

The *primes*, indicating TM or TE modes, are left out. We assume that it is clear, that depending on wether ξ is equal to e_z or h_z the variables k_z and k_t^2 refer to respectively TM or TE modes. Next, making use of Eq.(B.6) and $\nabla_t^2 \xi^*_j = -k_t^2 \xi^*_j$ we obtain

$$< \boldsymbol{\eta}_i, \boldsymbol{\eta}_j >= \frac{k_{z;i} k^*_{z;j}}{k^2_{t;i} k^2_{t;j}} \int_S \nabla_t \cdot (\xi_i \nabla_t \xi^*_j) + \xi_i \, k^2_{t;j} \, \xi^*_j \, d\sigma. \tag{B.19}$$

Applying *Gauss'* the 2-dimensional theorem to the first term under the integral results in

$$< \boldsymbol{\eta}_i, \boldsymbol{\eta}_j > = \frac{k_{z;i} k^*_{z;j}}{k^2_{t;i} k^2_{t;j}} \left(\oint_c \xi_i \nabla_t \xi^*_j \cdot \boldsymbol{\nu} dl + k^2_{t;j} \int_S \xi_i \, \xi^*_j \, d\sigma \right), \tag{B.20}$$

$$= \frac{k_{z;i} k^*_{z;j}}{k^2_{t;i} k^2_{t;j}} \left(\oint_c \xi_i \frac{\partial \xi^*_j}{\partial \nu} \, dl + k^2_{t;j} \int_S \xi_i \, \xi^*_j \, d\sigma \right), \tag{B.21}$$

Now, we are at a point similar to Eq.(B.11). Using the boundary conditions $e_z|_{\boldsymbol{\rho}=\boldsymbol{\rho}_\Gamma} = 0$ and $\partial h_z / \partial \nu|_{\boldsymbol{\rho}=\boldsymbol{\rho}_\Gamma} = 0$ for ξ, respectively equal to e_z, h_z, we conclude that the contour integral vanishes. The surface integral vanishes on account of Eq.(B.12). We end up with the conclusion that

$$< \mathbf{e}'_i, \mathbf{e}'_j > = 0, \qquad i \neq j, \tag{B.22}$$

$$< \mathbf{h}''_i, \mathbf{h}''_j > = 0, \qquad i \neq j. \tag{B.23}$$

i.e. the mode functions $\mathbf{e}'$ and $\mathbf{h}''$ are orthogonal.

B.2.2 Inner-product $\boldsymbol{\zeta}$

Looking at Eq.(B.14), the expressions for $\mathbf{h}'$ and $\mathbf{e}''$ are identical with the exception of h_z, e_z and the cross-product with $\mathbf{a}_z$. Again we will work with the substitute ξ for h_z and e_z. So we have

$$< \boldsymbol{\zeta}_i, \boldsymbol{\zeta}_j >= \frac{k_{z;i} k^*_{z;j}}{k^2_{t;i} k^2_{t;j}} \int_S (\mathbf{a}_z \times \nabla_t \xi_i) \cdot (\mathbf{a}_z \times \nabla_t \xi^*_j) \, d\sigma. \tag{B.24}$$

By applying the vector identities in Eq.(3.25) and Eq.(3.29) to the integrand we obtain

$$< \boldsymbol{\zeta}_i, \boldsymbol{\zeta}_j >= \frac{k_{z;i} k^*_{z;j}}{k^2_{t;i} k^2_{t;j}} \int_S \nabla_t \xi_i \cdot \nabla_t \xi^*_j \, d\sigma, \tag{B.25}$$

which is the same as equation Eq.(B.18). This brings us to the conclusion that $\mathbf{h}'$ and $\mathbf{e}''$ are also orthogonal

$$< \mathbf{h}'_i, \mathbf{h}'_j > = 0, \qquad i \neq j, \tag{B.26}$$

$$< \mathbf{e}''_i, \mathbf{e}''_j > = 0, \qquad i \neq j. \tag{B.27}$$

B.3 Mutual Orthogonal e',e'' and h',h''

We start with $\mathbf{e}'$ and $\mathbf{e}''$.

$$< \mathbf{e}'_i, \mathbf{e}''_j >= \frac{1}{k'^2_{t;i} k''^2_{t;j}} \int_S \nabla_t \phi_i \cdot (\nabla_t \psi^*_j \times \mathbf{a}_z)\, d\sigma = \frac{1}{k'^2_{t;i} k''^2_{t;j}} \int_S (\nabla_t \phi_i \times \nabla_t \psi^*_j) \cdot \mathbf{a}_z\, d\sigma. \tag{B.28}$$

Applying the right vector identity and *Stokes's* theorem yields

$$< \mathbf{e}'_i, \mathbf{e}''_j >= \frac{1}{k'^2_{t;i} k''^2_{t;j}} \oint_C \phi_i \frac{\partial \psi^*_j}{\partial \tau}\, dl = 0; \qquad \phi\,|_{\boldsymbol{\rho}=\boldsymbol{\rho}_\Gamma} = 0. \tag{B.29}$$

And by analogy with the above, of course

$$< \mathbf{h}'_i, \mathbf{h}''_j >= 0. \tag{B.30}$$

B.4 Real eigenvalue

In all the above we have made use of the fact that k_t^2 is real. This follows from

$$< (\nabla_t^2 + k^2_{t;i})\xi_i, \xi_i >=< \nabla_t^2 \xi_i, \xi_i > + k^2_{t;i} < \xi_i, \xi_i >= 0, \tag{B.31}$$

referring to Eq.(B.1) for ξ. Then using Eq.(B.7), *Gauss'* theorem and the boundary conditions $e_z|_{\boldsymbol{\rho}=\boldsymbol{\rho}_\Gamma} = 0$ and $\partial h_z/\partial \nu|_{\boldsymbol{\rho}=\boldsymbol{\rho}_\Gamma} = 0$ we obtain

$$k^2_{t;i} = \frac{\| \nabla_t \xi_i \|^2}{\| \xi_i \|^2}. \tag{B.32}$$

Hence $k^2_{t;i}$ is positive because of its quadratic form and real because of the quotient of two real valued numbers.

Appendix C

Waveguide modes for rectangular waveguide

In Secs.4.3.1 and 4.3.2, we ended up with a set of equations for TE modes, Eqs.(4.47)-(4.50), and TM modes, Eqs.(4.61)-(4.64). These equations are built from the scalar functions ψ and ϕ, respectively, or their gradients. However, up till now their exact expression form is still unknown, the only thing we know about them is that they obey an orthogonality relation, see Appendix B, since ψ and ϕ are proportional to h_z and e_z, respectively, and their L^2-norm is one. By solving the two dimensional scalar wave equations in Eqs.(4.47) and (4.61) we obtain explicit expressions for ψ and ϕ, respectively. If we accompany these wave equations with their specific boundary conditions, so that they become uniquely solvable, we get the well known Neumann boundary-value problem

$$(\nabla_t^2 + k_{t;i}^2)\,\psi_i = 0, \qquad \frac{\partial \psi_i}{\partial \nu}\Big|_{\boldsymbol{\rho}=\boldsymbol{\rho}_\Gamma} = 0, \tag{C.1}$$

and the Dirichlet boundary-value problem

$$(\nabla_t^2 + k_{t;i}^2)\phi_i = 0, \qquad \phi_i\big|_{\boldsymbol{\rho}=\boldsymbol{\rho}_\Gamma} = 0. \tag{C.2}$$

These boundary value problems will be solved for rectangular waveguides of arbitrary size. The x-dimension is indicated with A and y-dimension with B.

C.1 Solution to Neumann boundary-value problem

The simplest way to solve the differential equation in Eq.(C.1) is by applying the method of separation of variables (also called the product solution). Separation of variables is possible because there is a underlaying orthonormal (or at least a orthogonal) basis in the problem. Upon assuming a solution of the form

$$\psi_i(\boldsymbol{\rho}) = \psi_n(x)\psi_m(y), \qquad i = (n, m), \tag{C.3}$$

substituted in Eq.(C.1) and subsequently dividing, this total equation, by Eq.(C.3) yields

$$\frac{1}{\psi_n(x)}\frac{d^2\psi_n(x)}{dx^2}+\frac{1}{\psi_m(y)}\frac{d^2\psi_m(y)}{dy^2}=-k_{t;i}^2. \tag{C.4}$$

The terms on the left-hand side in above equation are independent and must be equal to the constant transverse wavenumber on the right-hand side for every combination of x and y. The solution to Eq.(C.4) can be found by writing the transverse wavenumber as a combination of the wavenumbers in the x-direction and the y-direction as follows

$$k_{t;i}^2=k_x^2+k_y^2. \tag{C.5}$$

This reduces Eq.(C.1) to two scalar second order differential equation

$$\left(\frac{d^2}{dx^2}+k_x^2\right)\psi_n(x)=0, \qquad \frac{d\psi_n(x)}{dx}=0 \text{ at } x=\{0,A\} \tag{C.6}$$

$$\left(\frac{d^2}{dy^2}+k_y^2\right)\psi_m(y)=0, \qquad \frac{d\psi_m(y)}{dy}=0 \text{ at } y=\{0,B\} \tag{C.7}$$

where k_x^2 and k_y^2 are the so-called *separation* constants.

Eqs.(C.6) and (C.7) can be recognize as problems of the Sturm-Liouville type. This implies that the eigenfunctions $\psi_n(x)$ and $\psi_m(y)$ form complete sets and possess orthogonality, and the eigenvalues are real and positive, [11, Sec.3.2],[18, Sec.4.7]. This supplements the facts that we found in Appendix B.

The general solution to Eq.(C.6) is

$$\psi_n(x)=c_1e^{-jk_xx}+c_2e^{jk_xx}, \tag{C.8}$$

where c_1 and c_2 are two unknown constants which we can solve by invoking the two boundary conditions along the x-directions, indicated in Eq.(C.6). From $\frac{d\psi_n}{dx}|_{x=0}$ we get $c_1=c_2$ and $\frac{d\psi_n}{dx}|_{x=A}$ yields $k_x=\frac{n\pi}{A}$. With these results we obtain a final expression of the following form

$$\psi_n(x)=\sqrt{\frac{\epsilon_n}{A}}\cos(k_xx), \quad k_x=\frac{n\pi}{A}, \quad \epsilon_n=\begin{cases}2, & n\neq 0,\\ 1, & n=0,\end{cases} \quad n=\{0,1,2,3,...\}. \tag{C.9}$$

The multiplicative constant $\sqrt{\frac{\epsilon_n}{A}}$ is due to the normalization of ψ_n to unity, as stated in Sec.4.3.1, and according to

$$<\psi_n,\psi_n>=\|\psi_n\|^2=\int_0^A\psi_n^2\,dx=1. \tag{C.10}$$

By analogy with the above derivation, it is now simple to find the solution to Eq.(C.7), which is

$$\psi_m(y)=\sqrt{\frac{\epsilon_m}{B}}\cos(k_yy), \quad k_y=\frac{m\pi}{B}, \quad \epsilon_m=\begin{cases}2, & m\neq 0,\\ 1, & m=0,\end{cases} \quad m=\{0,1,2,3,...\}. \tag{C.11}$$

Multiplying Eq.(C.9) and Eq.(C.11), according to Eq.(C.3), results in the final expression for the scalar function ψ_i

$$\psi_i(\boldsymbol{\rho}) = \sqrt{\frac{\epsilon_n \epsilon_m}{AB}} \cos(k_x x)\cos(k_y y), \tag{C.12}$$
$$\epsilon_m = \epsilon_n = \begin{cases} 2, & \text{n}\neq 0, \\ 1, & \text{n}=0, \end{cases} \qquad i = (n,m), \quad n,m = \{0,1,2,...\}.$$

The combination $n = 0 \wedge m = 0$ is excluded, because the result is a constant field.

C.2 Solution to Dirichlet boundary-value problem

To solve the Dirichlet boundary-value problem, we follow the same approach as above. Applying separation of variables reduces Eq.(C.2) to two one-dimensional second order differential equation

$$\left(\frac{d^2}{dx^2} + k_x^2\right)\phi_n(x) = 0, \qquad \phi_n(x) = 0 \text{ at } x = \{0, A\} \tag{C.13}$$
$$\left(\frac{d^2}{dy^2} + k_y^2\right)\phi_m(y) = 0, \qquad \phi_m(y) = 0 \text{ at } y = \{0, B\}. \tag{C.14}$$

Once again, these problems are of the Sturm-Liouville type. The solution to Eq.(C.13) is

$$\phi_n(x) = \sqrt{\frac{2}{A}}\sin(k_x x), \qquad k_x = \frac{n\pi}{A}, \qquad n = \{1,2,3,...\}, \tag{C.15}$$

$n = 0$ is a trivial case and thereby excluded. The constant $\sqrt{\frac{2}{A}}$ is due to the normalization of ϕ_n to unity, as in Eq.(C.10). The solution to $\phi_m(y)$ in Eq.(C.14) is as follows

$$\phi_m(y) = \sqrt{\frac{2}{B}}\sin(k_y y), \qquad k_y = \frac{m\pi}{B}, \qquad m = \{1,2,3,...\}, \tag{C.16}$$

Multiplying Eq.(C.15) and Eq.(C.16) leads to the final solution of Eq.(C.2)

$$\phi_i(\boldsymbol{\rho}) = \frac{2}{\sqrt{AB}}\sin(k_x x)\sin(k_y y), \qquad i = (n,m), \qquad n,m = \{1,2,3,...\}. \tag{C.17}$$

C.2.1 The TE and TM mode functions

Now that the scalar functions are calculated, it is rather simple to find the TE and TM mode functions, explicitly. Using Eqs.(4.49)-(4.50) and Eqs.(4.63)-(4.64) we find, respectively

$$\mathbf{h}_i'' = -\frac{1}{k_{t;i}''}\nabla_t \psi_i = \frac{\sqrt{\epsilon_n\epsilon_m}}{k_{t;i}''\sqrt{AB}}\begin{bmatrix} k_x''\sin(k_x''x)\cos(k_y''y) \\ k_y''\cos(k_x''x)\sin(k_y''y)\end{bmatrix}, \tag{C.18}$$

$$\mathbf{e}_i'' = -\frac{1}{k_{t;i}''^2}(\nabla_t \psi_i \times \mathbf{a}_z) = \frac{\sqrt{\epsilon_n\epsilon_m}}{k_{t;i}''\sqrt{AB}}\begin{bmatrix} k_y''\cos(k_x''x)\sin(k_y''y) \\ -k_y''\sin(k_x''x)\cos(k_y''y)\end{bmatrix}. \tag{C.19}$$

$$\mathbf{h}_i' = -\frac{1}{k_{t;i}'}\left(\mathbf{a}_z \times \nabla_t \phi_i\right) = \frac{-2}{k_{t;i}'\sqrt{AB}}\begin{bmatrix} -k_y' \sin(k_x' x)\cos(k_y' y) \\ k_x' \cos(k_x' x)\sin(k_y' y) \end{bmatrix}, \tag{C.20}$$

$$\mathbf{e}_i' = -\frac{1}{k_{t;i}'}\nabla_t \phi_i = \frac{-2}{k_{t;i}'\sqrt{AB}}\begin{bmatrix} k_x' \cos(k_x' x)\sin(k_y' y) \\ k_y' \sin(k_x' x)\cos(k_y' y) \end{bmatrix}, \tag{C.21}$$

Appendix D

Interim results transmission lines

In Chapter 5, equivalent transmission line equations have been derived. To arrive these equations, an inner-product has to be taken of a mode function with an other mode function on which the operator $\underline{\underline{\mathcal{L}}}$ is working, see Eq.(5.4). In this section we will give a short description of what the outcome is of this inner-product. Only in the case of the electric field mode functions a derivation wil be given. By analogy with the electric field mode function case, the inner-product for the magnetic field mode functions can be obtained.

Case 1: both the mode functions are α=β=TM mode types. The inner-product takes the following form

$$< \underbrace{\mathbf{e}'_i + \frac{1}{k^2}\nabla_t\nabla_t \cdot \mathbf{e}'_i}_{I_1}, \mathbf{e}'_j >, \tag{D.1}$$

where $\mathbf{e}'_i$ is found in Eq.(4.63). The underbraced expression, indicated by I_1, can be written as,

$$\begin{aligned} I_1 &= \frac{1}{k^2}[k^2\mathbf{e}'_i + \nabla_t\nabla_t \cdot \mathbf{e}'_i] = \frac{-1}{k^2 k'_{t;i}}[k^2\nabla_t\,\phi_i + \nabla_t\nabla_t \cdot \nabla_t\,\phi_i] \\ &= \frac{-1}{k^2 k'_{t;i}}\nabla_t(k'^2_{z;i}\phi_i + \underbrace{k'^2_{t;i}\phi_i + \nabla_t^2\,\phi_i}_{=0}) = \frac{-k'^2_{z;i}}{k^2 k'_{t;i}}\nabla_t\,\phi_i. \end{aligned} \tag{D.2}$$

In Eq.(D.2) we used the fact that the scalar Helmholtz equation for ϕ is zero. Now, if we substitute Eq.(D.2) back into Eq.(D.1) we obtain

$$< \frac{-k'^2_{z;i}}{k^2 k'_{t;i}}\nabla_t\,\phi_i, \frac{-1}{k'_{t;j}}\nabla_t\,\phi_j > = \frac{k'^2_{z;i}}{k^2 k'_{t;i} k'_{t;j}} \underbrace{\int_S \nabla_t\,\phi_i \cdot \nabla_t\,\phi_j^*\, d\sigma}_{I_2}. \tag{D.3}$$

The underbraced expression I_2 can be rewritten as

$$\begin{aligned} I_2 = \int_S \nabla_t \phi_i \cdot \nabla_t \phi_j^* \, d\sigma &= \int_S \nabla_t \cdot (\phi_i \nabla_t \phi_j^*) - \phi_i \nabla_t^2 \phi_j^* \, d\sigma \\ &= \oint_C \phi_i \frac{\partial \phi_j^*}{\partial \nu} \, dl + k_{t;j}'^2 \int_S \phi_i \, \phi_j^* \, d\sigma \\ &= k_{t;j}'^2 < \phi_i, \phi_j >= k_{t;j}'^2 \, \delta_{ij}. \end{aligned} \tag{D.4}$$

The contour integral is zero because ϕ vanishes upon approaching the waveguide wall, owing to the boundary condition. Note that we've already encountered an integral like I_2 in Eq.(B.18). Substituting the above expression for I_2 back into Eq.(D.3), we obtain the final form of Eq.(D.1)

$$< \mathbf{e}_i' + \frac{1}{k^2} \nabla_t \nabla_t \cdot \mathbf{e}_i', \mathbf{e}_j' >= \frac{k_{z;i}'^2 k_{t;j}'^2}{k^2 k_{t;i}' k_{t;j}'} < \phi_i, \phi_j >= \frac{k_{z;i}'^2}{k^2} \delta_{ij} \tag{D.5}$$

Case 2: both the mode functions are α=β=TE mode types. The inner-product now takes on the following form

$$< \underbrace{\mathbf{e}_i'' + \frac{1}{k^2} \nabla_t \nabla_t \cdot \mathbf{e}_i''}_{I_1}, \mathbf{e}_j'' >, \tag{D.6}$$

where $\mathbf{e}_i''$ is found in Eq.(4.50). We can write the underbraced expression, indicated by I_1, as,

$$\begin{aligned} I_1 &= \frac{-1}{k_{t;i}''} \left[(\nabla_t \psi_i \times \mathbf{a}_z) + \frac{1}{k^2} \nabla_t \nabla_t \cdot (\nabla_t \psi_i \times \mathbf{a}_z) \right] \\ &= \frac{-1}{k^2 k_{t;i}''} \left[k^2 (\nabla_t \psi_i \times \mathbf{a}_z) + \nabla_t \{ \mathbf{a}_z \cdot [\underbrace{\nabla_t \times (\nabla_t \psi_i)}_{=0}] - \nabla_t \psi_i \cdot (\underbrace{\nabla_t \times \mathbf{a}_z}_{=0}) \} \right] \\ &= \frac{-1}{k_{t;i}''} (\nabla_t \psi_i \times \mathbf{a}_z). \end{aligned} \tag{D.7}$$

With the help of I_1, Eq.(D.6) can then be rewritten as

$$< \frac{-1}{k_{t;i}''} (\nabla_t \psi_i \times \mathbf{a}_z), \frac{-1}{k_{t;j}''} (\nabla_t \psi_j \times \mathbf{a}_z) >= \frac{1}{k_{t;i}'' k_{t;j}''} \underbrace{\int_S (\nabla_t \psi_i \times \mathbf{a}_z) \cdot (\nabla_t \psi_j^* \times \mathbf{a}_z) \, d\sigma}_{I_2} \tag{D.8}$$

Expression I_2 can be rewritten as

$$\begin{aligned} I_2 &= \int_S \nabla_t \psi_i \cdot \nabla_t \psi_j^* \, d\sigma = \oint_C \psi_i \frac{\partial \psi_j^*}{\partial \nu} \, dl + k_{t;j}''^2 \int_S \psi_i \, \psi_j^* \, d\sigma \\ &= k_{t;j}''^2 < \psi_i, \psi_j >= k_{t;j}''^2 \, \delta_{ij}. \end{aligned} \tag{D.9}$$

Note that this integral has been encountered once before in Eq.(B.24). With help of the expression for I_2 in Eq.(D.9), Eq.(D.6) finally takes on the form

$$< \mathbf{e}_i'' + \frac{1}{k^2}\nabla_t\nabla_t \cdot \mathbf{e}_i'', \mathbf{e}_j'' >= \frac{k_{t;j}''^2}{k_{t;i}'' k_{t;j}''} < \psi_i, \psi_j >= \delta_{ij}. \tag{D.10}$$

Case 3: one of the mode functions is TM type and the other is TE type, which leads to the following inner-product

$$< \underbrace{\mathbf{e}_i' + \frac{1}{k^2}\nabla_t\nabla_t \cdot \mathbf{e}_i'}_{I_1}, \mathbf{e}_j'' > . \tag{D.11}$$

We can write the underbraced expression, indicated by I_1, as we did in Eq.(D.2)

$$I_1 = \frac{-k_{z;i}'^2}{k^2 k_{t;i}'}\nabla_t \phi_i. \tag{D.12}$$

Next, with Eqs.(4.50) and (D.12) we can rewrite Eq.(D.11) as

$$\begin{aligned} < \frac{-k_{z;i}'^2}{k^2 k_{t;i}'}\nabla_t \phi_i, \frac{-1}{k_{t;j}''}(\nabla_t \psi_j \times \mathbf{a}_z) > &= \frac{k_{z;i}'^2}{k^2 k_{t;i}' k_{t;j}''} \int_S \nabla_t \phi_i \cdot (\nabla_t \psi_j^* \times \mathbf{a}_z)\, d\sigma \\ &= \frac{k_{z;i}'^2}{k^2 k_{t;i}' k_{t;j}''} \underbrace{\int_S (\nabla_t \phi_i \times \nabla_t \psi_j^*) \cdot \mathbf{a}_z\, d\sigma}_{I_2} . \end{aligned} \tag{D.13}$$

Expression I_2 can be rewritten into

$$\int_S (\nabla_t \phi_i \times \nabla_t \psi_j^*) \cdot \mathbf{a}_z\, d\sigma = \int_S \nabla_t \times (\phi_i \nabla_t \psi_j^*) \cdot \mathbf{a}_z\, d\sigma - \int_S (\phi_i \underbrace{\nabla_t \times (\nabla_t \psi_j^*)}_{0}) \cdot \mathbf{a}_z\, d\sigma \tag{D.14}$$

Applying Stokes's theorem to the first term on the right-hand side and making use of the directional derivative, we are left with the equation

$$\int_S (\nabla_t \phi_i \times \nabla_t \psi_j^*) \cdot \mathbf{a}_z\, d\sigma = \oint_C \phi_i \frac{\partial \psi_j^*}{\partial \tau}\, dl \tag{D.15}$$

Invoking the boundary condition $\phi_i|_{\rho=\rho_\Gamma} = 0$, indicating that the scalar function vanishes upon approaching the waveguide wall, we see that Eq.(D.15) becomes equal to zero. With this fact we can come to the conclusion that Eq.(D.11) is equal to zero.

$$< \mathbf{e}_i' + \frac{1}{k^2}\nabla_t\nabla_t \cdot \mathbf{e}_i', \mathbf{e}_j'' >= 0. \tag{D.16}$$

Interchanging the TM and TE electric field mode functions in the inner-product of Eq.(D.11) has no effect on the outcome.

Summarizing, we have obtained the following results for electric field mode functions

$$< \underline{\underline{\mathcal{L}}}\mathbf{e}_i^{\alpha}, \mathbf{e}_j^{\beta} >= \begin{cases} \frac{k_{z;i}'^2}{k^2}\,\delta_{ij}, & \alpha = \beta\text{=TM}; \\ \delta_{ij}, & \alpha = \beta\text{=TE}; \\ 0, & \alpha \neq \beta. \end{cases} \tag{D.17}$$

By taking analogous steps, a similar derivation as above can be used to find the results in the case of the magnetic field mode functions. They are

$$< \underline{\underline{\mathcal{L}}}\mathbf{h}_i^{\alpha}, \mathbf{h}_j^{\beta} >= \begin{cases} \delta_{ij}, & \alpha = \beta\text{=TM}; \\ \frac{k_{z;i}''^2}{k^2}\,\delta_{ij}, & \alpha = \beta\text{=TE}; \\ 0, & \alpha \neq \beta. \end{cases} \tag{D.18}$$

Appendix E

Closed form integrals for iris

The following integrals have to be calculated:

$$\Pi^{\mathrm{I}}_{is} = \left\langle \mathbf{h}_i^{\alpha;\mathrm{I}}, \mathbf{w}_s \right\rangle, \tag{E.1}$$

$$\Pi^{\mathrm{I}}_{ri} = \left\langle \mathbf{f}_r, \mathbf{h}_i^{\alpha;\mathrm{I}} \right\rangle, \tag{E.2}$$

$$\Pi^{\mathrm{II}}_{ps} = \left\langle \mathbf{h}_p^{\alpha;\mathrm{II}}, \mathbf{w}_s \right\rangle, \tag{E.3}$$

$$\Pi^{\mathrm{II}}_{rp} = \left\langle \mathbf{f}_r, \mathbf{h}_p^{\alpha;\mathrm{II}} \right\rangle, \tag{E.4}$$

$$\Pi^{\mathrm{II}}_{qp} = \left\langle \mathbf{f}_q, \mathbf{h}_p^{\alpha;\mathrm{II}} \right\rangle, \tag{E.5}$$

$$\Pi^{\mathrm{III}}_{ql} = \left\langle \mathbf{f}_q, \mathbf{h}_l^{\alpha;\mathrm{III}} \right\rangle, \tag{E.6}$$

$$\Pi^{\mathrm{III}}_{ls} = \left\langle \mathbf{h}_l^{\alpha;\mathrm{III}}, \mathbf{w}_s \right\rangle, \tag{E.7}$$

restricted to case depicted in Fig.E.1. The integrals we will derive are valid for waveguide

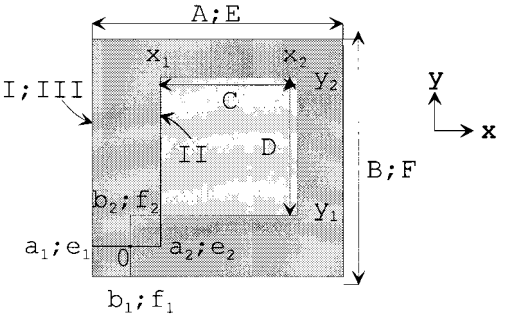

Figure E.1: *The outer rectangle is waveguide section I or III, the inner rectangle is waveguide section II. Both waveguides can have a displacement with respect to the origin "0", indicated by the small letters. The capitals indicate the waveguide dimensions.*

junctions, in which the cross section of waveguide section-II must be enclosed by or equal to the cross sections of waveguide sections-I and -III, as illustrated in Fig.E.1.

E.1 Integrals with $\mathbf{h}^{\alpha;\mathrm{II}}$, $\mathbf{h}^{\alpha;\mathrm{II}}$

Starting with Eqs.(E.3) and (E.4) and substituting the basis functions described in Sec.6.4.2 the following combinations are obtained

$$TM^{\mathrm{II}}TM^{\mathrm{II}}: \quad \left\langle \mathbf{h}_i^{\prime\mathrm{II}}, \mathbf{h}_j^{\prime\mathrm{II}} \right\rangle = \delta_{ij} \longrightarrow \left[\left\langle \mathbf{h}_i^{\prime\mathrm{II}}, \mathbf{h}_j^{\prime\mathrm{II}} \right\rangle \right] = [\underline{\underline{I}}]_{ii}, \tag{E.8}$$

$$TM^{\mathrm{II}}TE^{\mathrm{II}}: \quad \left\langle \mathbf{h}_i^{\prime\mathrm{II}}, \mathbf{h}_j^{\prime\prime\mathrm{II}} \right\rangle = 0, \tag{E.9}$$

$$TE^{\mathrm{II}}TM^{\mathrm{II}}: \quad \left\langle \mathbf{h}_i^{\prime\prime\mathrm{II}}, \mathbf{h}_j^{\prime\mathrm{II}} \right\rangle = 0, \tag{E.10}$$

$$TE^{\mathrm{II}}TE^{\mathrm{II}}: \quad \left\langle \mathbf{h}_i^{\prime\prime\mathrm{II}}, \mathbf{h}_j^{\prime\prime\mathrm{II}} \right\rangle = \delta_{ij} \longrightarrow \left[\left\langle \mathbf{h}_i^{\prime\prime\mathrm{II}}, \mathbf{h}_j^{\prime\prime\mathrm{II}} \right\rangle \right] = [\underline{\underline{I}}]_{ii} \tag{E.11}$$

At the end of Eqs.(E.8) and (E.11) the matrix notation given. $\underline{\underline{I}}_{ii}$ is the identity matrix of size $(i \times i)$. Henceforth, we use i and j as general mode number indication, to prevent from getting lost in different types of indications. Previously, we already mentioned that $i = p = l$. The subscripts I, II and III should give enough information over the waveguide section we're deling with and possibly point back to the corresponding mode indices.

E.2 Integrals with $\mathbf{h}^{\alpha;\mathrm{I}}$, $\mathbf{h}^{\alpha;\mathrm{II}}$

Then for Eqs.(E.1) and (E.2) we find, in the same way like above, the following integrals

$$TM^{\mathrm{I}}TM^{\mathrm{II}}: \quad \left\langle \mathbf{h}_i^{\prime\mathrm{I}}, \mathbf{h}_j^{\prime\mathrm{II}} \right\rangle, \tag{E.12}$$

$$TM^{\mathrm{I}}TE^{\mathrm{II}}: \quad \left\langle \mathbf{h}_i^{\prime\mathrm{I}}, \mathbf{h}_j^{\prime\prime\mathrm{II}} \right\rangle, \tag{E.13}$$

$$TE^{\mathrm{I}}TM^{\mathrm{II}}: \quad \left\langle \mathbf{h}_i^{\prime\prime\mathrm{I}}, \mathbf{h}_j^{\prime\mathrm{II}} \right\rangle, \tag{E.14}$$

$$TE^{\mathrm{I}}TE^{\mathrm{II}}: \quad \left\langle \mathbf{h}_i^{\prime\prime\mathrm{I}}, \mathbf{h}_j^{\prime\prime\mathrm{II}} \right\rangle. \tag{E.15}$$

By making use of the expressions in Eqs.(4.49) and (4.64) the integrals can be further simplified before we actually calculate them. Starting with Eq.(E.12).

E.2.1 TM^{I} $\mathrm{TM}^{\mathrm{II}}$ combination

The right-hand side term of Eq.(E.16) is derived by applying Eqs.(3.25) and (3.29) subsequently to the middle term of Eq.(E.16).

$$\left\langle \mathbf{h}_i^{\prime\mathrm{I}}, \mathbf{h}_j^{\prime\mathrm{II}} \right\rangle = \left\langle \frac{-1}{k_{t;i}^{\prime\mathrm{I}}} \left(\mathbf{a}_z \times \nabla_t \phi_i^{\mathrm{I}} \right), \frac{-1}{k_{t;j}^{\prime\mathrm{II}}} \left(\mathbf{a}_z \times \nabla_t \phi_j^{\mathrm{II}} \right) \right\rangle = \frac{1}{k_{t;i}^{\prime\mathrm{I}} k_{t;j}^{\prime\mathrm{II}}} \left\langle \nabla_t \phi_i^{\mathrm{I}}, \nabla_t \phi_j^{\mathrm{II}} \right\rangle \tag{E.16}$$

Then, with the use of Eq.(B.6) and $\nabla_t^2\phi^{*\mathrm{II}} = -k_t'^{2\,\mathrm{II}}\phi^{*\mathrm{II}}$, the right-hand side can cast into the form

$$\frac{1}{k_{t;i}'^{\mathrm{I}}k_{t;j}'^{\mathrm{II}}}\left\langle \nabla_t\,\phi_i^{\mathrm{I}}, \nabla_t\,\phi_j^{\mathrm{II}}\right\rangle = \frac{1}{k_{t;i}'^{\mathrm{I}}k_{t;j}'^{\mathrm{II}}}\int_{S_a^{\mathrm{II}}} \nabla_t\cdot(\phi_i^{\mathrm{I}}\,\nabla_t\,\phi_j^{*\mathrm{II}}) + \phi_i^{\mathrm{I}}\,k_{t;j}'^{2\,\mathrm{II}}\,\phi_j^{*\mathrm{II}}\,d\sigma. \tag{E.17}$$

The surface integral is over the cross-section[1] (aperture) of waveguide section-II and in Eq.(B.17) the inner-product is defined. This kind of integrals have been reviewed in Appendix B, so now and then we will point back and make use of already derived results. By invoking Gauss's theorem we find

$$= \frac{1}{k_{t;i}'^{\mathrm{I}}k_{t;j}'^{\mathrm{II}}}\left\{\oint_{\partial S_a^{\mathrm{II}}}\phi_i^{\mathrm{I}}\frac{\partial\phi_j^{*\mathrm{II}}}{\partial\nu}\,dl + \int_{S_a^{\mathrm{II}}}\phi_i^{\mathrm{I}}\,k_{t;j}'^{2\,\mathrm{II}}\,\phi_j^{*\mathrm{II}}\,d\sigma\right\} = \frac{k_{t;j}'^{\mathrm{II}}}{k_{t;i}'^{\mathrm{I}}}\int_{S_a^{\mathrm{II}}}\phi_i^{\mathrm{I}}\,\phi_j^{*\mathrm{II}}\,d\sigma. \tag{E.18}$$

Remember that $\phi_j^{*\mathrm{II}}|_{\partial S_a^{\mathrm{II}}} = 0$, where the edge, or contour, of surface S_a^{II} is indicated by $\partial S_a^{\mathrm{II}}$.

E.2.2 TM^{I} $\mathrm{TE}^{\mathrm{II}}$ combination

$$\left\langle \mathbf{h}_i'^{\mathrm{I}}, \mathbf{h}_j''^{\mathrm{II}}\right\rangle = \left\langle \frac{-1}{k_{t;i}'^{\mathrm{I}}}\left(\mathbf{a}_z\times\nabla_t\,\phi_i^{\mathrm{I}}\right), \frac{-1}{k_{t;j}''^{\mathrm{II}}}\nabla_t\,\psi_j^{\mathrm{II}}\right\rangle = \frac{1}{k_{t;i}'^{\mathrm{I}}k_{t;j}''^{\mathrm{II}}}\left\langle\left(\mathbf{a}_z\times\nabla_t\,\phi_i^{\mathrm{I}}\right), \nabla_t\,\psi_j^{\mathrm{II}}\right\rangle. \tag{E.19}$$

With the help of Eq.(3.29) and

$$\nabla_t\times(v\mathbf{A}) = \nabla_t v\times\mathbf{A} + v(\nabla_t\times\mathbf{A}), \tag{E.20}$$

the right-hand side of Eq.(E.19) can be written as

$$\frac{1}{k_{t;i}'^{\mathrm{I}}k_{t;j}''^{\mathrm{II}}}\left\langle\left(\mathbf{a}_z\times\nabla_t\,\phi_i^{\mathrm{I}}\right), \nabla_t\,\psi_j^{\mathrm{II}}\right\rangle = \frac{1}{k_{t;i}'^{\mathrm{I}}k_{t;j}''^{\mathrm{II}}}\left\{\int_{S_a^{\mathrm{II}}}\Big(\nabla_t\times(\phi_i^{\mathrm{I}}\nabla_t\,\psi_j^{*\mathrm{II}}) - \phi_i^{\mathrm{I}}(\nabla_t\times(\nabla_t\psi_j^{*\mathrm{II}}))\Big)\cdot\mathbf{a}_z\,d\sigma\right\}, \tag{E.21}$$

and be invoking Stokes's theorem we end up with

$$= \frac{1}{k_{t;i}'^{\mathrm{I}}k_{t;j}''^{\mathrm{II}}}\int_{S_a^{\mathrm{II}}}\left(\nabla_t\times(\phi_i^{\mathrm{I}}\nabla_t\,\psi_j^{*\mathrm{II}})\right)\cdot\mathbf{a}_z\,d\sigma = \frac{1}{k_{t;i}'^{\mathrm{I}}k_{t;j}''^{\mathrm{II}}}\oint_{\partial S_a^{\mathrm{II}}}\phi_i^{\mathrm{I}}\frac{\partial\psi_j^{*\mathrm{II}}}{\partial\tau}\,dl. \tag{E.22}$$

[1] This cross-section is indicated by S_a^{II} and can refer to S_1^a or S_2^a of Sec.6.4, which indicate the aperture surfaces (cross-sections) on the specific places z_1 and z_2. For now the specific place of the cross-section is of no importance. The main attention to calculate the integrals is the dimension of the waveguide cross-section and not the specific position of the junction.

E.2.3 TE^{I} TM^{II} combination

$$\left\langle \mathbf{h}_i^{\prime\prime\mathrm{I}}, \mathbf{h}_j^{\prime\prime\mathrm{II}} \right\rangle = \left\langle \frac{-1}{k_{t;i}^{\prime\prime\mathrm{I}}} \nabla_t \psi_i^{\mathrm{I}}, \frac{-1}{k_{t;j}^{\prime\prime\mathrm{II}}} \left(\mathbf{a}_z \times \nabla_t \phi_j^{\mathrm{II}} \right) \right\rangle = \frac{1}{k_{t;i}^{\prime\prime\mathrm{I}} k_{t;j}^{\prime\prime\mathrm{II}}} \left\langle \nabla_t \psi_i^{\mathrm{I}}, \left(\mathbf{a}_z \times \nabla_t \phi_j^{\mathrm{II}} \right) \right\rangle \quad \text{(E.23)}$$

By analogy with Sec.E.2.2 with obtain

$$\frac{1}{k_{t;i}^{\prime\prime\mathrm{I}} k_{t;j}^{\prime\prime\mathrm{II}}} \left\langle \nabla_t \psi_i^{\mathrm{I}}, \left(\mathbf{a}_z \times \nabla_t \phi_j^{\mathrm{II}} \right) \right\rangle = \frac{1}{k_{t;i}^{\prime\prime\mathrm{I}} k_{t;j}^{\prime\prime\mathrm{II}}} \oint_{\partial S_a^{\mathrm{II}}} \phi_i^{\mathrm{II}} \frac{\partial \psi_j^{*\mathrm{I}}}{\partial \tau} \, dl = 0. \quad \text{(E.24)}$$

The integral vanishes because the boundary condition $\phi_i^{\mathrm{II}}|_{\partial S_a^{\mathrm{II}}} = 0$ is satisfied. This means that the TE modes in the waveguide with the largest cross-section don't couple with the TM modes in the waveguide with the smaller cross-section.

Knowing this remarkable fact, it is worthwhile to point out to Eq.(E.22) and notice the following. If the case, presently under consideration, was the other way around, meaning that, the cross-section of waveguide section-I would be completely enclosed by the cross-section of waveguide section-II, then the TM modes in the waveguide with the smallest cross-section never couple with the TE modes in the waveguide with the largest cross-section, as consequence of the fact that the boundary condition $\phi_i^{\mathrm{I}}|_{\partial S_a^{\mathrm{I}}} = 0$ would be satisfied. Note that the integration area has become S_a^{I} instead of S_a^{II}. A larger integration surface would be superfluous because ϕ_i^{I} is confined to S_a^{I} and zero otherwise. These same results are obtain by Gentili G.G. [12].

E.2.4 TE^{I} TE^{II} combination

$$\left\langle \mathbf{h}_i^{\prime\prime\mathrm{I}}, \mathbf{h}_j^{\prime\prime\mathrm{II}} \right\rangle = \left\langle \frac{-1}{k_{t;i}^{\prime\prime\mathrm{I}}} \nabla_t \psi_i^{\mathrm{I}}, \frac{-1}{k_{t;j}^{\prime\prime\mathrm{II}}} \nabla_t \psi_j^{\mathrm{II}} \right\rangle = \frac{1}{k_{t;i}^{\prime\prime\mathrm{I}} k_{t;j}^{\prime\prime\mathrm{II}}} \left\langle \nabla_t \psi_i^{\mathrm{I}}, \nabla_t \psi_j^{\mathrm{II}} \right\rangle \quad \text{(E.25)}$$

By analogy with Sec.E.2.1, using Eq.(B.6), $\nabla_t^2 \psi^{*\mathrm{II}} = -k_t^{\prime\prime 2\mathrm{II}} \psi^{*\mathrm{II}}$ and Gauss's theorem we obtain

$$= \frac{1}{k_{t;i}^{\prime\prime\mathrm{I}} k_{t;j}^{\prime\prime\mathrm{II}}} \left\{ \oint_{\partial S_a^{\mathrm{II}}} \psi_i^{\mathrm{I}} \frac{\partial \psi_j^{*\mathrm{II}}}{\partial \nu} \, dl + \int_{S_a^{\mathrm{II}}} \psi_i^{\mathrm{I}} \, k_{t;j}^{\prime\prime 2\mathrm{II}} \, \psi_j^{*\mathrm{II}} \, d\sigma \right\} = \frac{k_{t;j}^{\prime\prime\mathrm{II}}}{k_{t;i}^{\prime\prime\mathrm{I}}} \int_{S_a^{\mathrm{II}}} \psi_i^{\mathrm{I}} \, \psi_j^{*\mathrm{II}} \, d\sigma, \quad \text{(E.26)}$$

with $\frac{\partial \psi_j^{*\mathrm{II}}}{\partial \nu}\big|_{\partial S_a^{\mathrm{II}}} = 0$, the boundary condition satisfied.

E.2.5 Integrals in their final form

With the integrals reduced to a more simple form we will have to give an explicit expression to the scalar functions ϕ and ψ. For waveguide section-I we define

$$\phi^{\mathrm{I}} = \frac{2}{\sqrt{AB}} \sin(k_x^{\mathrm{I}}[x + a_1]) \sin(k_y^{\mathrm{I}}[y + b_1]), \quad \text{(E.27)}$$

$$\psi^{\mathrm{I}} = \sqrt{\frac{\epsilon_n^{\mathrm{I}} \epsilon_m^{\mathrm{I}}}{AB}} \cos(k_x^{\mathrm{I}}[x + a_1]) \cos(k_y^{\mathrm{I}}[y + b_1]). \quad \text{(E.28)}$$

For waveguide section-II we define

$$\phi^{\mathrm{II}} = \frac{2}{\sqrt{CD}} \sin(k_x^{\mathrm{II}}[x-a_2]) \sin(k_y^{\mathrm{II}}[y-b_2]), \tag{E.29}$$

$$\psi^{\mathrm{II}} = \sqrt{\frac{\epsilon_n^{\mathrm{II}}\epsilon_m^{\mathrm{II}}}{CD}} \cos(k_x^{\mathrm{II}}[x-a_2]) \cos(k_y^{\mathrm{II}}[y-b_2]). \tag{E.30}$$

Appendix C and Fig.(E.1) clarify some of the parameters. Eqs.(E.27)-(E.30) substituted into the previously deduced integrals gives rise to

$$\begin{aligned}\left\langle \mathbf{h}_i^{\prime\mathrm{I}}, \mathbf{h}_j^{\prime\mathrm{II}} \right\rangle = \frac{k_{t;nm}^{\prime\mathrm{II}} 4}{k_{t;nm}^{\prime\mathrm{I}}\sqrt{ABCD}} \int_{x_1}^{x_2} \sin(k_x^{\mathrm{II}}[x-a_2]) \sin(k_x^{\mathrm{I}}[x+a_1])dx \\ \int_{y_1}^{y_2} \sin(k_y^{\mathrm{II}}[y-b_2]) \sin(k_y^{\mathrm{I}}[y+b_1])dy,\end{aligned} \tag{E.31}$$

$$\begin{aligned}\left\langle \mathbf{h}_i^{\prime\mathrm{I}}, \mathbf{h}_j^{\prime\prime\mathrm{II}} \right\rangle = \frac{-2\sqrt{\epsilon_n^{\mathrm{II}}\epsilon_m^{\mathrm{II}}}}{k_{t;nm}^{\prime\mathrm{I}} k_{t;nm}^{\prime\prime\mathrm{I\,I}}\sqrt{ABCD}} \Big\{ - k_x^{\mathrm{II}} k_y^{\mathrm{I}} \int_{x_1}^{x_2} \sin(k_x^{\mathrm{II}}[x-a_2]) \sin(k_x^{\mathrm{I}}[x+a_1])dx \\ \int_{y_1}^{y_2} \cos(k_y^{\mathrm{II}}[y-b_2]) \cos(k_y^{\mathrm{I}}[y+b_1])dy \\ + k_x^{\mathrm{I}} k_y^{\mathrm{II}} \int_{x_1}^{x_2} \cos(k_x^{\mathrm{II}}[x-a_2]) \cos(k_x^{\mathrm{I}}[x+a_1])dx \\ \int_{y_1}^{y_2} \sin(k_y^{\mathrm{II}}[y-b_2]) \sin(k_y^{\mathrm{I}}[y+b_1])dy \Big\}.\end{aligned} \tag{E.32}$$

$$\begin{aligned}\left\langle \mathbf{h}_i^{\prime\prime\mathrm{I}}, \mathbf{h}_j^{\prime\prime\mathrm{II}} \right\rangle = \frac{k_{t;nm}^{\prime\prime\mathrm{II}}\sqrt{\epsilon_n^{\mathrm{I}}\epsilon_m^{\mathrm{I}}\epsilon_n^{\mathrm{II}}\epsilon_m^{\mathrm{II}}}}{k_{t;nm}^{\prime\prime\mathrm{I}}\sqrt{ABCD}} \int_{x_1}^{x_2} \cos(k_x^{\mathrm{II}}[x-a_2]) \cos(k_x^{\mathrm{I}}[x+a_1])dx \\ \int_{y_1}^{y_2} \cos(k_y^{\mathrm{II}}[y-b_2]) \cos(k_y^{\mathrm{I}}[y+b_1])dy,\end{aligned} \tag{E.33}$$

For $\left\langle \mathbf{h}_i^{\prime\mathrm{I}}, \mathbf{h}_j^{\prime\prime\mathrm{II}} \right\rangle$, we do not use Eq.(E.22) but the right-hand side of Eq.(E.19). The reason for this is, if one looks at Eqs.(E.31)-(E.33), we see that it all comes down to solving two basic integrals and by properly combining them, the former equations can be constructed. The two remaining integrals are

$$INT_q^1(r,s,t,u,v,w) = \int_r^s \sin(v[q-u]) \sin(w[q+t])dq, \tag{E.34}$$

$$INT_q^2(r,s,t,u,v,w) = \int_r^s \cos(v[q-u]) \cos(w[q+t])dq. \tag{E.35}$$

For the proper combinations of variables, which one can find out by comparing the integrals in Eqs.(E.34) and (E.35) with the integrals in Eqs.(E.31)-(E.33), we obtain

$$\begin{aligned} INT_x^1(x_1,x_2,a_1,a_2,k_x^{\mathrm{II}},k_x^{\mathrm{I}}) &= \int_{x_1}^{x_2} \sin(k_x^{\mathrm{II}}[x-a_2])\sin(k_x^{\mathrm{I}}[x+a_1])dx \\ &= \frac{(x_2-x_1)}{2}[\alpha-\beta], \end{aligned} \tag{E.36}$$

$$INT_y^1(y_1,y_2,b_1,b_2,k_y^{\mathrm{II}},k_y^{\mathrm{I}}) = \frac{(y_2-y_1)}{2}[\xi-\gamma], \tag{E.37}$$

$$\begin{aligned} INT_x^2(x_1,x_2,a_1,a_2,k_x^{\mathrm{II}},k_x^{\mathrm{I}}) &= \int_{x_1}^{x_2} \cos(k_x^{\mathrm{II}}[x-a_2])\cos(k_x^{\mathrm{I}}[x+a_1])dx \\ &= \frac{(x_2-x_1)}{2}[\beta+\alpha], \end{aligned} \tag{E.38}$$

$$INT_y^2(y_1,y_2,b_1,b_2,k_y^{\mathrm{II}},k_y^{\mathrm{I}}) = \frac{(y_2-y_1)}{2}[\gamma+\xi]. \tag{E.39}$$

With

$$\alpha = \cos\left([-k_x^{\mathrm{II}}a_2 - k_x^{\mathrm{I}}a_1] + \frac{[x_2+x_1][k_x^{\mathrm{II}}-k_x^{\mathrm{I}}]}{2}\right) sinc\left(\frac{[x_2-x_1][k_x^{\mathrm{II}}-k_x^{\mathrm{I}}]}{2}\right), \tag{E.40}$$

$$\beta = \cos\left([-k_x^{\mathrm{II}}a_2 + k_x^{\mathrm{I}}a_1] + \frac{[x_2+x_1][k_x^{\mathrm{II}}+k_x^{\mathrm{I}}]}{2}\right) sinc\left(\frac{[x_2-x_1][k_x^{\mathrm{II}}+k_x^{\mathrm{I}}]}{2}\right), \tag{E.41}$$

$$\gamma = \cos\left([-k_y^{\mathrm{II}}b_2 + k_y^{\mathrm{I}}b_1] + \frac{[y_2+y_1][k_y^{\mathrm{II}}+k_y^{\mathrm{I}}]}{2}\right) sinc\left(\frac{[y_2-y_1][k_y^{\mathrm{II}}+k_y^{\mathrm{I}}]}{2}\right), \tag{E.42}$$

$$\xi = \cos\left([-k_y^{\mathrm{II}}b_2 - k_y^{\mathrm{I}}b_1] + \frac{[y_2+y_1][k_y^{\mathrm{II}}-k_y^{\mathrm{I}}]}{2}\right) sinc\left(\frac{[y_2-y_1][k_y^{\mathrm{II}}-k_y^{\mathrm{I}}]}{2}\right). \tag{E.43}$$

This gives us the final form

$$\left\langle \mathbf{h}_i^{\prime\mathrm{I}}, \mathbf{h}_j^{\prime\mathrm{II}} \right\rangle = \frac{k_{t;nm}^{\prime\mathrm{II}}(x_2-x_1)(y_2-y_1)}{k_{t;nm}^{\prime\mathrm{I}}\sqrt{ABCD}}[\alpha-\beta][\xi-\gamma], \tag{E.44}$$

$$\begin{aligned} \left\langle \mathbf{h}_i^{\prime\mathrm{I}}, \mathbf{h}_j^{\prime\prime\mathrm{II}} \right\rangle = \frac{-\sqrt{\epsilon_n^{\mathrm{II}}\epsilon_m^{\mathrm{II}}}(x_2-x_1)(y_2-y_1)}{2k_{t;nm}^{\prime\mathrm{I}}k_{t;nm}^{\prime\prime\mathrm{II}}\sqrt{ABCD}}\big\{&[\beta\xi-\alpha\gamma][k_x^{\mathrm{II}}k_y^{\mathrm{I}}+k_y^{\mathrm{II}}k_x^{\mathrm{I}}] \\ &+[\beta\gamma-\alpha\xi][k_x^{\mathrm{II}}k_y^{\mathrm{I}}-k_y^{\mathrm{II}}k_x^{\mathrm{I}}]\big\}, \end{aligned} \tag{E.45}$$

$$\left\langle \mathbf{h}_i^{\prime\mathrm{I}}, \mathbf{h}_j^{\prime\mathrm{II}} \right\rangle = 0, \tag{E.46}$$

$$\left\langle \mathbf{h}_i^{\prime\mathrm{I}}, \mathbf{h}_j^{\prime\prime\mathrm{II}} \right\rangle = \frac{k_{t;nm}^{\prime\prime\mathrm{II}}\sqrt{\epsilon_n^{\mathrm{I}}\epsilon_m^{\mathrm{I}}\epsilon_n^{\mathrm{II}}\epsilon_m^{\mathrm{II}}}(x_2-x_1)(y_2-y_1)}{4k_{t;nm}^{\prime\mathrm{I}}\sqrt{ABCD}}[\beta+\alpha][\gamma+\xi]. \tag{E.47}$$

E.3 Integrals with $\mathbf{h}^{\alpha;\mathrm{III}}$, $\mathbf{h}^{\alpha;\mathrm{II}}$

With the aid of the following substitutions, the integrals which we derived for the junction between section-I and -II, can be used for the junction between section-III and -II.

$$\begin{aligned} I &\longrightarrow III, \\ a_1 &\longrightarrow e_1, \\ a_2 &\longrightarrow e_2, \\ b_1 &\longrightarrow f_1, \\ b_2 &\longrightarrow f_2, \\ A &\longrightarrow E, \\ B &\longrightarrow F. \end{aligned} \tag{E.48}$$

Appendix F

Closed form integrals for patch

In order to solve the linear system at which we arrived by means of the MoM, the integrals it involves must be solved. The integrals are

$$\Pi_{ri}^{\mathrm{IV}} = \left\langle \mathbf{f}_r, \mathbf{h}_i^{\alpha;\mathrm{IV}} \right\rangle, \tag{F.1}$$

$$\Pi_{is}^{\mathrm{IV}} = \left\langle \mathbf{h}_i^{\alpha;\mathrm{IV}}, \mathbf{w}_s \right\rangle, \tag{F.2}$$

$$\Pi_{rp}^{\mathrm{V}} = \left\langle \mathbf{f}_r, \mathbf{h}_p^{\alpha;\mathrm{V}} \right\rangle, \tag{F.3}$$

$$\Pi_{ps}^{\mathrm{V}} = \left\langle \mathbf{h}_p^{\alpha;\mathrm{V}}, \mathbf{w}_s \right\rangle, \tag{F.4}$$

with $\mathbf{f}_r = \mathbf{w}_s$ stated in Eq.(7.25) and $\mathbf{h}_i^{\alpha}$ for TM modes stated in Eq.(4.64) and for TE modes in Eq.(4.49). Instead of trying to solve these surface integrals we will simplify them to line integrals. If we look closely, we see four resembling integrals. This reduces the number of integrals that need to be evaluated back to two viz., a TM mode weighted with a RWG and a TE mode weighted with a RWG. We will work them out for section-IV. By substitution of IV with V, the integrals for section-V are obtained.

F.1 Simplification of a TM-mode coupled to at RWG-function

$$\begin{aligned}\left\langle \mathbf{h}_i^{\prime\mathrm{IV}}, \mathbf{g}_n \right\rangle &= \left\langle \frac{-1}{k_{t;i}^{\prime\mathrm{IV}}} (\mathbf{a}_z \times \nabla_t \phi_i^{\mathrm{IV}}), \mathbf{g}_n \right\rangle = \frac{-1}{k_{t;i}^{\prime\mathrm{IV}}} \int_{S_{RWG}} (\mathbf{a}_z \times \nabla_t \phi_i^{\mathrm{IV}}) \cdot \mathbf{g}_n \, d\sigma \\ &= -\frac{1}{k_{t;i}^{\prime\mathrm{IV}}} \int_{T_n^+} (\mathbf{a}_z \times \nabla_t \phi_i^{\mathrm{IV}}) \cdot \mathbf{g}_n \, d\sigma - \frac{1}{k_{t;i}^{\prime\mathrm{IV}}} \int_{T_n^-} (\mathbf{a}_z \times \nabla_t \phi_i^{\mathrm{IV}}) \cdot \mathbf{g}_n \, d\sigma.\end{aligned} \tag{F.5}$$

The integrands in the last right-hand side term of above's expression can be handled by applying the vector identities in Eq.(3.29) and (E.20). We note that, in the vector identity of Eq.(E.20), we have made use of the fact that $\nabla_t \times \mathbf{A} = \nabla_t \times \mathbf{g}_n = \mathbf{0}$. Subsequently we

apply Stokes's theorem on the term, of the vector identity in Eq.(E.20), that is leftover, to end up with

$$\left\langle \mathbf{h}_i^{\prime \mathrm{IV}}, \mathbf{g}_n \right\rangle = -\frac{1}{k_{t;i}^{\prime \mathrm{IV}}} \oint_{\partial T_n^+} \phi_i^{\mathrm{IV}}\, \mathbf{g}_n \cdot \boldsymbol{\tau}\, dl - \frac{1}{k_{t;i}^{\prime \mathrm{IV}}} \oint_{\partial T_n^-} \phi_i^{\mathrm{IV}}\, \mathbf{g}_n \cdot \boldsymbol{\tau}\, dl. \tag{F.6}$$

F.2 Simplification of a TE-mode coupled to a RWG-function

$$\left\langle \mathbf{h}_i^{\prime\prime \mathrm{IV}}, \mathbf{g}_n \right\rangle = \left\langle \frac{-1}{k_{t;i}^{\prime\prime \mathrm{IV}}} \nabla_t \psi_i^{\mathrm{IV}}, \mathbf{g}_n \right\rangle = -\frac{1}{k_{t;i}^{\prime\prime \mathrm{IV}}} \int_{T_n^+} \nabla_t \psi_i^{\mathrm{IV}} \cdot \mathbf{g}_n d\sigma - \frac{1}{k_{t;i}^{\prime\prime \mathrm{IV}}} \int_{T_n^-} \nabla_t \psi_i^{\mathrm{IV}} \cdot \mathbf{g}_n d\sigma. \tag{F.7}$$

Again, the integrants are restated, but now with help of the vector identity

$$\nabla_t \cdot (v\mathbf{A}) = v\, \nabla_t \cdot \mathbf{A} + \mathbf{A} \cdot \nabla_t v. \tag{F.8}$$

Then, by investigating the vector identity we notice that, by applying Gauss' theorem for 2-dimensions and the divergence of the RWG basis function, we obtain

$$\begin{aligned} \left\langle \mathbf{h}_i^{\prime\prime \mathrm{IV}}, \mathbf{g}_n \right\rangle = &-\frac{1}{k_{t;i}^{\prime\prime \mathrm{IV}}} \oint_{\partial T_n^+} \psi_i^{\mathrm{IV}}\, \mathbf{g}_n \cdot \boldsymbol{\nu}\, dl + \frac{l_n}{k_{t;i}^{\prime\prime \mathrm{IV}} A_n^+} \int_{T_n^+} \psi_i^{\mathrm{IV}}\, d\sigma \\ &-\frac{1}{k_{t;i}^{\prime\prime \mathrm{IV}}} \oint_{\partial T_n^-} \psi_i^{\mathrm{IV}}\, \mathbf{g}_n \cdot \boldsymbol{\nu}\, dl + \frac{l_n}{k_{t;i}^{\prime\prime \mathrm{IV}} A_n^-} \int_{T_n^-} \psi_i^{\mathrm{IV}}\, d\sigma. \end{aligned} \tag{F.9}$$

Two surface integrals are still left. From Sec.4.3.1, Eq.(4.47), we remember that $(\nabla_t^2 + k_{t;i}^{\prime\prime 2})\psi_i = 0$ from which $\psi_i = \frac{-1}{k_{t;i}^{\prime\prime 2}} \nabla_t \cdot \nabla_t \psi_i$ follows. Substituting this last result into the surface integrals and again invoking Gauss' 2-dimensions theorem yields

$$\begin{aligned} \left\langle \mathbf{h}_i^{\prime\prime \mathrm{IV}}, \mathbf{g}_n \right\rangle = &-\frac{1}{k_{t;i}^{\prime\prime \mathrm{IV}}} \oint_{\partial T_n^+} \psi_i^{\mathrm{IV}}\, \mathbf{g}_n \cdot \boldsymbol{\nu}\, dl - \frac{l_n}{k_{t;i}^{\prime\prime \mathrm{IV}^3} A_n^+} \oint_{\partial T_n^+} \frac{\partial \psi_i^{\mathrm{IV}}}{\partial \nu}\, dl \\ &-\frac{1}{k_{t;i}^{\prime\prime \mathrm{IV}}} \oint_{\partial T_n^-} \psi_i^{\mathrm{IV}}\, \mathbf{g}_n \cdot \boldsymbol{\nu}\, dl - \frac{l_n}{k_{t;i}^{\prime\prime \mathrm{IV}^3} A_n^-} \oint_{\partial T_n^-} \frac{\partial \psi_i^{\mathrm{IV}}}{\partial \nu}\, dl. \end{aligned} \tag{F.10}$$

During the discussion in Sec.7.3.1 on the RWG basis function we have seen that the basis function has no component normal to the boundary of the surface, in the plane the two triangles form. The boundary is formed by the outer contour of two adjacent triangles (excluding the common edge). However, a component normal to the common edge exists. These facts reduce the closed contour integrals, which consists of inner-products of basis functions with boundary normal vectors, to single line integrals over the common edge, as

follows

$$\begin{aligned}\left\langle \mathbf{h}_i^{''\mathrm{IV}}, \mathbf{g}_n \right\rangle = &-\frac{1}{k_{t;i}^{''\mathrm{IV}}} \int\limits_{\text{common edge}^+} \psi_i^{\mathrm{IV}}\, \mathbf{g}_n \cdot \boldsymbol{\nu}\, dl - \frac{l_n}{k_{t;i}^{''\mathrm{IV}\,3} A_n^+} \oint_{\partial T_n^+} \frac{\partial \psi_i^{\mathrm{IV}}}{\partial \nu}\, dl \\ &-\frac{1}{k_{t;i}^{''\mathrm{IV}}} \int\limits_{\text{common edge}^-} \psi_i^{\mathrm{IV}}\, \mathbf{g}_n \cdot \boldsymbol{\nu}\, dl - \frac{l_n}{k_{t;i}^{''\mathrm{IV}\,3} A_n^-} \oint_{\partial T_n^-} \frac{\partial \psi_i^{\mathrm{IV}}}{\partial \nu}\, dl.\end{aligned} \tag{F.11}$$

F.3 Integral of a TM-mode with a RWG-function, final form

For the calculation of line integrals we find [1]

$$\int_K (\mathbf{v}, \mathbf{t}) ds, \quad \mathbf{t} = \frac{\dot{\mathbf{x}}}{|\dot{\mathbf{x}}|}, \quad ds = |\dot{\mathbf{x}}|\, dt, \quad K = \{\mathbf{x}(t) |\, a \leq t \leq b\}, \tag{F.12}$$

yielding

$$\int_a^b (\mathbf{v}(\mathbf{x}(t)), \dot{\mathbf{x}}(t))\, dt. \tag{F.13}$$

F.3.1 Integral over T_n^+

In Eq.(F.6) we see that we need to calculate a closed contour integral over the triangles T_n^+ and T_n^-. We will start with T_n^+.

The integral over the piecewise continuous contour ∂T_n^+ is split up in three sub-integrals over the three straight lines, for convenience, $\partial T_n^+ = l_{R^+ \to S^+} \cup l_{S^+ \to V^+} \cup l_{V^+ \to R^+}$. Fig.F.1 clarifies this notation. By adding the results of the sub-integrals, the total contribution is

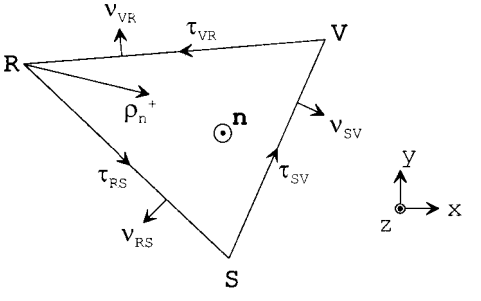

Figure F.1: *This is T_n^+, the basis function is departing from the free vertex (R). Visible are also the normal- and tangential-vectors of each line section.*

found. Recognising that $\mathbf{v} = \phi_i \, \mathbf{g}_n$ and $\mathbf{t} = \boldsymbol{\tau}$ we give the following parameter representation

$$\begin{aligned} R^+ \rightarrow S^+ : \mathbf{x}(t) &= \mathbf{x}_R + \frac{1}{2}(\mathbf{x}_S - \mathbf{x}_R) + \frac{t}{2}(\mathbf{x}_S - \mathbf{x}_R) \qquad t = [-1, 1] \\ &= \left(\frac{1}{2}[x_R + x_S] + \frac{t}{2}[x_S - x_R], \frac{1}{2}[y_R + y_S] + \frac{t}{2}[y_S - y_R] \right), \end{aligned} \tag{F.14}$$

$$\dot{\mathbf{x}}(t) = \left(\frac{1}{2}[x_S - x_R], \frac{1}{2}[y_S - y_R] \right), \tag{F.15}$$

$$\begin{aligned} \boldsymbol{\rho}_n^+(\mathbf{x}(t)) &= (\mathbf{r}(\mathbf{x}(t)) - \mathbf{r}_R) \\ &= \left(\frac{1}{2}[x_S - x_R][1 + t], \frac{1}{2}[y_S - y_R][1 + t] \right), \end{aligned} \tag{F.16}$$

$$\begin{aligned} \phi_i^{\mathrm{IV}}(\mathbf{x}(t)) = \frac{2}{\sqrt{GH}} &\sin \left\{ k_x^{\mathrm{IV}} \left(\frac{1}{2}[x_R + x_S] - q \right) + k_x^{\mathrm{IV}} \frac{t}{2}[x_S - x_R] \right\} \\ &\sin \left\{ k_y^{\mathrm{IV}} \left(\frac{1}{2}[y_R + y_S] - r \right) + k_y^{\mathrm{IV}} \frac{t}{2}[y_S - y_R] \right\}, \end{aligned} \tag{F.17}$$

$$\begin{aligned} S^+ \rightarrow V^+ : \mathbf{x}(t) &= \mathbf{x}_S + \frac{1}{2}(\mathbf{x}_V - \mathbf{x}_S) + \frac{t}{2}(\mathbf{x}_V - \mathbf{x}_S) \qquad t = [-1, 1] \\ &= \left(\frac{1}{2}[x_S + x_V] + \frac{t}{2}[x_V - x_S], \frac{1}{2}[y_S + y_V] + \frac{t}{2}[y_V - y_S] \right), \end{aligned} \tag{F.18}$$

$$\dot{\mathbf{x}}(t) = \left(\frac{1}{2}[x_V - x_S], \frac{1}{2}[y_V - y_S] \right), \tag{F.19}$$

$$\boldsymbol{\rho}_n^+(\mathbf{x}(t)) = \left(\frac{1}{2}[x_S + x_V] + \frac{t}{2}[x_V - x_S] - x_R, \frac{1}{2}[y_S + y_V] + \frac{t}{2}[y_V - y_S] - y_R \right), \tag{F.20}$$

$$\begin{aligned} \phi_i^{\mathrm{IV}}(\mathbf{x}(t)) = \frac{2}{\sqrt{GH}} &\sin \left\{ k_x^{\mathrm{IV}} \left(\frac{1}{2}[x_S + x_V] - q \right) + k_x^{\mathrm{IV}} \frac{t}{2}[x_V - x_S] \right\} \\ &\sin \left\{ k_y^{\mathrm{IV}} \left(\frac{1}{2}[y_S + y_V] - r \right) + k_y^{\mathrm{IV}} \frac{t}{2}[y_V - y_S] \right\}, \end{aligned} \tag{F.21}$$

$$\begin{aligned} V^+ \rightarrow R^+ : \mathbf{x}(t) &= \mathbf{x}_V + \frac{1}{2}(\mathbf{x}_R - \mathbf{x}_V) + \frac{t}{2}(\mathbf{x}_R - \mathbf{x}_V) \qquad t = [-1, 1] \\ &= \left(\frac{1}{2}[x_V + x_R] + \frac{t}{2}[x_R - x_V], \frac{1}{2}[y_V + y_R] + \frac{t}{2}[y_R - y_V] \right), \end{aligned} \tag{F.22}$$

$$\dot{\mathbf{x}}(t) = \left(\frac{1}{2}[x_R - x_V], \frac{1}{2}[y_R - y_V] \right), \tag{F.23}$$

$$\boldsymbol{\rho}_n^+(\mathbf{x}(t)) = \left(\frac{1}{2}[x_R - x_V][-1 + t], \frac{1}{2}[y_R - y_V][-1 + t] \right), \tag{F.24}$$

$$\phi_i^{\mathrm{IV}}(\mathbf{x}(t)) = \frac{2}{\sqrt{GH}} \sin\left\{k_x^{\mathrm{IV}}\left(\frac{1}{2}[x_V + x_R] - q\right) + k_x^{\mathrm{IV}}\frac{t}{2}[x_R - x_V]\right\} \sin\left\{k_y^{\mathrm{IV}}\left(\frac{1}{2}[y_V + y_R] - r\right) + k_y^{\mathrm{IV}}\frac{t}{2}[y_R - y_V]\right\}, \tag{F.25}$$

The "+" superscript at the vertex indices is just an indication that we're dealing with T_n^+. With these parameter representations, the following integral must be calculated, which is the first contour integral of Eq.(F.6). Note that, the normalization constant, $\frac{l_n}{2A_n^+}$, is left out.

$$\begin{aligned}\oint_{\partial T_n^+} \phi_i^{\mathrm{IV}}\, \boldsymbol{\rho}_n^+ \cdot \boldsymbol{\tau}\, dl = &\int_{l_{R^+\to S^+}} \phi_i^{\mathrm{IV}}(\mathbf{x}(t))\boldsymbol{\rho}_n^+(\mathbf{x}(t)) \cdot \dot{\mathbf{x}}(t)dt \\ &+ \int_{l_{S^+\to V^+}} \phi_i^{\mathrm{IV}}(\mathbf{x}(t))\boldsymbol{\rho}_n^+(\mathbf{x}(t)) \cdot \dot{\mathbf{x}}(t)dt \\ &+ \int_{l_{V^+\to R^+}} \phi_i^{\mathrm{IV}}(\mathbf{x}(t))\boldsymbol{\rho}_n^+(\mathbf{x}(t)) \cdot \dot{\mathbf{x}}(t)dt.\end{aligned} \tag{F.26}$$

With the integrals and variables stated in Sec.F.3.3, the integral in Eq.(F.26) can be written as

$$\begin{aligned}\oint_{\partial T_n^+} \phi_i^{\mathrm{IV}}\, \boldsymbol{\rho}_n^+ \cdot \boldsymbol{\tau}\, dl = &\frac{\sigma}{\sqrt{GH}}\left(I_1 - I_2 + I_3 - I_4\right)\Big|_{R^+\to S^+} \\ &+ \left[\frac{\sigma}{\sqrt{GH}}\left(I_1 - I_2\right) + \frac{\chi}{\sqrt{GH}}\left(I_3 - I_4\right)\right]\Big|_{S^+\to V^+} \\ &+ \frac{\sigma}{\sqrt{GH}}\left(-I_1 + I_2 + I_3 - I_4\right)\Big|_{V^+\to R^+}.\end{aligned} \tag{F.27}$$

F.3.2 Integral over T_n^-

Now, it is the turn for the integral over T_n^-. Here, we also split up the contour in three pieces, $\partial T_n^- = l_{U^-\to S^-} \cup l_{S^-\to V^-} \cup l_{V^-\to U^-}$. In Fig.F.2 the T_n^- is depicted with corresponding normal- and tangential-vectors. The parameter representation for the triangle under

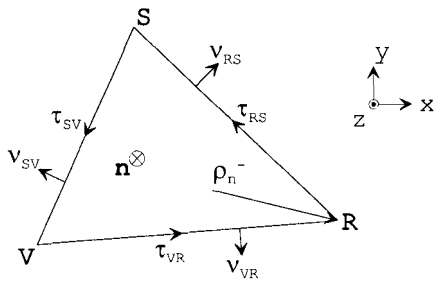

Figure F.2: *This is the T_n^-, the basis function is arriving in the free vertex (U).*

consideration is

$$\begin{aligned} U^- \to S^- : \mathbf{x}(t) &= \mathbf{x}_U + \frac{1}{2}(\mathbf{x}_S - \mathbf{x}_U) + \frac{t}{2}(\mathbf{x}_S - \mathbf{x}_U) \qquad t = [-1, 1] \\ &= \left(\frac{1}{2}[x_U + x_S] + \frac{t}{2}[x_S - x_U], \frac{1}{2}[y_U + y_S] + \frac{t}{2}[y_S - y_U]\right), \end{aligned} \tag{F.28}$$

$$\dot{\mathbf{x}}(t) = \left(\frac{1}{2}[x_S - x_U], \frac{1}{2}[y_S - y_U]\right), \tag{F.29}$$

$$\begin{aligned} \boldsymbol{\rho}_n^+(\mathbf{x}(t)) &= (\mathbf{r}_U - \mathbf{r}(\mathbf{x}(t))) \\ &= \left(\frac{-1}{2}[x_S - x_U][1 + t], \frac{-1}{2}[y_S - y_U][1 + t]\right), \end{aligned} \tag{F.30}$$

$$\begin{aligned} \phi_i^{\mathrm{IV}}(\mathbf{x}(t)) = \frac{2}{\sqrt{GH}} &\sin\left\{k_x^{\mathrm{IV}}\left(\frac{1}{2}[x_U + x_S] - q\right) + k_x^{\mathrm{IV}}\frac{t}{2}[x_S - x_U]\right\} \\ &\sin\left\{k_y^{\mathrm{IV}}\left(\frac{1}{2}[y_U + y_S] - r\right) + k_y^{\mathrm{IV}}\frac{t}{2}[y_S - y_U]\right\}, \end{aligned} \tag{F.31}$$

$$\begin{aligned} S^- \to V^- : \mathbf{x}(t) &= \mathbf{x}_S + \frac{1}{2}(\mathbf{x}_V - \mathbf{x}_S) + \frac{t}{2}(\mathbf{x}_V - \mathbf{x}_S) \qquad t = [-1, 1] \\ &= \left(\frac{1}{2}[x_S + x_V] + \frac{t}{2}[x_V - x_S], \frac{1}{2}[y_S + y_V] + \frac{t}{2}[y_V - y_S]\right), \end{aligned} \tag{F.32}$$

$$\dot{\mathbf{x}}(t) = \left(\frac{1}{2}[x_V - x_S], \frac{1}{2}[y_V - y_S]\right), \tag{F.33}$$

$$\boldsymbol{\rho}_n^+(\mathbf{x}(t)) = \left(x_U - \frac{1}{2}[x_S + x_V] - \frac{t}{2}[x_V - x_S], y_U - \frac{1}{2}[y_S + y_V] - \frac{t}{2}[y_V - y_S]\right), \tag{F.34}$$

$$\begin{aligned} \phi_i^{\mathrm{IV}}(\mathbf{x}(t)) = \frac{2}{\sqrt{GH}} &\sin\left\{k_x^{\mathrm{IV}}\left(\frac{1}{2}[x_S + x_V] - q\right) + k_x^{\mathrm{IV}}\frac{t}{2}[x_V - x_S]\right\} \\ &\sin\left\{k_y^{\mathrm{IV}}\left(\frac{1}{2}[y_S + y_V] - r\right) + k_y^{\mathrm{IV}}\frac{t}{2}[y_V - y_S]\right\}, \end{aligned} \tag{F.35}$$

$$
\begin{aligned}
V^- \to U^- : \mathbf{x}(t) &= \mathbf{x}_V + \frac{1}{2}(\mathbf{x}_U - \mathbf{x}_V) + \frac{t}{2}(\mathbf{x}_U - \mathbf{x}_V) \qquad t = [-1, 1] \\
&= \left(\frac{1}{2}[x_V + x_U] + \frac{t}{2}[x_U - x_V], \frac{1}{2}[y_V + y_U] + \frac{t}{2}[y_U - y_V]\right), \qquad \text{(F.36)} \\
\dot{\mathbf{x}}(t) &= \left(\frac{1}{2}[x_U - x_V], \frac{1}{2}[y_U - y_V]\right), \qquad \text{(F.37)} \\
\boldsymbol{\rho}_n^+(\mathbf{x}(t)) &= \left(\frac{1}{2}[x_U - x_V][1-t], \frac{1}{2}[y_U - y_V][1-t]\right), \qquad \text{(F.38)} \\
\phi_i^{\mathrm{IV}}(\mathbf{x}(t)) &= \frac{2}{\sqrt{GH}} \sin\left\{k_x^{\mathrm{IV}}\left(\frac{1}{2}[x_V + x_U] - q\right) + k_x^{\mathrm{IV}}\frac{t}{2}[x_U - x_V]\right\} \\
&\quad \sin\left\{k_y^{\mathrm{IV}}\left(\frac{1}{2}[y_V + y_U] - r\right) + k_y^{\mathrm{IV}}\frac{t}{2}[y_U - y_V]\right\}, \qquad \text{(F.39)}
\end{aligned}
$$

The "-" superscript at the vertex indices is just an indication that we're dealing with T_n^-. The parameter representations are used to solve the following integral, which is the second contour integral of Eq.(F.6). Note that, the normalization constant, $\frac{l_n}{2A_n^-}$, is left out.

$$
\begin{aligned}
\oint_{\partial T_n^-} \phi_i^{\mathrm{IV}}\, \boldsymbol{\rho}_n^- \cdot \boldsymbol{\tau}\, dl = &\int_{l_{U^- \to S^-}} \phi_i^{\mathrm{IV}}(\mathbf{x}(t))\boldsymbol{\rho}_n^-(\mathbf{x}(t)) \cdot \dot{\mathbf{x}}(t) dt \\
&+ \int_{l_{S^- \to V^-}} \phi_i^{\mathrm{IV}}(\mathbf{x}(t))\boldsymbol{\rho}_n^-(\mathbf{x}(t)) \cdot \dot{\mathbf{x}}(t) dt \qquad \text{(F.40)} \\
&+ \int_{l_{V^- \to U^-}} \phi_i^{\mathrm{IV}}(\mathbf{x}(t))\boldsymbol{\rho}_n^-(\mathbf{x}(t)) \cdot \dot{\mathbf{x}}(t) dt.
\end{aligned}
$$

With help of the definitions in Sec.F.3.3, Eq.(F.40) is rewritten as

$$
\begin{aligned}
\oint_{\partial T_n^-} \phi_i^{\mathrm{IV}}\, \boldsymbol{\rho}_n^- \cdot \boldsymbol{\tau}\, dl = &\frac{\sigma}{\sqrt{GH}}\left(I_1 - I_2 + I_3 - I_4\right)\Big|_{U^- \to S^-} \\
&+ \left[\frac{\sigma}{\sqrt{GH}}\left(I_1 - I_2\right) + \frac{\chi}{\sqrt{GH}}\left(I_3 - I_4\right)\right]\Big|_{S^- \to V^-} \qquad \text{(F.41)} \\
&+ \frac{\sigma}{\sqrt{GH}}\left(I_1 - I_2 - I_3 + I_4\right)\Big|_{V^- \to U^-}.
\end{aligned}
$$

With the Eqs.(F.27) and (F.41,) the closed form of Eq.(F.6) can be found, according to

$$\left\langle \mathbf{h}_i^{'\mathrm{IV}}, \mathbf{g}_n \right\rangle = -\frac{l_n}{2k'_{t;i}} \left\{ \frac{1}{A_n^+} \left[\frac{\sigma}{\sqrt{GH}} (I_1 - I_2 + I_3 - I_4) \Big|_{R^+ \to S^+} + \frac{\sigma}{\sqrt{GH}} (I_1 - I_2) \Big|_{S^+ \to V^+} \right.\right.$$
$$\left. + \frac{\chi}{\sqrt{GH}} (I_3 - I_4) \Big|_{S^+ \to V^+} + \frac{\sigma}{\sqrt{GH}} (-I_1 + I_2 + I_3 - I_4) \Big|_{V^+ \to R^+} \right]$$
$$- \frac{1}{A_n^-} \left[\frac{\sigma}{\sqrt{GH}} (I_1 - I_2 + I_3 - I_4) \Big|_{U^- \to S^-} + \frac{\sigma}{\sqrt{GH}} (I_1 - I_2) \Big|_{S^- \to V^-} \right.$$
$$\left.\left. + \frac{\chi}{\sqrt{GH}} (I_3 - I_4) \Big|_{S^- \to V^-} + \frac{\sigma}{\sqrt{GH}} (I_1 - I_2 - I_3 + I_4) \Big|_{V^- \to U^-} \right] \right\}. \tag{F.42}$$

Note that the contribution of T_n^- is subtracted form the contribution of T_n^+ instead of added. This is the result of the fact that T_n^+ is oriented counterclockwise and the T_n^- is oriented clockwise.

F.3.3 Defined integral variables

In Eqs.(F.27), (F.41) and (F.42) we introduced some variables, defined as follows.

$$I_1 = \int_a^b \cos[(\alpha - \zeta) + t(\beta - \xi)] dt = \cos\left[(\alpha - \zeta) + \frac{(\beta - \xi)(b + a)}{2}\right] \operatorname{sinc}\left[\frac{(\beta - \xi)(b - a)}{2}\right] (b - a), \tag{F.43}$$

$$I_2 = \int_a^b \cos[(\alpha + \zeta) + t(\beta + \xi)] dt = \cos\left[(\alpha + \zeta) + \frac{(\beta + \xi)(b + a)}{2}\right] \operatorname{sinc}\left[\frac{(\beta + \xi)(b - a)}{2}\right] (b - a), \tag{F.44}$$

$$I_3 = \int_a^b \cos[(\alpha - \zeta) + t(\beta - \xi)] t \, dt =$$
$$= \frac{1}{\beta - \xi} \{ b \sin[(\alpha - \zeta) + b(\beta - \xi)] - a \sin[(\alpha - \zeta) + a(\beta - \xi)] \}$$
$$+ \frac{1}{(\beta - \xi)^2} \{ \cos[(\alpha - \zeta) + b(\beta - \xi)] - \cos[(\alpha - \zeta) + a(\beta - \xi)] \} \, |_{|\beta - \xi| > \kappa}, \tag{F.45}$$

$$I_4 = \int_a^b \cos[(\alpha + \zeta) + t(\beta + \xi)] t \, dt$$
$$= \frac{1}{\beta + \xi} \{ b \sin[(\alpha + \zeta) + b(\beta + \xi)] - a \sin[(\alpha + \zeta) + a(\beta + \xi)] \}$$
$$+ \frac{1}{(\beta + \xi)^2} \{ \cos[(\alpha + \zeta) + b(\beta + \xi)] - \cos[(\alpha + \zeta) + a(\beta + \xi)] \} \, |_{|\beta + \xi| > \kappa},$$

(F.46)

$$
\begin{aligned}
R^+ \to S^+ : \alpha &= k_x^{\mathrm{IV}} \left[\frac{1}{2}(x_R + x_S) - q \right], \\
\zeta &= k_y^{\mathrm{IV}} \left[\frac{1}{2}(y_R + y_S) - r \right], \\
\sigma &= \frac{1}{4}(x_S - x_R)^2 + \frac{1}{4}(y_S - y_R)^2,
\end{aligned}
\qquad
\begin{aligned}
\beta &= k_x^{\mathrm{IV}} \frac{1}{2}(x_S - x_R), \\
\xi &= k_y^{\mathrm{IV}} \frac{1}{2}(y_S - y_R),
\end{aligned}
\tag{F.47}
$$

$$
\begin{aligned}
S^+ \to V^+ : \alpha &= k_x^{\mathrm{IV}} \left[\frac{1}{2}(x_S + x_V) - q \right], \\
\zeta &= k_y^{\mathrm{IV}} \left[\frac{1}{2}(y_V + y_S) - r \right], \\
\sigma &= \frac{1}{4}(x_V^2 - x_S^2) - \frac{x_R}{2}(x_V - x_S) \\
&\quad + \frac{1}{4}(y_V^2 - y_S^2) - \frac{y_R}{2}(y_V - y_S),
\end{aligned}
\qquad
\begin{aligned}
\beta &= k_x^{\mathrm{IV}} \frac{1}{2}(x_V - x_S), \\
\xi &= k_y^{\mathrm{IV}} \frac{1}{2}(y_V - y_S), \\
\chi &= \frac{1}{4}(x_V - x_S)^2 + \frac{1}{4}(y_V - y_S)^2,
\end{aligned}
\tag{F.48}
$$

$$
\begin{aligned}
V^+ \to R^+ : \alpha &= k_x^{\mathrm{IV}} \left[\frac{1}{2}(x_V + x_R) - q \right], \\
\zeta &= k_y^{\mathrm{IV}} \left[\frac{1}{2}(y_V + y_R) - r \right], \\
\sigma &= \frac{1}{4}(x_R - x_V)^2 + \frac{1}{4}(y_R - y_V)^2,
\end{aligned}
\qquad
\begin{aligned}
\beta &= k_x^{\mathrm{IV}} \frac{1}{2}(x_R - x_V), \\
\xi &= k_y^{\mathrm{IV}} \frac{1}{2}(y_R - y_V),
\end{aligned}
\tag{F.49}
$$

$$
\begin{aligned}
U^- \to S^- : \alpha &= k_x^{\mathrm{IV}} \left[\frac{1}{2}(x_U + x_S) - q \right], \\
\zeta &= k_y^{\mathrm{IV}} \left[\frac{1}{2}(y_U + y_S) - r \right], \\
\sigma &= \frac{-1}{4}(x_S - x_U)^2 - \frac{1}{4}(y_S - y_U)^2,
\end{aligned}
\qquad
\begin{aligned}
\beta &= k_x^{\mathrm{IV}} \frac{1}{2}(x_S - x_U), \\
\xi &= k_y^{\mathrm{IV}} \frac{1}{2}(y_S - y_U),
\end{aligned}
\tag{F.50}
$$

$$
\begin{aligned}
S^- \to V^- : \alpha &= k_x^{\mathrm{IV}} \left[\frac{1}{2}(x_S + x_V) - q \right], \\
\zeta &= k_y^{\mathrm{IV}} \left[\frac{1}{2}(y_S + y_V) - r \right], \\
\sigma &= \frac{x_U}{2}(x_V - x_S) - \frac{1}{4}(x_V^2 - x_S^2) \\
&\quad + \frac{y_U}{2}(y_V - y_S) - \frac{1}{4}(y_V^2 - y_S^2),
\end{aligned}
\qquad
\begin{aligned}
\beta &= k_x^{\mathrm{IV}} \frac{1}{2}(x_V - x_S), \\
\xi &= k_y^{\mathrm{IV}} \frac{1}{2}(y_V - y_S), \\
\chi &= \frac{-1}{4}(x_V - x_S)^2 - \frac{1}{4}(y_V - y_S)^2,
\end{aligned}
\tag{F.51}
$$

$$
\begin{aligned}
V^- \to U^- : \alpha &= k_x^{\mathrm{IV}} \left[\frac{1}{2}(x_V + x_U) - q\right], & \beta &= k_x^{\mathrm{IV}} \frac{1}{2}(x_U - x_V), \\
\zeta &= k_y^{\mathrm{IV}} \left[\frac{1}{2}(y_V + y_U) - r\right], & \xi &= k_y^{\mathrm{IV}} \frac{1}{2}(y_U - y_V), \\
\sigma &= \frac{1}{4}(x_U - x_V)^2 + \frac{1}{4}(y_U - y_V)^2,
\end{aligned}
\tag{F.52}
$$

F.3.4 Removable singularities

There is a possibility that equations (F.45) and (F.46) become singular. Therefore, we enforced the restrictions $|\beta - \xi| > \kappa$ and $|\beta + \xi| > \kappa$, with $\kappa > 0$. These singularities can be dealt with by an n-th order approximation of the integral, as follows. With a 3-rd order approximation for Eq.(F.45) we obtain

$$
\begin{aligned}
I_3 \big|_{|\beta-\xi|<\kappa} \approx \Bigg[\frac{1}{2}(b^2 - a^2)\cos(\alpha - \zeta) - \frac{(\beta - \xi)}{3}(b^3 - a^3)\sin(\alpha - \zeta) - \frac{(\beta - \xi)^2}{8}(b^4 - a^4) \\
\cos(\alpha - \zeta) + \frac{(\beta - \xi)^3}{120}(b^5 - a^5)\sin(\alpha - \zeta)\Bigg]_{|\beta-\xi|<\kappa},
\end{aligned}
\tag{F.53}
$$

and for Eq.(F.46)

$$
\begin{aligned}
I_4 \big|_{|\beta+\xi|<\kappa} \approx \Bigg[\frac{1}{2}(b^2 - a^2)\cos(\alpha + \zeta) - \frac{(\beta + \xi)}{3}(b^3 - a^3)\sin(\alpha + \zeta) - \frac{(\beta + \xi)^2}{8}(b^4 - a^4) \\
\cos(\alpha + \zeta) + \frac{(\beta + \xi)^3}{120}(b^5 - a^5)\sin(\alpha + \zeta)\Bigg]_{|\beta+\xi|<\kappa},
\end{aligned}
\tag{F.54}
$$

we use $\kappa = 10^{-6}$. Since $a = -1$ and $b = 1$, all the terms with even powers for a and b vanish, reducing Eqs.(F.53) and (F.54) to

$$
I_3 \approx -\frac{(\beta - \xi)}{3}(b^3 - a^3)\sin(\alpha - \zeta) + \frac{(\beta - \xi)^3}{120}(b^5 - a^5)\sin(\alpha - \zeta)|_{|\beta-\xi|<\kappa}, \tag{F.55}
$$

$$
I_4 \approx -\frac{(\beta + \xi)}{3}(b^3 - a^3)\sin(\alpha + \zeta) + \frac{(\beta + \xi)^3}{120}(b^5 - a^5)\sin(\alpha + \zeta)|_{|\beta+\xi|<\kappa}, \tag{F.56}
$$

F.4 Integral of a TE-mode with a RWG-function, final form

The definitions stated in Eq.(F.12) and (F.13) are also applicable in this case. Firstly we'll discuss the integrals concerning triangle T_n^+ and then the ones concerning triangle T_n^-.

F.4.1 Integral over T_n^+

With respect to T_n^+, both the integrals possess inner-products with a boundary normal vector ($\boldsymbol{\nu}$). According to the definition of a line integral we need an inner-product with a tangential vector ($\boldsymbol{\tau}$). Hence, we will use the following substitution $\boldsymbol{\nu} = \boldsymbol{\tau} \times \mathbf{n}$, where $\mathbf{n}$ is the surface normal of T_n^+ which on its turn is determined by the orientation of the tangent at the boundary of T_n^+ surface. This substitution results in the following integrands, with respect to T_n^+,

$$\frac{\partial \psi_i}{\partial \nu} = (\nabla_t \psi_i) \cdot \boldsymbol{\nu} = (\mathbf{a}_z \times \nabla_t \psi_i) \cdot \boldsymbol{\tau}, \tag{F.57}$$

$$\psi_i \, \boldsymbol{\rho}_n^+ \cdot \boldsymbol{\nu} = \psi_i \, (\mathbf{a}_z \times \boldsymbol{\rho}_n^+) \cdot \boldsymbol{\tau}. \tag{F.58}$$

The surface normal vector ($\mathbf{n}$) is equal to the z-directed unit vector, see Fig.F.1.

Again, the contour integral is split up into three parts, as in the preceding case, $\partial T_n^+ = l_{R^+ \to S^+} \cup l_{S^+ \to V^+} \cup l_{V^+ \to R^+}$. The required parameter representations are equal to those in Sec.F.3.1 except for ϕ. This one is to be replaced with a parameter representation for ψ. So therefore, we'll give the parameter representation for ψ and for the rest refer to Sec.F.3.1.

$R^+ \to S^+$: Eq.(F.14), Eq.(F.15), Eq.(F.16),

$$\psi_i^{\mathrm{IV}}(\mathbf{x}(t)) = \frac{\sqrt{\epsilon_n \epsilon_m}}{\sqrt{GH}} \cos\left\{ k_x^{\mathrm{IV}} \left(\frac{1}{2}\left[x_R + x_S\right] - q \right) + k_x^{\mathrm{IV}} \frac{t}{2}\left[x_S - x_R\right] \right\} \cos\left\{ k_y^{\mathrm{IV}} \left(\frac{1}{2}\left[y_R + y_S\right] - r \right) + k_y^{\mathrm{IV}} \frac{t}{2}\left[y_S - y_R\right] \right\}, \tag{F.59}$$

$S^+ \to V^+$: Eq.(F.18), Eq.(F.19), Eq.(F.20),

$$\psi_i^{\mathrm{IV}}(\mathbf{x}(t)) = \frac{\sqrt{\epsilon_n \epsilon_m}}{\sqrt{GH}} \cos\left\{ k_x^{\mathrm{IV}} \left(\frac{1}{2}\left[x_S + x_V\right] - q \right) + k_x^{\mathrm{IV}} \frac{t}{2}\left[x_V - x_S\right] \right\} \cos\left\{ k_y^{\mathrm{IV}} \left(\frac{1}{2}\left[y_S + y_V\right] - r \right) + k_y^{\mathrm{IV}} \frac{t}{2}\left[y_V - y_S\right] \right\}, \tag{F.60}$$

$V^+ \to R^+$: Eq.(F.22), Eq.(F.23), Eq.(F.24),

$$\psi_i^{\mathrm{IV}}(\mathbf{x}(t)) = \frac{\sqrt{\epsilon_n \epsilon_m}}{\sqrt{GH}} \cos\left\{ k_x^{\mathrm{IV}} \left(\frac{1}{2}\left[x_V + x_R\right] - q \right) + k_x^{\mathrm{IV}} \frac{t}{2}\left[x_R - x_V\right] \right\} \cos\left\{ k_y^{\mathrm{IV}} \left(\frac{1}{2}\left[y_V + y_R\right] - r \right) + k_y^{\mathrm{IV}} \frac{t}{2}\left[y_R - y_V\right] \right\}, \tag{F.61}$$

With these parameter representations, the following integrals can be calculated

$$\begin{aligned}\oint_{\partial T_n^+} \frac{\partial \psi_i^{\mathrm{IV}}}{\partial \nu}\, dl = &\int_{l_{R+\to S+}} [\mathbf{a}_z \times \nabla_t \psi_i^{\mathrm{IV}}(\mathbf{x}(t))] \cdot \dot{\mathbf{x}}(t) dt \\ &+ \int_{l_{S+\to V+}} [\mathbf{a}_z \times \nabla_t \psi_i^{\mathrm{IV}}(\mathbf{x}(t))] \cdot \dot{\mathbf{x}}(t) dt \\ &+ \int_{l_{V+\to R+}} [\mathbf{a}_z \times \nabla_t \psi_i^{\mathrm{IV}}(\mathbf{x}(t))] \cdot \dot{\mathbf{x}}(t) dt,\end{aligned} \tag{F.62}$$

which is the second term on the right hand-side of Eq.(F.11) and

$$\int_{\text{common edge}^+} \psi_i^{\mathrm{IV}}\, \boldsymbol{\rho}_n^+ \cdot \boldsymbol{\nu}\, dl = \int_{l_{S+\to V+}} \psi_i^{\mathrm{IV}}(\mathbf{x}(t))\, [\mathbf{a}_z \times \boldsymbol{\rho}_n^+(\mathbf{x}(t))] \cdot \dot{\mathbf{x}}(t) dt \tag{F.63}$$

which is the first term on the right hand-side of Eq.(F.11).

Eq.(F.62) results in

$$\begin{aligned}\oint_{\partial T_n^+} \frac{\partial \psi_i^{\mathrm{IV}}}{\partial \nu}\, dl = &\frac{\sqrt{\epsilon_n \epsilon_m}}{\sqrt{GH}} [I_3 - I_4]\Big|_{R+\to S+} \\ &+ \frac{\sqrt{\epsilon_n \epsilon_m}}{\sqrt{GH}} [I_3 - I_4]\Big|_{S+\to V+} \\ &+ \frac{\sqrt{\epsilon_n \epsilon_m}}{\sqrt{GH}} [I_3 - I_4]\Big|_{V+\to R+},\end{aligned} \tag{F.64}$$

and Eq.(F.63) results in

$$\int_{\text{common edge}^+} \psi_i^{\mathrm{IV}}\, \boldsymbol{\rho}_n^+ \cdot \boldsymbol{\nu}\, dl = \frac{\eta}{4} \frac{\sqrt{\epsilon_n \epsilon_m}}{\sqrt{GH}} [I_1 + I_2]\Big|_{S+\to V+}. \tag{F.65}$$

In Sec.F.4.3 the various variables are defined.

F.4.2 Integral over T_n^-

For the integrals over T_n^- we also have to deal with vectors normal to the boundary. In the same way as in Sec.F.4.1 we use the substitution $\boldsymbol{\nu} = \boldsymbol{\tau} \times \mathbf{n}$, only now, $\mathbf{n}$ is the normal vector on the surface of the 'minus'-triangle which is equal to $-\mathbf{a}_z$, see Fig.F.2. So, we end up with

$$\frac{\partial \psi_i}{\partial \nu} = -(\mathbf{a}_z \times \nabla_t \psi_i) \cdot \boldsymbol{\tau}, \tag{F.66}$$

$$\psi_i\, \boldsymbol{\rho}_n^+ \cdot \boldsymbol{\nu} = -\psi_i\, (\mathbf{a}_z \times \boldsymbol{\rho}_n^+) \cdot \boldsymbol{\tau}. \tag{F.67}$$

The corresponding parameter representation is

$$U^- \to S^- : \text{Eq.(F.28), Eq.(F.29), Eq.(F.30),}$$
$$\psi_i^{\mathrm{IV}}(\mathbf{x}(t)) = \frac{\sqrt{\epsilon_n \epsilon_m}}{\sqrt{GH}} \cos\left\{k_x^{\mathrm{IV}}\left(\frac{1}{2}\left[x_R + x_S\right] - q\right) + k_x^{\mathrm{IV}}\frac{t}{2}\left[x_S - x_R\right]\right\} \cos\left\{k_y^{\mathrm{IV}}\left(\frac{1}{2}\left[y_R + y_S\right] - r\right) + k_y^{\mathrm{IV}}\frac{t}{2}\left[y_S - y_R\right]\right\}, \tag{F.68}$$

$$S^+ \to V^+ : \text{Eq.(F.32), Eq.(F.33), Eq.(F.34),}$$
$$\psi_i^{\mathrm{IV}}(\mathbf{x}(t)) = \frac{\sqrt{\epsilon_n \epsilon_m}}{\sqrt{GH}} \cos\left\{k_x^{\mathrm{IV}}\left(\frac{1}{2}\left[x_S + x_V\right] - q\right) + k_x^{\mathrm{IV}}\frac{t}{2}\left[x_V - x_S\right]\right\} \cos\left\{k_y^{\mathrm{IV}}\left(\frac{1}{2}\left[y_S + y_V\right] - r\right) + k_y^{\mathrm{IV}}\frac{t}{2}\left[y_V - y_S\right]\right\}, \tag{F.69}$$

$$V^+ \to R^+ : \text{Eq.(F.36), Eq.(F.37), Eq.(F.38),}$$
$$\psi_i^{\mathrm{IV}}(\mathbf{x}(t)) = \frac{\sqrt{\epsilon_n \epsilon_m}}{\sqrt{GH}} \cos\left\{k_x^{\mathrm{IV}}\left(\frac{1}{2}\left[x_V + x_R\right] - q\right) + k_x^{\mathrm{IV}}\frac{t}{2}\left[x_R - x_V\right]\right\} \cos\left\{k_y^{\mathrm{IV}}\left(\frac{1}{2}\left[y_V + y_R\right] - r\right) + k_y^{\mathrm{IV}}\frac{t}{2}\left[y_R - y_V\right]\right\}, \tag{F.70}$$

With these parameter representations, the following integral can be calculated

$$\begin{aligned}\oint_{\partial T_n^-} \frac{\partial \psi_i^{\mathrm{IV}}}{\partial \nu}\, dl = &- \int_{l_{U^- \to S^-}} \left[\mathbf{a}_z \times \nabla_t\, \psi_i^{\mathrm{IV}}(\mathbf{x}(t))\right] \cdot \dot{\mathbf{x}}(t) dt \\ &- \int_{l_{S^- \to V^-}} \left[\mathbf{a}_z \times \nabla_t\, \psi_i^{\mathrm{IV}}(\mathbf{x}(t))\right] \cdot \dot{\mathbf{x}}(t) dt \\ &- \int_{l_{V^- \to U^-}} \left[\mathbf{a}_z \times \nabla_t\, \psi_i^{\mathrm{IV}}(\mathbf{x}(t))\right] \cdot \dot{\mathbf{x}}(t) dt,\end{aligned} \tag{F.71}$$

which is the fourth term on the right hand-side of Eq.(F.11) and

$$\int_{\text{common edge}^-} \psi_i^{\mathrm{IV}}\, \boldsymbol{\rho}_n^- \cdot \boldsymbol{\nu}\, dl = - \int_{l_{S^- \to V^-}} \psi_i^{\mathrm{IV}}(\mathbf{x}(t))\, \left[\mathbf{a}_z \times \boldsymbol{\rho}_n^+(\mathbf{x}(t))\right] \cdot \dot{\mathbf{x}}(t) dt \tag{F.72}$$

which is the third term on the right hand-side of Eq.(F.11).

Eq.(F.71) results in

$$\begin{aligned}\oint_{\partial T_n^-} \frac{\partial \psi_i^{\mathrm{IV}}}{\partial \nu}\, dl = &-\frac{\sqrt{\epsilon_n \epsilon_m}}{\sqrt{GH}}[I_3 - I_4]\Big|_{U^- \to S^-} \\ &- \frac{\sqrt{\epsilon_n \epsilon_m}}{\sqrt{GH}}[I_3 - I_4]\Big|_{S^- \to V^-} \\ &- \frac{\sqrt{\epsilon_n \epsilon_m}}{\sqrt{GH}}[I_3 - I_4]\Big|_{V^- \to U^-},\end{aligned} \tag{F.73}$$

and Eq.(F.72) results in

$$\int\limits_{\text{common edge}^-} \psi_i^{\mathrm{IV}}\, \boldsymbol{\rho}_n^- \cdot \boldsymbol{\nu}\, dl = -\frac{\eta}{4}\frac{\sqrt{\epsilon_n \epsilon_m}}{\sqrt{GH}}[I_1 + I_2]\Big|_{S^- \to V^-}. \tag{F.74}$$

In Sec.F.4.3 the pertaining variables are defined.

With Eqs.(F.64), (F.65), (F.73) and (F.74), a solution to Eq.(F.11) can be found in the form

$$\begin{aligned}\left\langle \mathbf{h}_i^{''\mathrm{IV}}, \mathbf{g}_n \right\rangle = &-\frac{l_n \eta \sqrt{\epsilon_n \epsilon_m}}{4 A_n^+ k_{t;i}'' \sqrt{GH}}[I_1 + I_2]\Big|_{S^+ \to V^+} - \frac{l_n \sqrt{\epsilon_n \epsilon_m}}{A_n^+ k_{t;i}''^{\,3} \sqrt{GH}}\Big\{[I_3 - I_4]\Big|_{R^+ \to S^+} \\ &+[I_3 - I_4]\Big|_{S^+ \to V^+} + [I_3 - I_4]\Big|_{V^+ \to R^+}\Big\} \\ &-\frac{l_n \eta \sqrt{\epsilon_n \epsilon_m}}{4 A_n^- k_{t;i}'' \sqrt{GH}}\{-[I_1 + I_2]\}\Big|_{S^- \to V^-} - \frac{l_n \sqrt{\epsilon_n \epsilon_m}}{A_n^- k_{t;i}''^{\,3} \sqrt{GH}}\Big\{ - [I_3 - I_4]\Big|_{U^- \to S^-} \\ &-[I_3 - I_4]\Big|_{S^- \to V^-} - [I_3 - I_4]\Big|_{V^- \to U^-}\Big\}.\end{aligned} \tag{F.75}$$

F.4.3 Defined integral variables

In Eqs.(F.64), (F.65), (F.73), (F.74) and (F.75) we introduced a number of variables, defined as follows.

I_1 is given by Eq.(F.43),

I_2 is given by Eq.(F.44),

$$\begin{aligned}I_3 &= \int_a^b \delta \cos(\alpha + t\beta) \sin(\zeta + t\xi)\, dt = \\ &= -\frac{\delta(a-b)}{2}\Big\{ \sin\left[(\zeta + \alpha) + \frac{(\xi + \beta)(a+b)}{2}\right] \operatorname{sinc}\left[\frac{(\xi + \beta)(a-b)}{2}\right] \\ &\qquad + \sin\left[(\zeta - \alpha) + \frac{(\xi - \beta)(a+b)}{2}\right] \operatorname{sinc}\left[\frac{(\xi - \beta)(a-b)}{2}\right]\Big\}\end{aligned} \tag{F.76}$$

$$
\begin{aligned}
I_4 &= \int_a^b \gamma \sin(\alpha + t\beta)\cos(\zeta + t\xi)\, dt = \\
&= -\frac{\gamma(a-b)}{2}\left\{ \sin\left[(\alpha+\zeta) + \frac{(\beta+\xi)(a+b)}{2}\right] \operatorname{sinc}\left[\frac{(\beta+\xi)(a-b)}{2}\right] \right. \\
&\qquad \left. + \sin\left[(\alpha-\zeta) + \frac{(\beta-\xi)(a+b)}{2}\right] \operatorname{sinc}\left[\frac{(\beta-\xi)(a-b)}{2}\right] \right\}
\end{aligned} \tag{F.77}
$$

The variables α, β, ξ and ζ for the various line sections can be found in Eqs.(F.47)-(F.52). The variables δ, γ and η for the various line sections are defined in Eqs.(F.78)-(F.83).

$$
\begin{aligned}
R^+ \to S^+ : \delta &= k_y^{\mathrm{IV}} \frac{1}{2}(x_S - x_R), \\
\gamma &= k_x^{\mathrm{IV}} \frac{1}{2}(y_S - y_R),
\end{aligned} \tag{F.78}
$$

$$
\begin{aligned}
S^+ \to V^+ : \delta &= k_y^{\mathrm{IV}} \frac{1}{2}(x_V - x_S), \\
\gamma &= k_x^{\mathrm{IV}} \frac{1}{2}(y_V - y_S), \\
\eta &= \frac{-1}{4}(y_S + y_V)(x_V - x_S) - \frac{y_R}{2}(x_V - x_S) \\
&\quad + \frac{1}{4}(x_S + x_V)(y_V - y_S) - \frac{x_R}{2}(y_V - y_S),
\end{aligned} \tag{F.79}
$$

$$
\begin{aligned}
V^+ \to R^+ : \delta &= k_y^{\mathrm{IV}} \frac{1}{2}(x_R - x_V), \\
\gamma &= k_x^{\mathrm{IV}} \frac{1}{2}(y_R - y_V),
\end{aligned} \tag{F.80}
$$

$$
\begin{aligned}
U^- \to S^- : \delta &= k_y^{\mathrm{IV}} \frac{1}{2}(x_S - x_U), \\
\gamma &= k_x^{\mathrm{IV}} \frac{1}{2}(y_S - y_U),
\end{aligned} \tag{F.81}
$$

$$
\begin{aligned}
S^- \to V^- : \delta &= k_y^{\mathrm{IV}} \frac{1}{2}(x_V - x_S), \\
\gamma &= k_x^{\mathrm{IV}} \frac{1}{2}(y_V - y_S), \\
\eta &= \frac{-y_U}{2}(x_V - x_S) + \frac{1}{4}(y_S + y_V)(x_V - x_S) \\
&\quad + \frac{x_U}{2}(y_V - y_S) - \frac{1}{4}(x_S + x_V)(y_V - y_S),
\end{aligned} \tag{F.82}
$$

$$
\begin{aligned}
V^- \to U^- : \delta &= k_y^{\mathrm{IV}} \frac{1}{2}(x_U - x_V), \\
\gamma &= k_x^{\mathrm{IV}} \frac{1}{2}(y_U - y_V),
\end{aligned} \tag{F.83}
$$

Appendix G

Programming details

Below, matrix formulations are presented, which are related to the iris.

$$[T^{\mathrm{I;II}}]_{sr} = [T^{\mathrm{I}}]_{sr} + [T^{\mathrm{II}}]_{sr}, \tag{G.1}$$

$$[T^{\mathrm{I}}]_{sr} = -[\Pi^{\mathrm{I}}]^T_{is}[Y^{\mathrm{I}}]_{ii}\,[\Pi^{\mathrm{I}}]^T_{ri}, \tag{G.2}$$

$$[T^{\mathrm{II}}]_{sr} = [\Pi^{\mathrm{II}}]^T_{ps}[\Lambda^{\mathrm{II}}]_{pp}\,[\Pi^{\mathrm{II}}]^T_{rp}, \tag{G.3}$$

$$[T^{\mathrm{II}}]_{sq} = -[\Pi^{\mathrm{II}}]^T_{ps}[\,\Xi^{\mathrm{II}}]_{pp}\,[\Pi^{\mathrm{II}}]^T_{qp}, \tag{G.4}$$

$$[Y^{\mathrm{I}}]_{ii} = Y^{\alpha;\mathrm{I}}_{\infty;i}\,\delta_{ij}, \tag{G.5}$$

$$[\,\Lambda^{\mathrm{II}}]_{pp} = \frac{Y^{\alpha;\mathrm{II}}_{\infty;p}\cos(k^{\alpha;\mathrm{II}}_{z;p}[z_1 - z_2])}{j\sin(k^{\alpha;\mathrm{II}}_{z;p}[z_1 - z_2])}\,\delta_{pj}, \tag{G.6}$$

$$[\,\Xi^{\mathrm{II}}]_{pp} = \frac{Y^{\alpha;\mathrm{II}}_{\infty;p}}{j\sin(k^{\alpha;\mathrm{II}}_{z;p}[z_1 - z_2])}\,\delta_{pj}, \tag{G.7}$$

$$[T^{\mathrm{II;III}}]_{sq} = [T^{\mathrm{II}}]_{sq} + [T^{\mathrm{III}}]_{sq}, \tag{G.8}$$

$$[T^{\mathrm{II}}]_{sq} = -[\Pi^{\mathrm{II}}]^T_{ps}[\,\Gamma^{\mathrm{II}}]_{pp}\,[\Pi^{\mathrm{II}}]^T_{qp}, \tag{G.9}$$

$$[T^{\mathrm{III}}]_{sp} = [\Pi^{\mathrm{III}}]^T_{ls}[Y^{\mathrm{III}}]_{ll}\,[\Pi^{\mathrm{III}}]^T_{ql}, \tag{G.10}$$

$$[T^{\mathrm{II}}]_{sr} = [\Pi^{\mathrm{II}}]^T_{ps}[\,\Xi^{\mathrm{II}}]_{pp}\,[\Pi^{\mathrm{II}}]^T_{rp}, \tag{G.11}$$

$$[\,\Gamma^{\mathrm{II}}]_{pp} = \frac{Y^{\alpha;\mathrm{II}}_{\infty;p}\cos(k^{\alpha;\mathrm{II}}_{z;p}[z_2 - z_1])}{j\sin(k^{\alpha;\mathrm{II}}_{z;p}[z_1 - z_2])}\,\delta_{pj}, \tag{G.12}$$

$$[Y^{\mathrm{III}}]_{ll} = Y^{\alpha;\mathrm{III}}_{\infty;l}\,\delta_{lj}, \tag{G.13}$$

$$[\Pi^{\mathrm{I}}]_{is} = \left\langle \mathbf{h}^{\alpha;\mathrm{I}}_i, \mathbf{w}_s \right\rangle, \tag{G.14}$$

$$[\Pi^{\mathrm{I}}]_{ri} = \left\langle \mathbf{f}_r, \mathbf{h}^{\alpha;\mathrm{I}}_i \right\rangle, \tag{G.15}$$

$$[\Pi^{\mathrm{II}}]_{ps} = \left\langle \mathbf{h}^{\alpha;\mathrm{II}}_p, \mathbf{w}_s \right\rangle, \tag{G.16}$$

$$[\Pi^{\mathrm{II}}]_{rp} = \left\langle \mathbf{f}_r, \mathbf{h}_p^{\alpha;\mathrm{II}} \right\rangle, \tag{G.17}$$

$$[\Pi^{\mathrm{II}}]_{qp} = \left\langle \mathbf{f}_q, \mathbf{h}_p^{\alpha;\mathrm{II}} \right\rangle, \tag{G.18}$$

$$[\Pi^{\mathrm{III}}]_{ql} = \left\langle \mathbf{f}_q, \mathbf{h}_l^{\alpha;\mathrm{III}} \right\rangle, \tag{G.19}$$

$$[\Pi^{\mathrm{III}}]_{ls} = \left\langle \mathbf{h}_l^{\alpha;\mathrm{III}}, \mathbf{w}_s \right\rangle, \tag{G.20}$$

$$[I^{\mathrm{I};ex}]_s = -2[\Pi^{\mathrm{I}}]_{is}^T [Y^{\mathrm{I}}]_{ii} [B^\alpha]_i, \tag{G.21}$$

$$[I^{\mathrm{III};ex}]_s = -2[\Pi^{\mathrm{III}}]_{ls}^T [Y^{\mathrm{III}}]_{ll} [-C^\alpha]_l. \tag{G.22}$$

The integrals in Eq.(G.14)-(G.20) are worked out in Appendix E.

Below, matrix formulations are presented, which are related to the patch.

$$[T^{\mathrm{IV;V}}]_{sr} = [T^{\mathrm{IV}}]_{sr} + [T^{\mathrm{V}}]_{sr}, \tag{G.23}$$

$$[T^{\mathrm{IV}}]_{sr} = [\Pi^{\mathrm{IV}}]_{is}^T [Y^{\mathrm{IV}}]_{ii} [\Pi^{\mathrm{IV}}]_{ri}^T, \tag{G.24}$$

$$[T^{\mathrm{V}}]_{sr} = [\Pi^{\mathrm{V}}]_{ps}^T [Y^{\mathrm{V}}]_{pp} [\Pi^{\mathrm{V}}]_{rp}^T, \tag{G.25}$$

$$[\Pi^{\mathrm{IV}}]_{is} = \left\langle \mathbf{h}_i^{\alpha;\mathrm{IV}}, \mathbf{w}_s \right\rangle, \tag{G.26}$$

$$[\Pi^{\mathrm{IV}}]_{ri} = \left\langle \mathbf{f}_r, \mathbf{h}_i^{\alpha;\mathrm{IV}} \right\rangle, \tag{G.27}$$

$$[\Pi^{\mathrm{V}}]_{ps} = \left\langle \mathbf{h}_p^{\alpha;\mathrm{V}}, \mathbf{w}_s \right\rangle, \tag{G.28}$$

$$[\Pi^{\mathrm{V}}]_{rp} = \left\langle \mathbf{f}_r, \mathbf{h}_p^{\alpha;\mathrm{V}} \right\rangle, \tag{G.29}$$

$$[Y^{\mathrm{IV}}]_{ii} = Y_{\infty;i}^{\alpha;\mathrm{IV}} \, \delta_{ij}, \tag{G.30}$$

$$[Y^{\mathrm{V}}]_{pp} = Y_{\infty;p}^{\alpha;\mathrm{V}} \, \delta_{pj}, \tag{G.31}$$

$$[I^{ex}]_s = [I^{\mathrm{IV};ex}]_s + [I^{\mathrm{V};ex}]_s, \tag{G.32}$$

$$[I^{\mathrm{IV};ex}]_s = 2[\Pi^{\mathrm{IV}}]_{is}^T [Y^{\mathrm{IV}}]_{ii} [B^\alpha]_i, \tag{G.33}$$

$$[I^{\mathrm{V};ex}]_s = -2[\Pi^{\mathrm{IV}}]_{ps}^T [Y^{\mathrm{V}}]_{pp} [-C^\alpha]_p, \tag{G.34}$$

The integrals in Eq.(G.26)-(G.29) are worked out in Appendix F.

Bibliography

[1] "Analyse3."
Eindhoven University of Technology, Department of Mathematics & Computing Science, Eindhoven.
Lecture notes. 1998/1999.

[2] Aberle, J.T. and D.M. Pozar
"Analysis of infinite arrays of one and two-probe-fed circular patches."
IEEE Trans. Antennas Propagat. Vol.38(No.4):p.421–432, April 1990.

[3] Aberle, J.T. and D.M. Pozar
"Analysis of infinite arrays of probe-fed rectangular microstrip patches using a rigorous feed model."
IEE Proc. Part-H. Vol.136(No.2):p.110–118, April 1989.

[4] Aberle, J.T.
"On the use of metallized cavities backing microstrip antennas."
IEEE Antennes and Propagation Society Symposiom 1991 Digest (Cat. No.91CH3036-1).IEEE New York, NY, USA; 1991; 3 vol. xii+1892 pp. p.60-3 vol.1.

[5] Au, Tsien Ming
"Performance of aperture-coupled dual-patch microstrip phased arrays."
IEEE Trans. Antennas Propagat. Vol.44(No.9):p.1290–1295, Sept. 1996.

[6] Balanis, C.A.
"Antenna theory; analysis and design." 2nd ed.
New York: John Wiley & Sons, Inc.,1982.

[7] Cheng, J.-C. and N.I. Dib, L.P.B. Katehi
"Theorectical modeling of cavity-backed patch antennas using a hybrid technique."
IEEE Trans. Antennas Propagat. Vol.43(No.9):p.1003–1013, Sept. 1995.

[8] Collin, R.E.
"Foundations for microwave engineering." 2nd ed.
New York: McGraw-Hill, Inc.,1992.
Electrical Engineering Series.

[9] Croq, F. and D.M. Pozar
"Millimeter-wave design of wide-band aperture-coupled stacked microstrip antennas."
IEEE Trans. Antennas Propagat. Vol.39(No.12):p.1770–1776, Dec. 1991.

[10] Das, B.N. and D.M. Pozar
"Printed antennas in multiple layers: general considerations and infinite array analysis by a unified method."
Sixth International Conference on Antennas and Propagation (ICAP 89) (Conf. Publ. No.301). IEE, London, UK; 1989; 2 vol. (xxii+546+xxii474) pp. p.364-8 vol.1.

[11] Felsen, L.B. and N. Marcuvitz
"Radiation and scattering of waves."
Prentic-Hall, Inc.,1994.
IEEE PRESS Series on Electromagnetic Waves.

[12] Gentili, G.G.
"Properties of TE-TM mode-matching techniques"
IEEE Trans. Microwave Theory Tech. Vol.39(No.9):p.1669–1673, Sept. 1991.

[13] Gonzalez de Aza, M.A. and J. Zapata, J.A. Encinar
"Broad-band cavity backed and capacitively probe-fed microstrip patch arrays."
IEEE Trans. Antennas Propagat. Vol.48(No.5):p.784–789, May 2000.

[14] Gonzalez de Aza, M.A. and J.A. Encinar, J. Zapata, M. Lambea
"Full-wave analysis of cavity backed, probe-fed microstrip patch arrays by a hybrid mode-matching generalized scattering matrix, and finite-element method."
IEEE Trans. Antennas Propagat. Vol.42(No.2):p.234–242, Feb. 1998.

[15] Harrington, R.F.
"Field computation by moment methods."
New York: IEEE Press ,1993.

[16] Hon, B.P. de
"Electromagnetisch golfgeleiders"
Eindhoven University of Technology, Department of Electrical Engineering, Electromagnetics Division, Eindhoven.
Lecture notes for:. 2000.

[17] Jones, D.S.
"The theory of electromagnetism."
Oxford: Pergamon, 1964.

[18] Kreyszig, E.
"Advanced engineering mathematics."
New York: John Wiley & Sons, 8-th ed., 1999.

[19] Kuester, E.F. and D.C. Chang
"Theory of waveguides and transmission lines."
University of Colorado, Department of Electrical and Computer Engineering, Electromagnetics Laboratory, Boulder 2000
Lecture notes for: ECEN 5114. 2000.

[20] Lubin, Y. and A. Hessel
"Wide band, wide angle microstrip stacked patch element phased arrays."
IEEE Trans. Antennas Propagat. Vol.39(No.8):p.1062–1070, Aug. 1991.

[21] Mailloux, R.J.
"On the use of metallized cavities in printed slot arrays with dielectric substrates."
IEEE Trans. Antennas Propagat. Vol.35(No.5):p.477–487, May 1987.

[22] N. Marcuvitz
"Waveguide handbook."
New York: McGraw-Hill, Inc.,1951.

[23] Pozar, D.M. and D.H. Schaubert
"Scan blindness in infinite phased arrays o printed dipoles"
IEEE Trans. Antennas Propagat. Vol.32(No.6):p.602–610, June 1984.

[24] Pozar, D.M.
"Analysis of an infinite phased array of aperture coupled microstrip patches."
IEEE Trans. Antennas Propagat. Vol.37(No.4):p.418–425, April 1989.

[25] Rao, S.M. and D.R. Wilton, A.W. Glisson
"Electromagnetic scattering by surfaces of arbitrary shape"
IEEE Trans. Antennas Propagat. Vol.30(No.3):p.409–418, May 1982.

[26] Rothwell, E.J. and M.J. Cloud
"Electromagnetics"
Boca Raton: CRC Press.

[27] Sadiku, M.N.O.
"Elements of electromagnetics." 2nd ed.
New York: Oxford University, Inc.,1995.

[28] Safavi-Naini, R. and R.H. Macphie
"Scattering at rectangular-to-rectangular waveguide junctions"
IEEE Trans. Microwave Theory Tech. Vol.30(No.11):p.2060–2063, Nov. 1982.

[29] Smolders, A.B.
"Electormagnetische Antennes 1."
Eindhoven University of Technology, Department of Electrical Engineering, Electromagnetics Division, Eindhoven.
Lecture notes:. 1999.

[30] Smolders, A.B.
"Microstrip phased-array antennas: A finite-array approach"
Eindhoven University of Technologie, 1994. PhD thesis.

[31] Waterhouse, R.B.
"Design and performance of large phased arrays of aperture stacked patches"
IEEE Trans. Antennas Propagat. Vol.49(No.2):p.292–297, Feb. 2001.

[32] Zavosh, F. and J.T. Aberle
"Infinite phased arrays of cavity-backed patches."
IEEE Trans. Antennes Propagat. Vol.42(No.3):p.390–398, March 1994.

[33] Zavosh, F. and J.T. Aberle
"Single and stacked circular microstrip patch antennas backed by a circular cavity."
IEEE Trans. Antennes Propagat. Vol.43(No.7):p.746–750, July 1995.